ABSTRACT

LIEBOV, NICHOLE S. Development of Methods for Hydrocarbon Functionalization (Under the direction of Professor T. Brent Gunnoe).

Natural gas, which consists primarily of methane, ethane and propane, is a plentiful domestic resource that accounts for nearly a quarter of global energy production. However, its transportation and utilization is complicated by its gaseous state under ambient conditions. Current methods for the conversion of natural gas to high value liquid products require high temperatures and pressures and are capital-intensive. As a result, sources of natural gas that are located in remote regions are left "stranded." Because methane is a potent greenhouse gas, with high global warming potential relative to CO_2, this stranded natural gas is often unproductively flared to produce CO_2. Globally, this flaring has been estimated to add 300 million tons of CO_2 to the atmosphere each year and represents a loss of approximately $2 billion per year. Thus, there is significant motivation to develop a more efficient method to convert methane and other light alkanes from natural gas to easily transportable liquid products at the wellhead. This liquid (*e.g.*, methanol) could then be used directly as a fuel or as a precursor to high-value chemicals.

The primary focus of this Dissertation is the development of a selective method for the direct partial oxidation of light alkanes. Iodine oxides and chloride salts have been demonstrated to be highly efficient for the oxy-esterification (OxE) of methane, ethane and propane to generate the corresponding esters in trifluoroacetic acid at temperatures < 200 °C and pressures ranging from 35-1000 psi. Ethylene is also functionalized under similar reaction conditions to generate a derivative of ethylene glycol.

A combined experimental and computational mechanistic study found that light alkane functionalization likely occurs through a radical-based pathway where chlorine radical or

IO_2 radical are predicted to abstract an H-atom from the starting alkane to generate alkyl radical. The alkyl radical is trapped by iodine which is generated *in situ* from the reduction of the iodine oxide oxidant to produce alkyl iodide which undergoes solvolysis in trifluoroacetic acid to produce alkyl trifluoroacetate. Although the C–H bond of MeTFA is weaker than that of methane, the alkyl ester was demonstrated to be stable under the highly oxidizing conditions with KCl/NH_4IO_3 in HTFA at 140 °C. The high selectivity for the alkyl ester product is proposed to be a manifestation of the polar effect, where the electron-withdrawing trifluoroacetate moiety of the alkyl ester prevents additional, undesired oxidation in the polar solvent by decreasing the polarity of the transition state.

Extension of the selective alkane OxE process to oxidants other than iodate was examined with the goal of identifying an oxidant which could generate species capable of H-atom abstraction and be regenerated easily using air. Nitrates and manganese-based oxidants have been demonstrated to be the most effective of those studied. Methane functionalization with these oxidants is stoichiometric rather than catalytic, but efforts to recycle the oxidants *in situ* are ongoing.

The iodine oxide and chloride system was also examined under photochemical conditions. The functionalization of methane, ethane and propane is highly efficient, producing functionalized products with percent yields of ~50%, 80% and ~40%, respectively. MeTFA is also highly stable under photochemical reaction conditions, likely enabling the high yield of the mono-functionalized product. The conversion of methane to alkyl esters has also been observed using other oxidant systems and the photocatalyst tetrabutylammonium decatungstate.

Additionally, the conversion of toluene and 1-pentene to pentenyltoluenes using the Rh catalyst precursor $[Rh(\mu\text{-}OAc)(\eta^2\text{-}C_2H_4)_2]_2$ has been studied. Rhodium-based catalysis enables high ratios of linear:branched pentenyltoluenes products (up to 11:1). These linear pentenyltoluenes, which cannot be produced using current acid-based industrial methods for arene alkylation, are precursors for the plastic polyethylene naphthalate (PEN), a derivative of polyethylene terephthalate (PET).

ACKNOWLEDGMENTS

I could not have reached this point without the help of many, many people. There is no way to thank everyone enough for all of their help, time, advice, patience, and kindness. Choosing to come to UVA is the best decision I have ever made. I have learned so much. This department has been incredibly supportive and I am grateful to have known everyone I have had the pleasure to meet here. Thank you all.

First, I have to thank my PI, Brent Gunnoe. Brent, thank you for everything you have done for me over the past five years. Thank you for taking a chance on me and accepting me into the graduate program and your lab. My life is undoubtedly better for it. I have loved being a part of the department and I am so lucky to have had you as my PI. You have been a great advisor and have kept me inspired even when I thought I had reached the end of my rope. Thanks for treating my project as important as the others and continuing with our subgroup meetings that were really just one-on-ones. Your leadership and generosity are unfailing and we would all do well to follow your example. You care about your students and that makes all the difference. It has been wonderful getting to know you, Trecia and Leah. See how much I appreciate you? I left out the Oxford comma. I wish you and your family all the best and am excited to hear where Leah’s brilliance and dedication take her.

Now, naturally, onto my honorary advisor. Dean Harman, while I may not have officially joined your lab, I joined your lab family. It fills me with pride when you say I’m an honorary member of your group because I know how much love you have for your students and how much we have for you. I have enjoyed getting to spend time with you and your group at your Classics or just down the hall. Lisa is wonderful, and I’m so glad

I’ve gotten to know you both. Thank you for always being there for me. Grad school is a challenging time, and you helped me so much when I was down. It has also been amazing getting to watch the dogs, even if we did get locked out that one time and had the lights turned off from across the world.

I have also been very fortunate to have had incredible mentors early on in my education. In particular, I have to thank Matt Mihordea, my fantastic high school chemistry teacher. I will always be incredibly grateful to him for inspiring me to pursue chemistry. Without him, I would not be where I am today. More recently, Robert Gilliard has been an amazing mentor. I feel very privileged to have known you as a graduate student, and am so thankful for your patience in training me when I didn’t know anything about working in a lab. I was sad when we went our separate ways from UGA and then was thrilled to hear that you planned to accept the offer to come to UVA. It was amazing and hilarious that I got to recruit you. It has been great getting to see your career flourish, and it has been so nice having you nearby again. I wish you the best of luck, not that you need it.

Research is a group effort, and I have been very fortunate to have worked with some fantastic collaborators. The DOE EERE AMO group has been so helpful in elucidating aspects of the OxE process. Special thanks to Bill Goddard, Smith Nielsen, Ross Fu, Jay Groves, Nick Boaz, Jon Goldberg, and Thompson Zhuang for all of their hard work. I wish Nathan, Evan, and all of those continuing this exciting and challenging project all the best!

The UVA Chemistry Department’s staff have made each and every day easier and better. In particular I am so grateful to Cindy Knight, Susie Marshall, Danny Via, Mike Birckhead, and Jerry Shifflett. Cindy, it has been so good to get to know you. It’s been my pleasure helping you out at graduation and, just like the undergrads, I think you’re the best.

You run this show. Susie, you have always been kind and unbelievably helpful. Thank you for all your reminders and help. Thanks to both of you for innumerable parking passes and room reservations. I feel very lucky to know Danny Via and Mike Birckhead in the stockroom. I love getting to see you two. You're both so wonderful and kind. I can't thank you enough. Thanks Jerry for always fixing everything and being a friendly face around the department. I also have to thank Jeff Ellena for all of his hard work and for always graciously fixing the NMRs whenever they wouldn't cooperate.

Thank you to the entire Gunnoe lab, past and present. There is absolutely no way I could have made it this far without you. There are a few past members I have to thank specifically. Steve Kalman, thank you for training me and introducing me to this project. George Fortman, well done for discovering that Rh is useless so that I could play with salts for years. Thank you so much for all of your incredibly gracious help via email long before we ever met. Kathleen Taylor, thank you for always being a ray of sunshine in our tiny office. I love how much you love cats and hope you get one soon. You're such a diligent worker and I hope you know how amazing you are. Thanks for introducing me to the ordering process and the awesome people in the stockroom. Thank you to John Dekarske and Bridgette Dale for being hilarious labmates. I've missed you guys.

Sometimes we're lucky enough to be friends with our colleagues. I am grateful to be able to call Mike Webster-Gardiner my friend. When I joined the lab, you were always so supportive. I remember that you pulled me aside after I gave group meeting in my first year to tell me I did a good job. That meant so much to me. You were always the golden child and your good opinion meant and means a great deal. You're a good scientist, but more importantly, you're a great person and are infectiously happy, selfless, and kind. Thank you for being a friend and groomsman and for planning my honeymoon, even though you also attended it. I had an amazing time in Australia. It was truly unforgettable, and I am so glad our group was able to reunite down under! I can't lie to you, as you well know, so believe me when I say I respect you and value your friendship more than I can say.

Someone who, like Mike, did impressive science, frequently sang falsetto around the lab, and calls me Megan, is Brad McKeown. I still can't believe I get to be friends with either of them. I remember hearing about Brad long before he came back to Charlottesville, as though he were this mythical creature who ate everything in sight and was incredibly productive and universally loved. When I met you, I understood right away and desperately wanted you to come back to UVA and am so grateful you did. I learned so much from you at work, and loved getting to know you and Katie. I have so many fond memories of us together and I am grateful for them all, though they are as difficult as they are wonderful. Thank you for letting me into your life and for being as into Thai food and Black Mirror as I am. I'm so glad we've been able to see each other since you left Charlottesville.

To the current Gunnoe lab, thank you all! Special thanks to those of you who helped edit my thesis! We're in the trenches every day and it's been great both having a cohort around for many years and getting to know new students and postdocs as they join. Evan Hall and Holly Tubbs, I wish you both the best of luck as you get started on your projects. Ana Geer, thank you for being a great addition to our lab. I can always rely on you when I have a random question, and it's been wonderful getting to know you. Ryan Holland, thanks for bringing your passion for science to our lab. Nathan Coutard, I wish you the best of luck with this project and I'm sorry we did not overlap more. The lab is lucky to have you. Fanji Kong, you're absolutely brilliant. You've helped me in countless ways and I am very grateful. Kaeleigh Olsen, I’m so glad I’ve gotten to know you. Like Yara, you’re a little shy at first, but you’re also hilarious and I’m so glad we’re desk neighbors. Thanks for always being there to share a glance and chat about whatever. I know science has been tough, but I also know you can get through it. Thanks to Ke Zhang for always being kind and for being a great reactor sharing partner. Shunyan Gu, you’ve always been so reliable and wonderful and I can’t thank you enough for taking over for ordering when I’m away and all of the other selfless things you do for me and the whole lab. Zhongwen Luo, thanks for your enthusiasm. Weihao Zhu, thank you for all the many things you do for everyone around the lab. Wear your sweatpants with pride.

I really can’t thank the next two labmates enough. Junqi Chen, you’ve been around since I started and I owe you so much. You can do anything. It’s been amazing seeing how far you’ve pushed different projects and how many things you do so well. You’ve completely changed the whole hydroarylation project for our lab. You got the 10,000 TO that we all thought was a laughably high goal, and now new people won’t realize how much of a long shot that seemed just a couple of years ago. You’ll be brilliant at whatever you do next. Thank you for always helping me out and being a great mentor. Finally, I am so excited to thank Xiaofan Jia. I’m so glad to have someone as awesome as you around. I love that we are in the same year, have always presented together at group meeting, and have always sat next each other in all of the three (soon to be four) offices we’ve shared. You’re so funny and unbelievably kind. You would do anything for anyone and the lab and department are so lucky to have you. Oh, and yeah, you’re also a great chemist, but everyone knows that. We’re technically peers, but I’ve always known you are head and shoulders above me. Thank you for teaching me so much, always helping me with whatever questions I have, and for sharing all your obsessions, from cats to Google Earth.

I am lucky enough to have a second lab family, or as I like to call them, a lab away from lab. To the entire Harman lab, thank you so much for everything. Thank you for accepting me into your group. I have loved spending time with you guys at work, at trivia, at Dean's house, and everywhere else around Charlottesville. Kevin Welch, I'm so glad you came back to UVA. You're hilarious and an invaluable trivia team member. I'm very lucky to call you my friend. To past Harman lab members, thank you guys and you are missed dearly. Jeff Myers, you gave me my first tour around the building! Thank you for all of your enthusiasm and kindness. Phil Shivokevich, I'm glad I've gotten to know you better. You're so good to your friends. Thank you, Hannah Nedzbala and Alex Heyer, you're both amazing and I have loved hanging out with you. You're seriously going to do great things. Steven Dakermanji, thank you for being your kind, selfless self. Thanks for always letting us swap HPs with you. Thank you, Jacob Smith, Justin Wilde, and Spenser Simpson, for always treating me like part of the lab. And no, I haven't forgotten about two very important members of the Harman lab...

Thankfully, I've had an amazing network of friends during my time in grad school. I'm particularly grateful to a few from home. Camily Williams and Carly Moskowitz, it was so hard to leave UGA knowing you guys were still there living it up (though I'm sure you probably had to study and stuff…). Thank you two for always supporting me and for being amazing bridesmaids! I love you both. Caroline Irvin, thank you for always being there for me since middle school. I'm so excited for this next chapter in your life. Who'd have thought you'd be in Alaska?

I'm especially grateful to have made new friends in Charlottesville. I was very nervous coming here, to a place where I didn't know anyone, but everything turned out better than I could have ever dreamed. I'm so thankful to have been warmly welcomed by the amazing grad students in the Chem department. Jen Martin, thank you for being the frequent leader of our little group. I'm so glad I've gotten to spend more time with you lately. You have the biggest heart and I'll be forever grateful that you rescued me when my Miata couldn't make it home in the snow. Thank you for sharing your wine and your pottery, and I've loved sharing my obsession for the GBBO with you. Ashton Brock Nelson, thanks for being your hilarious self. To you both, I'm so glad we were able to go to Australia together! I can't wait for our next adventure. Kim Stanek & Mike Hague, thanks for being amazing friends. You guys are so cool and you're very missed in Charlottesville. We'll all have to make a trip out to see you soon. I hear that vineyard is only 4 hours away! To Chris DeRosa, thank you for being a friend and one of the nicest people I've ever met. I never would have thought I'd like being called precious, but you pull it off. You love all of your friends so much and I hope you know how truly lucky we are to know you.

I am also very grateful to the Eagles Landing group. Eric Hunt, you are a remarkable person and seeing you in your element, playing sports or board games surrounded by friends, never fails to make me smile. Thanks for always being there for your friends and for all of the one-on-ones we've had. Maura Belanger, thanks for everything you do for me and the department with GSC. I'm very lucky to have you as my VP. Thank you, Andi Davis, Elizabeth Duselis, Jason Kuhn, and everyone else from Eagles. I've loved getting to play volleyball and games with you all.

I have to thank Katy Wilson. You are incredible and definitely one of the best people I've ever met. I'm so unbelievably lucky that you want to be my friend, even if it did take us a little while. You are kind, brilliant, and funny, but most of all I love how much you care about people. I have enjoyed sharing our love of sports, HIMYM, GBBO, chemistry, games, and of course, PowerSox. I also love that we're both super competitive, (usually) in the best way. You have always been there for me no matter what, and sometimes I have needed your support more than I would like to admit. I am so grateful you put up with me even though I don't like IPAs. Getting to be your friend really is The Dream. You were the perfect maid of honor and I will apologize again here for making you give a speech in front of everyone. That said, it was phenomenal and I loved every second of it. Thank you for making life better. Thank you for being one of my best friends. Thank you, Katy.

With that, I have to thank my family. Thank you, Joanna, Mom, Donna, Mark, and Emmett for always being there for me. I apologize for not coming home more often. Thank you for visiting during the summer. It's been wonderful getting to show off Charlottesville to you all. I'm so lucky to have your love and support. Thank you, Coleman, for showing me that chemistry was an option, and thanks, Eddie, for always believing in me. Thank you, Grandma Alice, for your love and help. I also want to thank Grandma Shirley and Papa. I love and miss you dearly. I hope I make you proud. I love my family, and I am so grateful you all love the final person I am beyond excited to thank.

I never thought I would be so lucky as to meet and fall in love with someone as incredible as you, Ben Liebov. As hard as grad school has been at times, you have always made it easier. I love the story of how we met and every moment we've shared since. Thank you for being my best friend and, now, my husband. I can't wait to spend the rest of my life with you. Thank you for your letters and good morning emails. Thank you for all our walks to and from work, and then, for the phone calls as we walked together, but separately. Thank you for helping me sort of join the Harman lab. Thank you for bringing me into your amazing circle of friends. Thank you for all of our adventures, from our trips to Wegmans to our Australian honeymoon with some of said amazing friends. Thank you for being so patient and kind. Thank you for everything you do for others. Thank you for making me feel at home with your family, who are now my family too. Thank you to the Liebov & Kaufman families for making me feel like a member of the family from the very beginning. Thank you, Ben, for everything. You are the best part of my life, and I can’t wait to see what our future holds. Thank you and I love you.

DEDICATION

To loved ones who are greatly missed and live on in fond memories

Katherine McKeown

Leroy Pate

Shirley Schwartz

TABLE OF CONTENTS

LIST OF SCHEMES

CHAPTER 1

CHAPTER 2

CHAPTER 3

CHAPTER 4

CHAPTER 5

CHAPTER 6

LIST OF FIGURES

CHAPTER 1

CHAPTER 2

CHAPTER 3

CHAPTER 4

CHAPTER 5

CHAPTER 6

LIST OF TABLES

CHAPTER 5

CHAPTER 6

1 Introduction to Light Alkane Functionalization

1.1 Natural Gas Overview

Natural gas accounts for nearly a quarter of global energy production and consists primarily of the light alkane methane (70-90% by volume) with smaller amounts of ethane and propane.[1-3] As a result of the shale gas boom, the supply of natural gas has increased exponentially in recent years, making it a plentiful and valuable domestic resource.[4] However, there are significant limitations associated with natural gas extraction and utilization. While petroleum, which is a liquid at ambient conditions, can be transported to processing plants using existing infrastructure, it is much more challenging to efficiently and safely transport natural gas. As a result, significant sources of natural gas are left economically "stranded" often resulting in significant methane emissions or flaring to produce CO_2.[5]

These emissions are problematic because methane is a potent greenhouse gas with a global warming potential 35 times greater than that of carbon dioxide.[6] Furthermore, methane also reacts in the atmosphere to produce ozone.[6-7] When natural gas cannot be transported to a synthesis gas plant (see below), it is typically flared to generate the less harmful greenhouse gas CO_2 in order to minimize methane emissions at the wellhead.[8] This flaring is performed on a large scale at some sites and can be seen from NASA satellite images at night (Figure 1.1). Furthermore, methane emissions are not limited to the wellhead. Levels of emissions across the supply chain have recently been demonstrated to be > 60% higher than previous estimates by the Environmental Protection Agency, with emissions accounting for > 2% of the domestic gross natural gas production.[9] This unproductive use of natural gas adds 300 million tons of CO_2 into the atmosphere annually and has been estimated to represent the loss of approximately \$2 billion/year.[8-9] Therefore, there is significant motivation to develop economical and effective methods to convert methane to an easily transportable liquid at the wellhead (*e.g.*, gas-to-liquid or GTL technologies). Ideally, this liquid could be used as a fuel or as a precursor to high-value chemicals.

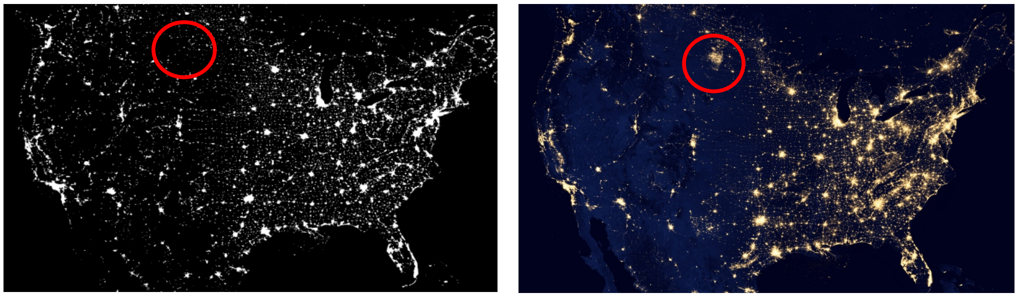

Figure 1.1. Satellite images of the United States taken at night in 2000 (left) before the shale gas boom and in 2012 after the boom (right) illustrate the scale of natural gas flaring. The Bakken oil fields of North Dakota are encircled in red.[10-11]

The current industrial route for methane functionalization involves steam reformation at ~900 °C to generate synthesis gas (syngas), a mixture of carbon monoxide and dihydrogen (Scheme 1.1).[12] Methanol is produced by reducing carbon monoxide with H_2 using Fischer-Tropsch chemistry with an iron catalyst and elevated reaction temperatures (260-450 °C) and pressures (~400 psi, Scheme 1.1).[13] Although effective, this process is energy-intensive and capital-intensive as syngas plant construction requires multi-billion dollar infrastructure investments and the syngas route to methanol produces large amounts of CO_2.[1] This investment cost effectively limits the implementation of this functionalization method as plants cannot be built in each isolated location natural gas is found. Thus, natural gas is often effectively "stranded" leading to the issues discussed previously.

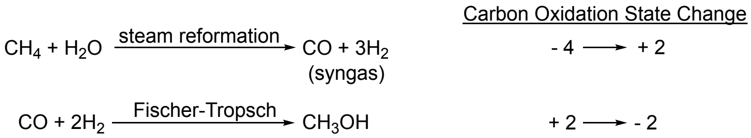

Scheme 1.1. Generation of methanol through the indirect syngas method.

The syngas method is inefficient as it oxidizes methane to carbon monoxide (-4 to +2 oxidation state change for carbon) and subsequently reduces carbon monoxide to methanol (+2 to -2 oxidation state change for carbon). It would be highly beneficial to forgo the over-oxidation and selectively partially oxidize methane to a useful liquid product (*e.g.*, methanol or a methanol equivalent) in a single step, particularly if the process could require minimal investment. For example, the direct conversion of methane to methanol (MTM), $CH_4 + \frac{1}{2}O_2 \rightarrow CH_3OH$ is a direct partial oxidation (-4 to -2 oxidation state change for carbon). The generation of liquid products would enable the facile transportation of functionalized natural gas without requiring the harsh storage conditions of liquefied natural gas. Methanol is a particularly useful product as it can be transported using existing infrastructure and used either as a fuel directly or as a precursor for a variety of higher-value commodity chemicals (Figure 1.2).[14] While global methanol demand already exceeds 80 million metric tons per year,[14] there is significant incentive for the development of a direct method for its production from methane. Such a process would enable more efficient use of natural gas and would reduce greenhouse gas emissions.

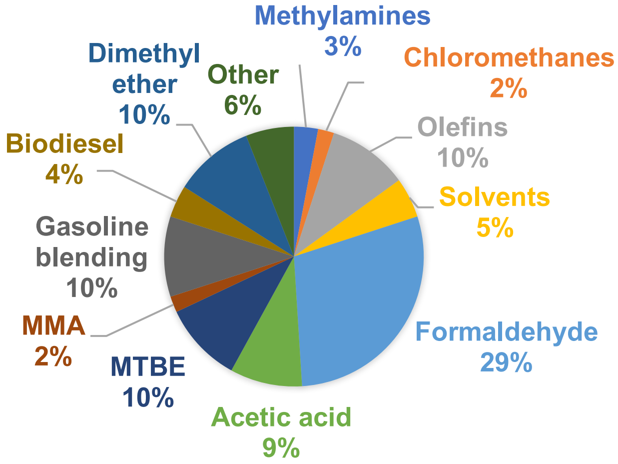

Figure 1.2. Relative demands for the various uses of methanol globally in 2015. Adapted from reference.[14] MTBE = methyl *tert*-butyl ether; MMA = methyl methacrylate.

In addition to current demand (Figure 1.2), less expensive and less energy-intense MTM could stimulate increased demand. For example, large scale conversion to dimethyl ether, a diesel fuel, could become a major fraction of automotive fuel in Europe.[15] Also, it is appreciated that at a particular methanol price, the conversion of methanol to ethylene and propylene becomes competitive with ethane and propane cracking. As methane is not currently converted to ethylene or propylene commercially, the development of a process that puts the price of methanol production below the tipping point could open an enormous new market (*i.e.*, the conversion of CH_4 to light olefins).

Methods for the selective partial oxidation of methane have been the subject of extensive study. Although the reaction of methane with ½ O_2 to yield methanol is exothermic and thermodynamically favorable, there are significant kinetic barriers for the reaction. Additionally, there is the added complication that the C–H bonds of functionalized products are weaker than those of the starting material (Scheme 1.2).[16] For example, the bond dissociation energy (BDE) for the C–H bonds of methane and methanol are 105 and 96 kcal/mol, respectively.[16] As the activation of weaker C–H bonds is generally favored for many C–H functionalization mechanisms, products like methanol are often more reactive than methane. The heightened reactivity of oxidized products often results in unselective functionalization, and over-oxidation is a chronic issue. Protection of these methyl products from over-oxidation is key to achieving the selective partial oxidation of methane as well as related light alkanes such as ethane and propane (*vide infra*).

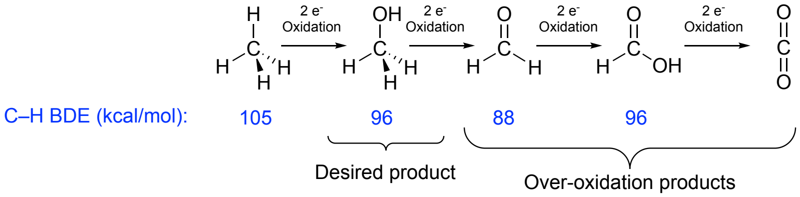

Scheme 1.2. C–H bond dissociation energies (BDEs) for methane and functionalized products.

1.2 C–H Bond Activation

The functionalization of light alkanes requires C–H bond activation, which has been reviewed extensively.[17-18] There are several traditional methods of non-radical transition metal-mediated C–H activation, including oxidative addition, electrophilic substitution, σ-bond metathesis and 1,2-C–H-addition across metal-heteroatom bonds (Scheme 1.3).[17] Oxidative addition involves the insertion of the metal center into the C–H bond to form a metal–hydride bond and a metal–hydrocarbyl bond and results in a formal two-electron oxidation of the metal center. Electrophilic substitution involves the activation of the alkane and loss of a proton (Scheme 1.3). σ-Bond metathesis is advantageous in cases where the metal center cannot be oxidized (*e.g.*, with d^0 complexes) as there is no formal change in the oxidation state of the metal. The four-membered transition state results in the formation of a metal–hydrocarbyl species and HY. The 1,2-C–H addition across metal-heteroatom bonds is similar to σ-bond metathesis as it typically does not involve oxidation of the metal center. However, in the case of 1,2-C–H addition, the metal typically has an imido, aryloxo or amino ligand. Each of these has a lone pair of electrons on the heteroatom, thus it has a four-membered six-electron transition state, whereas σ-bond metathesis has a four-membered four-electron transition state.[17] There are also metal-mediated C–H activation pathways involving homolytic bond cleavage, including metalloradical reactions and ligand-based H-atom abstractions.

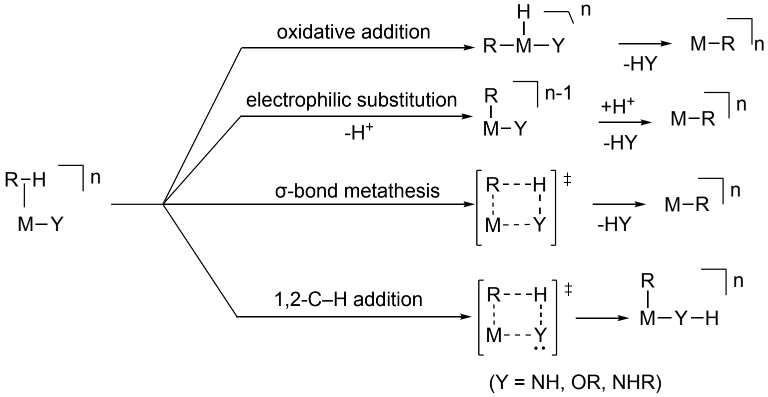

Scheme 1.3. Pathways for C–H activation from a metal-alkane coordination complex. Adapted from reference.[17]

C–H bonds can also be activated via additional radical-based reaction pathways which do not require interaction with a metal center (*e.g.*, hydrogen atom abstraction). These reactions result in homolytic C–H bond cleavage and the formation of an alkyl radical. Thus, hydrogen-atom abstraction involves a high-energy radical species capable of generating alkyl radicals from inert alkanes through the removal of an H-atom. Halogen radicals, produced in the presence of light or through the addition of an initiator, are effective agents for H-atom abstraction (Scheme 1.4). Although the overall reaction for free radical halogenation indicates that the mono-functionalized product is generated with an equivalent of HX (Scheme 1.4), this is not representative of the overall product distribution. As the cleavage of C–H bonds by free radical means typically occurs as a function of the C–H bond strength, weaker bonds are more easily broken.[19] Therefore, mono-halogenated alkyl products which have weaker C–H bonds than the starting alkane will undergo over-oxidation at higher conversions to generate undesired poly-halogenated alkanes.[20-21]

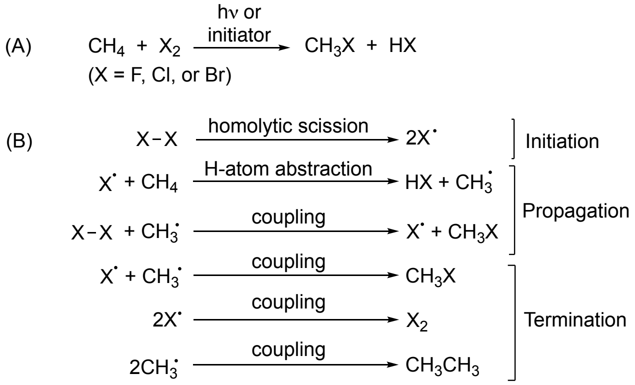

Scheme 1.4. (A) Overall reaction for the halogenation of methane and (B) steps for free radical-based functionalization.

1.3 Light Alkane Functionalization using Electrophilic Catalysts

1.3.1 Introduction

Although there is precedent regarding high-temperature methane conversion with metal oxides (> 500 °C), selectivity for mono-functionalized products is typically low at high conversions under such conditions (*vide infra*).[22-23] Using modeling to compare rates of over-oxidation relative to mono-functionalization with various radical species, it has been proposed that the best yield for selective mono-functionalization under high-temperature conditions is ~5%.[22] This value is in agreement with experimental data.[23] Thus, there is significant motivation to pursue lower-temperature functionalization methods.

There have been significant efforts to incorporate the above C–H bond activation pathways into catalytic processes for the selective partial oxidation of light alkanes under mild reaction conditions (≤ 250 °C).[24] This chemistry is challenging as methane is inert, nonpolar, and weakly basic (pKa = 50 in DMSO) with strong C–H bonds (BDE = 105 kcal/mol).[25] After years of research, low-temperature light alkane functionalization using electrophilic catalysts emerged as a promising strategy.

1.3.2 Metal-Based Electrophilic Processes

The activation of C–H bonds by electrophilic metals has been studied thoroughly. Shilov laid the groundwork for this chemistry with Pt(II) complexes that convert methane to methanol in aqueous solvent (Scheme 1.5).[26-30] However, although the process demonstrated the capability of electrophilic metals to partially oxidize methane, the process was limited by the uneconomical use of a stoichiometric amount of Pt(IV) as the oxidant (Scheme 1.6).

$$CH_4 + Pt^{IV}Cl_6^{2-} + H_2O \xrightarrow[120\ °C]{\text{cat. } PtCl_4^{2-}} MeOH + PtCl_4^{2-} + 2HCl$$

Scheme 1.5. Shilov system for partial methane functionalization.[31]

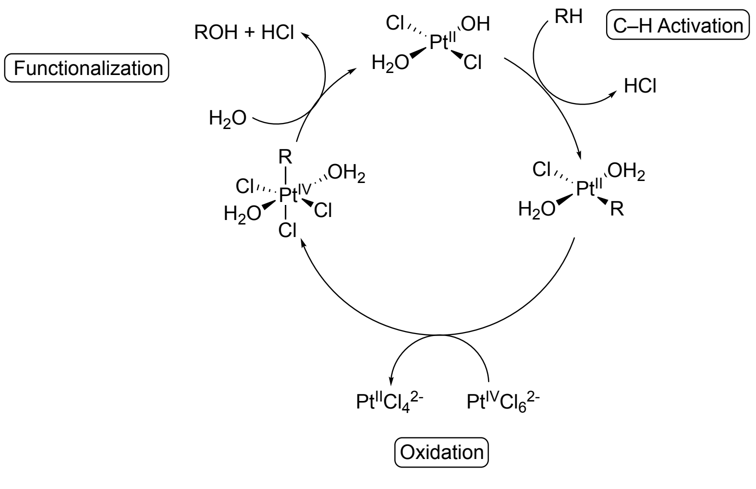

Scheme 1.6. Proposed mechanism for methane functionalization by the Shilov Pt(II) system.[18, 31]

In an attempt to extend Shilov's findings to more commercially viable catalytic processes, Periana and coworkers developed a series of electrophilic catalysts based on a variety of metals including Hg, Pd, Au and Pt.[32-37] Of these, the Pt(II) catalyst (bpym)PtCl$_2$ (bpym = 2,2'-bipyrimidinyl) (Scheme 1.7), sometimes called the Catalytica system, remains one of the most efficient processes for the direct partial oxidation of methane to methyl bisulfate (a methanol derivative) at low temperatures (100-220 °C).[37] One-pass yields of > 70% were obtained with > 90% selectivity for methyl bisulfate with product concentrations of up to ~1 M. Conversion to inactive Pt(IV) was prevented through a type of "self-repair," which helped to improve the catalyst's longevity.[38] The significant advancement of the Catalytica system is its use of fuming sulfuric acid (oleum) as the solvent, air-regenerable oxidant, and as the source of the protecting group for the product.[39]

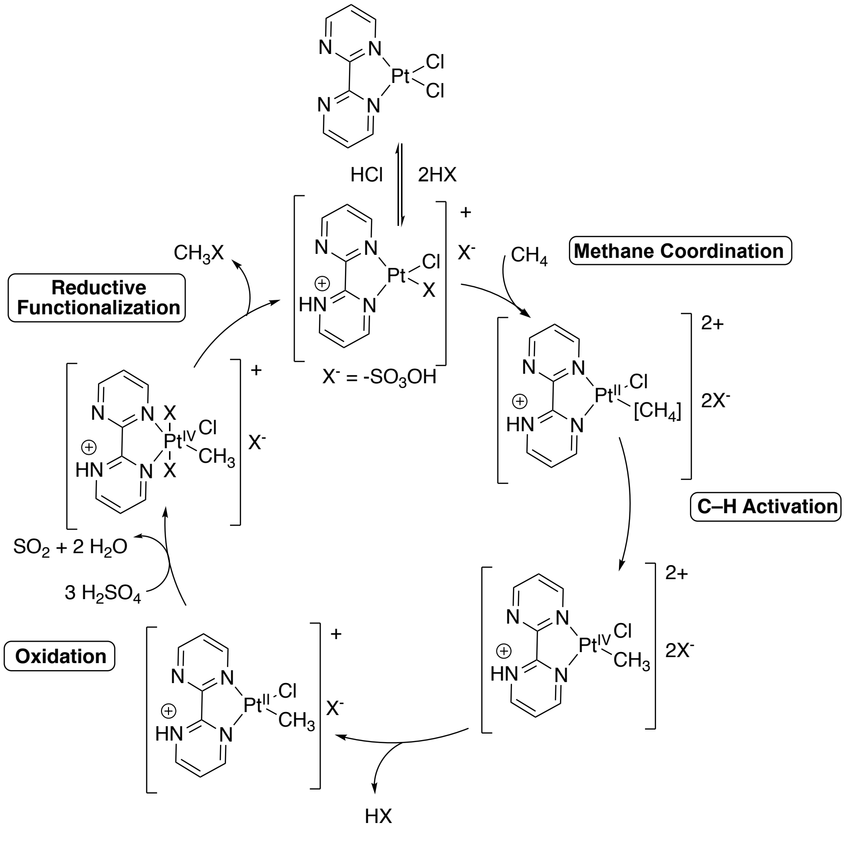

Scheme 1.7. Proposed mechanism for the Catalytica system.[24, 37] Adapted from reference.[24]

Since over-oxidation is one of the greatest challenges in the field, product protection strategies are crucial. The Periana group's use of the bisulfate moiety was inspired by the partial oxidation reports from Sen and Moiseev which used the electron-withdrawing trifluoroacetate (TFA) group to protect the methanol derivative methyl trifluoroacetate (MeTFA) formed in their studies with Pd(II) and Co(III) salts in trifluoroacetic acid.[40-41] The electron-poor C–H bonds of MeTFA or $MeOSO_3H$ are proposed to be deactivated toward further, undesired oxidation by the electrophilic metal catalysts. In the Catalytica system, the bisulfate group proved to be a particularly capable protecting group, making the product ~100 times less reactive than methane under the highly oxidizing conditions.[25] As a result, high yields of mono-functionalized product were observed with minimal over-oxidation.

Although the Catalytica system demonstrated high methane conversion with minimal over-oxidation, several limitations prevented its continued development. Primary complications included the difficulties related to reaction rates, product separation and water intolerance.[42] The rate of the reaction is significantly lower than similar industrial processes ($\sim 2.8\times10^{-3}$ s^{-1} versus $> 2.8\times10^{-1}$ s^{-1}).[43] The hydrolysis of methyl bisulfate to produce methanol and sulfuric acid is unfavorable and requires dilution of the reaction mixture by ~50%.[44] As the Catalytica system is significantly inhibited by water, sulfuric acid must be recycled and concentrated at a great energetic expense.

Several strategies have been pursued to address these challenges. Contrary to claims in the initial report,[37] the Schüth group has demonstrated that simple platinum salts (*e.g.*, K_2PtCl_4) act as efficient catalysts for methane functionalization in oleum with a maximum turnover frequency (TOF) ~20 times higher than with the original (bpym)$PtCl_2$ catalyst (Scheme 1.8).[43] The TOF with platinum salts is on par with other industrial processes, and the process operates with 99% selectivity for methyl bisulfate.

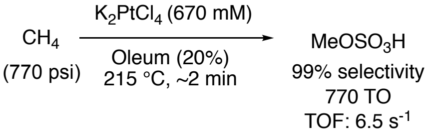

Scheme 1.8. Methane functionalization with K_2PtCl_4 in oleum to produce methyl bisulfate with high TOF and selectivity.[43]

Two major approaches have been taken to avoid the problematic dilution of the reaction mixture to obtain methanol. First, it has been demonstrated that the addition of an organic solvent enables more facile separation of methyl bisulfate from aqueous sulfuric aicd.[45] Another notable method to enable more effective separation involves the use of low pressure membrane distillation (LPMD).[44] With LPMD, a recyclable membrane separates methyl bisulfate and SO_3 from sulfuric acid. SO_3 can then added back to the concentrated sulfuric acid and used again. Methyl bisulfate can be hydrolyzed to give methanol without diluting the reaction media.

Efforts to address the intolerance of the Pt(II) catalysts to water have involved the use of ionic liquids (ILs) as co-solvents due to their thermal stability and low volatility.[46-48] ILs have been demonstrated to solubilize a variety of platinum salts, and thus could be combined with the progress made by the Schüth group in efforts to improve reaction rates.[46, 48] Imidazolium and pyrazolium-based IL-sulfuric acid mixtures were shown to be effective for methane functionalization with a variety of platinum catalysts including (bpym)$PtCl_2$.[46] The water tolerance exhibited by the IL mixture enabled higher yields of methyl bisulfate at lower concentrations of sulfuric acid.

1.3.3 Main Group-Based Electrophilic Processes

Given the success of the metal-based electrophilic processes, the Periana group extended the motif of electrophilic functionalization to include main group-based compounds such as $Tl(TFA)_3$ and $Pb(TFA)_4$.[33] These compounds are efficient for the stoichiometric functionalization of methane, ethane and propane in non-superacidic solvents {*e.g.*, trifluoroacetic acid (HTFA) and HOAc} to generate the corresponding methyl esters. The authors reported that MeTFA was stable to over-oxidation, as $^{13}CO_2$ was not detected as a product of the $^{13}CH_4$ functionalization. Control reactions studied the stability of the ester products under reaction conditions with $Tl(TFA)_3$ and found them to be unreactive. These findings were in agreement with calculations that predicted the ΔG for C–H activation of MeTFA would be ~9 kcal/mol higher than that of methane. Experimental and computational studies indicated that a non-radical-based C–H activation mechanism is most likely operative.

Iodine has also been studied as an electrophile for light alkane functionalization. Periana and co-workers used molecular iodine as a catalyst for methane functionalization in oleum (Scheme 1.9).[36] Yields of methyl bisulfate of 45% with respect to methane were obtained with > 90% selectivity for methyl bisulfate. Methane functionalization is not observed in reaction media less acidic than 98% H_2SO_4 or in the absence of SO_3. Periana and coworkers proposed $I_2^+HS_2O_7^-$ as a potential active catalyst under the reaction conditions. The addition of O_2 or $K_2S_2O_8$ did not result in changes to the rate or selectivity of the reaction, providing evidence against a radical-based C–H activation mechanism. A blue species forms on the addition of iodine to oleum, characteristic of a I_2^+ species. However, Davico found experimentally and computationally that I^+ is more likely to be the active intermediate in this electrophilic C–H activation process.[49] Gang and coworkers found that using a variety of other iodine-containing species including KI, NaI, I_2O_5, KIO_3 and KIO_4 in oleum gave similar results, indicating that all might funnel to the same active intermediate as in the earlier report.[50]

$$CH_4 + 2SO_3 \xrightarrow[\text{Oleum}]{\text{cat. } I_2} CH_3OSO_3H + SO_2$$

Scheme 1.9. Iodine mediated methane functionalization in oleum. Adapted from reference.[25]

Recent efforts have been used to demonstrate that hypervalent iodine oxidants are capable of light alkane functionalization in non-superacidic media. Periana, Ess, Gunnoe, Groves and coworkers demonstrated the efficacy of the perfluoroarene iodine(III) complex $(C_6F_5)I^{III}(TFA)_2$ for methane, ethane and propane functionalization in HTFA (Scheme 1.10).[51] MeTFA is selectively produced from methane, but the MeTFA yield is limited to ~5% relative to $(C_6F_5)I^{III}(TFA)_2$. Ethane and propane were converted in higher yields to the corresponding mono-functionalized and 1,2-di-functionalized products (Scheme 1.10). Computational studies supported the electrophilic C–H activation mechanism proposed by the authors, similar to that of the Tl- and Pb-based processes. A primary limitation of the process is the inability to readily regenerate $(C_6F_5)I^{III}(TFA)_2$ from $(C_6F_5)I^{I}$ with O_2.[25]

$$C_6F_5I^{III}(TFA)_2 + RH \xrightarrow[150\ ^\circ C,\ 3\ h]{HTFA/TFAA} C_6F_5I^{I} + RTFA + 1,2\text{-}Y(TFA)_2$$

$Y = CH_2CH_2$ (with EtH)
CH_2CHCH_3 (with PrH)

Alkane	**Product (Yield relative to $C_6F_5I(TFA)_2$)**
MeH	MeTFA (5%)
EtH	EtTFA (73%); 1,2-Y$(TFA)_2$ (3%)
PrH	PrTFA (30%); 1,2-Y$(TFA)_2$ (27%)

Scheme 1.10. Alkane functionalization by $(C_6F_5)I^{III}(TFA)_2$. Yields are reported relative to $(C_6F_5)I^{III}(TFA)_2$. Di-functionalized product yields are calculated assuming that 2 equivalents of $(C_6F_5)I^{III}(TFA)_2$ are consumed per 1 eq. of product. Adapted from reference.[51]

1.4 Radical-Based Processes

1.4.1 Introduction

The development of effective electrophilic catalysts for methane functionalization is challenging and requires specific modulation of the electrophilicity of the metal center.

Depending on the rate-limiting step of the process, increasing the electrophilicity of the metal center increases the barrier of the methane coordination step, hindering functionalization, or reduces the barrier for C–H activation, aiding functionalization.[33] Radical-based C–H activation (*e.g.*, H-atom abstraction) offers an alternative and there has been extensive study of such systems for light alkane functionalization.

1.4.2 Biological and Biomimetic Approaches

In nature, bacteria known as methanotrophs exist in harsh methane-rich environments have developed metalloenzymes to convert methane to methanol.[52] There are two primary methane monooxygenase enzymes, soluble methane monooxygenase (sMMO) and membrane-bound particulate methane monooxygenase (pMMO). sMMO, which has a diiron(IV) center, has been studied thoroughly.[53] sMMO functionalizes methane by H-atom abstraction by a high-valent bis-μ-oxo-diiron species (compound Q) and subsequent radical rebound to form methanol (Scheme 1.11).[52, 54] Studies of pMMO have been limited by the instability of the enzyme outside of its native environment, but its active site likely contains a di- or tri-copper cluster.[55-56] As a function of their evolution, these enzymes operate under specific environmental conditions and cannot be readily adapted for use in industrial processes as they often require cofactors and are not sufficiently stable to solvents, elevated temperatures or high-pressure conditions.[57]

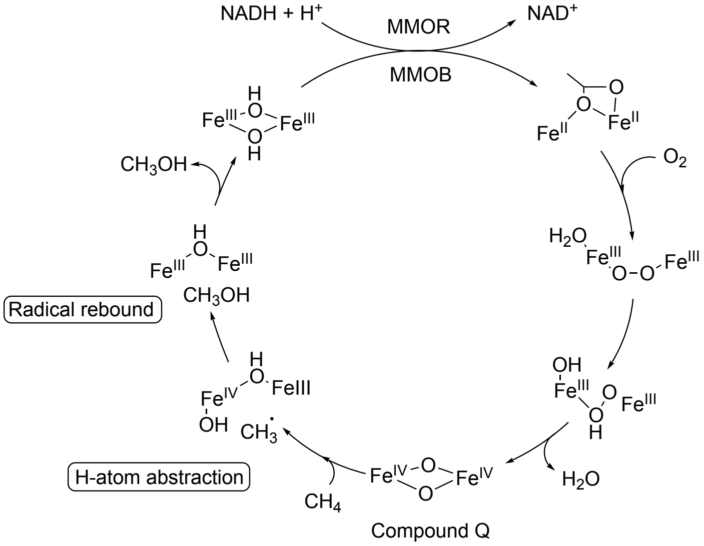

Scheme 1.11. C–H functionalization by H-atom abstraction and radical rebound to generate MeOH from methane. MMOR = reductase protein component; MMOB = effector protein component. Adapted from references.[53-54]

Biomimetic approaches, those using insight from biological systems, to develop related catalysts for partial methane oxidation have focused on the development of synthetic enzymes and zeolite systems.[57] There have been extensive efforts to generate model systems for sMMO based on porphyrinoid complexes which seek to apply the selective radical-based functionalization observed with sMMO.[54] Often, these porphyrinoid systems have diiron-based active sites. A diiron phthaocyanine complex was reported to oxidize methane to formic acid and formaldehyde with 437 TON using H_2O_2 as the oxidant (Scheme 1.12).[58] As H_2O_2 cannot be recycled easily using O_2,[59] the industrially desired terminal oxidant, the scale-up of processes utilizing H_2O_2 as the oxidant is not economically viable. A similar system utilizing mCPBA as the oxidant has also been reported.[60] These processes are proposed to operate by an H-atom abstraction pathway, similar to the enzymes themselves. Synthetic models of pMMO include a tri-nuclear copper complex which can yield ~6 TO of methanol using H_2O_2 as the oxidant.[61] DFT studies found that in the presence of O_2 the complex forms a reactive μ-O intermediate capable of oxene transfer to methane and net oxygen insertion into a C–H bond of methane (Scheme 1.13).[61]

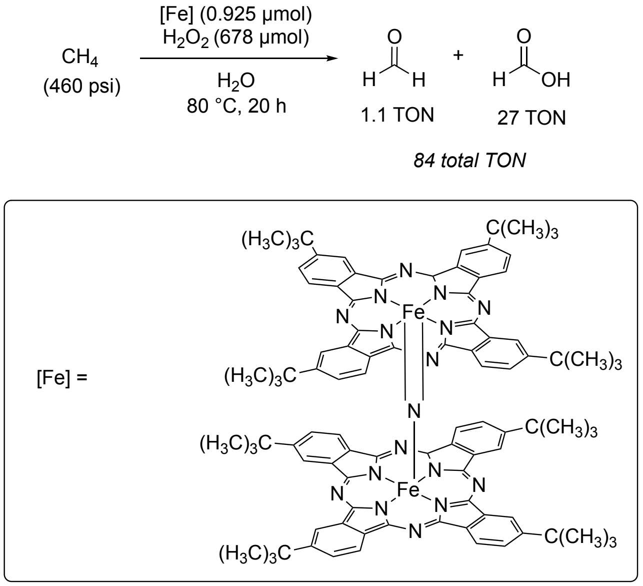

Scheme 1.12. Diiron phthalocyanine complex for partial methane oxidation in water.[58] Methanol was not observed. Total TON was calculated as (3 × formic acid/catalyst) + (2 × formaldehyde/catalyst) to account for over-oxidation.

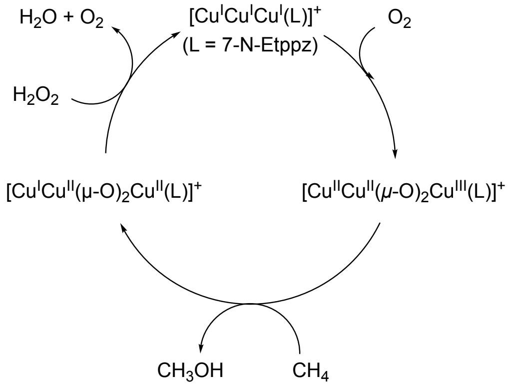

Scheme 1.13. Proposed mechanism for partial methane oxidation by $Cu^{I}Cu^{I}Cu^{I}$(7-N-Etppz)$^{+}$ (7-N-Etppz = 3,3’-(1,4-diazepane-1,4-diyl)bis[1-(4-ethylpiperazine-1-yl)propan-2-ol]).[61]

Zeolites, microporous (alumino)silicates, offer the high level of stability necessary for industrial applications and have defined transition-metal based active sites capable of cycling through a range of oxidation states.[57] Iron-containing zeolites such as Fe-ZSM-5 (parent ZSM-5 shown in Figure 1.3) have been demonstrated to convert methane to methanol at room temperature using N_2O as the oxidant.[62] The reaction was found to operate by H-atom abstraction from methane by a reactive surface oxygen species to generate hydroxy and methoxy species which react to form methanol. However, the use of oxygen as the oxidant with Fe-ZSM-5 required higher reaction temperatures (> 350 °C).[63] Another iron-containing zeolite iron sodalite converted methane to methanol with 70% selectivity at ~6% conversion at > 400 °C.[64] In general, although selectivity for methanol can approach 90% with a mixed iron-copper zeolite, conversion is typically limited to < 10%, and is < 1% under conditions where high selectivity for methanol is observed.[65]

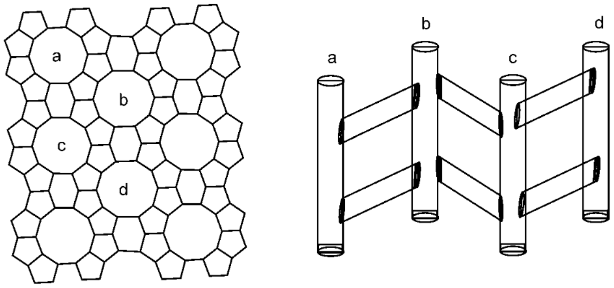

Figure 1.3. Structure of the zeolite ZSM-5 with two orientations (A) and (B) to show the pore channels (a-d). Vertices represent Si atoms. O atoms omitted for clarity. Copyright 2009 John Wiley and Sons. Used with permission from Macquarrie, D. J. Industrial Friedel-Crafts Chemistry. In *Catalytic Asymmetric Friedel-Crafts Alkylations*; Bandini, M.; Umani-Ronchi, A., Eds.; Wiley-VCH: Weinheim, 2009, 271-278.

A variety of copper-containing zeolites have also been examined for the partial oxidation of methane. While often capable of operating with high selectivities for methanol (> 98%),[66] their active sites remain the subject of controversy similar to that of pMMO.[57] Researchers indicate that either mono-, di- or tri-copper clusters are responsible for methane functionalization.[57] The copper-based zeolite systems have several drawbacks. First, early reactions required high temperatures for oxygen activation and a separate extraction in order to isolate the product as methanol did not desorb under reaction conditions.[57] This extraction with water was problematic as it resulted in the deactivation of copper sites. This was addressed through the use of a water, oxygen and methane gas mixture, enabling methanol selectivity of 70% using Cu-ZSM-5 with temperatures ~200 °C.[57] However, the amount of methane conversion could not be quantified under these conditions, limiting conclusions about selectivity at high conversion.[57] While these zeolites are able to functionalize methane, additional optimization is required to obtain a catalyst which can operate with high selectivity at high conversion.

1.4.3 Halogenation and Oxyhalogenation

Light alkane chlorination is well-established and follows the radical-based mechanism outlined previously (see Scheme 1.4). Gas-phase alkane chlorination was first reported in 1840 using chlorine and marsh gas, of which methane is a major component.[67] Carbon tetrachloride was produced in the initial report, but in a study from 1858, methyl chloride, which can by hydrolyzed to give methanol, was isolated.[68] The Hoechst process to produce chloromethanes was commercialized in 1923 in which recycled MeCl and unreacted methane are used to generate higher chloromethanes (Scheme 1.14).[68] However as the reactions are unselective for the mono-functionalized product and 50% of the chlorine was converted reduced to HCl, which was not marketable at the time,[69] alternatives routes for methane functionalization were desired.

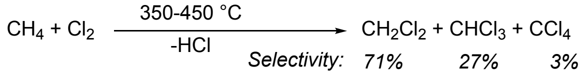

$$CH_4 + Cl_2 \xrightarrow[\text{-HCl}]{\text{350-450 °C}} \underset{71\%}{CH_2Cl_2} + \underset{27\%}{CHCl_3} + \underset{3\%}{CCl_4} \quad \textit{Selectivity}$$

Scheme 1.14. Hoechst process for the formation of chloromethanes.[68]

The use of fluorine, iodine and bromine for light alkane halogenation has also been studied. Methane fluorination is highly exothermic and can be explosive.[70] Methane iodination is endothermic and thermodynamically unfavorable, and the generation of MeI requires temperatures > 600 °C.[70] Bromination, however is a more promising method of methane functionalization.[2] As the H–Br bond is ~15 kcal/mol weaker than that of H–Cl,[2] there is a higher barrier to over-oxidation with bromination than chlorination. Thus, methane bromination operates with higher selectivity for the lower bromomethanes MeBr and CH_2Br_2. Simulations indicate that selectivity for dibromomethane can approach 90% at high conversion (~80%).[70] The selectivity for the mono-functionalized product MeBr can be significantly improved through the addition of a small amount of iodine (Scheme 1.15).[71] Iodine is proposed to enable reproportionation between CH_4 and CH_2Br_2.[71] Significant progress has been made, but as chlorine is more widely available and less expensive than bromine, the development of selective chlorine-based processes remains highly desirable.

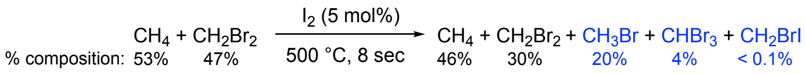

Scheme 1.15. Effect of added iodine of the product distribution of methane bromination.[71] The I_2 mol% is given relative to CH_2Br_2.

Oxyhalogenation chemistry, which typically involves the use heterogeneous catalysts such as copper or iron halides, HX (X = Cl, Br) and O_2 for alkane functionalization, avoids a key drawback of the halogenation systems as halogens can be used with high atom economy (Scheme 1.16).[2] However, the introduction of oxygen often results in significant over-oxidation to higher halomethanes.[2] Thus, in addition to being stable toward harsh reaction conditions (*e.g.*, corrosive gases and elevated temperatures), catalysts must be designed to minimize over-oxidation.[2]

Halogenation

$$CH_4 + X_2 \longrightarrow HX + CH_3X$$

Oxyhalogenation

$$CH_4 + HX + 1/2O_2 \xrightarrow{cat.} CH_3X + H_2O$$

Scheme 1.16. Overview of methane halogenation and oxyhalogenation.[2] Over-oxidation to higher halomethanes is omitted for clarity. X = Cl, Br.

Initially, catalysts found to be successful for ethylene oxychlorination were examined for light alkane oxychlorination. These were typically silica- or alumina-supported copper chloride-based catalysts.[2] Although these were able to achieve 60-85% selectivity for MeCl at 18-43% conversion of methane, selectivity and conversion are inversely related, where the highest selectivity for MeCl (85%) is obtained at the lowest methane conversion (18%).[72] The high temperatures (> 400 °C) required for methane oxychlorination result in damage to the catalyst and over-oxidation of the halomethane products.[2] Promoters (*e.g.*, $LaCl_3$ and KCl) have been found to minimize catalyst decomposition but their use does not result in more selective formation of MeCl. The mechanism of copper chloride-based systems for oxychlorination, though generally accepted to be radical-based, is not fully understood. Oxychlorination has been proposed to operate via liberation of molecular chlorine from the heterogeneous catalyst.[2]

Due to the shortcomings of these copper chloride-based materials, other catalysts based on La, Ru and Ce oxides have been developed for methane oxychlorination at elevated temperatures (> 400 °C).[2] These typically exhibit greater thermal stability than the copper chloride catalysts, but the selectivity for MeCl remains low at reasonable methane conversions. An iron-doped ceria catalyst was able to achieve 74% selectivity for MeCl with 23% conversion.[73] Further, mechanistic studies indicate that methane activation by these catalysts likely occurs by non-radical pathways.[2] With LaOCl and $LaCl_3$, surface

OCl^- is proposed to react with methane.[74] $K_4Ru_2OCl_{10}/TiO_2$ has been proposed to activate methane via O-atom insertion into the C–H bond with simultaneous removal of a proton by a basic site on the catalyst to produce a methoxy species which reacts with HCl to give MeCl.[75] The mechanism of methane activation has not been elucidated for the cerium-based catalysts as a greater understanding of the surface chemistry is required.[2]

Oxybromination offers potential advantages relative to oxychlorination, similar to those demonstrated for bromination versus chlorination (*i.e.*, higher selectivity for MeBr than MeCl).[2, 76] However, HBr is significantly more expensive than HCl and is more corrosive in the presence of water, which is produced and aids in the removal of heat that is released during the reaction.[2] Catalysts for oxybromination include those based on noble metals (*e.g.*, Rh and Ru), non-noble metal oxides based on V, Ce, Mo, Ba and W, and Fe- and V-based phosphates.[77] With Rh- and Ru-based catalysts on inert supports (*e.g.*, SiO_2), selectivities for MeBr of > 90% at conversions ~20-40% were observed.[78-79] These processes were proposed to operate by a radical chain mechanism similar to that of traditional bromination chemistry.[77] The non-noble metal oxides were less selective for MeBr (*i.e.*, 50% selective at ~40% conversion) and resulted in significant CO production.[80] A variety of iron phosphates are stable under the reaction conditions and are capable of methane oxybromination, however at useful methane conversions the selectivity for MeBr is similar to that of the non-noble metal oxide catalysts.[81] In contrast, vanadium phosphates such as $(VO)_2P_2O_7$ are efficient catalysts for the selective formation of MeBr via methane oxybromination, operating with > 92% selectivity, albeit at low conversions (< 7%).[82] Although oxybromination offers a selectivity advantage over oxychlorination, these high selectivities are generally limited to < 10% methane conversion.

Bromine-mediated methane functionalization in zone reactors developed by Stucky and McFarland has similarities to oxybromination and bromination (Scheme 1.17).[83-86] The alkane is first brominated to give alkyl bromides and HBr. On reaction with a metal oxide (*e.g.*, 50/50 CuO/ZrO_2, 47/3/50 $Co_3O_4/Sm_2O_3/ZrO_2$),[85] HBr is neutralized and the alkyl bromides are oxygenated to produce the corresponding alcohol (or dialkyl ether or alkene) and metal bromide. Both reactors operate at moderate temperatures (200-350 °C) which are lower than those typically used for oxyhalogenation. Oxygen is then used to oxidize the metal bromide to regenerate the metal oxide catalyst and bromine. The metal oxide can be recycled > 50 times without a loss in activity and the process is not inhibited by common impurities in natural gas (*e.g.*, sulfur).[85-86] Higher alkane and alkene products were observed as a result of MeBr coupling under these conditions.[85, 87]

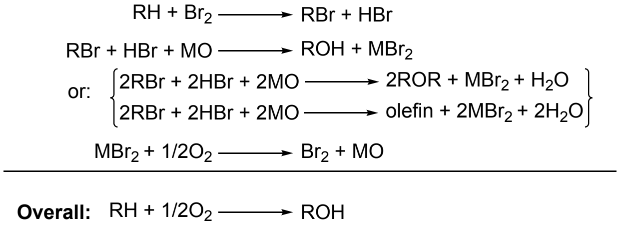

Scheme 1.17. Overall scheme for bromine-mediated alkane functionalization. Potential side pathways also shown. MO = metal oxide. Adapted from reference.[85]

1.4.4 Radical Functionalization in Acidic Media

Light alkane functionalization can also occur by radical pathways in acidic media. The Sen group demonstrated the use of $HgSO_4$, $Ce(SO_4)_2$ and $K_2S_2O_8$ as radical initiators for methane and ethane functionalization in oleum to produce the corresponding alkanesulfonic acid or alkyl bisulfate (Scheme 1.18).[88] Although the process operated similarly to the Catalytica system by using oleum as the solvent and SO_3 as the oxidant, the authors proposed that the oxidation with $HgSO_4$ occurred by a radical pathway rather than the electrophilic pathway proposed for Periana's Pt(II) and Hg(II) systems.[32, 37] The reactions with radical initiators operated from 90-160 °C, but yields relative to methane and overall methane conversion were not disclosed.

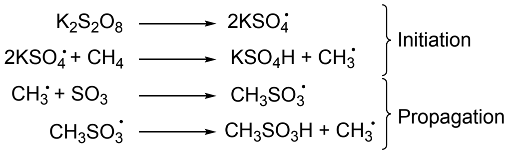

Scheme 1.18. Proposed mechanism for formation of methanesulfonic acid from methane with $K_2S_2O_8$. Adapted from reference.[88]

The use of $K_2S_2O_8$ as an oxidant is impractical as it cannot be easily recycled with oxygen. Thus, there is motivation to develop radical-based processes for light alkane functionalization using air or oxygen as the terminal oxidant. Cobalt- and manganese-based catalysts have been reported to oxidize methane in HTFA by radical mechanisms and can be recycled with oxygen.[41, 89-90] A process using Mn_2O_3 in the presence of air achieved 36% yield of MeTFA relative to methane with >95% selectivity for MeTFA (Scheme 1.19).[89] Cobalt(III) trifluoroacetate has been demonstrated to oxidize alkanes in HTFA stoichiometrically in the absence of oxygen[90] and catalytically in the presence of oxygen.[41] Vargaftik and coworkers demonstrated ~400% yield of MeTFA relative to $Co(TFA)_3$ in the presence of O_2 (Scheme 1.20).[41] Strassner and coworkers expanded this study to include a variety of Co(III) and Mn(III) sources, obtaining 50% yield based on methane under optimized conditions with $Co(OAc)_2{\cdot}4H_2O$ and O_2 (Scheme 1.21).[91]

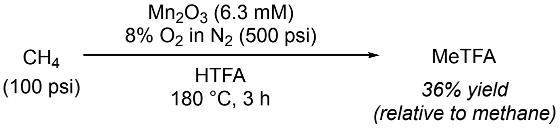

Scheme 1.19. Mn_2O_3-catalyzed methane oxidation to MeTFA in HTFA.[89]

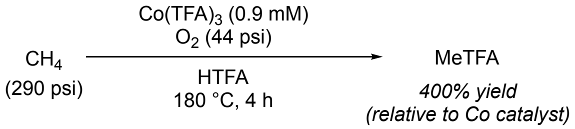

Scheme 1.20. Co(TFA)$_3$-catalyzed methane oxidation to MeTFA in HTFA.[41]

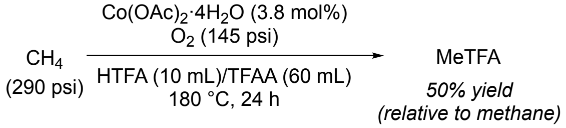

Scheme 1.21. Co(OAc)$_2$·4H$_2$O-catalyzed methane oxidation to MeTFA in HTFA.[91] The mol% of Co(OAc)$_2$·4H$_2$O is reported relative to methane.

Other radical-based processes utilize peroxides,[45, 92-95] which can be regenerated using dioxygen,[25] as initiators. Though less convenient than using O$_2$ directly, these methods offer potential advantages as O$_2$ can serve as a radical trap and in turn inhibit functionalization.[25] These peroxide-based systems functionalize methane by H-atom abstraction. The generated methyl radicals are then trapped, typically as methanesulfonic acid.[25] Calcium and barium peroxides were the most efficient of those studied, with 91% conversion of SO$_3$ to methanesulfonic acid under optimized conditions (Scheme 1.22).[94] The effect of additives was also examined. RhCl$_3$ was found to be the most efficient of those tested.[95] The authors proposed that RhCl$_3$ converted to a hydroperoxo or rhodium-peroxo species *in situ* which acted as an initiator.[95]

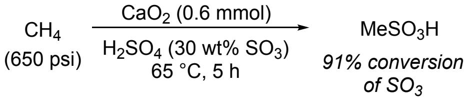

Scheme 1.22. Calcium peroxide in H$_2$SO$_4$ for the conversion of methane to methanesulfonic acid.[94]

1.5 Thesis Aims

This Dissertation is primarily focused on the mechanistic elucidation of the previously published studies by our group that illustrated the efficacy of simple chloride and iodate or periodate salts for light alkane functionalization[96-97] and on efforts to apply the principles of those original processes to other oxidant systems. Chapter 2 details the mechanistic studies of the oxyesterification (OxE) process, a collaborative effort with the Goddard (Caltech) and Groves (Princeton) groups. From these studies, it could be concluded that the functionalization of light alkanes occurs by a radical-based mechanism, and operates with high selectivity. The protection of the RTFA (R = Me, Et, Pr; TFA = trifluoroacetate) product against over-oxidation enables high yields and selectivity for the mono-functionalization process. In an effort to improve the efficiency of the OxE process for olefin functionalization, Chapter 3 discusses the optimization of ethylene functionalization using iodate and periodate oxidants. Using the mechanistic insight discussed in Chapter 2, Chapter 4 demonstrates the extension of the OxE process to other oxidants, namely bismuth-, manganese-, and iron-based oxidants. As the OxE process with iodate/chloride was demonstrated to occur by a radical-based pathway, the generation of active species under photochemical conditions was probed in Chapter 5. Given the success of the OxE process under these mild photochemical conditions, the photochemical OxE process was extended to other oxidants as well as the photocatalyst tetrabutylammonium decatungstate. Chapter 6 details results related to another project in the Gunnoe group, oxidative olefin hydroarylation. Specifically, the use of toluene for the oxidative hydroarylation of 1-pentene was studied due to the relevance of generated pentenyltoluenes as precursors for the improved plastic polyethylene naphthalate. Catalysis was examined as a function of pentene concentration, copper oxidant and reaction temperature, among other conditions.

1.6 References

1. Kinday, A. J.; Parrish, W. R., *Fundamentals of Natural Gas Processing*. CRC Press: Boca Raton, 2006.

2. Lin, R.; Amrute, A. P.; Pérez-Ramírez, J. *Chem. Rev.* **2017**, *117*, 4182-4247.

3. Horn, R.; Schlögl, R. *Catal. Lett.* **2015**, *145*, 23-39.

4. Wang, Q.; Chen, X.; Jha, A. N.; Rogers, H. *Renewable Sustainable Energy Rev.* **2014**, *30*, 1-28.

5. Golombok, M.; Teunissen, W. *Ind. Eng. Chem. Res.* **2003**, *42*, 5003-5006.

6. *Fourth National Climate Assessment*; United States Global Change Research Program: 2018.

7. Sarofim, M. C.; Waldhoff, S. T.; Anenberg, S. C. *Environ. Resource Econ.* **2017**, *66*, 45-63.

8. Zero Routing Flaring by 2030. http://www.worldbank.org/en/programs/zero-routine-flaring-by-2030.

9. Alvarez, R. A.; Zavala-Araiza, D.; Lyon, D. R.; Allen, D. T.; Barkley, Z. R.; Brandt, A. R.; Davis, K. E.; Herndon, S. C.; Jacob, D. J.; Karion, A.; Kort, E. A.; Lamb, B. K.; Lauvaux, T.; Maasakkers, J. D.; Marchese, A. J.; Omara, M.; Pacala, S. W.; Townsend-Small, A.; Wofsy, S. C.; Hamburg, S. P. *Science* **2018**, *361*, 186-188.

10. The United States at Night. https://apod.nasa.gov/apod/ap000708.html.

11. NASA-NOAA satellite reveals new views of earth at night. https://www.nasa.gov/mission_pages/NPP/news/earth-at-night.html.

12. Webb, J. R.; Bolaño, T.; Gunnoe, T. B. *ChemSusChem* **2011**, *4* (1), 37-49.

13. Malik, A.; Mantri, V., Gas-to-Liquids Plants Face Challenges in the U.S. Market. In *Today in Energy*, U.S. Energy Information Administration: Online, 2014.

14. Alvarado, M. *IHS Chem. Bull.* **2016**, *3*, 10-11.

15. Patten, J.; McWha, T. *Dimethyl ether fuel literature review*; National Research Council Canada: Canada, 2016.

16. Blanksby, S. J.; Ellison, G. B. *Acc. Chem. Res.* **2003**, *36* (4), 255-263.

17. Gunnoe, T. B., Metal-Mediated Carbon-Hydrogen Bond Activation. In *Physical Inorganic Chemistry: Reactions, Processes, and Appications*, Bakac, A., Ed. John Wiley & Sons: Hoboken, New Jersey, 2010; pp 495-549.

18. Goldman, A. S.; Goldberg, K. I., Organometallic C–H bond activation:An introduction. In *Activation and Functionalization of C–H Bonds*, Goldberg, K. I.; Goldman, A. S., Eds. American Chemical Society: 2004; Vol. 885, pp 1-43.

19. Klein, D., Radical Reactions. In *Organic Chemistry* 2nd ed.; John Wiley and Sons: Hoboken, NJ, 2015; pp 500-539.

20. Crabtree, R. H. *Chem. Rev.* **1995**, *95* (4), 987-1007.

21. Egloff, G.; Schaad, R. E.; Lowry, C. D. *Chem. Rev.* **1931**, *8* (1), 1-80.

22. Labinger, J. A. *J. Mol. Catal. A: Chem.* **2004**, *220* (1), 27-35.

23. Grant, J. T.; Venegas, J. M.; McDermott, W. P.; Hermans, I. *Chem. Rev.* **2018**, *118* (5), 2769-2815.

24. Hashiguchi, B. G.; Bischof, S. M.; Konnick, M. M.; Periana, R. A. *Acc. Chem. Res.* **2012**, *45* (6), 885-898.

25. Gunsalus, N. J.; Koppaka, A.; Park, S. H.; Bischof, S. M.; Hashiguchi, B. G.; Periana, R. A. *Chem. Rev.* **2017**, *117* (13), 8521-8573.

26. Shilov, A. E.; Shul'pin, G. B. *Chem. Rev.* **1997**, *97* (8), 2879-2932.

27. Crabtree, R. H. *J. Organomet. Chem.* **2004**, *689* (24), 4083-4091.

28. Crabtree, R. H. *J. Organomet. Chem.* **2015**, *793*, 41-46.

29. Labinger, J. A.; Bercaw, J. E. *J. Organomet. Chem.* **2015**, *793*, 47-53.

30. Shteinman, A. A. *J. Organomet. Chem.* **2015**, *793*, 34-40.

31. Labinger, J. A.; Bercaw, J. E. *Nature* **2002**, *417* (6888), 507-514.

32. Periana, R. A.; Taube, D. J.; Evitt, E. R.; Löffler, D. G.; Wentrcek, P. R.; Voss, G.; Masuda, T. *Science* **1993**, *259* (5093), 340-343.

33. Hashiguchi, B. G.; Konnick, M. M.; Bischof, S. M.; Gustafson, S. J.; Devarajan, D.; Gunsalus, N.; Ess, D. H.; Periana, R. A. *Science* **2014**, *343*, 1232-1237.

34. Periana, R. A.; Mironov, O.; Taube, D.; Bhalla, G.; Jones, C. *Science* **2003**, *301* (5634), 814-818.

35. Jones, C. J.; Taube, D.; Ziatdinov, V. R.; Periana, R. A.; Nielsen, R. J.; Oxgaard, J.; Goddard, W. A. *Angew. Chem., Int. Ed.* **2004**, *116* (35), 4726-4729.

36. Periana, R. A.; Mirinov, O.; Taube, D. J.; Gamble, S. *Chem. Commun.* **2002**, (20), 2376-2377.

37. Periana, R. A.; Taube, D. J.; Gamble, S.; Taube, H.; Satoh, T.; Fujii, H. *Science* **1998**, *280*, 560-564.

38. Mironov, O. A.; Bischof, S. M.; Konnick, M. M.; Hashiguchi, B. G.; Ziatdinov, V. R.; Goddard, W. A.; Ahlquist, M.; Periana, R. A. *J. Am. Chem. Soc.* **2013**, *135* (39), 14644-14658.

39. Ahlquist, M.; Nielsen, R. J.; Periana, R. A.; Goddard III, W. A. *J. Am. Chem. Soc.* **2009**, *131* (47), 17110-17115.

40. Gretz, E.; Oliver, T. F.; Sen, A. *J. Am. Chem. Soc.* **1987**, *109* (8109-8111).

41. Vargaftik, M. N.; Stolarov, I. P.; Moiseev, I. I. *J. C.S. Chem. Commun.* **1990,** (15), 1049-1050.

42. Conley, B. L.; Tenn, W. J.; Young, K. J. H.; Ganesh, S. K.; Meier, S. K.; Ziatdinov, V. R.; Mironov, O.; Oxgaard, J.; Gonzales, J.; Goddard, W. A.; Periana, R. A. *J. Mol. Catal. A: Chem.* **2006**, *251* (1-2), 8-23.

43. Zimmermann, T.; Soorholtz, M.; Bilke, M.; Schüth, F. *J. Am. Chem. Soc.* **2016**, *138*, 1239-12400.

44. Michalkiewicz, B.; Ziebro, J.; Tomaszewska, M. *J. Membr. Sci.* **2006**, *286* (1), 223-227.

45. Mukhopadhyay, S.; Zerella, M.; Bell, A. T. *Adv. Synth. Catal.* **2005**, *347*, 1203-1206.

46. Cheng, J.; Li, Z.; Haught, M.; Tang, Y. *Chem. Commun.* **2006**, 4617-4619.

47. Chepaikin, E. G.; Bezruchko, A. P.; Menchikova, G. N.; Moiseeva, N. I.; Gekhman, A. E. *Pet. Chem.* **2014**, *54*, 374-381.

48. Xu, Z.; Oxgaard, J.; Goddard, W. A., III. *Organometallics* **2008**, *27*, 3770-3773.

49. Davico, G. E. *J. Phys. Chem. A* **2005**, *109* (15), 3433-3437.

50. Gang, X.; Zhu, Y.; Birch, H.; Hjuler, H. A.; Bjerrum, N. J. *Appl. Catal., A* **2004**, *261* (1), 91-98.

51. Konnick, M. M.; Hashiguchi, B. G.; Devarajan, D.; Boaz, N. C.; Gunnoe, T. B.; Groves, J. T.; Ess, D. H.; Periana, R. A. *Angew. Chem. Int. Ed.* **2014**, *53* (39), 10490-10494.

52. Sirajuddin, S.; Rosenzweig, A. C. *Biochemistry* **2015**, *54* (14), 2283-2294.

53. Brazeau, B. J.; Austin, R. N.; Tarr, C.; Groves, J. T.; Lipscomb, J. D. *J. Am. Chem. Soc.* **2001**, *123* (48), 11831-11837.

54. Huang, X.; Groves, J. T. *J. Biol. Inorg. Chem.* **2017**, *22*, 185–207

55. Balasubramanian, R.; Smith, S. M.; Rawat, S.; Yatsunyk, L. A.; Stemmler, T. L.; Rosenzweig, A. C. *Nature* **2010**, *465*, 115-119.

56. Chan, S. I.; Yu, S. S.-F. *Acc. Chem. Res.* **2008**, *41* (8), 969-979.

57. Snyder, B. E. R.; Bols, M. L.; Schoonheydt, R. A.; Sels, B. F.; Solomon, E. I., *Chem. Rev.* **2018**, *118* (5), 2718-2768.

58. Sorokin, A. B.; Kudrik, E. V.; Bouchu, D. *Chem. Commun.* **2008**, 2562-2564.

59. Goor, G.; Glenneberg, J.; Jacobi, S., Hydrogen peroxide. In *Ullmann's Encyclopedia of Industrial Chemistry*, Wiley: Weinheim, Germany, 2007; pp 12068-12103.

60. Kudrik, E. V.; Afanasiev, P.; Alvarez, L. X.; Dubourdeaux, P.; Clémancey, M.; Latour, J. M.; Blondin, G.; Bouchu, D.; Albrieux, F.; Nefedov, S. E.; Sorokin, A. B. *Nat. Chem.* **2012**, *4*, 1024-1029.

61. Chen, P. P.-Y.; Nagababu, P.; Yu, S. S.-F.; Chan, S. I. *ChemCatChem* **2014**, *6*, 429-437.

62. Sobolev, V. I.; Dubkov, K. A.; Panna, O. V.; Panov, G. I. *Catal. Today* **1995**, *24* (3), 251-252.

63. Michalkiewicz, B. *Appl. Catal. A* **2004**, *277*, 147-153.

64. Lyons, J. E.; Ellis, P. E., Jr.; Durante, V. A. *Stud. Surf. Sci. Catal.* **1991,** *67*, 99-116.

65. Xu, J.; Armstrong, R. D.; Shaw, G.; Dummer, N. F.; Freakley, S. J.; Taylor, S. H.; Hutchings, G. J. *Catal. Today* **2016**, *270*, 93-100.

66. Groothaert, M. H.; Smeets, P. J.; Sels, B. F.; Jacobs, P. A.; Schoonheydt, R. A. *J. Am. Chem. Soc.* **2005**, *127* (5), 1394-1395.

67. Dumas, J. *Liebigs Ann.* **1840**, *33*, 187-189.

68. Rossberg, M.; Lendle, W.; Pfleiderer, G.; Tögel, A.; Dreher, E.-L.; Langer, E.; Rassaerts, H.; Kleinschmidt, P.; Strack, H.; Cook, R.; Beck, U.; Lipper, K.-A.; Torkelson, T. R.; Löser, E.; Beutel, K. K.; Mann, T., Chlorinated Hydrocarbons. In *Ullmann's Encyclopedia of Industrial Chemistry*, Wiley-VCH Weinheim, 2006.

69. Gorin, E.; Fontana, C. M.; Kidder, G. A. *Ind. Eng. Chem.* **1948**, *40* (11), 2128-2134.

70. Degirmenci, V.; Uner, D.; Yilmaz, A. *Catal. Today* **2005,** *106*, 252-255.

71. Ding, K.; Metiu, H.; Stucky, G. D. *ACS Catal.* **2013**, *3*, 474-477.

72. Taylor, C. E.; Noceti, R. P.; Schehl, R. R. *Stud. Surf. Sci. Catal.* **1988**, *36*, 483-489.

73. He, J.; Xu, T.; Wang, Z.; Zhang, Q.; Deng, W.; Wang, Y. *Angew. Chem. Int. Ed.* **2012**, *2488-2492*.

74. Podkolzin, S. G.; Stangland, E. E.; Jones, M. E.; Peringer, E.; Lercher, J. A. *J. Am. Chem. Soc.* **2007**, *129* (9), 2569-2576.

75. Shalygin, A.; Paukshtis, E.; Kovalyov, E.; Bal'zhinimaev, B. *Front. Chem. Sci. Eng.* **2013**, *7* (3), 279-288.

76. Zichittella, G.; Paunovic, V.; Amrute, A. P.; Perez-Ramirez, J. *ACS Catal.* **2017**, *7* (3), 1805-1817.

77. Ravi, M.; Ranocchiari, M.; van Bokhoven, J. A. *Angew. Chem. Int. Ed.* **2017**, *56* (52), 16464-16483.

78. Wang, K. X.; Xu, H. F.; Li, W. S.; Au, C. T.; Zhou, X. P. *Appl. Catal. A* **2006**, *304*, 168-177.

79. Liu, Z.; Li, W.; Zhou, X. *J. Nat. Gas Chem.* **2010**, *19* (5), 522-529.

80. Lin, R.; Ding, Y.; Gong, L.; Li, J.; Chen, W.; Yan, L.; Lu, Y. *Appl. Catal. A: Chem.* **2009**, *353*, 87-92.

81. Wang, R.; Lin, R.; Ding, Y.; Liu, J. *Catal. Lett.* **2014**, *144*, 1384-1392.

82. Paunović, V.; Zichittella, G.; Moser, M.; Amrute, A. P.; Pérez-Ramírez, J. *Nat. Chem.* **2016**, *8*, 803-809.

83. Zhou, X. P.; Lorkovic, I. M.; Stucky, G. D.; Ford, P. C.; Sherman, J. H.; Grosso, P. Integrated process for synthesizing alcohols and ethers from alkanes. US 6,462,243 B1 2002.

84. Zhou, X.; Yilmaz, A.; Yilmaz, G. A.; Lorkovic, I. M.; Laverman, L. E.; Weiss, M.; Sherman, J. H.; McFarland, E. W.; Stucky, G. D.; Ford, P. C. *Chem. Commun.* **2003**, 2294-2295.

85. Lorkovic, I. M.; Yilmaz, A.; Yilmaz, G. A.; Zhou, X.; Laverman, L. E.; Sun, S.; Schaefer, J. H.; McFarland, E. W.; Stucky, G. D.; Ford, P. C. *Catal. Today* **2004**, *98*, 317-322.

86. Breed, A.; Doherty, M. F.; Gadewar, S.; Grosso, P.; Lorkovic, I. M.; McFarland, E. W.; Weiss, M. *Catal. Today* **2005**, *106*, 301-304.

87. Lorkovic, I. M.; Noy, M.; Weiss, M.; Sherman, J.; McFarland, E.; Stucky, G. D.; Ford, P. C. *Chem. Commun.* **2004**, (5), 566-567.

88. Basickes, N.; Hogan, T. E.; Sen, A. *J. Am. Chem. Soc.* **1996**, *118* (51), 13111-13112.

89. Chen, W.; Kocal, J. A.; Brandvold, T. A.; Bricker, M. L.; Bare, S. R.; Broach, R. W.; Greenlay, N.; Popp, K.; Walenga, J. T.; Yang, S. S.; Low, J. J. *Catal. Today* **2009,** *140*, 157-161.

90. Tang, R.; Kochi, J. K. *J. Inorg. Nucl. Chem.* **1973**, *35* (11), 3845-3856.

91. Strassner, T.; Ahrens, S.; Muehlhofer, M.; Munz, D.; Zeller, A. *Eur. J. Inorg. Chem.* **2013**, *2013* (21), 3659-3663.

92. Mukhopadhyay, S.; Bell, A. T. *Org. Proc. Res. Dev.* **2003**, *7* (2), 161-163.

93. Mukhopadhyay, S.; Bell, A. T. *Angew. Chem. Int. Ed.* **2003**, *42*, 2990-2993.

94. Mukhopadhyay, S.; Bell, A. T. *Angew. Chem. Int. Ed.* **2003**, *42* (9), 1019-1021.

95. Mukhopadhyay, S.; Bell, A. T. *Org. Proc. Res. Dev.* **2003**, *7* (5), 754-757.

96. Fortman, G. C.; Boaz, N. C.; Munz, D.; Konnick, M. M.; Periana, R. A.; Groves, J. T.; Gunnoe, T. B. *J. Am. Chem. Soc.* **2014**, *136*, 8393-8401.

97. Kalman, S. E.; Munz, D.; Fortman, G. C.; Boaz, N. C.; Groves, J. T.; Gunnoe, T. B. *Dalton Trans.* **2015**, *44*, 5294-5298.

2 Elucidation of the Mechanism for the Thermal Functionalization of Hydrocarbons Using Chloride and Hypervalent Iodine Oxidants

This chapter is adapted from "Schwartz, N. A.; Boaz, N. C.; Kalman, S. E.; Zhuang, T.; Goldberg, J. M.; Fu, R.; Nielsen, R. J.; Goddard, W. A., III; Groves, J. T.; Gunnoe, T. B. Mechanism of Hydrocarbon Functionalization by an Iodate/Chloride System: The Role of Ester Protection. ACS Catal. 2018, 8, 3138-3149." Copyright 2018 American Chemical Society

2.1 Introduction

2.1.1 Oxy-Esterification (OxE) Process using Iodate and Chloride

Mixtures of iodate and chloride convert light alkanes (*e.g.*, methane, ethane and propane) to their respective alkyl esters in trifluoroacetic acid (HTFA) solvent in high yield and selectivity, as reported prior to my work by Gunnoe and coworkers in a process termed oxy-esterification (OxE).[1] For methane, methyl trifluoroacetate (MeTFA) yields based on methane exceed 20% with > 85% selectivity for MeTFA. The selectivity denotes the preference for alkyl trifluoroacetates relative to alkyl chlorides (*e.g.*, MeCl) which are detected as byproducts of this reaction. The OxE process is also highly effective for ethane and propane functionalization, with 30% yield of EtTFA relative to ethane and ~20% yield of mono- and di-functionalized propyl trifluoroacetate esters relative to propane.

To understand the scope of this reaction, a variety of halide and iodate sources were examined. A broad range of chloride and iodate sources are efficient in this process, with the best being KCl and NH_4IO_3, while very minimal reactivity was observed when other halides are used (Figure 2.1). Sub-stoichiometric amounts of chloride are necessary for the reaction, as only trace reactivity was observed when methane reacted with iodate alone in HTFA.

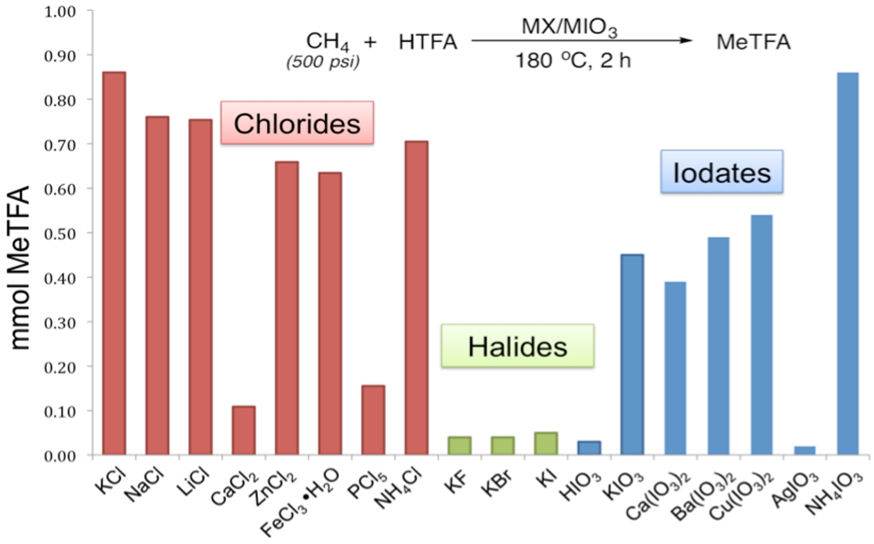

Figure 2.1. Comparison of chloride sources, halides and iodate sources for the partial oxidation of methane. Conditions: 0.338 mmol of X^-; 2.26 mmol of IO_3^-; 2.0 mL of HTFA; $p_{CH_4/Ne}$ = 5520 kPa; 180 °C; 2 h; 600 rpm. NH_4IO_3 was used as the oxidant for the reactions involving $M^{n+}Cl_n$ and KX. KCl was used in the reactions involving $M^{n+}(IO_3)_n$. Reprinted with permission from "Fortman, G. C.; Boaz, N. C.; Munz, D.; Konnick, M. M.; Periana, R. A.; Groves, J. T.; Gunnoe, T. B. Selective Monooxidation of Light Alkanes Using Chloride and Iodate. *J. Am. Chem. Soc.* 2014, 136, 8393-8401. Copyright 2014 American Chemical Society.

The OxE process is similar to oxychlorination (see Section 1.4.3) in that chloride is involved in both functionalization processes as KCl and HCl, respectively, and an oxidant is used in both processes. However, the oxidants of the OxE process and oxychlorination differ, with iodate being used for the former and oxygen (with a heterogeneous catalyst) being used for the latter. While oxychlorination occurs by a radical-based mechanism for alkane functionalization and favors the formation of chlorinated products,[2] our OxE process gives higher conversions and yields than is typically observed for oxychlorination. Importantly, the OxE process results in the selective formation of alkyl esters rather than alkyl chlorides, which of course is not possible for oxychlorination as no ester source is present. MeCl does not convert rapidly to MeTFA under the OxE reaction conditions and thus is unlikely to be a viable intermediate in this process. The possible involvement of iodine as an active intermediate was considered, but the abstraction of an H-atom from methane by an iodine radical is highly endothermic.[3] To probe whether the iodate/chloride reaction occurs by a radical pathway, the addition of dioxygen, an efficient alkyl radical trap, was examined.[4] As identical yields were obtained in the absence or presence of dioxygen, a conclusion could not be drawn. However, these results provide evidence against the formation of alkyl free radical intermediates.

Given the unique selectivity of the OxE process, initially our mechanistic hypotheses tended to avoid the involvement of free radical mediated C–H bond cleavage as this would be expected to react more rapidly with alkyl esters than alkanes. Thus, several possible reaction mechanisms for C–H bond cleavage were considered, and some examples are shown in Scheme 2.1. As UV-vis data and DFT calculations indicate that IX_3 (X = Cl, TFA) species may form under reaction conditions with iodate or periodate and chloride in HTFA (*vide infra*), Scheme 2.1 shows possible pathways starting from IX_3 species.[1, 5] Mechanism A shows an electrophilic C–H activation reaction pathway where methane is activated in a two-electron process to give an I(III) species and ultimately MeTFA on reaction with HTFA solvent. A similar mechanism has been proposed for a perfluoroarene iodine(III) compound.[6] In mechanism B, conversion of IX_3 where at least one X = TFA to an iodine-centered radical species and trifluoroacetyl radical could result in the formation of MeTFA. Mechanism C shows a concerted metalation deprotonation-type mechanism where activation of methane is enabled by the formation of trifluoroacetic acid. Other mechanisms beginning from the initial IO_x^- species are shown in D & E, where the former demonstrates a possible 1,2-C–H addition across an I–O bond and the latter shows a possible radical-based pathway where an I–OH species is formed. Both of these are akin to known transition metal oxo based reactivity, but, to our knowledge, do not have precedent in iodine oxide chemistry. In pathway F, iodate or periodate oxidize chloride to chlorine to produce chlorine radical, which results in traditional halogenation-type chemistry which could generate MeTFA in HTFA. DFT calculations by the Goddard group (calculations were performed by Ross Fu and Smith Nielsen) did not locate viable energies for any of the pathways shown in Scheme 2.1 or related reactions. As described in this chapter, our efforts to understand the reaction pathway and selectivity for the OxE process moved in different directions.

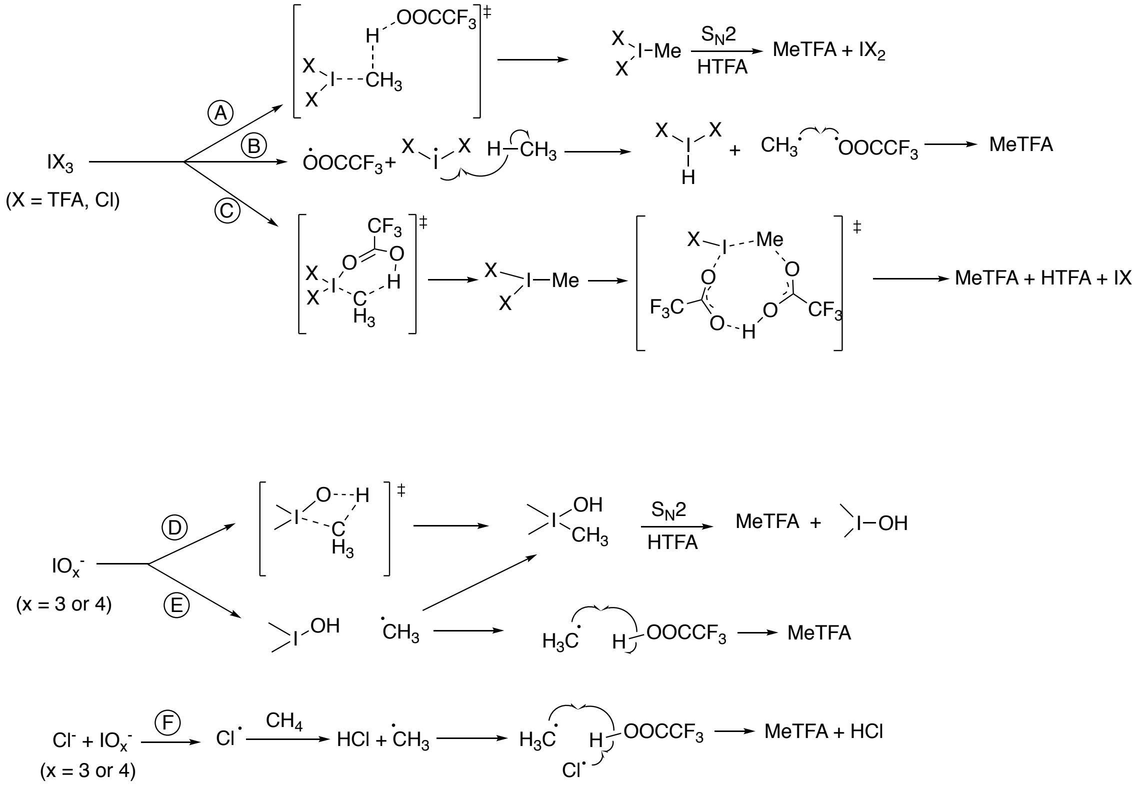

Scheme 2.1. Proposed reaction mechanisms for the iodate/chloride methane functionalization process. Bonds from iodine for mechanisms D & E represent a generic coordination sphere. Pathways D-F were also explored for IO_2 and IO^+ species.

Further efforts sought to determine the active species of this reaction by examining iodine sources, as MeI was demonstrated to convert rapidly to MeTFA under the reaction conditions. As I^+ originating from I_2 is known to be an effective catalyst for methane oxidation in oleum,[7-9] methane oxidation in the presence of I_2 was tested in our reaction solvent, HTFA. With I_2 alone or in the presence of KCl or NH_4IO_3 without chloride, only trace reactivity was observed. Low yields of MeTFA were also observed when using ICl or ICl_3. Several other iodine oxides and hypervalent iodine oxidants (*i.e.*, I_2O_4, $I(TFA)_3$, $(IO_2)_2S_2O_7$ and $(IO)_2SO_4$) gave high yields of MeTFA when substoichiometric amounts of chloride were added, indicating that the OxE process is not limited to using iodate as the oxidant. This initial report concluded that an iodine oxide is likely an active intermediate for the OxE process.[1]

2.1.2 OxE Process using Periodate and Chloride

Given the success of the OxE process with light alkanes using iodate, Gunnoe and coworkers also examined the use of periodate (IO_4^-) as an oxidant. Similar to the reactions with iodate and chloride, periodate and chloride also functionalized light alkanes in high yields to their respective alkyl trifluoroacetate esters in HTFA solvent.[10] Yields of methane functionalization are higher in the periodate system, with a maximum of > 40% yield of MeTFA relative to methane with > 97% selectivity observed under optimized conditions. Ethane and propane can also be functionalized in ~20% yield to their respective alkyl esters with periodate and chloride, however the reactions are much less selective for EtTFA versus EtCl than in the iodate process. Chloride is also essential for the OxE process with periodate, however the focus of this report was the optimization of the process with periodate rather than mechanistic elucidation.

2.2 Experimental Elucidation of the Mechanism of the OxE Process

The experimental results in this chapter have been published and the computational results have been submitted for publication and are attached as an appendix to this Dissertation.[5, 11] Efforts to elucidate the mechanism of the OxE process are a collaboration between the Gunnoe group, the Groves group (Princeton University) and the Goddard group (Caltech). Dr. Nicholas Boaz and Thompson Zhuang of the Groves group performed UV-visible studies, reactions using adamantane as a model substrate, and reactions with *tert*-butyl propaneperoxoate, an ethyl radical source. Dr. Steven Kalman of the Gunnoe group performed the first reactions with ethane in acetic acid to probe for ethyl iodide formation. Drs. Ross Fu and Robert (Smith) Nielsen from the Goddard group performed the computational studies based on the experimental results in this chapter and in the initial publications of the OxE process.

2.2.1 Findings from UV-Visible Spectroscopy

Efforts to elucidate the mechanism of the OxE process have used UV-visible spectroscopy to probe for reactive intermediates. The combination of the colorless chloride and iodate salts in HTFA generates a golden-yellow mixture (Figure 2.2). The UV-visible spectrum of this solution is consistent with the production of Cl_2 (~330 nm) and ICl and/or ICl_3 (~460 nm) (Figure 2.3). The absorption consistent with the interhalogen species cannot be assigned due to the overlap between the absorptions from authentic ICl and ICl_3 standards.

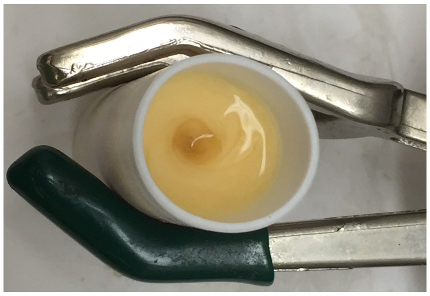

Figure 2.2. Addition of HTFA to KCl/NH_4IO_3 gives a golden-yellow mixture. Conditions: KCl (0.67 mmol), NH_4IO_3 (7.7 mmol) and HTFA (8 mL).

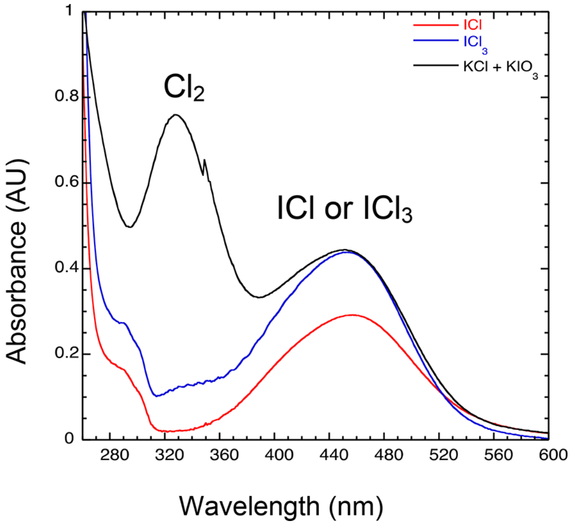

Figure 2.3. UV-vis spectra of the golden-yellow mixture of potassium chloride and potassium iodate in HTFA (top, black), pure ICl (bottom, red) and pure ICl_3 (middle, blue). Conditions for the black spectrum: 0.15 mmol of KCl, 1.0 mmol of KIO_3, and HTFA at room temperature. The peak for Cl_2 was assigned by experimentally preparing an authentic standard in HTFA.

The initial report of the OxE chemistry tested both ICl and ICl_3 as potential active species using the standard methane functionalization conditions in the absence of added KCl ($p_{CH_4/Ne}$ = 3450 kPa, 180 °C, 1 h).[1] Methane was not functionalized when ICl was used as the oxidant. However, when ICl_3 was used, MeTFA and MeCl were generated, with MeCl as the major product. The selectivity observed with ICl_3 differs significantly compared to the OxE process using iodate and chloride, for which MeCl is the minor product. Therefore, neither ICl nor ICl_3 is proposed to be a likely active intermediate. The formation of chlorine, also demonstrated by UV-vis spectroscopy, indicates that functionalization could occur by a pathway involving chlorine radicals since H-atom abstraction from CH_4 by chlorine radical is exothermic and exergonic (Scheme 2.2).[5, 12]

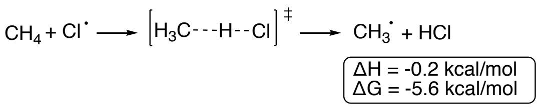

$$CH_4 + Cl^{\bullet} \longrightarrow \left[H_3C{-}{-}{-}H{-}{-}Cl\right]^{\ddagger} \longrightarrow CH_3^{\bullet} + HCl \qquad \boxed{\begin{array}{l}\Delta H = -0.2\ \text{kcal/mol}\\ \Delta G = -5.6\ \text{kcal/mol}\end{array}}$$

Scheme 2.2. H-atom abstraction from methane by chlorine radical.[5, 12]

2.2.2 Comparison of the OxE Process to Chlorination

Adamantane was used as a model substrate for light alkanes to compare the selectivity for chlorination to that of the iodate/chloride reaction as it contains multiple secondary and tertiary C–H bonds. The iodate/chloride reaction is also extremely efficient for the oxidation of adamantane (Scheme 2.3), giving 95% yield of the tertiary TFA ester based on adamantane. Dark crystals, identified as iodine by UV-vis spectroscopy, were also observed in this reaction (Figure 2.4). Iodine production was quantified by UV-vis spectroscopy using a calibration curve (Figure 2.5).

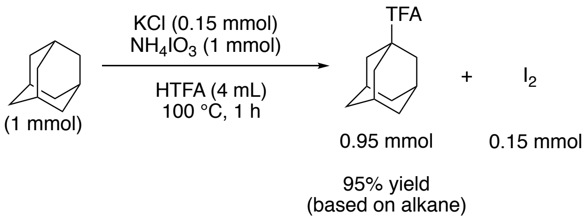

Scheme 2.3. Oxidation of adamantane by KCl/NH_4IO_3 in HTFA solvent.

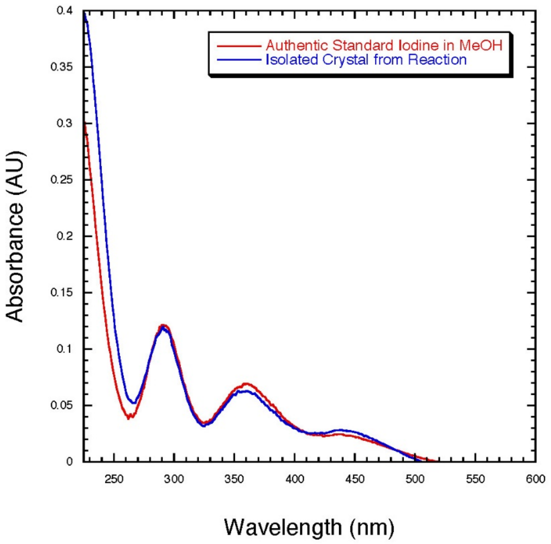

Figure 2.4. UV-vis spectra of a crystal isolated from the reaction in Scheme 2.1 (blue) and of an authentic standard of iodine (red).

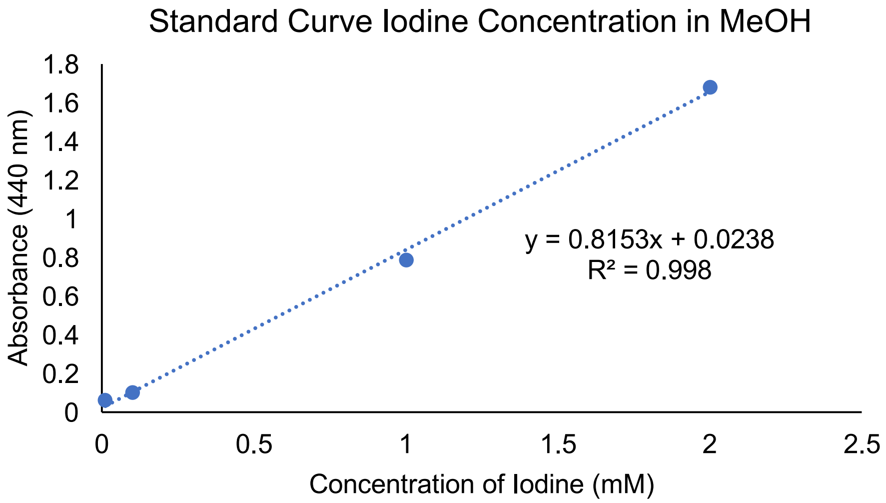

Figure 2.5. Calibration curve of the concentration of iodine in methanol by UV-vis spectroscopy, using the absorbance at 440 nm.

It was observed that 2-adamantyl trifluoroacetate rapidly rearranges to the tertiary 1-adamantyl trifluoroacetate in HTFA. Thus, this conversion would inhibit the ability to obtain useful data related to secondary versus tertiary kinetic selectivity. Because rearrangement was observed between secondary and tertiary functionalized adamantanes in HTFA, experiments probing the selectivity of the reaction were performed in acetic acid

(HOAc) because this conversion to the tertiary ester was not observed in HOAc (Scheme 2.4).

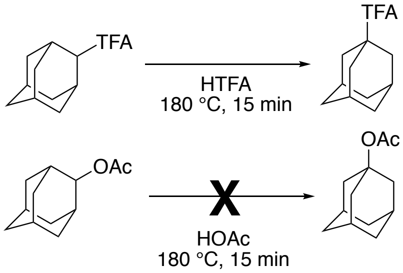

Scheme 2.4. Heating the secondary adamantyl ester derivative in acid generates the tertiary product in HTFA but not in HOAc.

Due to the similarities between the OxE process and radical-based functionalization with chlorine for light alkane functionalization (see Introduction to this chapter), the model studies with adamantane sought to compare the selectivity of the OxE process and chlorination. Chlorination of adamantane was performed using *N*-chlorosuccinimide (NCS), which is known to yield chlorine radicals in the presence of an initiator such as benzoyl peroxide.[13] The iodate/chloride reaction and chlorination by NCS/benzoyl peroxide both yield 3°:2° selectivity of ~5.2:1 on a per-hydrogen basis (Scheme 2.5). Radical chlorination of adamantane using NCS or Cl_2 has been reported to result in similar 3°:2° selectivity on a per-hydrogen basis, 4.9:1 and 4.7:1, respectively.[14-15] In both cases, only mono-functionalized products were generated. Kinetic isotope effects (KIEs) for these functionalization methods were also probed using a 1:1 mixture of perprotio- and perdeuteroadamantane. The KIEs for the two reactions are statistically identical, as shown in Scheme 2.6, with a k_H/k_D = 1.52(3) for the oxidation using iodate and chloride and k_H/k_D = 1.6(3) for both the acetate and chloride derivatives using NCS and benzoyl peroxide. The KIE and selectivity results are consistent with the likelihood that the iodate/chloride reaction involves chlorine radical species. The use of NCS as an unambiguous source of chlorine atoms has been contested,[16] however, it was utilized in this study to provide a reference for radical-based functionalization resulting in the overall chlorination of the substrate.

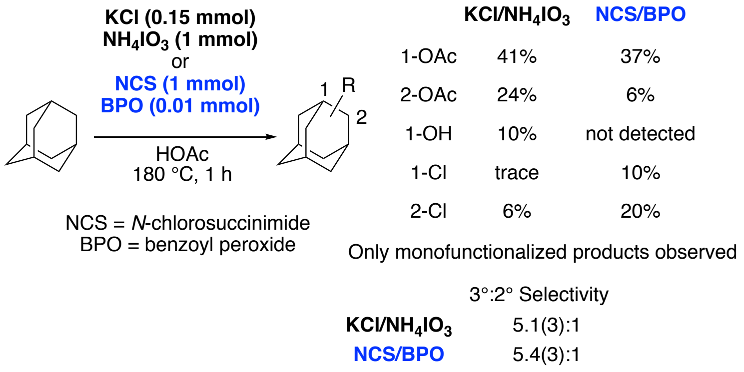

	KCl/NH_4IO_3	NCS/BPO
1-OAc	41%	37%
2-OAc	24%	6%
1-OH	10%	not detected
1-Cl	trace	10%
2-Cl	6%	20%

Only monofunctionalized products observed

	3°:2° Selectivity
KCl/NH_4IO_3	5.1(3):1
NCS/BPO	5.4(3):1

Scheme 2.5. Oxidation of adamantane by iodate/chloride (black) or NCS/BPO (NCS =*N*-chlorosuccinimide; BPO = benzoyl peroxide, in blue) in HOAc. Data are from three separate experiments with averages and standard deviations shown for 3°:2° selectivity ratios.

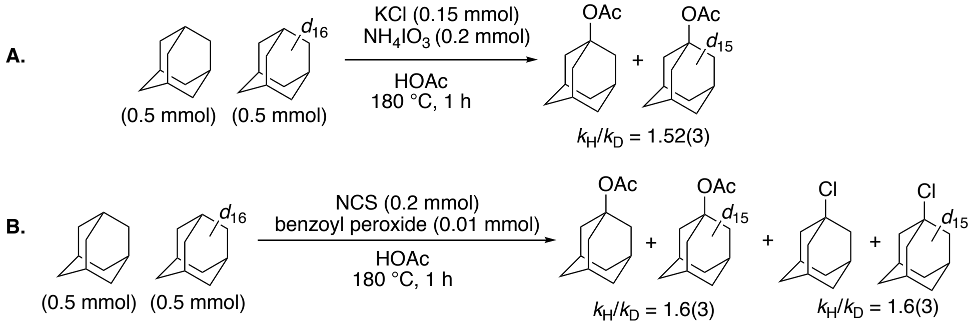

Scheme 2.6. (A) Intermolecular deuterium KIE for the oxidation of adamantane by iodate/chloride in HOAc and (B) intermolecular deuterium KIE for radical chlorination of adamantane. Values are given as averages with standard deviations based on at least three experiments.

2.2.3 The Role of Iodine

The similarities between the ratio of 3°:2° products and the KIEs for the functionalization of adamantane via chlorination with NCS and the OxE process suggest that the two processes may operate by similar mechanisms. This led to further investigation of potential radical-based reaction pathways for the OxE process. As the OxE process is tolerant of dioxygen, and dioxygen traps alkyl radicals at rates approaching diffusion limits,[17] it was previously anticipated that the presence of dioxygen would prevent the formation of the observed alkyl ester products. Thus, when the addition of oxygen to the methane functionalization reaction with KCl/NH_4IO_3 in HTFA did not result in decreased yields, the initial conclusion was that a radical pathway was likely not operative.[1] However, iodine, which is generated by the *in situ* reduction of iodate (see above), is also a well-established alkyl radical trap with a rate nearly half that of dioxygen (2.5×10^9 mol^{-1} s^{-1} for I_2 vs. 4.9×10^9 mol^{-1} s^{-1} for O_2).[17-19] Thus, if iodine is present in sufficient concentrations, it competes with dioxygen to trap alkyl radicals as alkyl iodides. Alkyl iodides were initially proposed as possible intermediates for the OxE process,[1] as MeI was shown to react rapidly with iodate in HTFA to generate MeTFA in approximately quantitative yield, in agreement with previous reports which demonstrated that RI species convert to alcohols or esters under highly oxidizing conditions. As a result, the detection of MeI during the reaction is unlikely.[20-24]

In order to determine if iodine could be acting as a trapping agent under aerobic conditions, *tert*-butyl propaneperoxoate, an ethyl radical precursor, was heated with I_2 in HOAc in the presence of O_2 (Scheme 2.7). EtI was generated as the major product in 50(11)% yield, demonstrating that iodine can compete with dioxygen to trap alkyl radicals as alkyl iodide species. Also, these experiments show that the conversion of EtI to EtOAc is not rapid enough to preclude the observation of EtI, which is in contrast with our results with MeI. Subsequent studies sought to observe EtI from ethane functionalization with the iodate/chloride process. Ethane functionalization by the iodate/chloride process was tested in HOAc, wherein EtI was observed by ^1H NMR spectroscopy (Scheme 2.8). These results, in combination with those of the ethyl radical trapping, are consistent with the formation of ethyl radicals under iodate/chloride functionalization conditions. Ethyl radical is then trapped by iodine, which is generated *in situ* from iodate and HTFA. Accordingly, it has been proposed that this process occurs with methane in HTFA as well. However, it is likely that due to the rapid conversion of MeI to MeTFA that it is not possible to observe the formation of MeI.

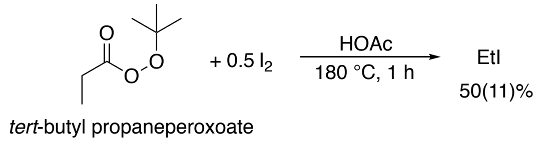

Scheme 2.7. Heating *tert*-butyl propaneperoxoate in the presence of iodine generates ethyl iodide. EtI yield is given as an average and standard deviation of four trials.

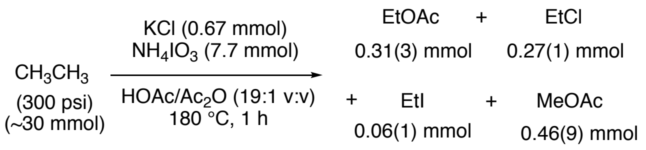

$$\underset{\substack{(300\text{ psi})\\(\sim 30\text{ mmol})}}{CH_3CH_3} \xrightarrow[\substack{HOAc/Ac_2O\ (19{:}1\ v{:}v)\\180\ °C,\ 1\ h}]{\substack{KCl\ (0.67\ mmol)\\NH_4IO_3\ (7.7\ mmol)}} \underset{0.31(3)\text{ mmol}}{EtOAc} + \underset{0.27(1)\text{ mmol}}{EtCl} + \underset{0.06(1)\text{ mmol}}{EtI} + \underset{0.46(9)\text{ mmol}}{MeOAc}$$

Scheme 2.8. Ethane functionalization by the iodate/chloride process yields EtI, EtOAc, EtCl and MeOAc. Error bars denote standard deviations based on at least three experiments. See section 2.2.6 for further details regarding the formation of MeOAc.

A standard set of conditions was developed to systematically determine and compare the relative stabilities of RI and RTFA species (R = Me, Et) under the iodate/chloride functionalization conditions (Schemes 2.9 and 2.10). After 20 min of reaction at 180 °C, MeI and EtI are both fully consumed under these conditions,. MeI converts to MeTFA and MeCl. In contrast, EtI, which was stable in HOAc, rapidly converts in HTFA to EtTFA, EtCl and the difunctionalized ester product 1,2-bis(trifluoroacetyl)ethane. In contrast, both alkyl trifluoroacetates MeTFA and EtTFA are relatively stable under those reaction conditions, with 90% and 55%, respectively, remaining after 20 min at 180 °C in the presence of chloride and iodate. The products of MeTFA and EtTFA over-oxidation were not characterized. The greater stability of the ester species relative to the alkyl iodides, especially of MeTFA, under highly oxidizing conditions led to additional studies.

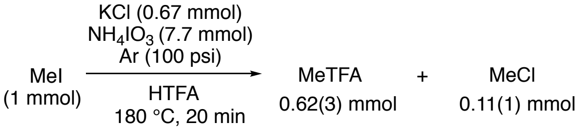

Scheme 2.9. MeI conversion to MeTFA and MeCl under iodate/chloride functionalization conditions. Yields are given as averages with standard deviations based on at least three experiments.

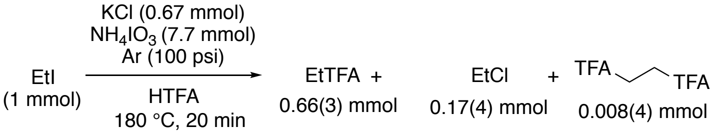

Scheme 2.10. EtI conversion to EtTFA, EtCl and difunctionalized ester product under iodate/chloride functionalization conditions. Yields are given as averages with standard deviations based on at least three experiments.

2.2.4 Alkyl Trifluoroacetate Stability

One of the major limitations of light alkane oxidation processes is undesired over-oxidation. To compare the rate of this over-oxidation relative to alkane functionalization, the functionalization of RH to form RTFA products and the oxidative consumption of RTFA were studied under identical conditions at 140 °C (R = Me, Et; Figures 2.6 and 2.7). The lower reaction temperature was used in order to study the alkane functionalization reactions over longer periods of time, as methane functionalization to MeTFA reaches completion within 1 h at 180 °C. This allowed better quantification of reaction rates. Over-oxidation products in RTFA consumption experiments were not characterized with the exception of 1,2-bis(trifluoroacetyl)ethane in the EtTFA experiments, which was observed by ^{1}H NMR spectroscopy. MeTFA is highly stable under these conditions at 140 °C, with 85% of the starting amount remaining after 16 h (Figure 2.6). Furthermore, MeTFA is somewhat volatile. Thus, the 85% retention of MeTFA serves as an upper limit to the amount lost as a result of chemical oxidation since it is possible that some of the 15% loss is due to volatility rather than oxidation. Although EtTFA is less stable than MeTFA, 41% of the starting amount of EtTFA remains after 8 h at 140 °C (Figure 2.7). The partial oxidation of methane to MeTFA is linear versus time and is complete within 8 h at 140 °C (Figure 2.6). Ethane functionalization to EtTFA, EtCl and 1,2-bis(trifluoroacetyl)ethane is complete within 6 h (Figure 2.7). For both methane and ethane functionalization, the major product of each reaction is the corresponding alkyl trifluoroacetate ester. The plots of functionalization versus decay cannot be used to directly and rigorously compare the rates as the concentration of alkane in solution during the reaction is unknown. However, the relative rates of decay and functionalization can be obtained from the slopes of these plots of MeTFA decay and production over time. Although the plot of MeX (X = TFA, Cl) production versus time is linear through the first 8 h of the reaction, it is not for EtX production. In order to compare the rates of RX generation consistently, the rate of product formation was determined by fitting a line to each of the first data points for RX production from the origin (Figure 2.8). As the RTFA decay data versus time are linear for both R = Me and Et (Figures 2.6 and 2.7), the slope of the linear fits of each data set were used (Figure 2.8). As a result, the ratios of RX production versus RTFA decay are 13 and 8 for R = Me and Et, respectively.

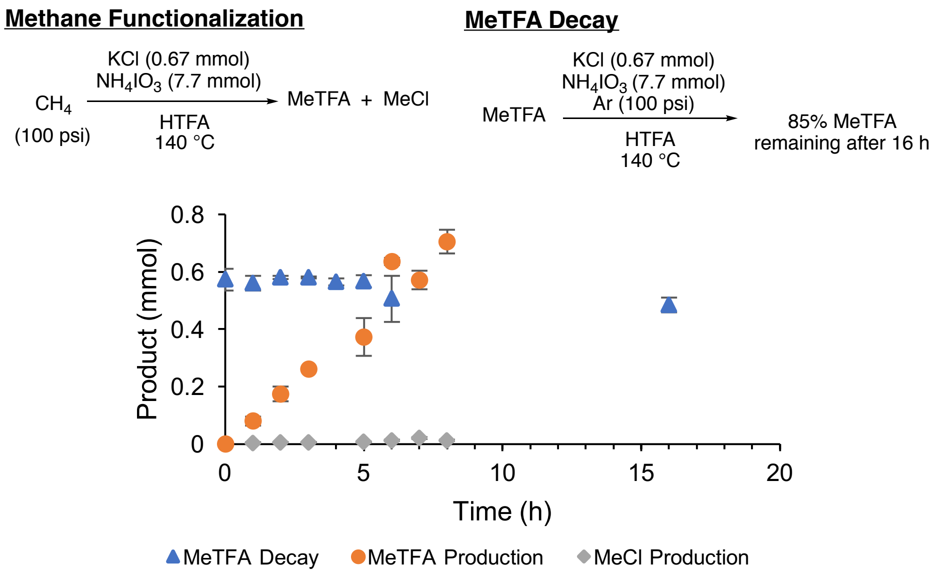

Figure 2.6. Methane functionalization and MeTFA decay in the presence of KCl, NH_4IO_3 and HTFA at 140 °C as a function of time. Error bars denote standard deviations based on at least three experiments.

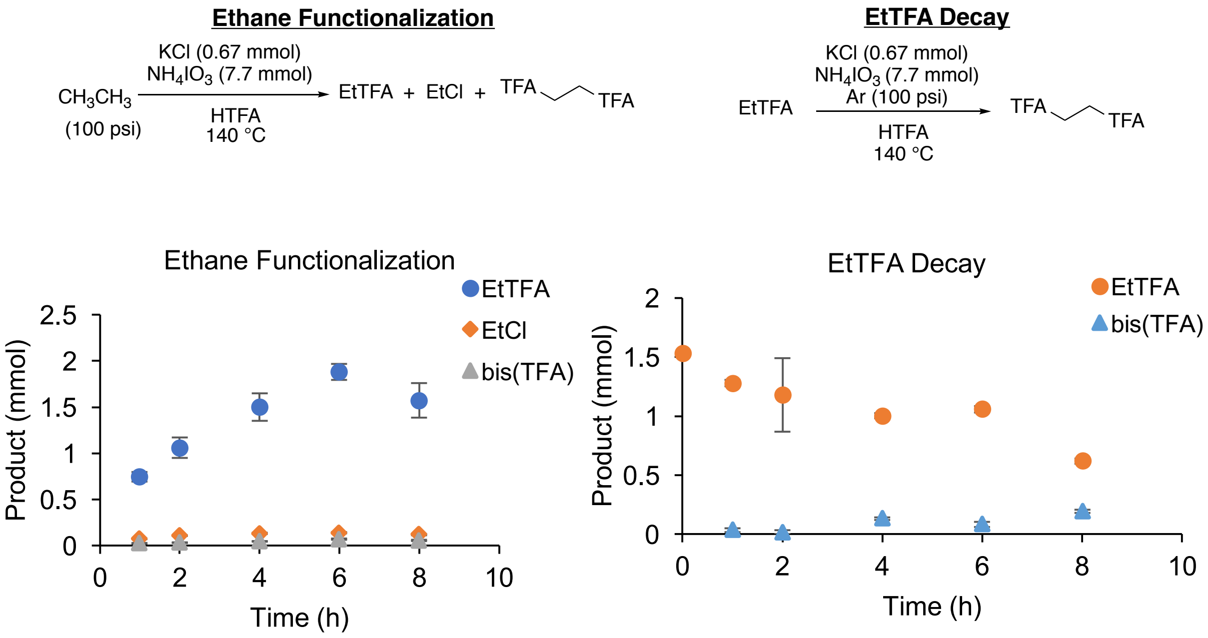

Figure 2.7. Ethane functionalization and EtTFA decay in the presence of KCl, NH_4IO_3 and HTFA at 140 °C as a function of time. Error bars, denoting standard deviations based on at least three experiments, are provided for all data, but are too small to be seen for several time points for EtTFFA decay. Bis(TFA) = 1,2-bis(trifluoroacetyl)ethane.

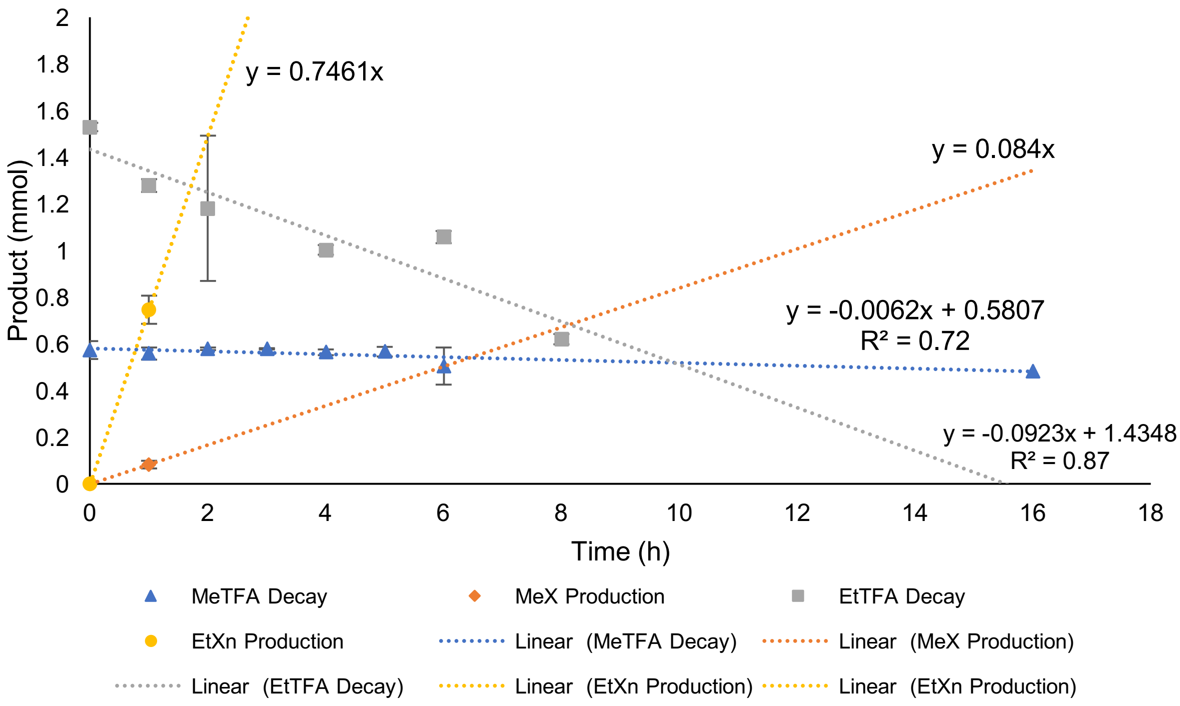

Figure 2.8. Plots of methane and ethane functionalization and MeTFA and EtTFA decay data. Ratios of functionalization to decay are obtained by dividing the absolute value of the slope of the fit of the functionalization data by the slope of the fit of the decay data.

Using the data from Figure 2.8, we can use the relative rates of methane functionalization and MeTFA decay/consumption to simulate the rates of a methane to MeTFA and MeTFA consumption to estimate the best possible yield from our OxE process. As methane functionalization is approximately 13 times faster than MeTFA consumption, the relative rate of conversion of MeTFA to over-oxidized products versus methane to MeTFA rate can be set to 1/13. A kinetic first-order plot for the reactions of methane to MeTFA and MeTFA to over-oxidized products demonstrates that an approximate maximum 75% yield of MeTFA based on methane is theoretically possible, due to the slow over-oxidation of the ester product relative to methane functionalization (Figure 2.9). We propose that current yields may be lower than the theoretical maximum due to undesired consumption of the oxidant through solvent oxidation. Moving forward, quantification of solvent oxidation will be important for reaction optimization, and a primary focus to improve the OxE process will be the use of less easily oxidized solvent media. The high theoretical yield demonstrates the potential viability of a functionalization process which likely operates by a radical-based mechanism.

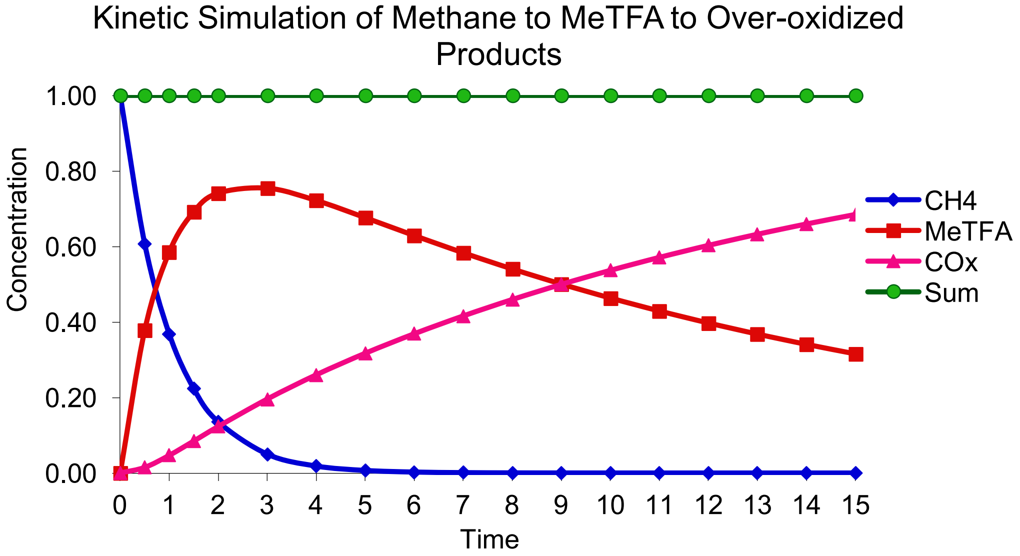

Figure 2.9. Kinetic simulation for a first-order reaction of methane to MeTFA and subsequent first-order over-oxidation (labeled as CO_x) showing the change in concentration over time. The ratio of functionalization to over-oxidation is set to 13, as was determined from Figure 2.8. The axes represent concentration and time as arbitrarily set scales.[25]

2.2.5 Comparison of OxE to Chlorination with Light Alkanes

For an apparent radical-based mechanism, the iodate/chloride process operates with surprising selectivity to generate the mono-functionalized product MeTFA, which led to further studies toward mechanistic elucidation. As products of functionalization reactions typically contain weaker bonds than methane, over-oxidation is a significant complication for free-radical-based functionalization methods. For example, the C–H bond dissociation energy (BDEs) of methane is greater than those of MeOH, MeCl and MeTFA (Scheme 2.11). The nature of the high selectivity of the iodate/chloride process could be a result of a protecting effect from the TFA ester moiety against over-oxidation, as demonstrated by the relative rates of reaction of RI and RTFA species (see above).

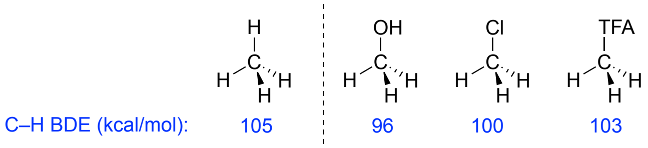

Scheme 2.11. Bond dissociation energies for the C–H bonds of methane, MeOH, MeCl and MeTFA in kcal/mol.[5, 26-27]

Chlorination of methane with NCS and benzoyl peroxide in HTFA solvent does not result in the formation of MeTFA (Figure 2.10). This result is in agreement with previous findings demonstrating that MeCl does not convert rapidly to MeTFA in HTFA in the presence of KCl and NH_4IO_3 at 180 °C.[1] However, on the addition of small amounts of iodine to the chlorination reaction, MeTFA is formed (Figure 2.10). However, the amount of MeTFA generated decreases when > 0.34 mmol of I_2 are added. The cause of this decrease is uncertain, but it may be a result of I_2 trapping radical intermediate species that are necessary for methane functionalization to yield alkyl radical species. The formation of MeTFA under chlorination conditions with added iodine is particularly notable, as it shows that I_2 is an efficient radical trap which can rapidly intercept methyl radicals, trapping them as MeI which is then converted *in situ* to the protected ester product, MeTFA. For comparison, iodine was also added to iodate/chloride functionalization reactions with methane (Figure 2.11). Similar to the observations from the chlorination reactions, the addition of > 0.3 mmol of I_2 to the reaction also results in decreased MeTFA yields when chloride and iodate are utilized.

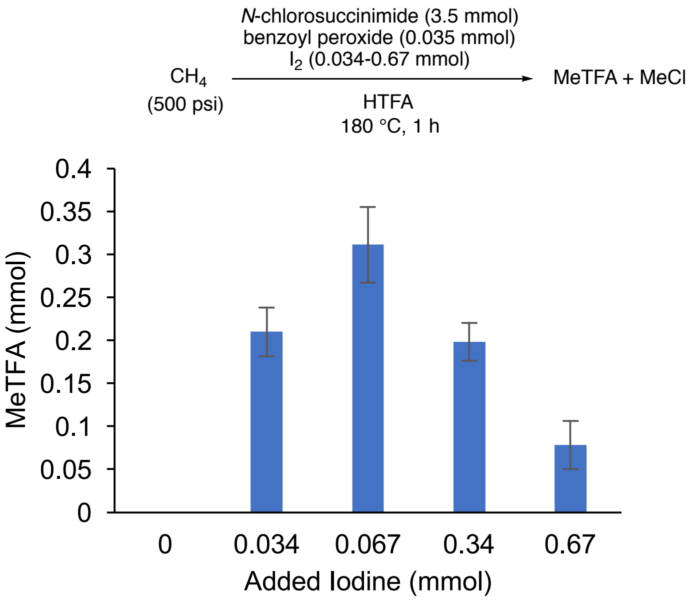

Figure 2.10. Radical chlorination of methane in the presence of added iodine produces MeTFA and MeCl. MeCl production was not quantified due to overlap in the ^{1}H NMR spectrum with the peak for succinimide with that of MeCl. Error bars denote standard deviations based on at least three experiments.

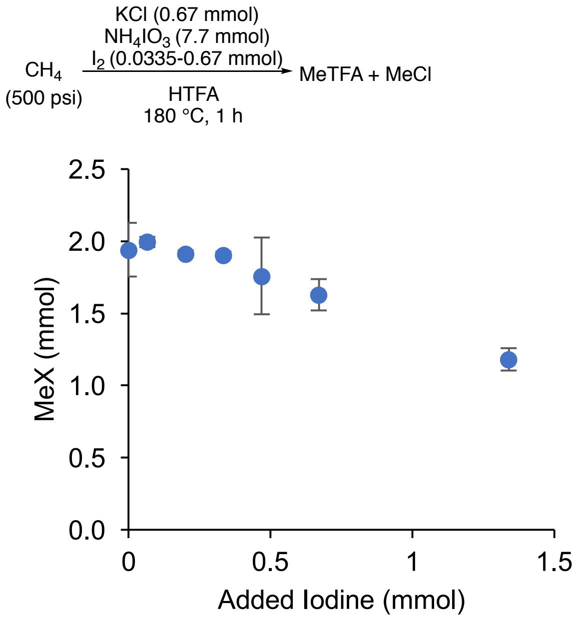

Figure 2.11. Addition of iodine to methane functionalization reaction with KCl (0.67 mmol) and NH_4IO_3 (7.7 mmol) in HTFA for 1 h at 180 °C yields MeTFA and MeCl. Error bars denote standard deviations based on at least three experiments.

The stability of MeTFA was also tested under chlorination conditions to determine if the protection effect observed in the iodate/chloride reactions was transferable to a radical-based functionalization process. Similar to the previously described MeTFA decay studies for the iodate/chloride functionalization process, MeTFA was heated in the presence of NCS and benzoyl peroxide at 180 °C for 1 h (Scheme 2.12). MeTFA is relatively stable under these chlorination conditions, with 83% remaining after 1 h at 180 °C, indicating that the protection of the TFA ester is not limited to the iodate/chloride process.

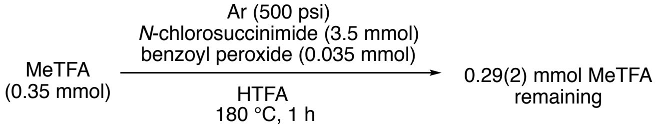

Scheme 2.12. Stability of MeTFA under chlorination conditions with NCS and benzoyl peroxide in HTFA. The amount of MeTFA remaining is given as an average with the standard deviation based on at least three experiments.

To compare the model studies using adamantane, which revealed statistically identical 3°:2° selectivities and kinetic isotope effects for iodate/chloride versus chlorination by NCS/benzoyl peroxide (Schemes 2.3 and 2.4), to light alkane functionalization the partial oxidation of propane using either iodate/chloride or chlorination by NCS/benzoyl peroxide was studied at 120 °C for 30 min (Scheme 2.13). The lower temperature and short reaction time were used in order to minimize production of di-functionalized products, which were not used to calculate the selectivity for mono-functionalized products as the order in which functionalization occurred is unknown. In the case of propane, the selectivity for 2°:1° functionalization differed between the two functionalization methods. The ratios of 2°:1° functionalization of a per-hydrogen basis were 17.0(8):1 and 5.6(6):1 for iodate/chloride and NCS/benzoyl peroxide, respectively. This finding is indicative that the iodate/chloride process could involve intermediates other than chlorine radicals, which led to computational studies of the reaction mechanism (see Section 2.3).

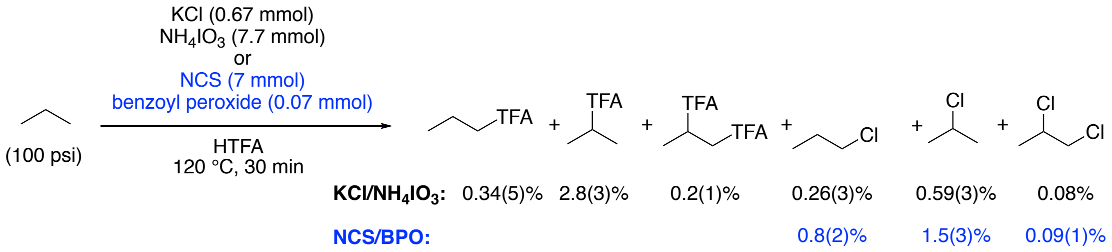

	2° : 1° Selectivity
KCl/NH_4IO_3	17.0(8) : 1
NCS/benzoyl peroxide	5.6(6) : 1

Scheme 2.13. Functionalization of propane with KCl/NH_4IO_3 or *N*-chlorosuccinimide/benzoyl peroxide in HTFA, with yields of functionalized products and the ratio of 2°:1° products on a per-hydrogen basis. Yields are calculated with respect to propane and are given as the average of three experiments with the standard deviation. Di-functionalized products are not included in the calculation of 2°:1° selectivity.

2.2.6 Solvent Effects on the OxE Process

The effect of changing the reaction solvent for the OxE process was described in the initial report by Fortman and coworkers where HTFA, perfluorobutyric acid, and acetic acid (HOAc) were shown to produce the corresponding methyl esters from methane with KCl and NH_4IO_3, whereas H_2SO_4 and H_2O led to only trace mono-functionalization of methane.[1] However, recent UV-vis analysis indicates that potential reactive intermediate Cl_2 as well as interhalogens ICl/ICl_3 are not produced from the combination of KCl and NH_4IO_3 in HOAc (Figure 2.12). This discrepancy led to further experimental analysis regarding the functionalization of light alkanes in HOAc. Recent data demonstrate that the formation of methyl acetate (MeOAc) under OxE conditions with methane is the result of solvent oxidation rather than methane functionalization. Statistically identical yields of MeOAc are obtained when pressurizing a HOAc solution of KCl and NH_4IO_3 with either methane or argon (Scheme 2.14). Additionally, the reaction of perprotiomethane with KCl and NH_4IO_3 in acetic acid-*d*$_4$ was shown to produce the fully deuterated product,

$CD_3CO_2CD_3$, by GC-MS (Scheme 2.15). This fully deuterated derivative of MeOAc accounted for > 90% of MeOAc production, while the product from methane functionalization $CD_3CO_2CH_3$, accounted for < 2% of the MeOAc product. Further, this provides a rationale for the formation of MeOAc in the ethane functionalization reaction in HOAc (Scheme 2.7). These findings are consistent with the UV-vis analysis indicating that the reactive species required for OxE alkane functionalization are not produced in HOAc, likely because of its decreased acidity relative to HTFA.

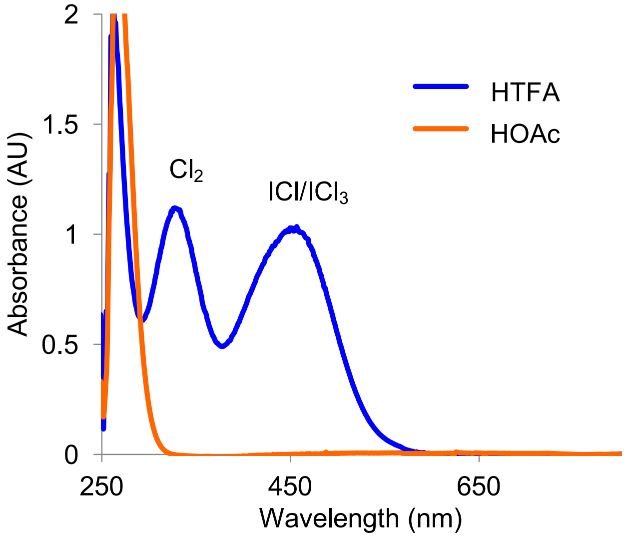

Figure 2.12. UV-Vis spectra of mixtures of KCl (0.10 mmol) and NH_4IO_3 (1 mmol) in 3 mL HTFA or HOAc.

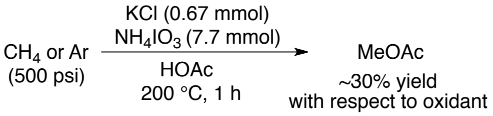

Scheme 2.14. Reaction of either methane or argon under OxE conditions with KCl/NH_4IO_3 in HOAc generates equivalent amounts of MeOAc.

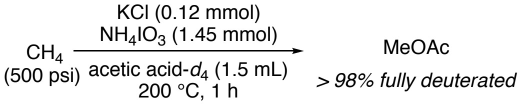

Scheme 2.15. Reaction of perprotiomethane with KCl/NH_4IO_3 in acetic acid-d_4.

Water often serves as a hindrance for traditional alkane functionalization processes which can require superacidic solvents.[28] While the OxE process is minimally active in neat H_2O,[1] water should be generated as iodate is reduced during the reaction. To determine how much water is produced during the OxE reaction, a calibration curve was first generated by monitoring the shift of the ^1H NMR resonance for a series of DTFA/H_2O mixtures using methylene chloride as an internal standard. As the concentration of water increases, the resonance shifts further upfield (Figure 2.13). Subsequently the methane functionalization reaction using KCl and NH_4IO_3 was performed in neat DTFA. After the reaction, the reaction mixtures were analyzed by ^1H NMR spectroscopy using methylene chloride as the internal standard in order to utilize the calibration curve. For all three replicates, the resonance for HTFA was observed from δ 10.32-10.33 ppm, which corresponds to the generation of ~1.6 mmol H_2O. This amount corresponds to a 28% yield of H_2O based on the starting amount of iodate, where 100% yield of H_2O would be achieved through the formation of three equivalents of H_2O per equivalent of iodate. Thus, there is experimental support for the formation of water during the OxE process, indicating that dilution of HTFA does not prohibit light alkane functionalization under these conditions, in contrast with other catalysts that require superacidic solvent to achieve reasonable rates.[28]

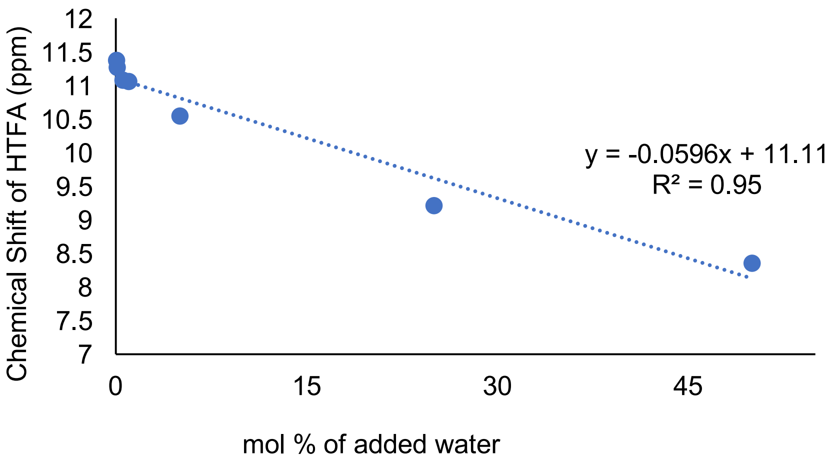

Figure 2.13. Calibration curve for the relationship of the chemical shift of the ^{1}H NMR resonance of HTFA in ppm to the mol% of added water to a DTFA solution.

2.2.7 Computational Study of the OxE Mechanism

The experimental data are consistent with the possibility of a radical-based functionalization mechanism, and computational studies using density functional theory (DFT) were performed to give further insight into the reaction mechanism. Computational modeling predicts that $IO_2Cl_2^-$ and $IOCl_4^-$ are likely formed as transient intermediates in the OxE process. Calculations also indicate that both of these species result in the formation of $IO_2\cdot$ and $Cl\cdot$ radicals (Scheme 2.16), both of which are predicted to be capable of H-atom abstraction from methane under OxE reaction conditions (Scheme 2.17).

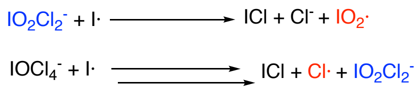

Scheme 2.16. Predicted intermediates that could generate $IO_2\cdot$ and $Cl\cdot$ radicals capable of H-atom abstraction from methane.

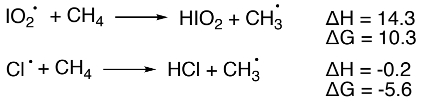

Scheme 2.17. DFT calculations of ΔH and ΔG for H-atom abstraction from methane by IO_2 radical and chlorine radical.[5] Values are given in kcal/mol.

The potential for $IO_2\cdot$ generation and activity in H-atom abstraction could explain the differences in the selectivity studies between adamantane and propane with iodate/chloride and NCS/benzoyl peroxide. Either $IO_2\cdot$ and $Cl\cdot$ could react with the starting alkane substrate to produce alkyl radicals, which are in turn likely trapped by iodine that is produced *in situ* from the reduction of iodate to give alkyl iodides, which have been shown experimentally to convert rapidly to alkyl esters in HTFA. These alkyl esters are protected from over-oxidation, which has also been modeled computationally. Computational and experimental findings are in good agreement with this proposed reaction pathway.

2.2.8 Protection of Alkyl Esters against Over-Oxidation

The minimal over-oxidation of alkyl ester products of the OxE process was a major focus of these mechanistic studies. Although the bond dissociation energy of the C–H bond of MeTFA is predicted to be 2.3 kcal/mol weaker than that of methane,[5] the reaction of MeTFA under reaction conditions is relatively slow (Figure 2.6). Moreover, the reaction rate of OxE of propane has been demonstrated to vary inversely as a function of the C–H bond energy through the propane selectivity studies as the weaker internal C–H bond reacts more rapidly than the stronger terminal C–H bond.[1, 11] The OxE reaction favors production of the internal product, 2-trifluoroacetylpropane, over the terminal product, 1-trifluoroacetylpropane. Thus, we first proposed that the process does not involve homolytic C–H bond breaking. However, some data are consistent with homolytic C–H cleavage.

Our data indicate the possibility that the OxE process involves C–H abstraction by free radicals, yet the oxidation of MeTFA appears to be quite a bit slower than the oxidation of methane. Generally, relative rates of homolytic cleavage of different C–H bonds are considered to depend primarily on the different C–H BDEs with weaker C–H bonds reacting more rapidly than stronger C–H bonds. However, other factors can certainly impact the rates of homolytic C–H bond cleavage including the position of the transition state (*i.e.*, early versus late transition state), steric effects, the nucleophilicity or electrophilicity of the radical species, electron delocalization, and the polarity of the transition state.[29] The OxE process occurs in the polar solvent HTFA. Hence, it is anticipated that the polarity of the transition state for C–H cleavage might influence the activation barrier. Thus, we propose that the unique stability of MeTFA is likely due to a polar effect, which was originally described by Walling et al.[30]

In effect, the ester moiety has a more nuanced influence on the rate of C–H abstraction from alkyl esters than just the impact on the C–H bond energy by stabilization of the CH_2TFA radical. Although the nature of the polar effect and its implications regarding the OxE process are not yet entirely understood, the TFA group may reduce the polarity of the transition state for H-atom abstraction. For example, a comparison of the transition states for H-atom abstraction for methane and MeTFA by chlorine radical ($H_3C\cdots H\cdots Cl$ vs. $TFA–C(H)_2\cdots H\cdots Cl$) shows that the transition state for H-atom abstraction from MeTFA could be much less polar due to the C→Cl and C→TFA dipoles partially cancelling. In the polar solvent HTFA, a decrease in the polarity of the transition state for C–H cleavage of MeTFA could result in an increase in the activation barrier for H-atom abstraction relative to that of the starting alkane.[29] Strongly electron-withdrawing moieties have recently been calculated by DFT to have a significant effect (~10 kcal/mol) on barriers for abstraction of H-atoms by chlorine atoms.[31] Therefore, the stability of MeTFA under OxE conditions could potentially be extended to other radical-based functionalization processes beyond our iodate/chloride process.

2.3 Conclusions

Combined experimental and computational studies support the proposed hypothesis that the OxE process operates through a radical-based pathway. $IO_2\cdot$ and Cl· radicals are calculated to be likely reactive intermediates generated *in situ* from the combination of chloride and iodate in HTFA solvent capable of H-atom abstraction from the light alkane substrate. A simplified overview of the proposed mechanism is shown in Scheme 2.18, wherein the catalytic nature of chloride is highlighted. Under reaction conditions, as observed by UV-vis spectroscopy, Cl_2 forms *in situ* and is likely homolytically cleaved to give chlorine radicals, which in addition to $IO_2\cdot$, are predicted to abstract an H-atom from the alkane substrate to generate an alkyl radical. The alkyl radical is then trapped by iodine, formed *in situ* through the reduction of the iodate oxidant to give alkyl iodide species. In HTFA, alkyl iodides readily undergo solvolysis to produce the protected alkyl esters (*e.g.*, MeTFA). These alkyl esters can be hydrolyzed to give alcohols, thus the OxE process is a candidate for the highly sought-after gas-to-liquid technologies for the conversion of methane to methanol.

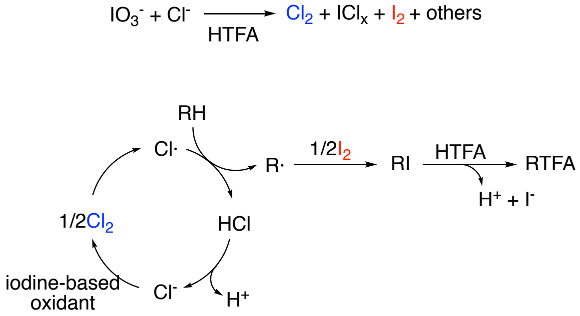

Scheme 2.18. Overview of the proposed mechanism for alkane oxidation by the OxE process, demonstrating the catalytic nature of chloride. Potential H-atom abstraction by $IO_2\cdot$ is omitted for clarity.

Alkyl esters, produced through the iodine trapping pathway, are favored in the OxE process relative to alkyl chlorides which would be generated if alkyl radicals are trapped by chlorine radicals. This preference for alkyl esters enables the remarkable selectivity and yields of the OxE process as the alkyl esters are protected against over-oxidation, unlike alkyl chlorides. In fact, the propensity for alkyl chlorides to be over-oxidized is one of the major limitations of oxychlorination chemistry. Through the selective production of alkyl esters, the OxE process is able to functionalize light alkanes in high yield with high selectivity. The fundamental advancement of this work is the elucidation of a selective radical-based pathway for the partial oxidation of hydrocarbons through the generation of protected products.

2.4 Future Directions

The OxE process demonstrates that light alkanes can be selectively oxidized to mono-functionalized products using a reaction pathway that likely involves homolytic C–H bond cleavage by free radical intermediates. Notably the C–H bonds of MeTFA are weaker than those of methane but are significantly less reactive. This is quite unique as weaker C–H bonds of alkane partial oxidation products have long thought to be a non-starter for processes that involve C–H bond breaking by free radical intermediates. Experimental and computational studies indicate that the OxE process operates by H-atom abstraction and requires the use of an oxidant to generate these species. Although this has not yet been studied, the polar nature of the solvent might be important to the ester protecting effect since H-bonding between the ester group and the protic solvent could play a role. Future experiments are being designed to address this question. For example, we are now working with the group of Zili Wu (Oak Ridge National Lab) to prepare gas flow reactors and study the relatives rate of alkane and alkyl ester oxidation.

Importantly, our new understanding of the iodate/chloride alkane oxidation suggests that the OxE process should not be limited to the use of iodate as the oxidant or to chloride as an H-atom abstraction source. That is, the key element is the ester protection. Therefore, moving forward, this process will be extended to other oxidant systems, namely to metal oxides that have been demonstrated to functionalize light alkanes but have heretofore suffered from poor selectivity for mono-functionalized products. This low selectivity is a result of the radical-based mechanism which favors functionalization of weaker C–H bonds. The use of a polar solvent and a protecting group could enable productive use of these heterogeneous catalysts. The generation of protected products which can be hydrolyzed to generate desired alcohols could revitalize the field of metal oxide catalyzed light alkane functionalization and enable high yields and selectivity for mono-functionalized products.

Although the OxE process has been an advancement in the field, enabling high yields and selectivities for light alkane oxidation, several challenges must be overcome to permit commercialization of the process. First, although the thermodynamics of the oxidation of iodate to iodine with oxygen are favorable, unfavorable kinetics have prevented facile recyclability of the iodate oxidant. To be a potential commercial route, the OxE process must be adapted to utilize an oxidant which can easily be recycled from air. Chapter 4 describes the extension of this work to other oxidant systems.

Furthermore, the OxE process is limited by solvent over-oxidation. Although over-oxidation of the alkane substrate and alkyl ester products is minimal, oxidant is wasted as

HTFA is oxidized under reaction conditions. Future efforts will focus on transitioning the OxE process to less corrosive and easily oxidizable solvents, such as certain ionic liquids, supercritical carbon dioxide and perfluorinated solvents.

2.5 Experimental Section

General Considerations. *Caution: Many of the reagents and conditions described herein are potentially hazardous.*[32] *Safety procedures should be consulted prior to the use of concentrated acids, mixtures of hydrocarbons and oxygen and strong oxidants.*

Unless noted otherwise, all reactions were performed under ambient atmosphere. All chemicals were purchased from commercial sources, and other than *N*-chlorosuccinimide, all were used as received. *N*-Chlorosuccinimide was recrystallized from acetic acid prior to use. Gases were purchases from GTS-Welco and were used as received. Standards of adamantyl ester products were synthesized according to published literature methods from commercially available alcohols.[33] NMR analysis was performed using a Bruker 300 Avance, Avance III 800, Avance III 600 or Avance DRX-600 or a Varian 500 spectrometer. NMR spectra of reaction mixtures from the functionalization of methane, ethane and propane were obtained using neat HTFA or HOAc with a C_6D_6 capillary as an internal lock reference. Nitromethane or dichloromethane were added as internal standards and used to reference ^{1}H NMR spectra (δ 4.18 and 2.04, respectively). UV-vis spectra were obtained using a Carey Varian Bio 300 UV-vis spectrophotometer. GC-MS analysis was performed using a Shimadzu GC-MS-QP2010 Plus system with a 30 m × 0.25 mm SHRXI-5MS column with a 0.25 μ thickness using electron impact ionization or an Agilent Technologies 7890A gas chromatograph equipped with a fused silica column and electron impact mass analyzer. High pressure reactions were performed in custom-built Swagelok stainless steel reactors.

General Procedures

Conversion of Adamantyl Esters in Acid. A custom-built stainless-steel reactor with a Teflon liner[1, 10] was charged with a stir bar, secondary adamantyl ester (trifluoroacetate or acetate) and corresponding acid (4 mL, HTFA or glacial HOAc). The reactor was sealed and pressurized with 100 psi of argon. After stirring at 800 rpm and heating at 180 °C for 15 min, the reactor was allowed to cool to room temperature. After venting, nitromethane was added as an internal standard, and the reaction mixture was stirred. Then, 5 mL of dichloromethane were added. The reaction mixture was washed with water (2 × 10 mL) and the organic washings were dried over $MgSO_4$ before they were analyzed by GC-MS. Each condition was run in triplicate.

Oxidation of Adamantane Using Potassium Chloride and Ammonium Iodate in Acetic or Trifluoroacetic Acid. An 8 mL microwave vial was charged with a stir bar, ammonium iodate (1 mmol), adamantane (1 mmol) and potassium chloride (0.15 mmol). Neat acid (4 mL) was added and the vial was sealed with a crimp cap. The reaction was heated in an oil bath at 180 °C for 1 h with 1150 rpm stirring. After 1 h, the vial was allowed to cool to room temperature and a solution of dodecane (1 mmol) in chloroform (5 mL) was added as an internal standard. The mixture was extracted twice with 10 mL H_2O and the organic washings were dried over $MgSO_4$. The product mixture was analyzed by GC-MS. Each condition was repeated a minimum of three times with the average of all reactions reported.

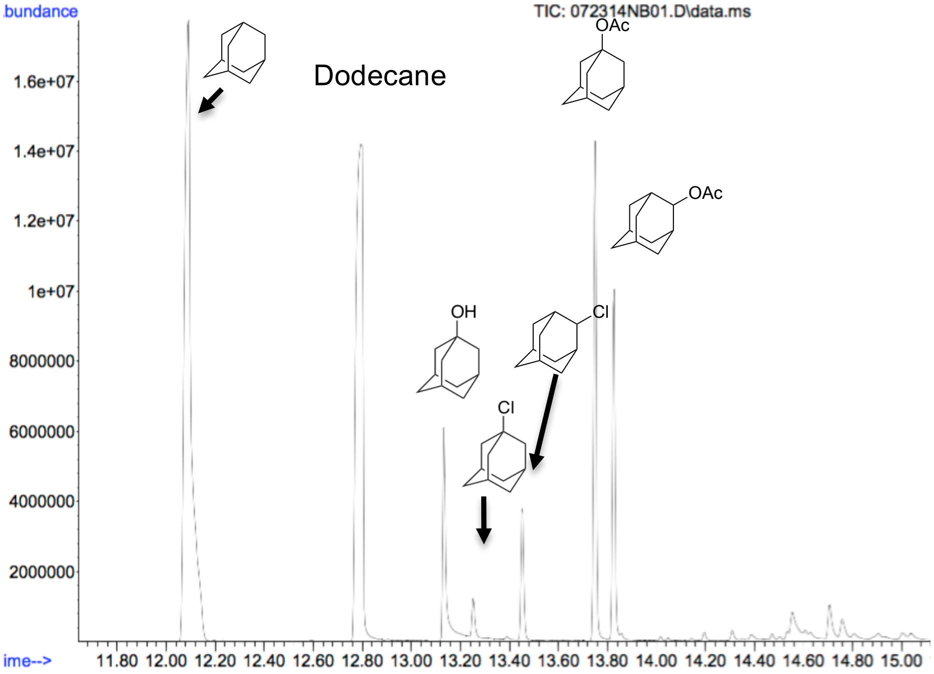

Figure 2.14. GC-MS trace of adamantane functionalization by KCl/NH_4IO_3 in HOAc. Conditions: Adamantane (1 mmol), KCl (0.15 mmol), NH_4IO_3 (1 mmol), HOAc (4 mL), 180 °C, 1h.

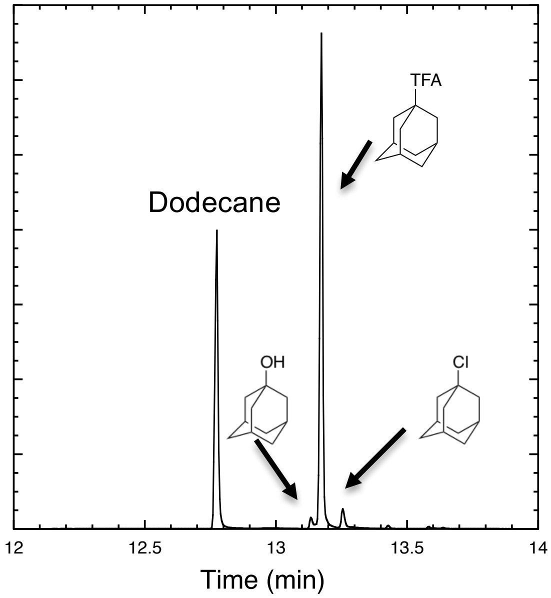

Figure 2.15. GC-MS trace of adamantane functionalization with KCl/NH_4IO_3 in HTFA. Conditions: Adamantane (1 mmol), KCl (0.15 mmol), NH_4IO_3 (1 mmol) HTFA (4 mL), 100 °C, 1 h. Dodecane (1 mmol) was added as an internal standard after the reaction.

Chlorination of Adamantane with *N*-Chlorosuccinimide and Benzoyl Peroxide. Adamantane chlorination was performed according to a literature procedure.[34] An 8 mL microwave vial was charged with a stir bar, adamantane (1 mmol), *N*-chlorosuccinimide (1 mmol) and benzoyl peroxide (0.01 mmol, as a radical initiator), and was then sealed with a crimp cap with a Teflon septum. The vial was flushed with argon for 20 min. Glacial acetic acid was degassed by refluxing under argon for 1 h before being added to the vial. The reaction was subsequently heated to 180 °C for 1 h in an oil bath stirring at 1150 rpm. After 1 h, the reaction mixture was allowed to cool to room temperature and a solution of dodecane (1 mmol) in chloroform (5 mL) was added as an internal standard. The mixture was extracted twice with 10 mL H_2O and the organic washings were dried over $MgSO_4$. The product mixture was analyzed by GC-MS. Each condition was repeated a minimum of three times with the average of all reactions reported.

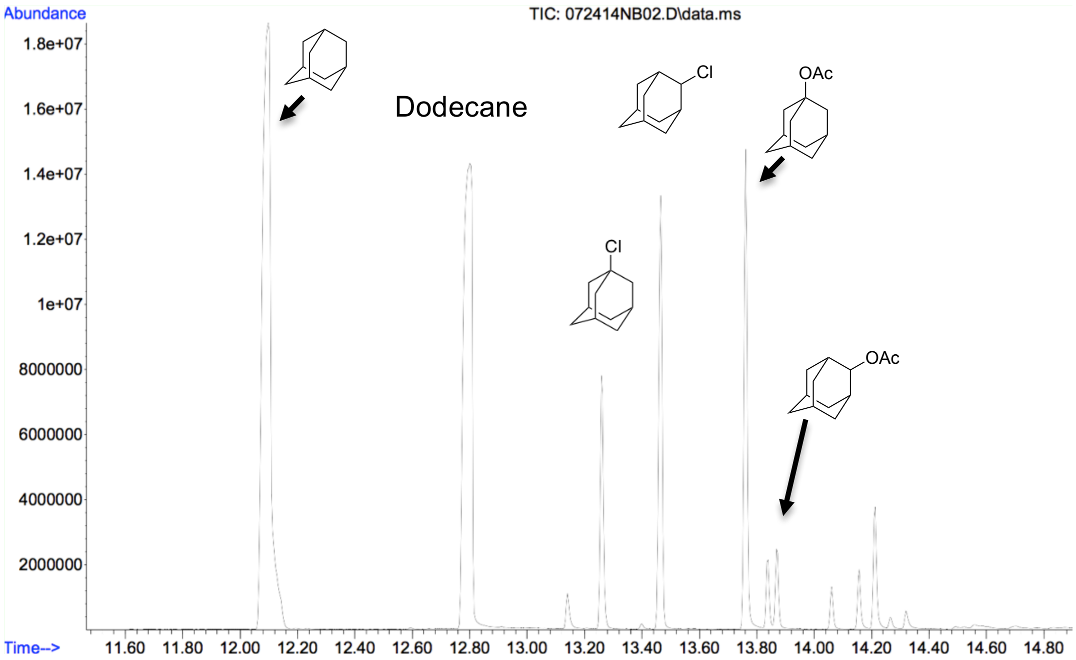

Figure 2.16. Sample GC-MS trace of adamantane functionalization by *N*-chlorosuccinimide/benzoyl peroxide in HOAc. Conditions: Adamantane (1 mmol), *N*-chlorosuccinimide (0.5 mmol), benzoyl peroxide (0.01 mmol), HOAc (4 mL), 180 °C, 1 h.

Determination of Intermolecular KIE for the Functionalization of Adamantane by KCl/NH_4IO_3 and *N*-Chlorosuccinimide/Benzoyl Peroxide. Intermolecular KIEs for functionalized adamantyl products were determined using a 1:1 stoichiometric ratio of perprotioadamantane and perdeuteroadamantane (0.5 mmol each). The oxidant loading was reduced to 20 mol% relative to the substrate to ensure that conversion remained below 20%. The intermolecular KIE was then obtained using the ratio of protio to deutero product by GC-MS. The KIE is reported as the average of at least three individual experiments with the standard deviation.

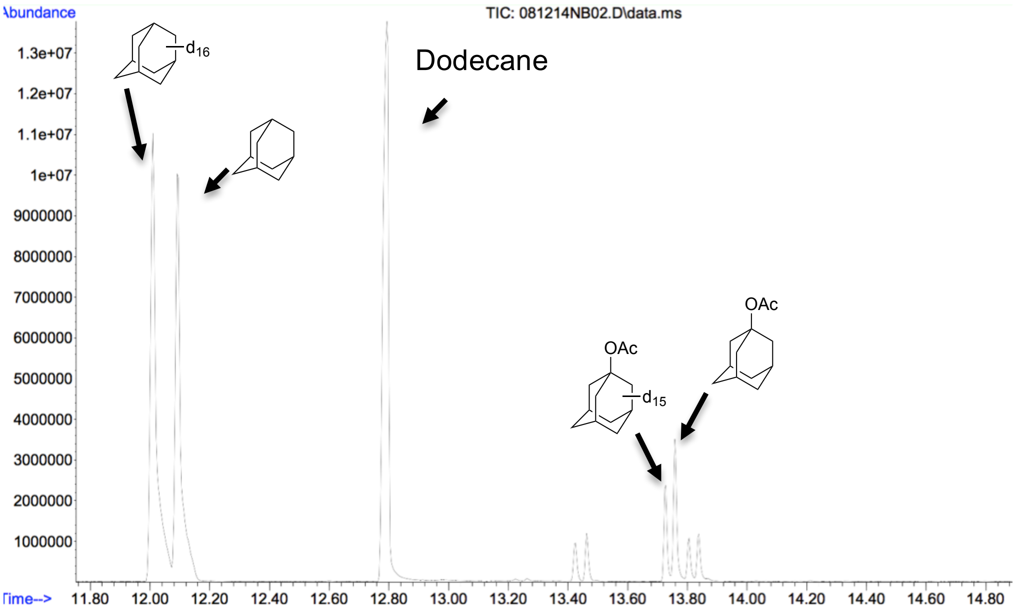

Figure 2.17. GC-MS trace of adamantane/adamantane-d_{16} (1:1) functionalization by KCl/NH_4IO_3 (1:1) in HOAc. Conditions: Adamantane (0.5 mmol), adamantane-d_{16} (0.5 mmol), KCl (0.15 mmol), NH_4IO_3 (0.2 mmol), HOAc (4 mL), 180 °C, 1 h.

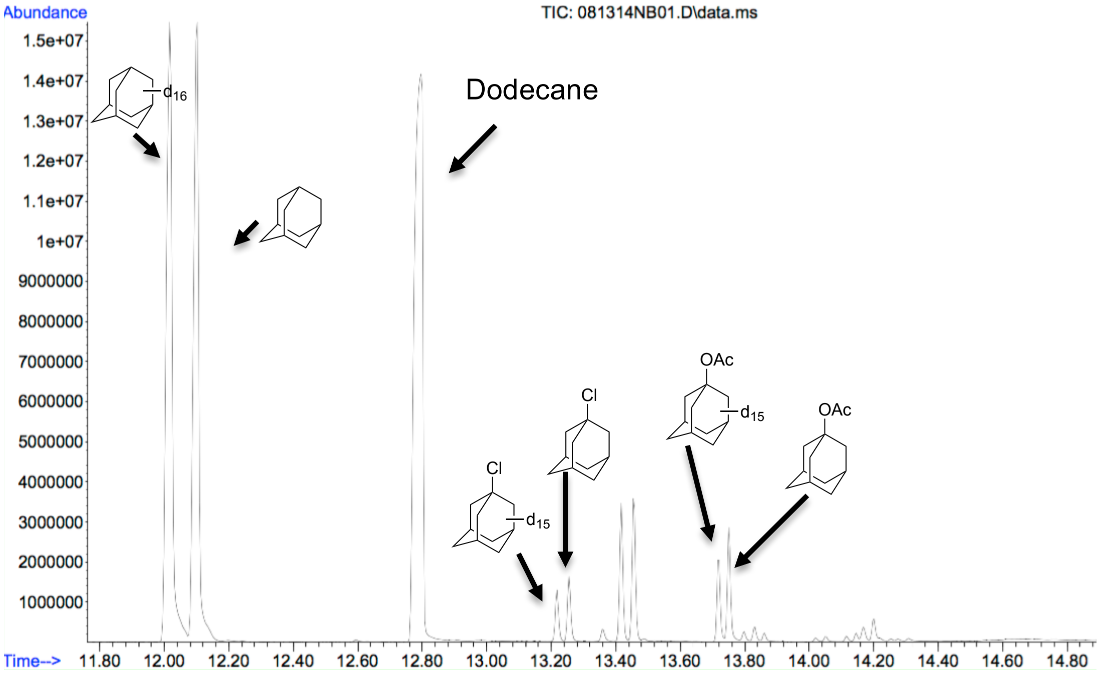

Figure 2.18. GC-MS trace of adamantane/adamantane-d_{16} (1:1) functionalization by *N*-chlorosuccinimide/benzoyl peroxide in HOAc. Conditions: Adamantane (0.5 mmol), adamantane-d_{16} (0.5 mmol), *N*-chlorosuccinimide (0.2 mmol), benzoyl peroxide (0.01 mmol), HOAc (4 mL), 180 °C, 1 h.

Synthesis of *tert*-Butyl Peroxypropionate. The compound was synthesized by adapting the procedure reported by Yur'ev and coworkers.[35] A 100 mL round-bottom flask was charged with a stir bar, $CDCl_3$ (5 mL) and propionic acid (5 mmol). The reaction flask was cooled to 0 °C, and pyridine (5 mmol) was added dropwise to the vigorously stirring solution. The solution continued to stir for 15 min at 0 °C. *Tert*-butyl hydroperoxide (3 mmol) and pyridine (5 mmol) were then added dropwise to the stirring solution. After an additional 45 min of stirring, the reaction mixture was allowed to warm to room temperature. The reaction mixture was washed with a saturated solution of sodium bicarbonate (3 × 5 mL) and 1 M HCl (2 × 5 mL) and the organic washings were then dried over $MgSO_4$. The solution was concentrated under vacuum behind a blast shield to yield the desired compound. ^{1}H NMR ($CDCl_3$, 300 MHz, δ): 2.27 (q, $CH_3CH_2CO_3C(CH_3)_3$, $^3J_{HH}$ = 8 Hz, 2 H), 1.13 (t, $CH_3CH_2CO_3C(CH_3)_3$, $^3J_{HH}$ = 8 Hz, 3H). ^{13}C NMR ($CDCl_3$, 125 MHz, δ): 172.1 ($CH_3CH_2CO_3C(CH_3)_3$), 83.6 ($CH_3CH_2CO_3C(CH_3)_3$), 26.4 ($CH_3CH_2CO_3C(CH_3)_3$, 25.0 ($CH_3CH_2CO_3C(CH_3)_3$), 9.5 ($CH_3CH_2CO_3C(CH_3)_3$).

Pyrolysis of *tert*-Butyl Peroxypropionate in the Presence of Iodine. A J. Young NMR tube was charged with *tert*-butyl peroxypropionate (0.1 mmol), iodine (0.05 mmol), cyclopentane (0.05 mmol, internal standard), and acetic acid-d_4 (1 mL). The NMR tube was sealed and heated at 180 °C in an oil bath for 1 h. After 1 h, the NMR tube was allowed to cool to room temperature and was analyzed by ^{1}H NMR. Ethyl iodide production was quantified relative to cyclopentane, and its identity was confirmed through the addition of a known standard of ethyl iodide. The reaction was repeated four times and the yield is reported as the average and standard deviation of those data.

Oxidation of Ethane with the OxE Process in Acetic Acid. A custom-built stainless-steel reactor with a Teflon liner[1, 10] was charged with a stir bar, KCl (0.67 mmol), NH_4IO_3 (7.7 mmol) and HOAc/Ac_2O (8 mL, 19:1 v/v). The reactor was sealed, purged with argon, and then pressurized with ethane to 300 psi. The reactor was heated at 180 °C for 1 h and stirred at 800 rpm. After the reaction, the reactor was allowed to cool to room temperature and was then carefully vented. Methylene chloride was added as an internal standard and the mixture stirred. An aliquot of the reaction mixture was centrifuged and analyzed by ^{1}H NMR spectroscopy. The yields are reported as an average of three trials with the standard deviations.

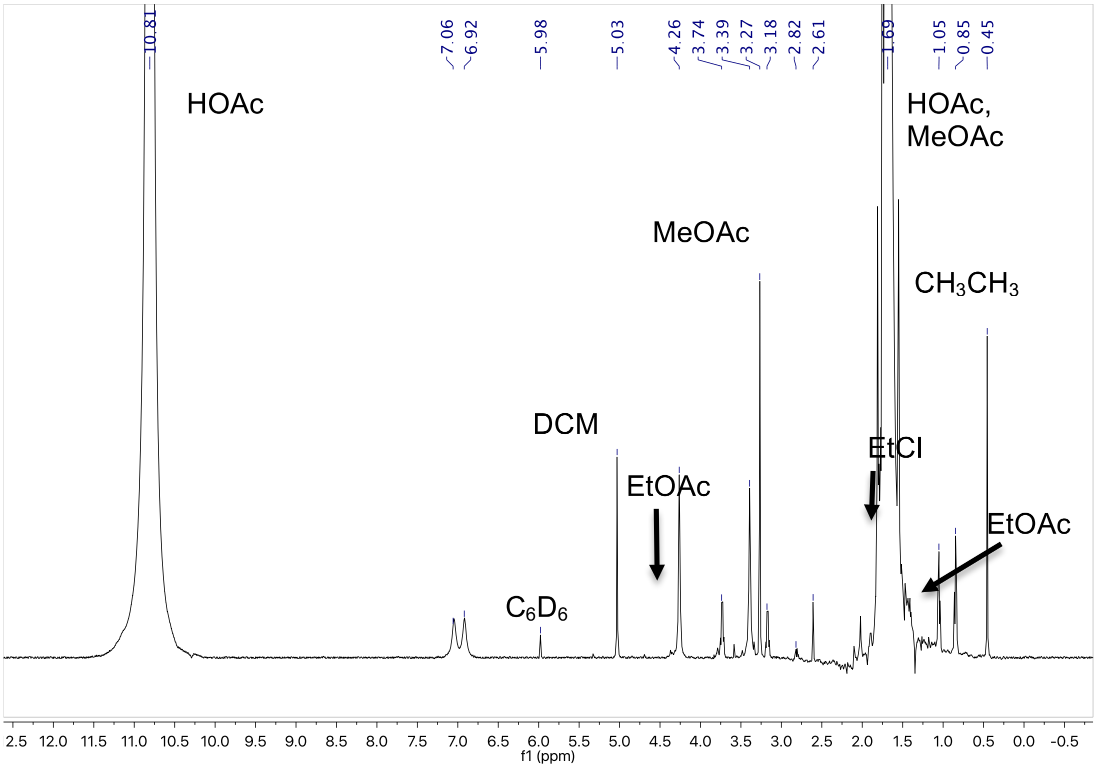

Figure 2.19. Representative ^{1}H NMR spectrum of the functionalization of ethane by KCl/NH_4IO_3 in HOAc/Ac_2O. Conditions: Ethane (300 psi, 14.3 mmol), KCl (0.67 mmol), NH_4IO_3 (7.7 mmol), HOAc/Ac_2O (8 mL, 19:1 v:v), 180 °C, 1 h. Dichloromethane (0.469 mmol) was added as an internal standard.

Consumption of Functionalized Products (RI and RTFA, R = Me, Et) under OxE Conditions. A custom-built stainless-steel reactor with a Teflon liner[1, 10] was charged with a stir bar, RI or RTFA (1 mmol, R = Me, Et), KCl (0.67 mmol), NH_4IO_3 (7.7 mmol) and HTFA (8 mL). The reactor was sealed and pressurized with 100 psi of argon. After the mixture was stirred at 800 rpm at 180 °C for 20 min, the reactor was allowed to cool to room temperature. The reactor was then vented carefully, and nitromethane was added as an internal standard. After stirring, an aliquot was removed for centrifugation. The supernatant was analyzed by ^{1}H NMR spectroscopy. This procedure was performed in triplicate.

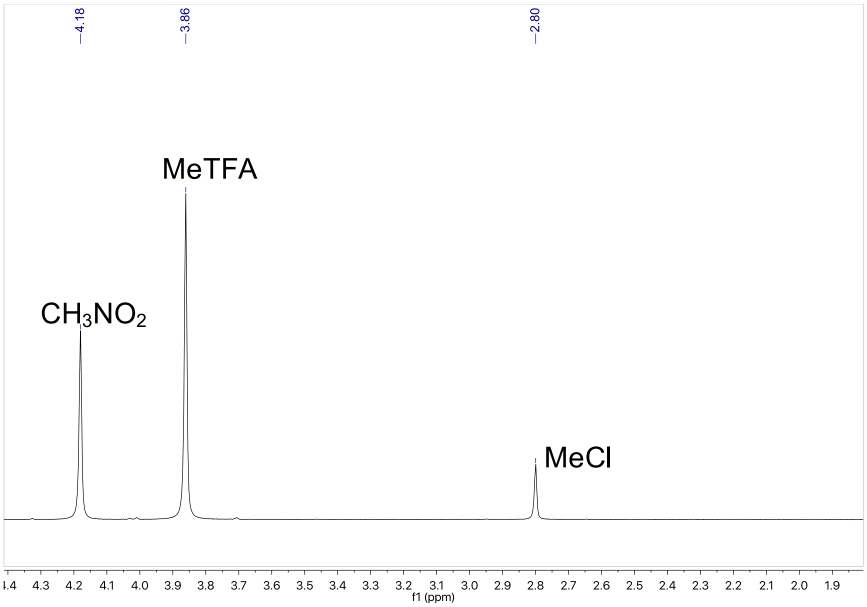

Figure 2.20. Representative ^{1}H NMR spectrum of the functionalization of methyl iodide by KCl/NH_4IO_3 in HTFA. Conditions: Argon (100 psi), MeI (1 mmol), KCl (0.67 mmol), NH_4IO_3 (7.7 mmol), 180 °C, 20 min. CH_3NO_2 (0.374 mmol) was added as an internal standard after the reaction. MeI has been fully consumed (MeI resonance: δ 1.91).

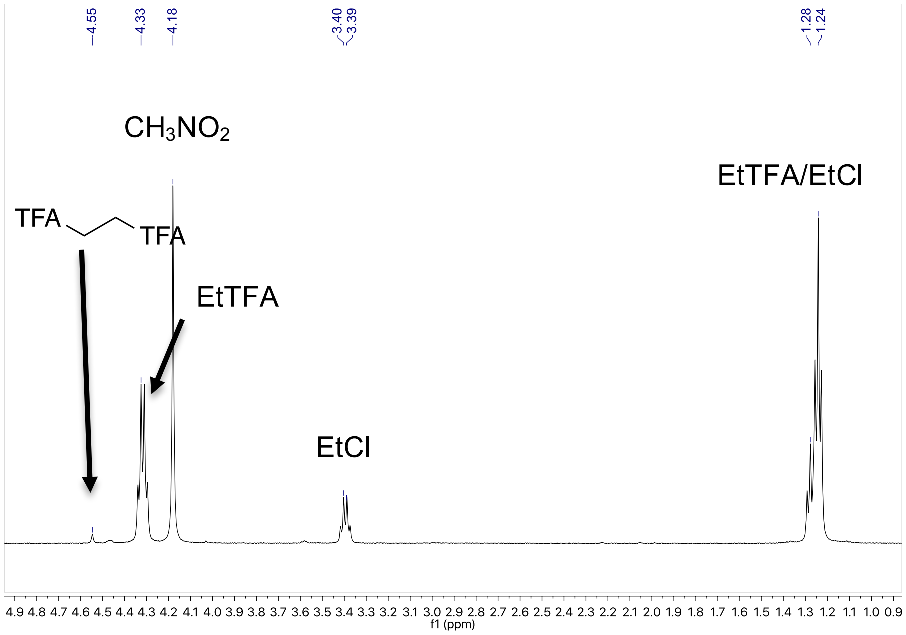

Figure 2.21. Representative ^{1}H NMR spectrum of the functionalization of ethyl iodide by KCl/NH_4IO_3 in HTFA. Conditions: Argon (100 psi), EtI (1 mmol), KCl (0.67 mmol), NH_4IO_3 (7.7 mmol), 180 °C, 20 min. CH_3NO_2 (0.374 mmol) was added as an internal standard after the reaction.

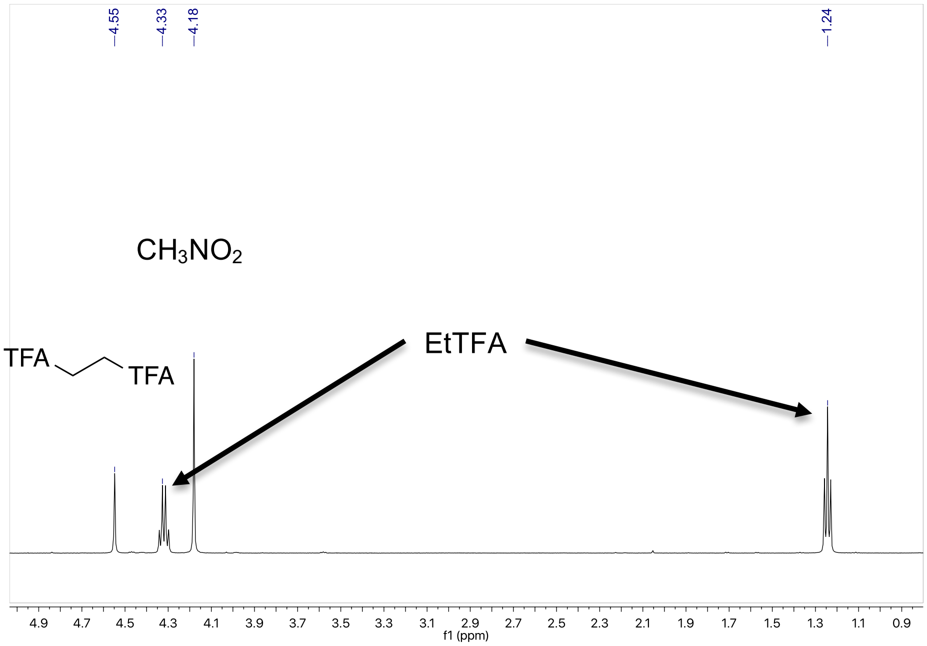

Figure 2.22. Representative ^{1}H NMR spectrum of the reaction of ethyl trifluoroacetate with KCl/NH_4IO_3 in HTFA. Conditions: Argon (100 psi), EtTFA (1 mmol), KCl (0.67 mmol), NH_4IO_3 (7.7 mmol), 180 °C, 20 min. CH_3NO_2 (0.374 mmol) was added as an internal standard after the reaction.

OxE of Methane or Ethane. A custom-built stainless-steel reactor with a Teflon liner[1, 10] was charged with a stir bar, KCl (0.67 mmol), NH_4IO_3 (7.7 mmol) and HTFA (8 mL). The reactor was sealed and pressurized with 100 psi of methane or ethane. After the mixture was stirred at 800 rpm at 140 °C for the desired amount of time, the reactor was allowed to cool to room temperature. The reactor was then vented carefully, and nitromethane was added as an internal standard. After stirring, an aliquot was removed for centrifugation. The supernatant was analyzed by ^{1}H NMR spectroscopy. This procedure was performed in triplicate.

MeTFA and EtTFA Decay under OxE Conditions. A custom-built stainless-steel reactor with a Teflon liner[1, 10] was charged with a stir bar, KCl (0.67 mmol), NH_4IO_3 (7.7 mmol), MeTFA (0.65 mmol) or EtTFA (1.51 mmol) and HTFA (8 mL). The reactor was sealed and pressurized with 100 psi of argon. After the mixture was stirred at 800 rpm at

140 °C for the desired amount of time, the reactor was allowed to cool to room temperature. The reactor was then vented carefully, and nitromethane was added as an internal standard. After stirring, an aliquot was removed for centrifugation. The supernatant was analyzed by ^{1}H NMR spectroscopy. This procedure was performed in triplicate.

Methane Oxidation with *N*-Chlorosuccinimide and Benzoyl Peroxide with or without Added Iodine. A custom-built stainless-steel reactor with a Teflon liner[1, 10] was charged with a stir bar, *N*-chlorosuccinimide (3.5 mmol), benzoyl peroxide (0.035 mmol), HTFA (8 mL) and iodine (0.0335, 0.067, 0.335, or 0.67 mmol, if added) in the glovebox. HTFA was refluxed under nitrogen for 1 h prior to being added to the reactor. The reactor was sealed and pressurized with 500 psi of methane. After stirring at 800 rpm and heating at 180 °C for 1 h, the reactor was allowed to cool to room temperature. The reactor was then vented carefully, and acetic acid was added as an internal standard. After stirring, an aliquot was removed for centrifugation. The supernatant was analyzed by ^{1}H NMR spectroscopy. This procedure was performed in triplicate.

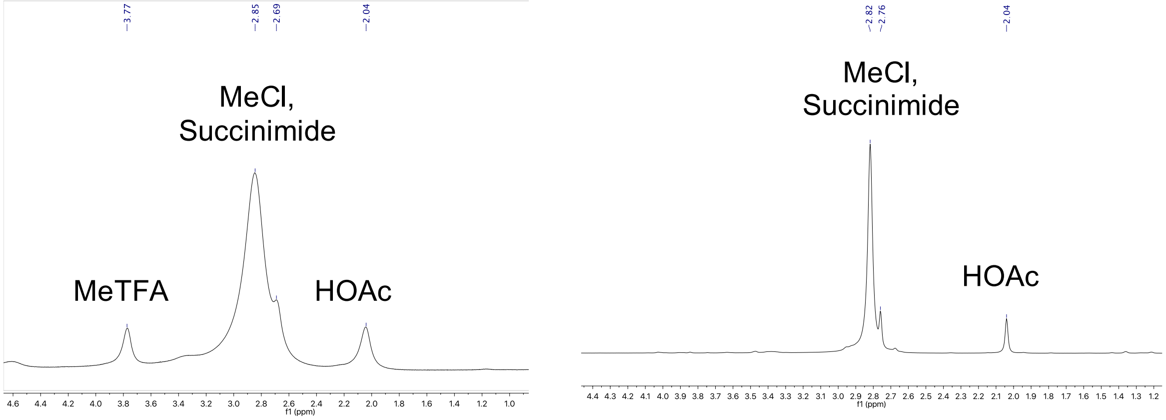

Figure 2.23. Representative ^{1}H NMR spectra of the functionalization of methane by *N*-chlorosuccinimide/benzoyl peroxide with (left) and without (right) added iodine. Conditions: Methane (500 psi), *N*-chlorosuccinimide (3.5 mmol), benzoyl peroxide (0.035 mmol), I_2 (left, 0 mmol; right, 0.067 mmol), HTFA (8 mL), 180 °C, 1 h. HOAc (0.35 mmol) was added as an internal standard following the reaction.

Iodine Addition to Methane OxE. A custom-built stainless-steel reactor with a Teflon liner[1, 10] was charged with a stir bar, KCl (0.67 mmol), NH_4IO_3 (7.7 mmol), I_2 (0-1.34 mmol) and HTFA (8 mL). The reactor was sealed and pressurized with 500 psi of methane. After the mixture was stirred at 800 rpm at 180 °C for 1 h, the reactor was allowed to cool to room temperature. The reactor was then vented carefully, and nitromethane was added as an internal standard. After stirring, an aliquot was removed for centrifugation. The supernatant was analyzed by ^1H NMR spectroscopy. This procedure was performed in triplicate.

Consumption of MeTFA under Radical Chlorination Conditions. A custom-built stainless-steel reactor with a Teflon liner[1, 10] was charged with a stir bar, *N*-chlorosuccinimide (3.5 mmol), benzoyl peroxide (0.035 mmol), HTFA (8 mL) and MeTFA (0.35 mmol) in the glovebox. HTFA was refluxed under nitrogen for 1 h prior to being added to the reactor. The reactor was sealed and pressurized with 500 psi of argon. After stirring at 800 rpm and heating at 180 °C for 1 h, the reactor was allowed to cool to room temperature. The reactor was then vented carefully, and acetic acid was added as an internal standard. After stirring, an aliquot was removed for centrifugation. The supernatant was analyzed by ^1H NMR spectroscopy. This procedure was performed in triplicate.

OxE of Propane. A custom-built stainless-steel reactor with a Teflon liner[1, 10] was charged with a stir bar, KCl (0.67 mmol), NH_4IO_3 (7.7 mmol) and HTFA (8 mL). The reactor was sealed and pressurized with 100 psi of propane. After the mixture was stirred at 800 rpm at 120 °C for 30 min, the reactor was allowed to cool to room temperature. The reactor was then vented carefully, and acetic acid was added as an internal standard. After stirring, an aliquot was removed for centrifugation. The supernatant was analyzed by ^1H

NMR spectroscopy. This procedure was performed in triplicate.

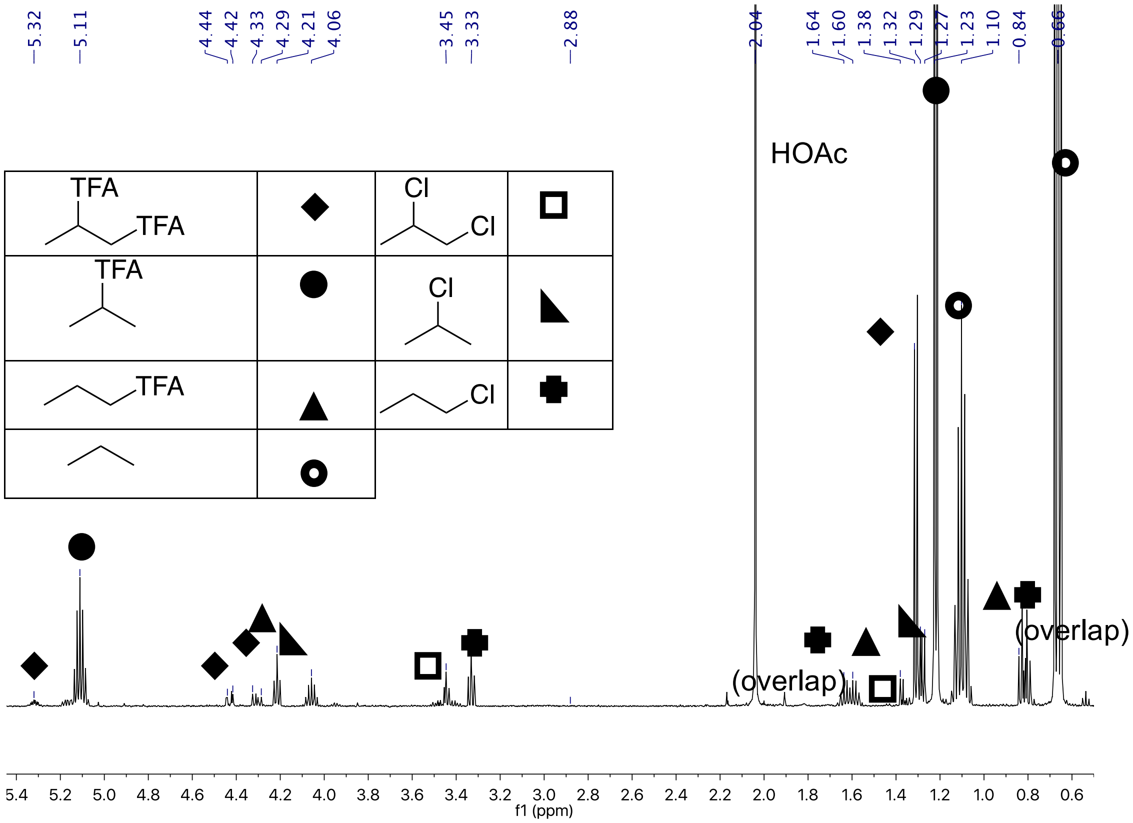

Figure 2.24. Representative ^{1}H NMR spectrum of the functionalization of propane by KCl/NH_4IO_3 in HTFA. Conditions: Propane (100 psi, ~9 mmol), KCl (0.67 mmol), NH_4IO_3 (7.7 mmol), HTFA (8 mL), 120 °C, 30 min. HOAc (0.35 mmol) was added as an internal standard following the reaction.

Oxidation of Propane with *N*-Chlorosuccinimide and Benzoyl Peroxide. A custom-built stainless-steel reactor with a Teflon liner[1, 10] was charged with a stir bar, *N*-chlorosuccinimide (7 mmol), benzoyl peroxide (0.07 mmol) and HTFA (8 mL) in the glovebox. HTFA was refluxed under nitrogen for 1 h prior to being added to the reactor. The reactor was sealed and pressurized with 100 psi of propane. After the mixture was stirred at 800 rpm at 120 °C for 30 min, the reactor was allowed to cool to room temperature. The reactor was then vented carefully, and acetic acid was added as an internal standard. After stirring, an aliquot was removed for centrifugation. The supernatant was analyzed by ^{1}H NMR. This procedure was performed in triplicate.

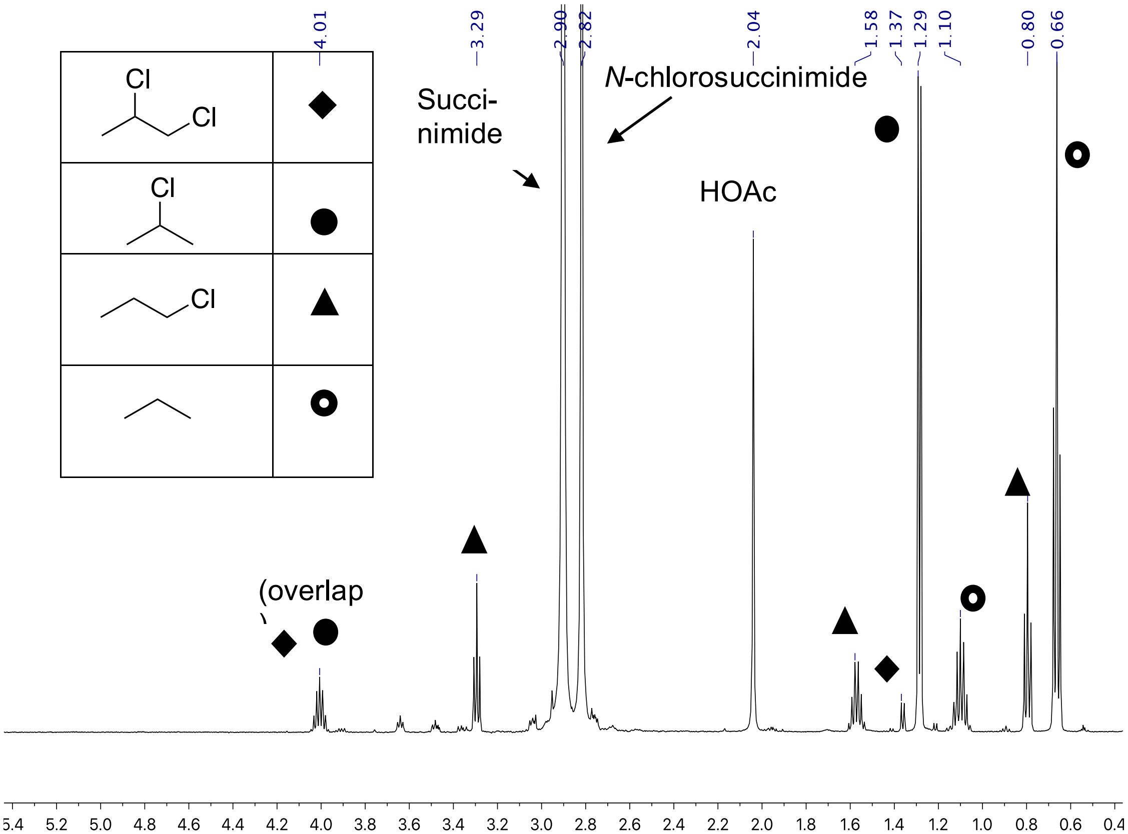

Figure 2.25. Representative ^{1}H NMR spectrum of the functionalization of propane by *N*-chlorosuccinimide/benzoyl peroxide in HTFA. Conditions: Propane (100 psi, ~ 9 mmol), *N*-chlorosuccinimide (7 mmol), benzoyl peroxide (0.07 mmol), HTFA (8 mL), 120 °C, 30 min. HOAc (0.35 mmol) was added as an internal standard following the reaction.

Acetic Acid as a Solvent for OxE. A custom-built stainless-steel reactor with a Teflon liner[1, 10] was charged with a stir bar, KCl (0.67 mmol), NH_4IO_3 (7.7 mmol) and HOAc (8 mL). The reactor was sealed and pressurized with 500 psi of methane or argon. After the mixture was stirred at 800 rpm at 200 °C for 1 h, the reactor was allowed to cool to room temperature. The reactor was then vented carefully, and nitromethane was added as an internal standard. After stirring, an aliquot was removed for centrifugation. The supernatant was analyzed by ^{1}H NMR spectroscopy. This procedure was performed in triplicate.

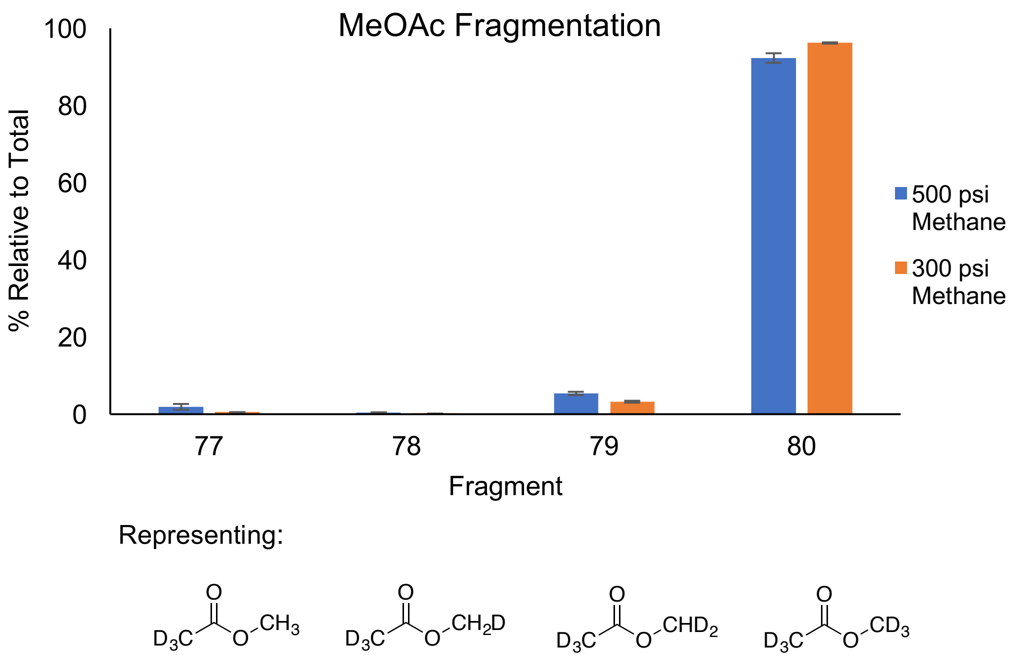

Figure 2.26. Ratio of m/z for MeOAc from the reaction of perprotio-methane in acetic acid-*d*$_4$. Conditions: Methane (300 or 500 psi), KCl (0.12 mmol), NH_4IO_3 (1.44 mmol), acetic acid-*d*$_4$ (1.5 mL), 200 °C, 1 h.

Calibration Curve for the Quantification of Water Production. A series of DTFA (99.5% D)/H_2O mixtures were prepared by serially diluting a 50 mol% H_2O and DTFA solution. Each was analyzed by ^1H NMR spectroscopy using a C_6D_6 capillary as a lock reference with dry dichloromethane as an internal standard, referenced to δ 5.03 ppm. The shifts of the HTFA resonances varied as function of the water concentration.

Methane OxE in DTFA. A custom-built stainless-steel reactor with a Teflon liner[1, 10] was charged with a stir bar, KCl (0.17 mmol), NH_4IO_3 (1.9 mmol) and DTFA (2 mL). The reaction was run in triplicate with each reaction using DTFA from the same ampule. The reactor was sealed and pressurized with 100 psi of methane. The reactions were heated at 180 °C for 1 h and stirred at 800 rpm. The reactions were worked up and analyzed as in the previously mentioned light alkane functionalization reactions using a C_6D_6 capillary as an internal lock reference. The calibration curve discussed above was used to determine the mol% of generated water on the basis of the chemical shift of the HTFA resonance. To determine the amount of water that was produced, the total volume of the mixture following the reaction was measured and used to calculate an amount using the calculated mol%.

2.6 References

1. Fortman, G. C.; Boaz, N. C.; Munz, D.; Konnick, M. M.; Periana, R. A.; Groves, J. T.; Gunnoe, T. B. *J. Am. Chem. Soc.* **2014**, *136*, 8393-8401.

2. Lin, R.; Amrute, A. P.; Pérez-Ramírez, J. *Chem. Rev.* **2017**, *117*, 4182-4247.

3. Golden, D. M.; Benson, S. W. *Chem. Rev.* **1969**, *69*, 125-134.

4. Barton, D. H. R.; Martell, A. E.; Sawyer, D. T. In *The Activation of Dioxygen and Homogeneous Catalytic Oxidation*, Fifth International Symposium on the Activation of Dioxygen and Homogeneous Catalytic Oxidation, College Station, TX, Barton, D. H. R.; Martell, A. E.; Sawyer, D. T., Eds. Springer Science and Business Media, LLC: College Station, TX, 1993.

5. Fu, R.; Nielsen, R. J.; Schwartz, N. A.; Goddard III, W. A.; Gunnoe, T. B.; Groves, J. T., DFT Mechanistic Study of Methane Monooxygenation by Hypervalent Iodine Alkane Oxidation (HIAO) Process. *Manuscript submitted* **2018**.

6. Konnick, M. M.; Hashiguchi, B. G.; Devarajan, D.; Boaz, N. C.; Gunnoe, T. B.; Groves, J. T.; Gunsalus, N.; Ess, D. H.; Periana, R. A. *Angew. Chem. Int. Ed.* **2014**, *53* (39), 10490-10494.

7. Periana, R. A.; Mirinov, O.; Taube, D. J.; Gamble, S. *Chem. Commun.* **2002**, (20), 2376-2377.

8. Gang, X.; Zhu, Y.; Birch, H.; Hjuler, H. A.; Bjerrum, N. J. *Appl. Catal., A* **2004**, *261* (1), 91-98.

9. Michalkiewicz, B.; Jarosinska, M.; Lukasiewicz, I. *Chem. Eng. J.* **2009**, *154* (1-3), 156-161.

10. Kalman, S. E.; Munz, D.; Fortman, G. C.; Boaz, N. C.; Groves, J. T.; Gunnoe, T. B. *Dalton Trans.* **2015**, *44*, 5294-5298.

11. Schwartz, N. A.; Boaz, N. C.; Kalman, S. E.; Zhuang, T.; Goldberg, J. M.; Fu, R.; Nielsen, R. J.; Goddard III, W. A.; Groves, J. T.; Gunnoe, T. B. *ACS Catal.* **2018**, *8*, 3138-3149.

12. Speight, J., *Lange's Handbook of Chemistry*. 17th ed.; McGraw-Hill: Boston, MA, 2016.

13. Koval, I. V. *Russ J Org Chem* **2002**, *38* (3), 301-337.

14. Smith, G. W.; Williams, H. D. *J. Org. Chem.* **1961**, *26* (7), 2207-2212.

15. Tabushi, I.; Hamuro, J.; Oda, R. *J. Am. Chem. Soc.* **1967**, *89* (26), 7127-7129.

16. Day, J. C.; Lindstrom, M. J.; Skell, P. S. *J. Am. Chem. Soc.* **1974**, *96* (17), 5616-5617.

17. Marchaj, A.; Kelley, D. G.; Bakac, A.; Espenson, J. H. *J. Phys. Chem.* **1991**, *95* (11), 4440-4441.

18. Hook, S. C. W.; Saville, B. *J. Chem. Soc., Perkin Trans. 2* **1975**, (6), 589-593.

19. Mezyk, S. P.; Madden, K. P. *J. Phys. Chem.* **1996**, *100* (22), 9360-9364.

20. Zefirov, N. S.; Zhdankin, V. V.; Makhon'kova, G. V.; Dan'kov, Y. V.; Koz'min, A. S. *J. Org. Chem.* **1985**, *50* (11), 1872-1876.

21. Davidson, R. I.; Kropp, P. J. *J. Org. Chem.* **1982**, *47*, 1904-1909.

22. Cambie, R. C.; Chambers, D.; Lindsay, B. G.; Rutledge, P. S.; Woodgate, P. D. *J. Chem. Soc., Perkin Trans. 1* **1980**, (3), 822-827.

23. Macdonald, T. L.; Narasimhan, N.; Burka, L. T. *J. Am. Chem. Soc.* **1980**, *102*, 7760-7765.

24. Bering, L.; Antonchick, A. P. *Chem. Sci.* **2017**, *8*, 452-457.

25. Sinex, S. A. Interactive Excel Spreadsheets for General Chemistry. (accessed September 10).

26. Blanksby, S. J.; Ellison, G. B. *Acc. Chem. Res.* **2003**, *36* (4), 255-263.

27. Labinger, J. A. *J. Mol. Catal. A: Chem.* **2004**, *220* (1), 27-35.

28. Conley, B. L.; Tenn, W. J.; Young, K. J. H.; Ganesh, S. K.; Meier, S. K.; Ziatdinov, V. R.; Mironov, O.; Oxgaard, J.; Gonzales, J.; Goddard, W. A.; Periana, R. A., *J. Mol. Catal. A: Chem.* **2006**, *251* (1-2), 8-23.

29. Tedder, J. M. *Angew. Chem. Int. Ed.* **1982**, *21*, 401-410.

30. Walling, C.; Mayahi, M. F. *J. Am. Chem. Soc.* **1959**, *81*, 1485-1489.

31. Chan, B.; Easton, C. J.; Radom, L. *J. Phys. Chem. A* **2015**, *119*, 3843-3847.

32. Solymosi, F.; Jáky, K. *J. Inorg. Nucl. Chem.* **1971**, *33*, 2829-2838.

33. Sakakura, A.; Kawajiri, K.; Ohkubo, T.; Kosugi, Y.; Ishihara, K. *J. Am. Chem. Soc.* **2007**, *129* (47), 14775-14779.

34. Mosher, M. W.; Estes, G. W. *J. Am. Chem. Soc.* **1977**, *99* (21), 6928-6932.

35. Donchak, V. A.; Voronov, S. A.; Yur'ev, R. S. *Russ J Org Chem* **2006**, *42* (4), 487-490.

3 Extension of the OxE Process to the Functionalization of Ethylene

3.1 Introduction

While previous Chapters have focused on the importance of light alkane (*e.g.*, methane, ethane and propane) functionalization and demonstrated the efficacy of the OxE process with iodate/chloride for such functionalization, this Chapter discusses extension of the OxE process with iodate/chloride to the functionalization of ethylene. Here, we sought to study an alternative route to convert ethylene to ethylene glycol.

Ethylene glycol, used as a component of antifreeze and other coolants, is produced on a 31 million ton scale annually[1] and is used primarily as a precursor for polyesters.[2-4] Polyethylene terephthalate (PET) is the most common of these polyesters as result of its thermal stability and resistance to water, acids, and other solvents.[5] These desirable properties enable the use of PET in the textile industry as a material for clothing and in the food and beverage industries as a component for bottles.[5-6]

Industrially, the majority of ethylene glycol is produced from the thermal hydrolysis of ethylene oxide,[4] which is generated from the oxidation of ethylene with O_2 over a silver catalyst (Scheme 3.1).[7-8] Ethylene is generated via ethane cracking at high temperatures and pressures.[9] As the Environmental Protection Agency has concluded that ethylene oxide is carcinogenic to humans,[10] an alternative route to produce ethylene glycol is desirable. Here, we sought to determine if our iodate/chloride process could convert ethylene to the corresponding di-functionalized alkyl ester, which could be hydrolyzed to generate ethylene glycol.

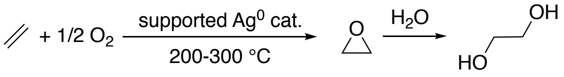

Scheme 3.1. Generation of ethylene oxide from ethylene and oxygen and subsequent hydrolysis to yield ethylene glycol.[7, 11-12]

3.2 Ethylene Functionalization using Iodate

The first report of the OxE process included a preliminary reaction with KCl and NH_4IO_3 with ethylene to demonstrate the scope and versatility of the oxidation process (Scheme 3.2).[13] A yield of 1,2-bis(trifluoroacetyl)ethane of ~50% with respect to ethylene was obtained using the standard OxE conditions (*i.e.*, 0.67 mmol KCl, 7.7 mmol NH_4IO_3). The production of 1,2-bis(trifluoroacetyl)ethane is exciting as it can be hydrolyzed to generate ethylene glycol. This screening demonstrated the utility of the OxE process with ethylene, but was not developed further.

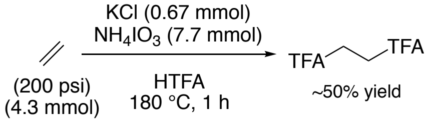

Scheme 3.2. Functionalization of ethylene to 1,2-bis(trifluoroacetyl)ethane in the original OxE report. Conditions: ethylene (200 psi), KCl (0.67 mmol), NH_4IO_3 (7.7 mmol), HTFA, 180 °C, 1 h.[13]

Because of limitations and complications associated with the high-pressure reactors used in the original report, new high-pressure reactors were custom-built to continue this study. Repeating the conditions in the original report with the new set of reactors resulted in a yield of 15(4)% yield based on ethylene of 1,2-bis(trifluoroacetyl)ethane, the ethylene glycol precursor (Scheme 3.3). However, 1,2-bis(trifluoroacetyl)ethane was not the only product of the reaction. 1-Trifluoroacetyl-2-iodoethane, 1-trifluoroacetyl-2-chloroethane, 1,2-dichloroethane and 1,2-diiodoethane were also observed, as were trace amounts of ethyl trifluoroacetate (Scheme 3.3). As the new reactors had a greater headspace than the reactors in the previous study, the 15(4)% yield of 1,2-bis(trifluoroacetyl)ethane corresponds to 3.2(5) mmol of product, while the previous report of ~50% yield provided 2.2 mmol of product.[13] Therefore, although the percent yield of the ethylene glycol precursor relative to ethylene is lower than in the original report,[13] overall production is higher using the new reactors.

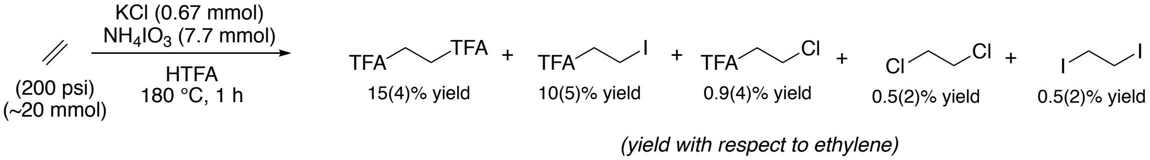

Scheme 3.3. Ethylene functionalization using KCl/NH_4IO_3 with the newly developed high-pressure reactor. Conditions: Ethylene (200 psi), KCl (0.67 mmol), NH_4IO_3 (7.6 mmol), HTFA (8 mL), 180 °C, 1 h. Ethyl trifluoroacetate was also produced in trace amounts. Yields are given as the average of six experiments with standard deviations.

Subsequent optimization focused on the effect of the reaction temperature. Functionalization is observed from 90-200 °C (Figure 3.1) and the highest yields of functionalized products are obtained from 170-180 °C. At 180 °C, the reaction has the highest yield of and selectivity for the desired glycol product, ~25% and ~66%, respectively. Increasing the temperature further to 200 °C results in decreased products. Thus, in additional studies, 180 °C was used as the reaction temperature.

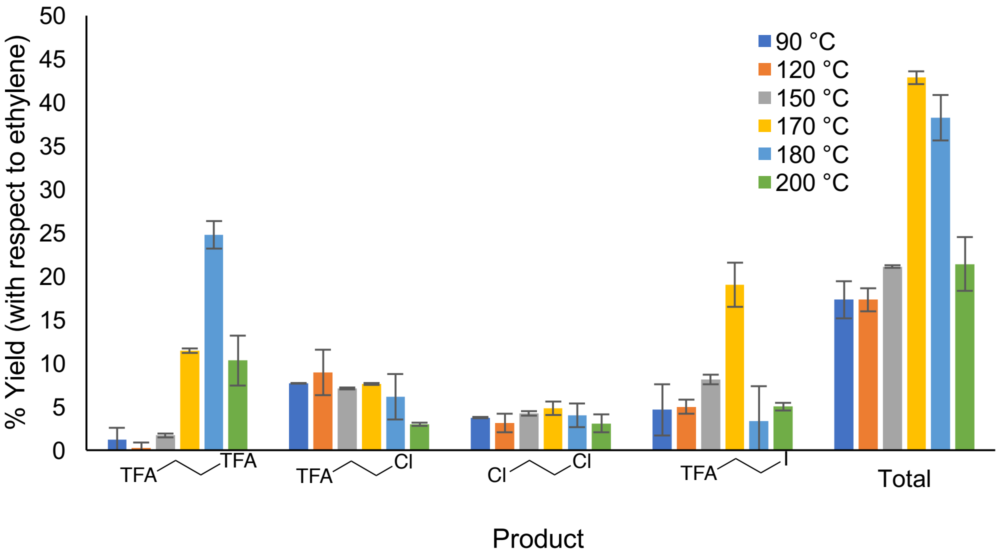

Figure 3.1. Temperature screening for ethylene functionalization with KCl/NH_4IO_3 in HTFA. Conditions: ethylene (50 psi), KCl (0.67 mmol), NH_4IO_3 (7.6 mmol), HTFA (8 mL), 1 h. Error bars denote standard deviations based on three experiments.

To compare the ethylene functionalization process with the OxE process for light alkane functionalization, various halide salts were examined as additives. For alkanes, minimal functionalization was observed when halide salts other than chlorides were used.[13] With ethylene, chloride does not provide an enhancement for glycol production over other KBr or KI (Figure 3.2). The total yield is slightly higher but the reaction is less selective when chloride is used, but the difference in yield is not statistically significant. Further, the reaction is less selective for the desired glycol product when KCl is used, as additional di-functionalized products 1-trifluoroacetyl-2-chloroethane and 1,2-dichloroethane are observed. This is indicative of a difference between the ethylene and light alkane functionalization processes.

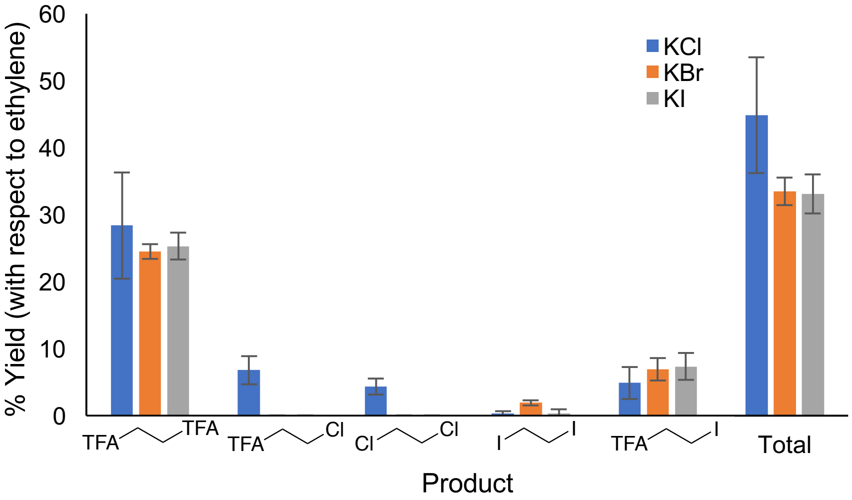

Figure 3.2. Effect of halide identity on ethylene functionalization with NH_4IO_3. Conditions: ethylene (50 psi), halide (0.67 mmol; KCl, KBr or KI), NH_4IO_3 (7.6 mmol), HTFA (8 mL), 180 °C, 2 h. Error bars denote standard deviations based on at least three experiments.

The effect of added iodine was also examined (Figure 3.3). The total yield of functionalized products increases from 38(2)% in the absence of added I_2 to 50(2)% on the addition of 0.34 mmol of I_2 at the beginning of the reaction. As ethylene could be undergoing an addition reaction with I_2 to generate 1,2-diiodoethane which could convert to the glycol product *in situ*, the reactivity of ethylene with iodine in the absence of iodate was examined (Scheme 3.4). With 0.50 mmol of I_2 in HTFA, ~4% yield of functionalized products was observed. Thus, although functionalization is observed in the absence of iodate, the presence of the iodate oxidant appears to be important for appreciable functionalization.

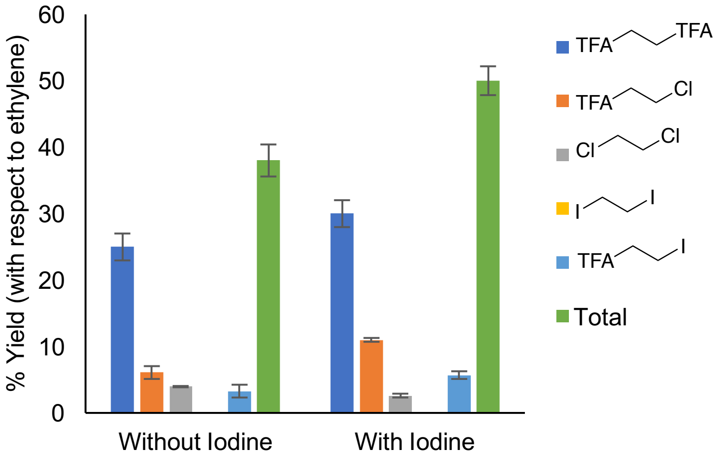

Figure 3.3. Effect of added iodine on ethylene functionalization with KCl/NH_4IO_3. Conditions: ethylene (50 psi), KCl (0.67 mmol), NH_4IO_3 (7.6 mmol), I_2 (0.34 mmol, if added), HTFA (8 mL), 180 °C, 1 h. Error bars denote standard deviations based on three experiments.

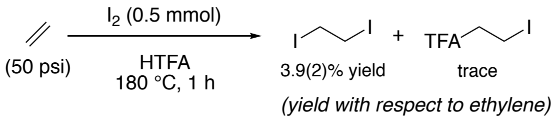

Scheme 3.4. Ethylene functionalization with I_2 in HTFA. Conditions: ethylene (50 psi), I_2 (0.5 mmol), HTFA (8 mL), 180 °C, 1 h. Yields are the average of three experiments with standard deviations.

3.3 Ethylene Functionalization Using Periodate

As potassium periodate (KIO_4) was also demonstrated to be effective for the functionalization of methane, ethane and propane using the OxE approach,[14] it was subsequently studied as a potential oxidant for the partial oxidation of ethylene. First, the use of KIO_4 in the absence of chloride was tested as a benchmark. Notably, without optimization, the partial oxidation of ethylene by KIO_4 in the absence of additives gave 33(3)% yield of 1,2-bis(trifluoroacetyl)ethane and minor amounts of 1-trifluoroacetyl-2-iodoethane (Scheme 3.5). To compare the reactivity to NH_4IO_3 directly, the optimized conditions with iodate were performed with KIO_4. KIO_4 proved to be a much more efficient oxidant, providing an increase in 1,2-bis(trifluoroacetyl)ethane yield from

25(2)% with NH_4IO_3 to 42(3)% with KIO_4 (Figure 3.4). Byproducts of the reactions were generated in similar amounts with both oxidants.

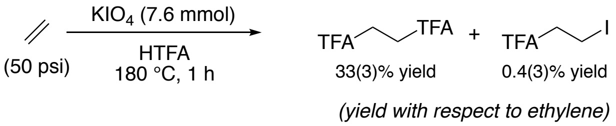

Scheme 3.5. Ethylene functionalization with KIO_4 at 150 °C. Conditions: ethylene (50 psi), KIO_4 (7.6 mmol), HTFA (8 mL), 180 °C, 1 h. Yields are given as the average of three experiments with standard deviations.

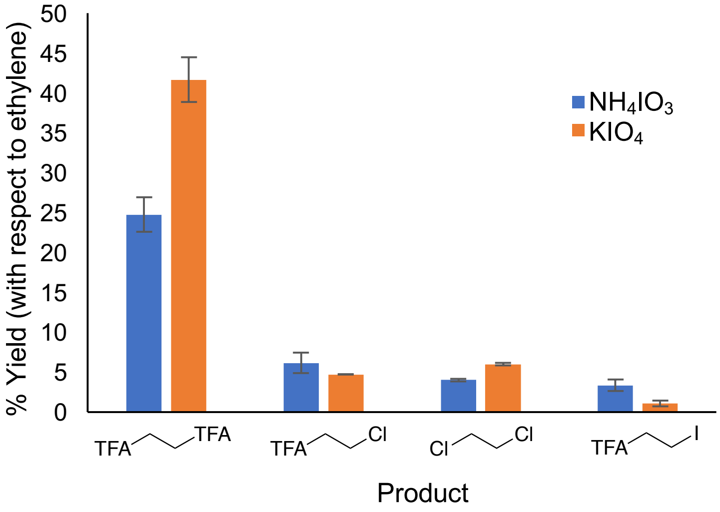

Figure 3.4. Comparison of ethylene functionalization using NH_4IO_3 versus KIO_4. Conditions: ethylene (50 psi), KCl (0.67 mmol), NH_4IO_3 or KIO_4 (7.6 mmol), HTFA (8 mL), 180 °C, 1 h. Error bars denote standard deviations based on three experiments.

Because the addition of iodine improved yields of ethylene functionalization using NH_4IO_3, an iodine addition screening was also performed with periodate. Yields of 1,2-bis(trifluoroacetyl)ethane were particularly affected by the addition of iodine under reaction conditions with KCl/KIO_4 (Figure 3.5). The optimal iodine loading was determined to be 0.5 mmol, at which the yield of 1,2-bis(trifluoroacetyl)ethane improved from 42(3)% to 61(3)%. Yields of byproducts were also increased with increased iodine loadings. The total yield of the functionalization products under these optimized conditions is > 75% with respect to ethylene, a marked increase from the ~50% obtained in the absence of iodine.

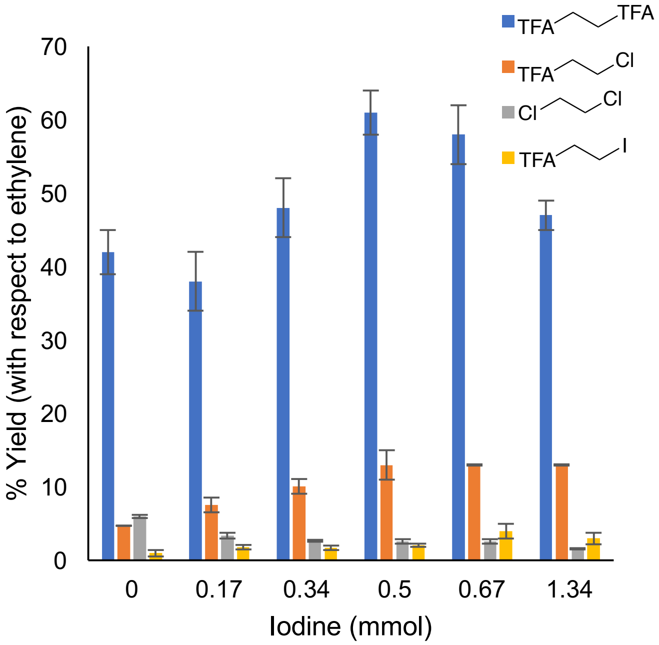

Figure 3.5. Effect of added iodine on ethylene functionalization with KCl/KIO_4. Conditions: ethylene (50 psi), KCl (0.67 mmol), KIO_4 (7.6 mmol), HTFA (8 mL), 180 °C, 1 h. Error bars denote standard deviations based on three experiments.

The original report of the iodate/chloride chemistry demonstrated that methane functionalization was minimal in the absence of chloride or with halides other than chloride.[13] However, given the significance of adding iodine to the ethylene functionalization reaction and the high yield in the initial screening of periodate in the absence of chloride (Scheme 3.5), the effect of additives was studied further using optimized conditions with KIO_4 and I_2. Remarkably, for reactions without added chloride, with KCl, and with KI, the yields of 1,2-bis(trifluoroacetyl)ethane were statistically identical, each ~60% with respect to ethylene (Figure 3.6). This finding represents a substantive difference between the original OxE process and its applications with ethylene. The addition of KCl is not necessary for ethylene functionalization, nor does it provide higher yields of 1,2-bis(trifluoroacetyl)ethane than those obtained on the addition of KI. However, overall yields of functionalized product are higher when KCl is added, due to the production of chlorine-containing byproducts, which account for ~15% yield relative to ethylene (Figure 3.6).

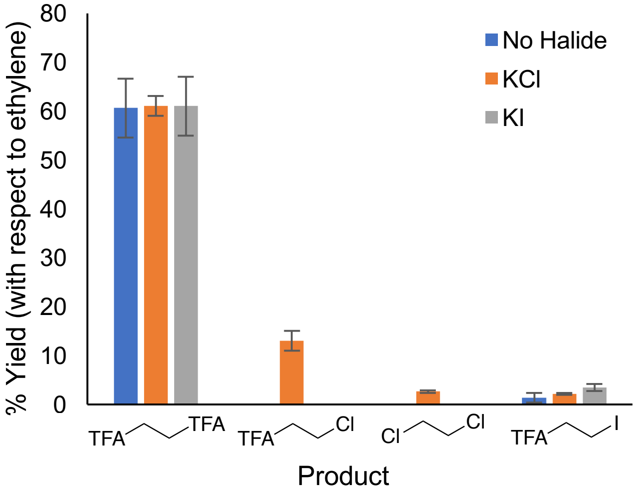

Figure 3.6. Effect of halide on ethylene functionalization with KIO_4/I_2. Conditions: ethylene (50 psi), KIO_4 (7.6 mmol), I_2 (0.5 mmol), KCl or KI (0.67 mmol, if added), HTFA (8 mL), 180 °C, 1 h. Error bars denote standard deviations based on three experiments.

Because ethylene functionalization was demonstrated to occur efficiently in the absence of halide salts, none were added in additional optimization studies. Although the additive optimization proved useful, resulting in significant increases in yields of functionalized products, this did not address one of the most challenging complications of the OxE chemistry, solvent oxidation. Periodate is a particularly strong oxidant and at high temperatures, trifluoroacetic acid can be oxidized by iodine oxide oxidants.[13] In addition to consuming trifluoroacetic acid, a costly reagent, this oxidation also hinders catalysis by unproductively utilizing the periodate oxidant. Therefore, in an effort to reduce solvent oxidation, the reaction temperature was decreased from 180 °C to 150 °C

(Scheme 3.6). On reducing the reaction temperature by 30 °C, a significant increase in the yield of 1,2-bis(trifluoroacetyl)ethane was observed. Previously, the highest yield of 1,2-bis(trifluoroacetyl)ethane with respect to ethylene was ~60%. At 150 °C with KIO_4 and I_2, the yield of 1,2-bis(trifluoroacetyl)ethane increased to 82(6)% (Scheme 3.6). The reaction with KIO_4/I_2 at 150 °C is also highly selective for 1,2-bis(trifluoroacetyl)ethane, with < 2% yield of other byproducts. Decreasing the reaction temperature further to 90 °C also resulted in an increase in the yield of 1,2-bis(trifluoroacetyl)ethane to 88(9)% yield with respect to ethylene (Scheme 3.7). These increases in the yield of functionalized products demonstrates how imperative reducing unproductive solvent oxidation is. At lower reaction temperatures, yields of 1,2-bis(trifluoroacetyl)ethane relative to the starting alkene approach 90%.

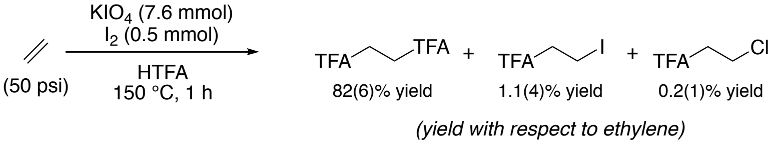

Scheme 3.6. Ethylene functionalization with KIO_4/I_2 at 150 °C. Conditions: Ethylene (50 psi), KIO_4 (7.6 mmol), I_2 (0.5 mmol), HTFA, 150 °C, 1 h. Yields are given as the average of three experiments with standard deviations.

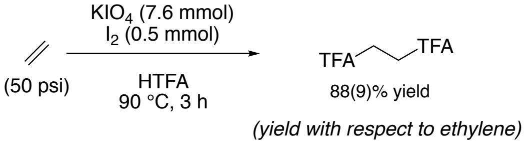

Scheme 3.7. Ethylene functionalization with KIO_4/I_2 at 90 °C. Conditions: Ethylene (50 psi), KIO_4 (7.6 mmol), I_2 (0.5 mmol), HTFA, 90 °C, 3 h. Yields are given as the average of three experiments with standard deviations.

3.4 Conclusions and Future Directions

Ethylene functionalization using iodate and periodate salts was successful. Under optimized conditions with periodate, the desired glycol product, which can be hydrolyzed to give ethylene glycol, was obtained in nearly quantitative yield. The process for ethylene functionalization differs from the original light alkane functionalization process wherein the presence of a chloride salt was necessary. This indicates that distinct reaction mechanisms may be operative for the two processes. Further mechanistic studies are required to elucidate these differences.

Following this study, we discovered a similar report of ethylene functionalization in the literature which had not been translated from the original Japanese.[15] As a result, this study was not pursued further using ethylene as the substrate. Instead, the extension of the OxE process focused on the use of alternative oxidants which could be more easily regenerated using air. Additionally, photochemical reaction conditions were studied in an effort to generate species capable of light alkane functionalization using lower reaction temperatures to minimize solvent oxidation.

3.5 Experimental Section

General Considerations. *Caution: Many of the reagents and conditions described herein are potentially hazardous. Safety procedures should be consulted prior to the use of concentrated acids, mixtures of hydrocarbons and oxygen and strong oxidants.*

Unless stated otherwise, all reactions were performed under ambient atmosphere. All chemicals were purchased from commercial sources and used as received. Ethylene was obtained from Matheson and was used as received. 1-TFA-2-chloroethane (TFCE) was synthesized according to a literature procedure.[16] ^{1}H NMR spectra were recorded on a Varian 500 MHz or Bruker 600 MHz spectrometer. Spectra were taken using a C_6D_6 capillary and were referenced with respect to an internal standard, dichloromethane (δ 5.03), glacial HOAc (δ 2.04), or nitromethane (δ 4.17 ppm). All reactions were performed in custom-built Swagelok stainless steel high pressure reactors with a Teflon liner.[13-14]

General Procedures

Ethylene functionalization using KX/NH_4IO_3. A custom-built stainless-steel reactor with a Teflon liner[13-14] was charged with a stir bar, KX (X = Cl, Br, I; 0.67 mmol), NH_4IO_3 (7.6 mmol), I_2 (0.34 mmol, if added) and HTFA (8 mL). The reactor was sealed and pressurized with 50 psi of ethylene. After the mixture was stirred at 800 rpm at 180 °C for 1 h, the reactor was allowed to cool to room temperature. The reactor was then vented carefully, and nitromethane was added as an internal standard. After stirring, an aliquot was removed for centrifugation. The supernatant was analyzed by ^1H NMR. A representative ^1H NMR spectrum is shown below. This procedure was performed in triplicate.

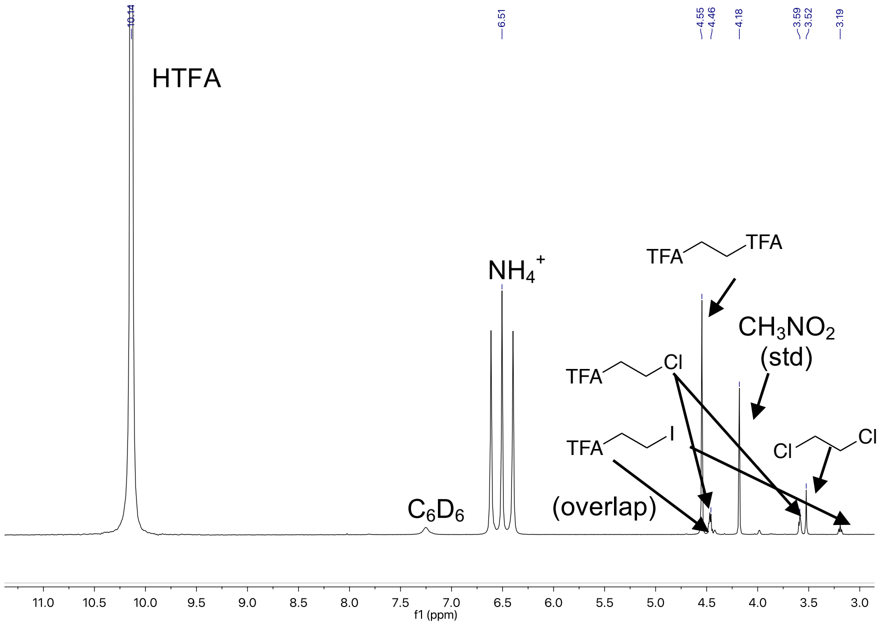

Figure 3.7. Representative ^{1}H NMR spectrum of ethylene functionalization using KCl/NH_4IO_3. Conditions: Ethylene (50 psi), KCl (0.67 mmol), NH_4IO_3 (7.6 mmol), HTFA (8 mL), 180 °C, 1 h. Nitromethane (0.56 mmol) was added as an internal standard.

Ethylene functionalization with I_2 in HTFA. A custom-built stainless-steel reactor with a Teflon liner[13-14] was charged with a stir bar, I_2 (0.67 mmol) and HTFA (8 mL) under either under ambient atmosphere. The reactor was sealed and pressurized with 50 psi of ethylene. After the mixture was stirred at 800 rpm at 180 °C for 1 h, the reactor was allowed to cool to room temperature. The reactor was then vented carefully, and nitromethane was added as an internal standard. After stirring, an aliquot was removed for centrifugation. The supernatant was analyzed by ^{1}H NMR. A representative ^{1}H NMR spectrum is shown below. This procedure was performed in triplicate.

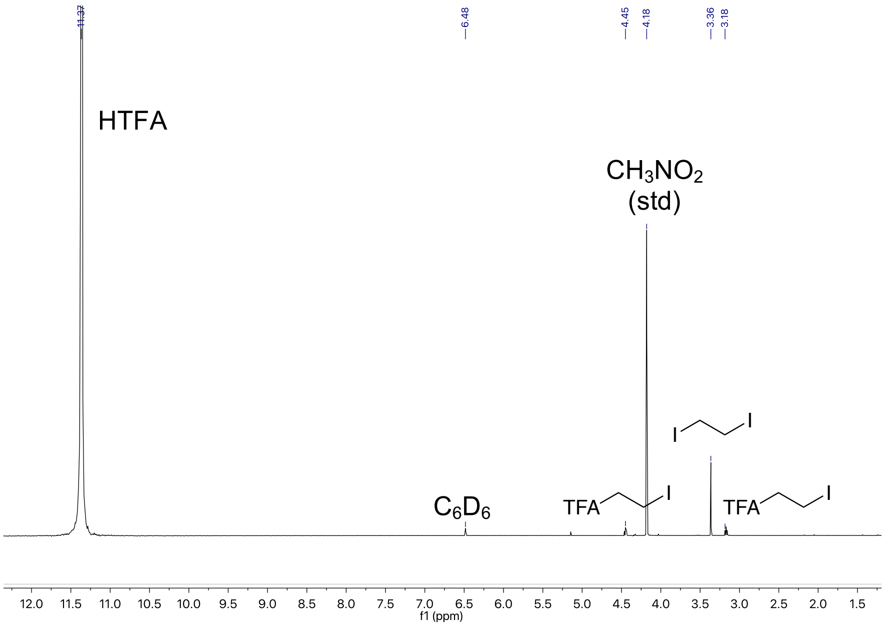

Figure 3.8. Representative ^{1}H NMR spectrum of ethylene functionalization using I_2 in HTFA. Conditions: Ethylene (50 psi), I_2 (0.67 mmol), HTFA (8 mL), 180 °C, 1 h. Nitromethane (0.56 mmol) was added as an internal standard.

Ethylene functionalization with KIO_4. A custom-built stainless-steel reactor with a Teflon liner[13-14] was charged with a stir bar, KIO_4 (7.6 mmol) and HTFA (8 mL). The reactor was sealed and pressurized with 50 psi of ethylene. After the mixture was stirred at 800 rpm at 180 °C for 1 h, the reactor was allowed to cool to room temperature. The reactor was then vented carefully, and nitromethane was added as an internal standard. After stirring, an aliquot was removed for centrifugation. The supernatant was analyzed by ^{1}H NMR. A representative ^{1}H NMR spectrum is shown below. This procedure was performed in triplicate.

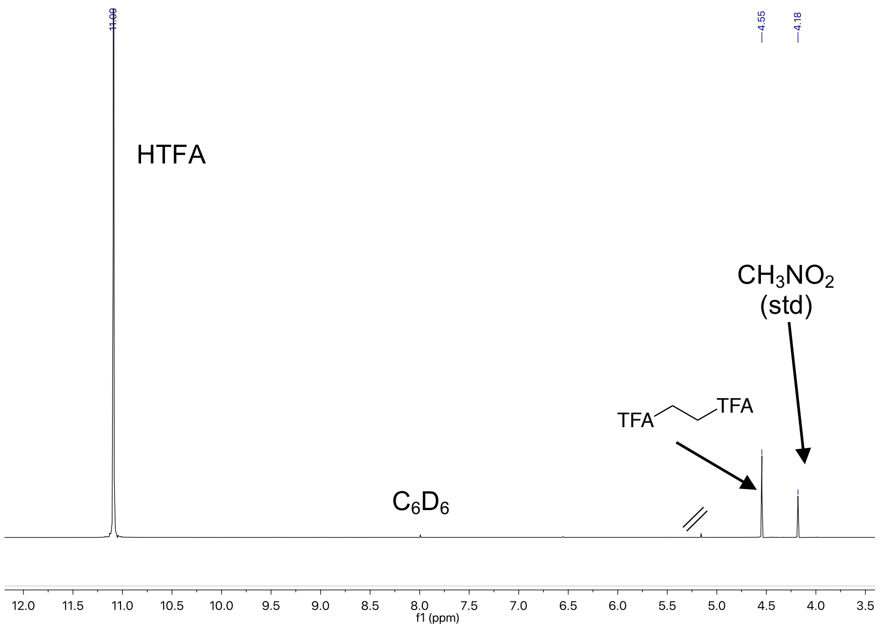

Figure 3.9. Representative ^{1}H NMR spectrum of ethylene functionalization using KIO_4. Conditions: Ethylene (50 psi), KIO_4 (7.6 mmol), HTFA (8 mL), 180 °C, 1 h. Nitromethane (0.56 mmol) was added as an internal standard.

Ethylene functionalization using KCl/KIO_4. A custom-built stainless-steel reactor with a Teflon liner[13-14] was charged with a stir bar, KCl (0.67 mmol), KIO_4 (7.6 mmol) and HTFA (8 mL). The reactor was sealed and pressurized with 50 psi of ethylene. After the mixture was stirred at 800 rpm at 180 °C for 1 h, the reactor was allowed to cool to room temperature. The reactor was then vented carefully, and nitromethane was added as an internal standard. After stirring, an aliquot was removed for centrifugation. The supernatant was analyzed by ^{1}H NMR. A representative ^{1}H NMR spectrum is shown below. This procedure was performed in triplicate.

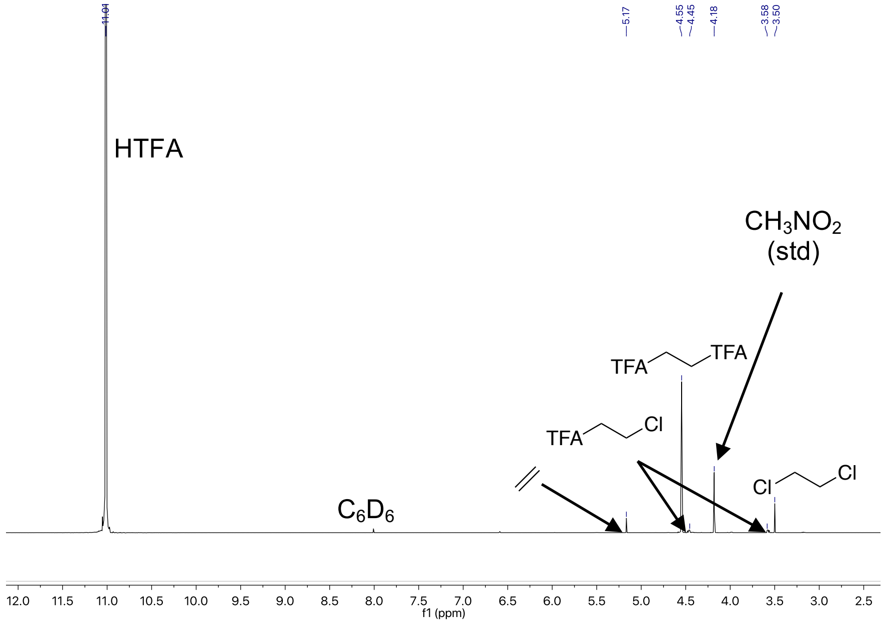

Figure 3.10. Representative ^1H NMR spectrum of ethylene functionalization using KCl/KIO_4. Conditions: Ethylene (50 psi), KCl (0.67 mmol), KIO_4 (7.6 mmol), HTFA (8 mL), 180 °C, 1 h.

3.6 References

1. Tremblay, J.-F., Polyester made from coal? China is betting on it. *Chem. Eng. News* 2019.

2. Burdick, D. L.; Leffler, W. L., Ethylene Oxide and Ethylene Glycol. In *Petrochemicals in Nontechnical Language*, PennWell: 2001.

3. Yue, H.; Zhao, Y.; Ma, X.; Gong, J. *Chem. Soc. Rev.* **2012,** *41*, 4218-4244.

4. Rebsdat, S.; Mayer, D., Ethylene Glycol. In *Ullmann's Encyclopedia of Industrial Chemistry*, Wiley-VCH: 2012; Vol. 13, pp 531-546.

5. Li-na, J. I. *Appl. Mech. Mater.* **2013,** *312*, 406-410.

6. Köpnick, H.; Schmidt, M.; Brügging, W.; Rüter, J.; Kaminsky, W., Polyesters. In *Ullmann's Encyclopedia of Industrial Chemistry*, Wiley-VCH: 2012; Vol. 13, pp 29898-29925.

7. Rebsdat, S.; Mayer, D., Ethylene Oxide. In *Ullmann's Encyclopedia of Industrial Chemistry*, Wiley-VCH: 2012; Vol. 13, pp 547-572.

8. Lefort, T. E. Process for the production of ethylene oxide. 1,998,872, 1935.

9. Zimmermann, H.; Walzl, R., Ethylene. In *Ullmann's Encyclopedia of Industrial Chemistry*, Wiley-VCH: 2009; Vol. 12, pp 531-583.

10. *Evaluation of the Inhalation Carcinogenicity of Ethylene Oxide: In Support of Summary Information on the Integrated Risk Information System (IRIS)*; National Center for Environmental Assessment, Office of Research & Development: Washington, DC, 2016.

11. Maurer, T.; Gitter, M.; Rosowski, F. Method for production of ethylene oxide in a microchannel reactor. US20090270640A1, 2009.

12. Verhaak, M. J. F. M.; Van Westrenen, J. Process for the production of ethylene oxide. US9260266B2, 2016.

13. Fortman, G. C.; Boaz, N. C.; Munz, D.; Konnick, M. M.; Periana, R. A.; Groves, J. T.; Gunnoe, T. B. *J. Am. Chem. Soc.* **2014,** *136*, 8393-8401.

14. Kalman, S. E.; Munz, D.; Fortman, G. C.; Boaz, N. C.; Groves, J. T.; Gunnoe, T. B. *Dalton Trans.* **2015,** *44*, 5294-5298.

15. Koyano, T.; Kaneko, K.; Watanabe, O. *J. Chem. Soc. Jpn., Ind. Chem. Sect.* **1971,** *74* (2), 207-210.

16. Hung, M. H. *Macromolecules* **1993,** *26* (22), 5829-5834.

4 Extension of the OxE Process to Oxidants other than Iodine Oxides

4.1 Introduction

Previous efforts related to the OxE process were focused on the use of iodine oxides for light alkane functionalization. Although the conversion of iodine and iodide to iodate with dioxygen is thermodynamically favorable,[1] using known thermal routes this is not a kinetically facile process.[2] Due to this significant limitation and the expense of iodate and periodate, the OxE process as originally developed cannot be readily commercialized. The focus of the studies in this Chapter is to extend the achievements of the OxE process toward the goal of selective partial oxidation with oxidants that can be easily recycled using air or pure dioxygen.

The work discussed in this chapter was a collaborative effort involving the Gunnoe group (UVA), the Groves group (Princeton University), the Goddard group (Caltech), the Wu group (Oak Ridge National Laboratory) and Dr. Ling Tao (National Renewable Energy Laboratory). Dr. Jonathan Goldberg of the Groves group performed studies of cyclohexane oxidation. Dr. Smith Nielsen of the Goddard group performed computational studies to determine likely reaction pathways. Dr. Zili Wu provided expertise regarding oxidant candidates and focused on development of OxE in a flow reactor. Dr. Ling Tao provided techno-economical analysis for variations of the OxE process. Dr. Bill Schinski (Chevron, retired) served as an additional advisor for this work.

4.2 Extension of the OxE Process to Nitrates

To shift the OxE process away from the use of iodate or periodate, alternative oxidants were investigated as potential replacements. A set of screening conditions was developed to assess potential replacements and to compare them to the standard OxE process using

NH_4IO_3. To reduce cost and the formation of hazardous waste, these screening conditions scaled down the amounts of KCl and oxidant in typical OxE reactions by seven-fold. Unless noted otherwise, yields in this Chapter are relative to oxidant, rather than the starting alkane.

Nitrate salts, NO_3^-, are well-known as powerful oxidizers and bear clear similarities to iodate, IO_3^-. Additionally, depending on the active species in solution, it may be possible to recycle a reduced nitrogen oxide to an active oxidized form using dioxygen,[3-4] a longstanding goal of this chemistry. Cerium-based oxidants were identified as promising candidates from their presence in the oxychlorination literature,[5-7] thus ceric ammonium nitrate (CAN) was a logical starting point for the extension of the OxE process to alternative oxidants.

The combination of KCl and CAN resulted in the formation of ~5% yield of both MeTFA and $MeNO_2$ after reaction at 180 °C for 1 h, whereas > 40% yield of MeTFA was obtained under those conditions with NH_4IO_3 (Figure 4.1). The formation of $MeNO_2$ under these conditions was confirmed by spiking a reaction mixture with a known standard and taking a ^1H NMR spectrum. Although the use of CAN resulted in lower yields of functionalized product relative to iodate, methane functionalization was observed. To test if the use of cerium(IV) was necessary or if a simple nitrate salt would suffice, NH_4NO_3 was studied. Methane was also partially oxidized using NH_4NO_3 (Figure 4.1). The yield of MeTFA was similar to that with CAN, while the yield of $MeNO_2$ decreased. Minimal amounts of MeCl were also observed with CAN, NH_4NO_3 and NH_4IO_3 under these conditions. Given that NH_4NO_3 exhibited a similar performance to CAN, the use of nitrate as a stoichiometric oxidant was examined further.

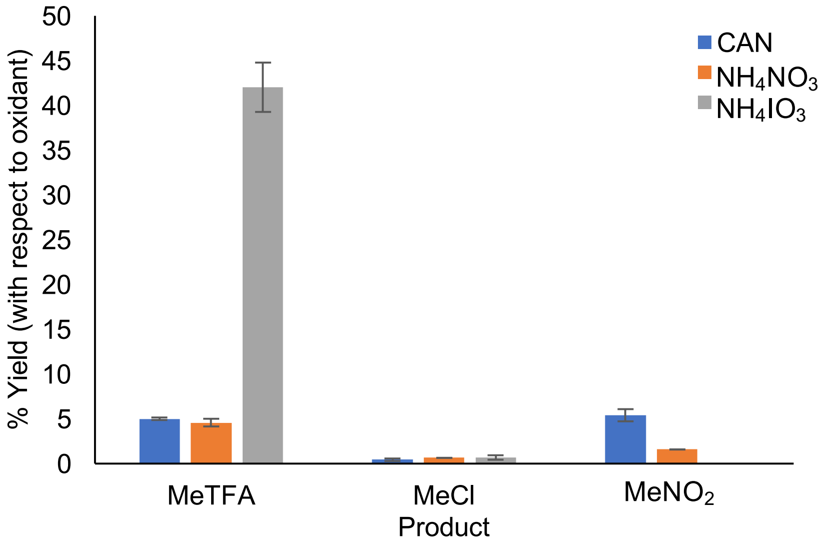

Figure 4.1. Functionalization of methane with KCl and ceric ammonium nitrate (CAN), NH_4NO_3 or NH_4IO_3. Conditions: CH_4 (300 psi), KCl (0.1 mmol), oxidant (1.1 mmol; CAN, NH_4NO_3, NH_4IO_3), HTFA (8 mL), 180 °C, 1 h. Error bars denote standard deviations based on at least three experiments.

As iodine was proposed to be a crucial intermediate in the OxE process, acting as a radical trap to intercept alkyl radicals and minimize over-oxidation,[8] it was proposed that the addition of iodine would be beneficial when using a nitrate oxidant. Although the OxE process did not give an increase in yield of mono-functionalized product on the addition of iodine at the start of the reaction, iodine was generated *in situ* as iodate was reduced.[8] With NH_4NO_3, the addition of iodine resulted in significantly higher yields of MeTFA, with an increase from 4.4(6)% yield in the absence of iodine to 18(1)% yield with 0.1 mmol of iodine (Figure 4.2). Similar to the OxE process with iodate, there is a point at which the addition of a larger amount of iodine results in decreased yields. Under the conditions studied using ammonium nitrate (see Figure 4.2), the addition of 0.2 mmol of iodine resulted in a MeTFA yield of 10.0(5)% with respect to oxidant, whereas 18(1)% yield was observed when 0.1 mmol of iodine was added. This decrease in yield is potentially a result of iodine radicals trapping intermediates required for methane functionalization.[8]

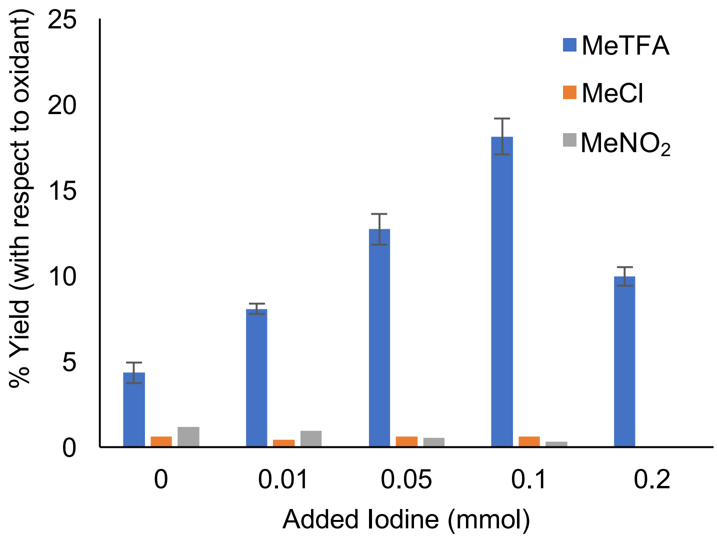

Figure 4.2. Functionalization of methane with KCl/NH_4NO_3 as a function of added iodine. Conditions: CH_4 (300 psi), KCl (0.1 mmol), NH_4NO_3 (1.1 mmol), I_2 (0-0.2 mmol), HTFA (8 mL), 180 °C, 2 h. Error bars denote standard deviations based on at least three experiments.

Chloride was found to be necessary for the OxE process with iodate or periodate as the oxidant, and yields of functionalized products improved with increased amounts of chloride.[9-10] To study the effect of added chloride on the reaction with NH_4NO_3, a variety of chloride loadings were tested, from 0 to 0.5 mmol (Figure 4.3). In the absence of chloride, the MeTFA yield decreased to 10.5(8)% from 18(1)% with 0.1 mmol of added KCl. With > 0.1 mmol of KCl, yields of functionalized products were similar or slightly less than with 0.1 mmol. When using 0.5 mmol of KCl, the yield of MeCl increased slightly, as was observed in the OxE process with iodate.[9] Extending the reaction time with optimized chloride and iodine loadings resulted in ~25% total yield of MeX (X = TFA, Cl, NO_2) (Scheme 4.1).

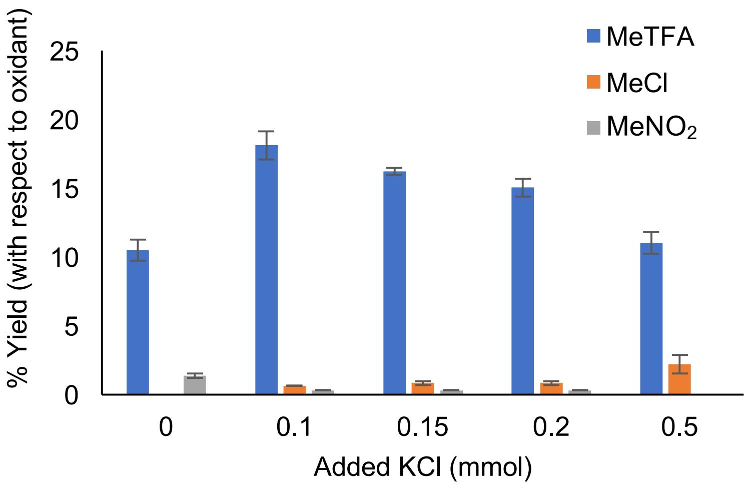

Figure 4.3. Functionalization of methane with NH_4NO_3/I_2 as a function of added chloride. Conditions: CH_4 (300 psi), KCl (0-0.5 mmol), NH_4NO_3 (1.1 mmol), I_2 (0.1 mmol), HTFA (8 mL), 180 °C, 2 h. Error bars denote standard deviations based on at least three experiments.

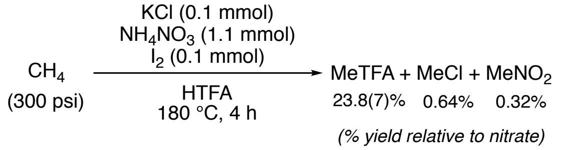

$$\underset{\text{(300 psi)}}{CH_4} \xrightarrow[\text{HTFA, 180 °C, 4 h}]{\text{KCl (0.1 mmol), }NH_4NO_3\text{ (1.1 mmol), }I_2\text{ (0.1 mmol)}} \underset{23.8(7)\%}{\text{MeTFA}} + \underset{0.64\%}{\text{MeCl}} + \underset{0.32\%}{MeNO_2}$$

Scheme 4.1. Methane functionalization under optimized conditions with KCl, NH_4NO_3 and I_2. Conditions: CH_4 (300 psi), KCl (0.1 mmol), NH_4NO_3 (1.1 mmol), I_2 (0.1 mmol), HTFA (8 mL), 180 °C, 4 h. Yields are based on three experiments with a standard deviation shown for MeTFA. The yields of MeCl and $MeNO_2$ were identical for all three trials.

As demonstrated in the initial report using iodate,[9] the counter-ion of the oxidant can have a significant effect on alkane functionalization. Although the nature of this effect is not yet understood, the trend observed with iodate where yields with KIO_3 are lower than those with NH_4IO_3 is also seen with nitrate oxidants (Figure 4.4). The effect is more pronounced with nitrate oxidants. With iodate, the yield of MeTFA was about ~50% lower with KIO_3 compared to NH_4IO_3,[9] while only minimal amounts of MeTFA are obtained when KNO_3 is used (Figure 4.4).

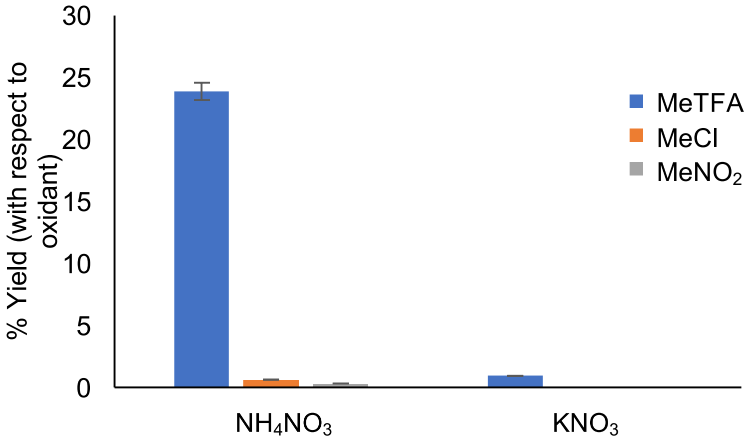

Figure 4.4. Comparison of methane functionalization with NH_4NO_3 versus KNO_3 under optimized conditions. Conditions: CH_4 (300 psi), KCl (0.1 mmol), NH_4NO_3 or KNO_3 (1.1 mmol), I_2 (0.1 mmol), HTFA (8 mL), 180 °C, 4 h. Error bars denote standard deviations based on at least three experiments.

NH_4NO_3 was also tested as an oxidant for ethane functionalization (Scheme 4.2). This served to demonstrate the potential scope of reactivity of NH_4NO_3 and provided further evidence for the formation of RNO_2 from RH (R = Me, Et) when nitrates were used as the oxidant. Spiking a reaction mixture with a known standard of nitroethane supported the conclusion that it was generated during the reaction. When using methane as the substrate, spiking the resulting reaction mixture with nitromethane was also consistent with the formation of $MeNO_2$. Thus, $MeNO_2$ and $EtNO_2$ were concluded to be functionalization products from the reactions with methane and ethane, respectively. Yields relative to nitrate for ethane functionalization are higher than those observed with methane under similar conditions, with ~40% total yield of EtX (X = TFA, NO_2) (Scheme 4.2). The simple nitrate oxidant is selective for the partial oxidation of both methane and ethane, indicating the ability of oxidants other than iodine oxides to be successful in the OxE reaction without deleterious effects with respect to over-oxidation.

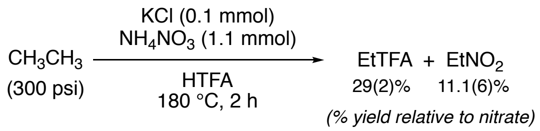

Scheme 4.2. Ethane functionalization under optimized conditions with KCl and NH_4NO_3. Conditions: CH_4 (300 psi), KCl (0.1 mmol), NH_4NO_3 (1.1 mmol), HTFA (8 mL), 180 °C, 2 h. Yields and standard deviations based on three experiments are shown.

4.3 Extension of the OxE Process to a Bismuth Oxidant

For our initial screening, sodium bismuth oxide ($NaBiO_3$) was examined as a candidate for the OxE process. Under the standard set of conditions examined for the nitrate oxidants (see above), $NaBiO_3$ results in slightly lower yields of MeX (X = TFA, Cl) than were observed for the nitrates (Figure 4.5, orange). In contrast to the nitrate study, the addition of 0.05 mmol of iodine resulted in somewhat lower average yields of MeX, though yields remain statistically identical to those observed in the absence of added iodine (Figure 4.5, blue).

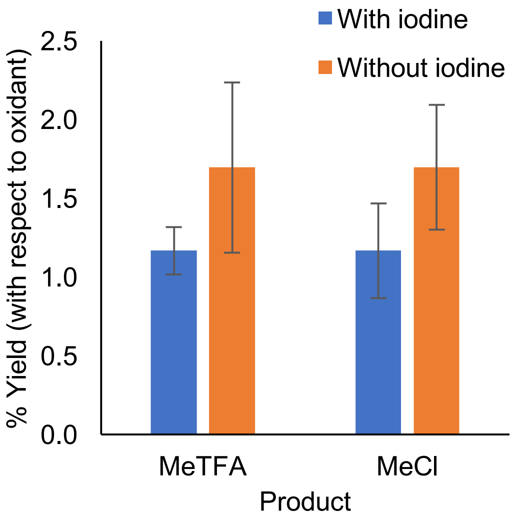

Figure 4.5. Functionalization of methane as a function of added iodine with KCl/$NaBiO_3$. Conditions: CH_4 (300 psi), KCl (0.1 mmol), $NaBiO_3$ (1.1 mmol), I_2 (if added, 0.05 mmol), HTFA (8 mL), 180 °C, 1 h. Error bars denote standard deviations based on three experiments.

In an effort to determine if the lower observed yields of MeTFA were a result of its instability under reaction conditions with $NaBiO_3$, MeTFA decay was studied at 80 °C for 2 h with $NaBiO_3$ in HTFA in the absence or presence of KCl (Scheme 4.3). MeTFA decay was observed with $NaBiO_3$ at 80 °C with ~85% and ~90% remaining after 2 h in the presence and absence of KCl, respectively (Scheme 4.3). At 140 °C, the consumption of MeTFA is comparable, with 82(4)% remaining after 1 h under reaction conditions in the absence of KCl (Scheme 4.4).[8] In contrast, with KCl/NH_4IO_3 > 85% of MeTFA remains after 16 h of heating (see Chapter 2). This difference indicates that MeTFA is likely less stable under functionalization conditions with $NaBiO_3$, providing a potential rationalization for the lower yields that are observed.

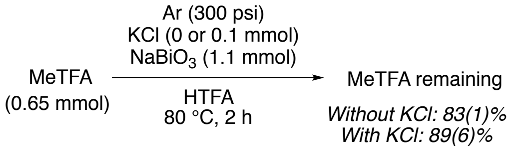

Scheme 4.3. Stability of MeTFA with $NaBiO_3$ with or without added KCl at 80 °C. Conditions: Ar (300 psi), MeTFA (0.65 mmol), KCl (if added, 0.1 mmol), $NaBiO_3$ (1.1 mmol), HTFA (8 mL), 80 °C, 2 h. Yields and standard deviations based on three experiments are shown.

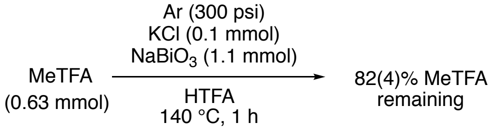

Scheme 4.4. Stability of MeTFA with $NaBiO_3$ at 140 °C. Conditions: Ar (300 psi), MeTFA (0.63 mmol), KCl (0.1 mmol), $NaBiO_3$ (1.1 mmol), HTFA (8 mL), 140 °C, 1 h. Yield and standard deviation based on three experiments are shown. Without heating, 97(3)% of MeTFA remains.

Ethane and propane were also examined as substrates for partial oxidation with $NaBiO_3$. These reactions were performed at lower temperatures to minimize product over-oxidation. Although yields with ethane are slightly higher than those with methane, the total product yields of ethane functionalization are < 5%, whether or not KCl is added

(Figure 4.6). Increasing the temperature to 120 °C or increasing the reaction time did not improve product yields. For propane, yields are somewhat higher, particularly when chloride is added. With added chloride, ~9% total yield of functionalized product is obtained, with the formation of 1-trifluoroacetylethane (1-TFA) and 2-trifluoroacetylethane (2-TFA) highly favored over other products which are observed in trace amounts (Figure 4.7).

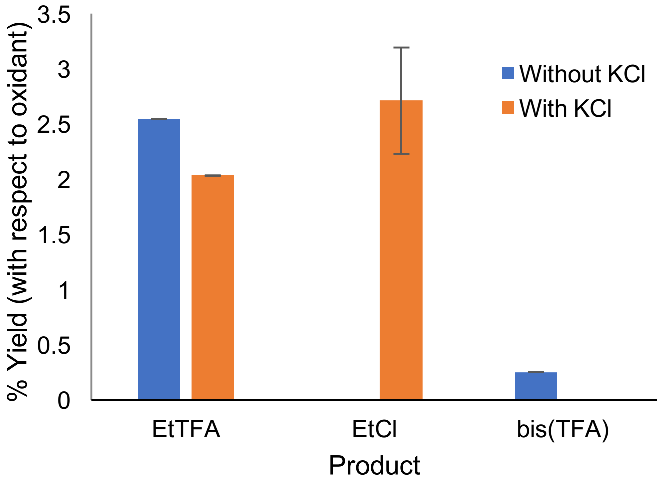

Figure 4.6. Functionalization of ethane as a function of added chloride with $NaBiO_3$. Conditions: CH_3CH_3 (300 psi), KCl (if added, 0.1 mmol), $NaBiO_3$ (1.1 mmol), HTFA (8 mL), 80 °C, 2 h. Bis(TFA) = 1,2-bis(trifluoroacetyl)ethane. Error bars denote standard deviations based on three experiments.

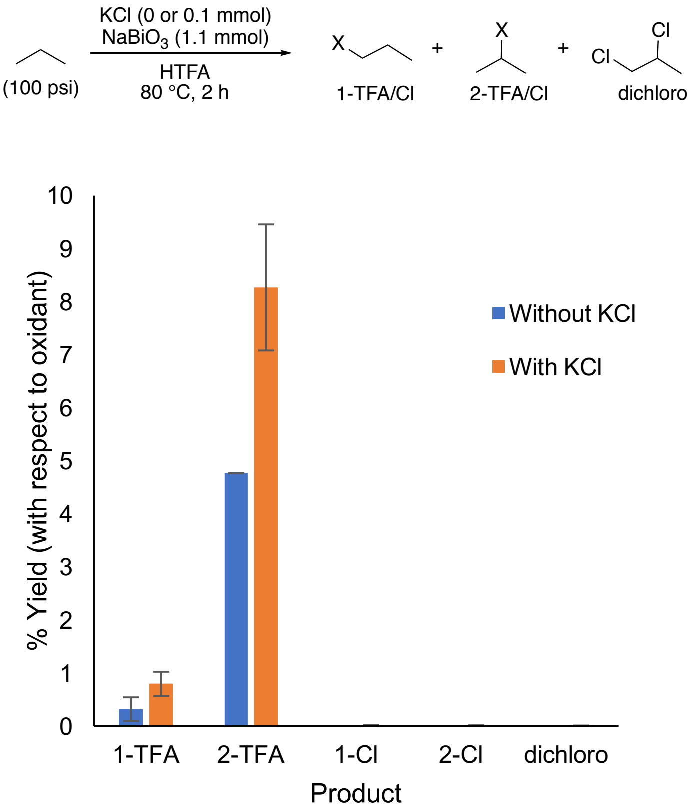

Figure 4.7. Functionalization of propane as a function of added chloride with $NaBiO_3$. Conditions: Propane (100 psi), KCl (if added, 0.1 mmol), $NaBiO_3$ (1.1 mmol), HTFA (8 mL), 80 °C, 2 h. Error bars denote standard deviations based on three experiments.

Although light alkane functionalization is observed using $NaBiO_3$, yields of functionalized products are significantly lower than those observed with iodate/chloride. For example, under identical conditions with 300 psi CH_4, 0.1 mmol KCl, 1.1 mmol oxidant in HTFA at 180 °C for 1 h, MeTFA yields with $NaBiO_3$ and iodate/chloride relative to oxidant are ~1.5% and ~42%, respectively (see Figures 4.1 and 4.5). The initial report of the OxE chemistry demonstrated that the ammonium iodate was the most effective, and as such, it is possible that bismuthate salts with ammonium or other counter-ions may be more efficient for light alkane functionalization. Further, as chloride is not required for alkane functionalization with $NaBiO_3$, the reaction may occur by a different mechanism than the OxE process with iodate/chloride. Further studies are required to elucidate the nature of these differences and to further optimize the process with bismuth oxidants.

4.4 Extension of the OxE Process to a Cerium Oxidant

Although using CAN as the oxidant did not result in higher yields of MeTFA than NH_4NO_3, the prevalence of cerium-based oxidants for oxychlorination chemistry[5-7] led us to study the ability of ceria, CeO_2, as a potential oxidant for the OxE system. Under the standard set of conditions for screening, CeO_2 resulted in MeTFA formation, but in poor yield with 0.6(2)% relative to oxidant (Scheme 4.5). In an effort toward optimization, the addition of 0.1 mmol of I_2 was tested. However, as was observed with $NaBiO_3$, the addition of iodine did not result in improved product yields. In fact, only trace amounts of MeTFA were observed when iodine was added to the reaction mixture (Scheme 4.6). Increasing the chloride loading for the $KCl/CeO_2/I_2$ process similarly did not improve yields of functionalized products (Scheme 4.7).

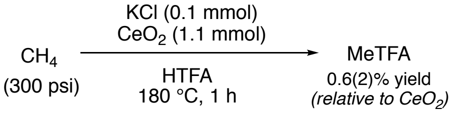

Scheme 4.5. Methane functionalization using KCl/CeO_2 in HTFA. Conditions: CH_4 (300 psi), KCl (0.1 mmol), CeO_2 (1.1 mmol), HTFA (8 mL), 180 °C, 1 h. Yield and standard deviation are based on three experiments.

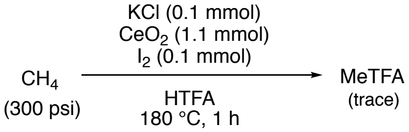

Scheme 4.6. Methane functionalization using $KCl/CeO_2/I_2$ in HTFA. Conditions: CH_4 (300 psi), KCl (0.1 mmol), CeO_2 (1.1 mmol), I_2 (0.1 mmol), HTFA (8 mL), 180 °C, 1 h. Trace MeTFA was observed in three experiments.

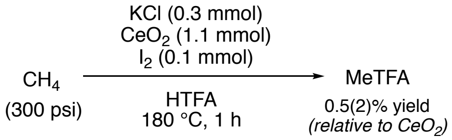

Scheme 4.7. Methane functionalization using KCl (0.3 mmol)/CeO_2/I_2 in HTFA. Conditions: CH_4 (300 psi), KCl (0.3 mmol), CeO_2 (1.1 mmol), I_2 (0.1 mmol), HTFA (8 mL), 180 °C, 1 h. Yield and standard deviation are based on three experiments.

Increasing the reaction temperature from 180 °C to 200 °C gave a slight increase in the yield of MeTFA from 0.6(2)% to 2.2(7)% (Figure 4.8), but the yield remained low. Due to restrictions in our reaction set-up, we are unable to examine temperatures higher than 200 °C, but that will be a future direction for this chemistry as we begin to examine the process in flow with the Wu group at ORNL.

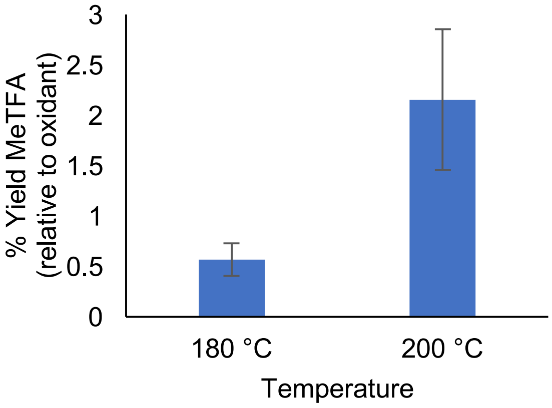

Figure 4.8. Methane functionalization using KCl/CeO_2 in HTFA at 180 °C and 200 °C. Conditions: CH_4 (300 psi), KCl (0.1 mmol), CeO_2 (1.1 mmol), HTFA (8 mL), 180 or 200 °C, 1 h.

4.5 Extension of the OxE Process to Manganese Oxidants

Manganese-based oxidants are highly oxidizing and can potentially be recycled using dioxygen.[11] They have also been demonstrated to functionalize methane,[11-12] making them promising candidates for this study to improve upon the OxE process. Additionally, many forms of heterogeneous manganese oxides exist,[13] enabling a broad screening with different oxidation states of manganese. Manganese(IV) oxide (MnO_2) was tested initially due to its availability, low cost and lower oxidation state than traditional strong Mn-based oxidants such as $KMnO_4$.

Using manganese-based oxidants for the OxE process under the standard screening conditions tested for the nitrate-, bismuth- and cerium-based oxidants (see above), ^1H NMR spectroscopy data were difficult to interpret due to significant peak broadening. This broadening was minimized through the development of a work-up procedure involving oxidation of reduced manganese species using $NaBiO_3$ following the reaction to minimize peak shifts and broadening due to paramagnetic resonances. The $NaBiO_3$ work-up was utilized for all reactions with manganese-based oxidants. The addition of iodine at the start of the reaction was also critical. Without added iodine, the resonances remain very broad and yields of MeTFA are ~20% with respect to oxidant. However, the addition of 0.1 mmol of I_2 to the standard conditions with KCl/MnO_2 resulted in a clean ^1H NMR spectrum (see Figure 4.29) and the selective production of MeTFA, in 60(1)% yield (Figure 4.9, right). This finding prompted further investigation into the role of additives in this reaction. Chloride was subsequently excluded from the reaction, and the combination of MnO_2 and I_2 in HTFA resulted in 59(2)% yield of MeTFA, indicating that chloride was not necessary for the reaction (Figure 4.9, left). Consequently, chloride was not added to future reactions studying light alkane functionalization with MnO_2.

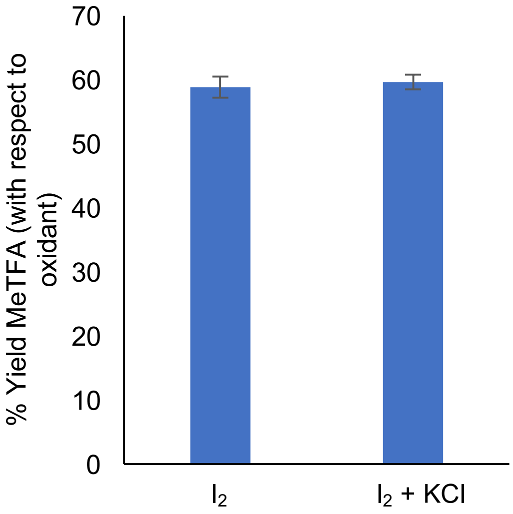

Figure 4.9. Functionalization of methane as a function of additives with MnO_2. Conditions: CH_4 (300 psi), KCl (0.1 mmol, if added), MnO_2 (1.1 mmol), I_2 (0.1 mmol), HTFA (8 mL), 180 °C, 1 h. Error bars denote standard deviations based on three experiments.

In contrast to chloride, the addition of iodine had a marked effect on the reaction. Thus, a screening of different iodine loadings was performed. As shown in Figure 4.10, highest yields of MeTFA were obtained using 0.15 mmol of iodine, and this amount was used in additional optimization studies. The addition of > 0.15 mmol of iodine resulted in lower yields of MeTFA (Figure 4.10), similar to what was observed in the original OxE process using iodate as the oxidant.[8]

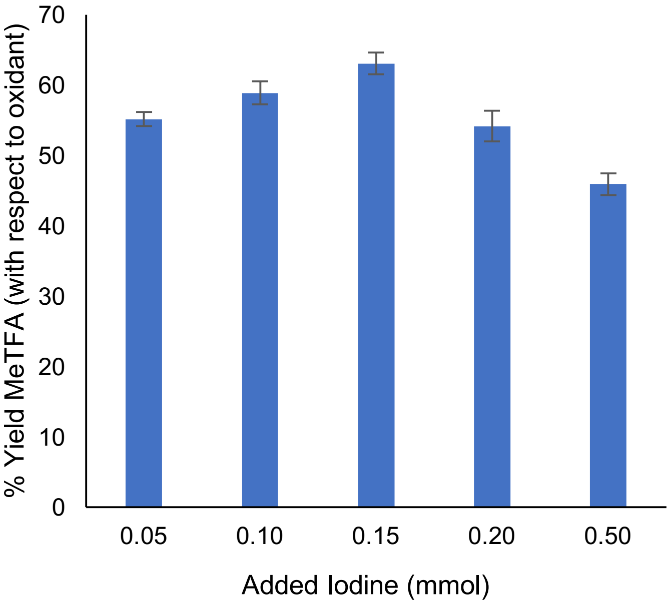

Figure 4.10. Methane functionalization with MnO_2 as a function of added iodine. Conditions: CH_4 (300 psi), MnO_2 (1.1 mmol), HTFA (8 mL), 180 °C, 1 h. Error bars denote standard deviations based on three experiments.

A range of manganese-based oxidants were tested under the identified optimal additive conditions with MnO_2 and 0.15 mmol of iodine (Figure 4.10). Interestingly, MnO_2, Mn_2O_3 and Mn_3O_4 each gave ~63% yield of MeTFA, whereas $KMnO_4$, K_2MnO_4 and $Mn(OAc)_3 \cdot 2H_2O$ resulted in significantly lower yields of MeTFA of ~20-35%. The lower yields obtained using oxidants with manganese in higher oxidation states were surprising given their strong oxidizing power. Examining the stability of MeTFA under reaction conditions with $KMnO_4$ provides a possible rationalization for the lower observed MeTFA yields (Scheme 4.8). Whereas > 80% of MeTFA remains under identical conditions at 140 °C with MnO_2/I_2 (Figure 4.16), only 69(1)% remains with $KMnO_4/I_2$. This may indicate that the protecting effect of the TFA moiety may not be strong enough to prevent over-oxidation of MeTFA by $KMnO_4$. Another possible issue with $KMnO_4$ is a greater degree of solvent oxidation, which would limit yields of functionalized product.

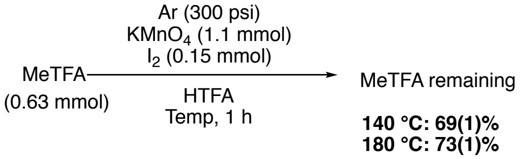

Scheme 4.8. MeTFA stability under reaction conditions with $KMnO_4/I_2$. Conditions: MeTFA (0.63 mmol), Ar (300 psi), $KMnO_4$ (1.1 mmol), I_2 (0.15 mmol), HTFA (8 mL), 140 °C or 160 °C, 1 h.

These results do not appear to follow a clear trend related to the oxidation state of manganese, as Mn(III) oxidants gave the highest and lowest yields in the screening (Figure 4.11). However, several manganese oxides were identified as effective oxidants for methane functionalization and gave extremely similar yields to one another, indicating that they might all funnel to the same active intermediate or follow the same mechanistic pathway. It was proposed that these oxidants may undergo disproportionation to generate more strongly oxidizing species under reaction conditions. Mechanistic studies are underway to determine the operative pathway through which functionalization occurs using these oxidants. As MnO_2 was one of the highest-yielding oxidants, it was used in additional optimization studies.

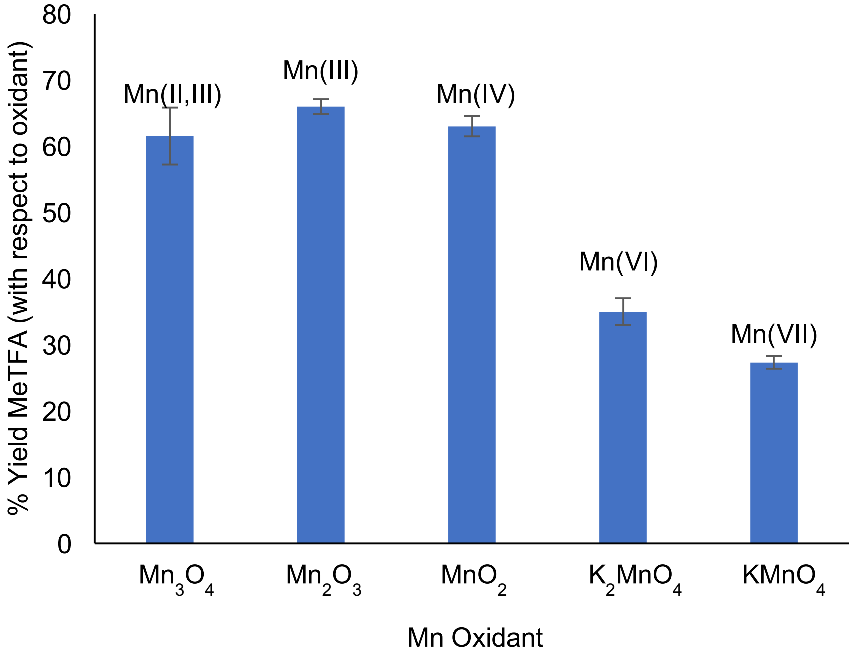

Figure 4.11. Screening Mn oxidants for methane functionalization. Conditions: CH_4 (300 psi), Mn source (1.1 mmol), I_2 (0.15 mmol), HTFA (8 mL), 180 °C, 1 h. Error bars denote standard deviations based on three experiments. Inset are the oxidations states of each oxidant. Yields are calculated by (mmol MeTFA)/(mmol oxidant)*100 not on a per-manganese basis.

Methane pressures were lowered to determine if higher MeTFA yields relative to methane could be obtained. With a lower pressure of methane, the yield of MeTFA relative to oxidant decreased significantly, thus the yield of MeTFA relative to methane remained statistically identical (Figure 4.12). Additional studies sought to understand this effect. First, higher loadings of MnO_2 oxidant were examined (Figure 4.13). With higher oxidant loadings, yields of MeTFA relative to methane yields increased, though not by an amount proportional to the increased amount of oxidant. Thus, an increase in MeTFA yield from 2.79(1)% to 3.89(6)% was observed with 1.1 and 2.2 mmol of MnO_2, respectively. However, the MeTFA yield relative to MnO_2 decreased from 63(2)% to 46(1)% with 1.1 and 2.2 mmol of MnO_2. Similarly, increasing the MnO_2 loading to 3.3 mmol did not result in a three-fold increase relative to reactions with 1.1 mmol, in fact, the yield of MeTFA was only 1.8 times higher with 3.3 mmol of MnO_2. However, this demonstrated that MeTFA yields of up to 5% with respect to methane could be obtained using the MnO_2/I_2 process in HTFA.

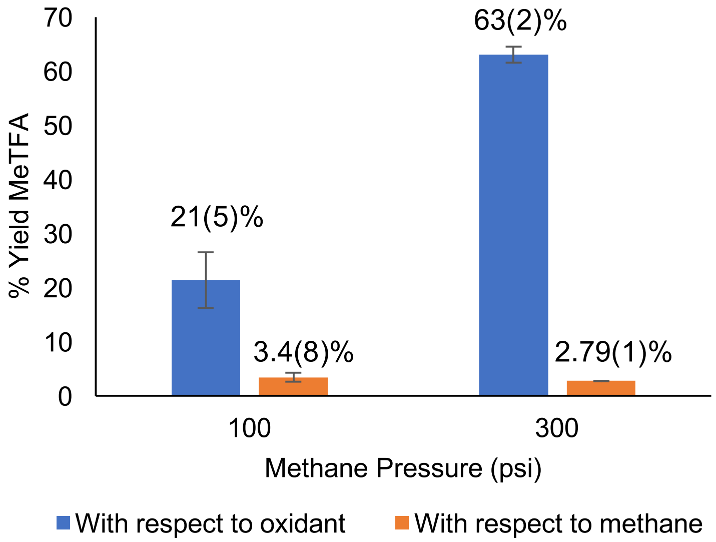

Figure 4.12. Methane functionalization with MnO_2/I_2 as a function of methane pressure. Conditions: CH_4 (100 or 300 psi), MnO_2 (1.1 mmol), I_2 (0.15 mmol), HTFA (8 mL), 180 °C, 1 h. Error bars denote standard deviations based on three experiments.

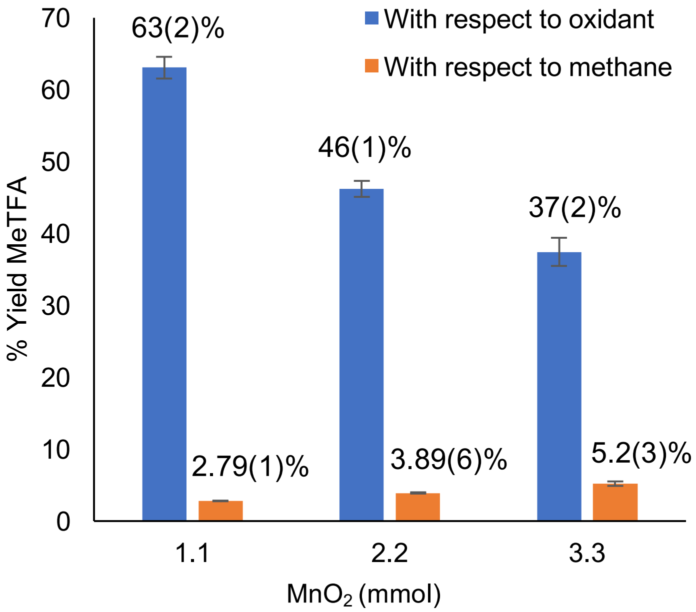

Figure 4.13. Methane functionalization with MnO_2/I_2 as a function of MnO_2 loading. Conditions: CH_4 (300 psi), MnO_2 (1.1-3.3 mmol), I_2 (0.15 mmol), HTFA (8 mL), 180 °C, 1 h. Error bars denote standard deviations based on three experiments.

In contrast, increasing the oxidant loading with $Mn(OAc)_3 \cdot 2H_2O$ did result in proportional increases in MeTFA yields with respect to methane as the yield relative to oxidant remained constant (Figure 4.14). Although the yields are lower than those observed with MnO_2, this effective scale-up has led to a re-evaluation of $Mn(OAc)_3 \cdot 2H_2O$ as an oxidant for the OxE system, and additional studies to determine the differences between the reactions with $Mn(OAc)_3 \cdot 2H_2O$ and MnO_2 are required.

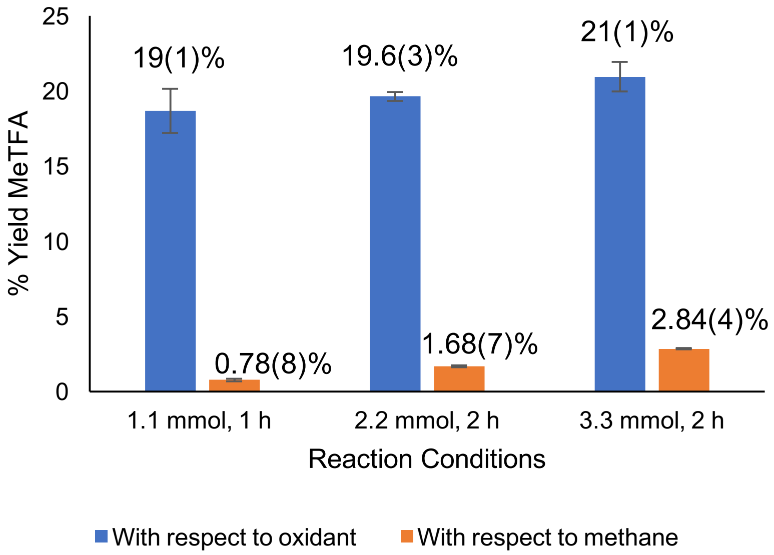

Figure 4.14. Methane functionalization with $Mn(OAc)_3 \cdot 2H_2O/I_2$ as a function of I_2 loading. Conditions: CH_4 (300 psi), $Mn(OAc)_3 \cdot 2H_2O$ (1.1, 2.2 or 3.3 mmol), I_2 (0.15 mmol), HTFA (8 mL), 180 °C, 1 or 2 h. Error bars denote standard deviations based on three experiments. Yields are calculated by (mmol MeTFA)/(mmol oxidant)*100 not on a per-manganese basis.

To determine if increasing the amount of iodine in proportion with the increase in oxidant would result in higher yields of MeTFA, the reaction with doubled loadings of MnO_2 and I_2 (Figure 4.15, right) was compared to the reaction wherein solely the oxidant loading was scaled up (Figure 4.15, left). This alteration did not have a significant effect on MeTFA yield, which was surprising given the inhibition observed previously when excess iodine was added (Figure 4.10).

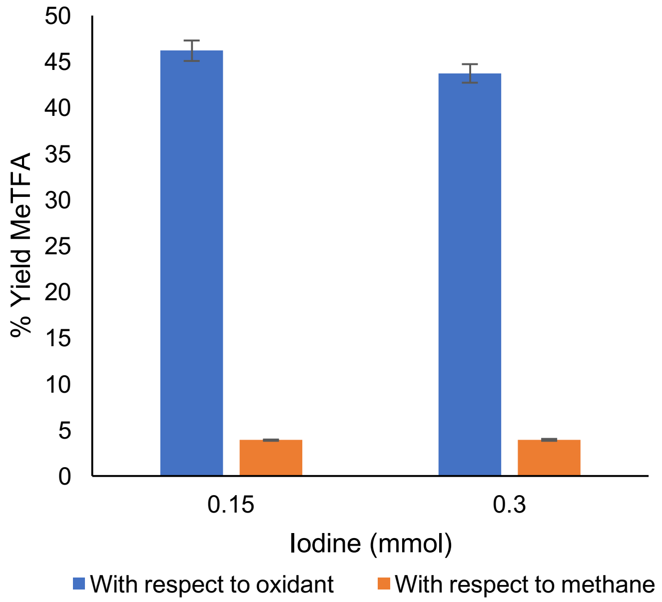

Figure 4.15. Methane functionalization with MnO_2/I_2 as a function of I_2 loading. Conditions: CH_4 (300 psi), MnO_2 (2.2 mmol), I_2 (0.15 or 0.3 mmol), HTFA (8 mL), 180 °C, 1 h. Error bars denote standard deviations based on three experiments.

One of the hallmarks of the OxE process is its selectivity for mono-functionalized products. As the manganese-based oxidants also exhibit selectivity for MeTFA formation, the stability of MeTFA under reaction conditions was studied to compare the oxidation of MeTFA with MnO_2/I_2 versus iodate/chloride. Reaction conditions for methane functionalization and MeTFA decay similar to those in Chapter 2 were used for MnO_2-based functionalization and decay (Figure 4.16). The reaction temperature was decreased to 140 °C to slow the rate of functionalization in order to compare it to the rate of decay over time. Methane functionalization is complete after 4 h. Although the MeTFA decay data are less consistent than was previously observed using iodate/chloride, MeTFA is also stable under the reaction conditions with MnO_2/I_2. After 16 h under oxidizing conditions, > 80% of the starting MeTFA remains. Under identical reaction conditions with iodate/chloride, ~85% remained after that amount of time. These results demonstrate that the rate of over-oxidation of MeTFA is slow compared to the rate of methane functionalization. Using the linear fit of the MeX production that was forced through zero (Figure 4.16, dark blue), the ratio of methane functionalization to MeTFA decay with MnO_2/I_2 is approximately 35. Using a linear fit of the data through four hours without forcing the fit through zero (Figure 4.16, light blue), the ratio of methane functionalization to MeTFA decay is higher, approximately 54. These values are significantly higher than the ratio of 13 observed using iodate/chloride. It should be noted that the R^2 of the fit for the MeTFA decay data is low. However, these data demonstrate that MeTFA decay is significantly slower than methane functionalization with MnO_2/I_2, as was also observed with iodate/chloride.

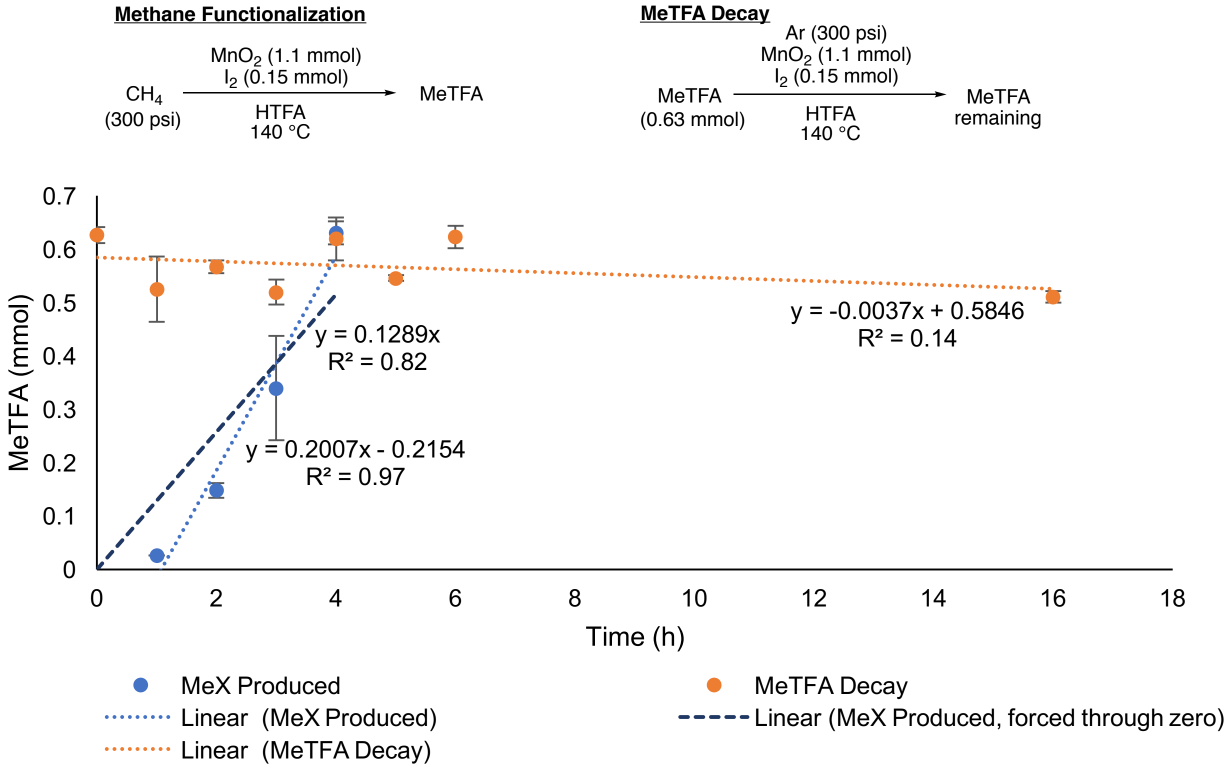

Figure 4.16. Methane functionalization versus MeTFA decay using MnO_2/I_2. Methane functionalization conditions: CH_4 (300 psi), MnO_2 (1.1 mmol), I_2 (0.15 mmol), HTFA (8 mL), 140 °C. MeTFA decay conditions: MeTFA (0.63 mmol), Ar (300 psi), MnO_2 (1.1 mmol), I_2 (0.15 mmol), HTFA (8 mL), 140 °C. Error bars denote standard deviations based on three experiments.

As we seek to shift away from the use of HTFA as a solvent for the OxE process, dilute HTFA and HOAc were also tested as potential solvents for methane functionalization with MnO_2/I_2 (Figure 4.17). Formation of MeX (X = TFA, OAc) is observed in both solvents, however yields are significantly lower than those obtained in neat HTFA. This indicates that strongly acidic media is likely necessary for the generation of active species, as was observed in the original OxE process using iodate/chloride.[8, 14]

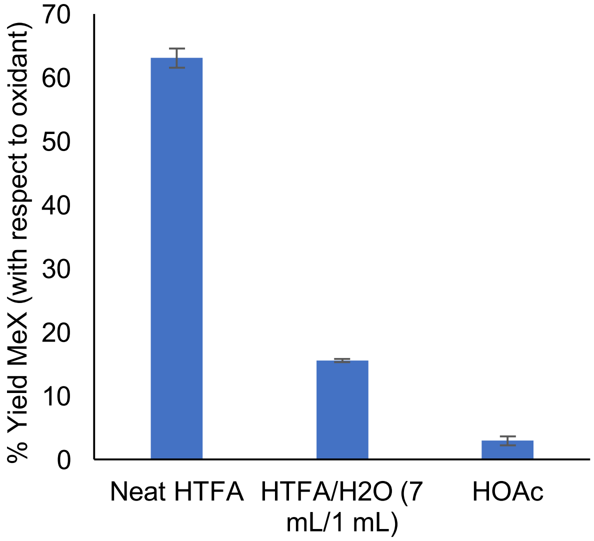

Figure 4.17. Methane functionalization using MnO_2/I_2 as a function of solvent. Conditions: CH_4 (300 psi), MnO_2 (1.1 mmol), I_2 (0.15 mmol), 8 mL solvent, 180 °C, 1 h. Error bars denote standard deviations based on three experiments.

4.6 Extension of the OxE Process to Iron Oxidants

Iron-based catalysts have also been demonstrated to partially oxidize light alkanes under oxychlorination conditions,[15-17] and the metal-organic framework iron 1,3,5-benzenetricarboxylate (Fe-BTC) has been studied for the oxidation of alkanes and benzylic compounds.[18-22] As an initial screening, iron(III) chloride, iron(III) oxide and Fe-BTC were examined as potential Fe-based oxidants for the OxE process. Under the standard screening conditions used for new oxidants, Fe-BTC gave high yields of MeTFA, > 60% relative to oxidant, while Fe_2O_3 produced only trace amounts of MeTFA and $FeCl_3$ did not produce

MeTFA (Figure 4.18). Thus, initial optimization studies focused on the use of Fe-BTC. Surprisingly, varying the chloride loading, adding iodine or omitting both chloride and iodine gave nearly identical yields of MeTFA, all ~60% (Figure 4.19). These results indicate that the reaction with Fe-BTC may operate by a different mechanism than the process with iodate/chloride, where the presence of chloride was essential for efficient methane functionalization (see Section 4.7).

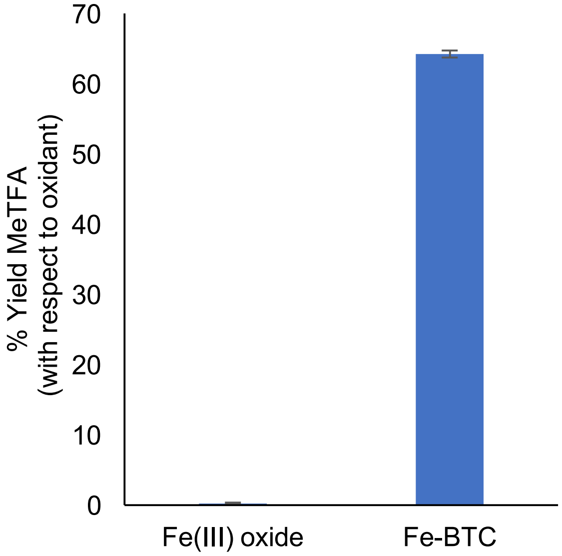

Figure 4.18. Methane functionalization using iron-based oxidants with KCl in HTFA. Conditions: CH_4 (300 psi), Fe_2O_3 or Fe-BTC (1.1 mmol), HTFA (8 mL), 180 °C, 1 h. Error bars denote standard deviations based on three experiments. Yields are calculated by (mmol MeTFA)/(mmol oxidant)*100 not on a per-iron basis.

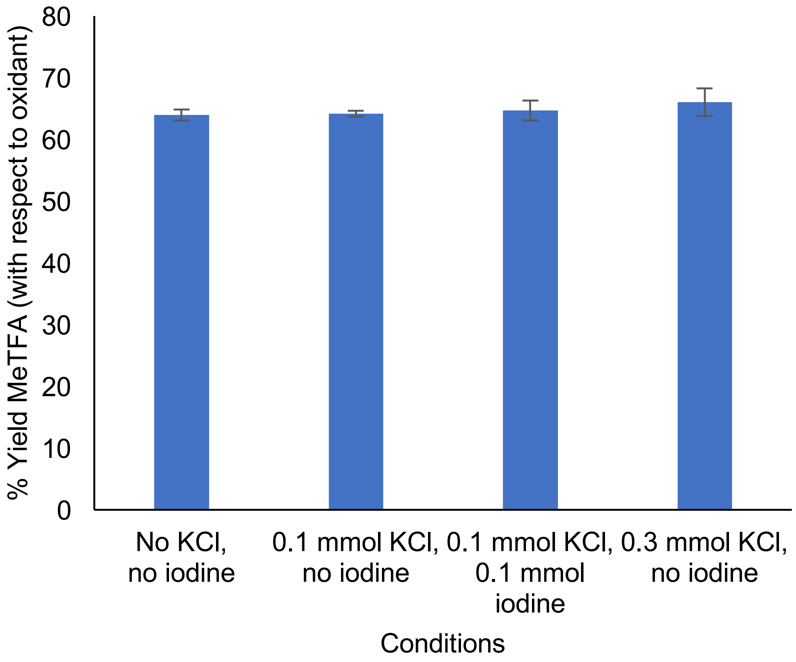

Figure 4.19. Additive screening using Fe-BTC for methane functionalization. Conditions: CH_4 (300 psi), Fe-BTC (1.1 mmol), KCl (0-0.3 mmol), I_2 (0-0.1 mmol), HTFA (8 mL), 180 °C, 1 h. Error bars denote standard deviations based on three experiments. Yields are calculated by (mmol MeTFA)/(mmol oxidant)*100 not on a per-iron basis.

4.7 Extension of the OxE Process to a Copper(II) Oxidant

As Fe-BTC was demonstrated to be a capable oxidant for the partial oxidation of methane, the Cu(II) derivative of the MOF (Cu-BTC), which has also been studied for the oxidation of alkanes and benzylic compounds,[20, 22-24] was also examined. The reactivity of Cu-BTC was first studied in the absence of KCl and I_2 as those additives did not affect the methane functionalization reaction with Fe-BTC. In the absence of additives, Cu-BTC mediates the conversion of methane to MeTFA in HTFA in 87(3)% yield relative to oxidant (calculated based on mmol of oxidant, not calculated on a per-copper basis), outperforming Fe-BTC under identical reaction conditions (Figure 4.20). However, using the conditions in Figure 4.20 with argon instead of methane, 58(2)% and 93(2)% yields of MeTFA were observed with Fe-BTC and Cu-BTC, respectively. These results indicate that the MeTFA observed with these oxidants is likely the result of methanol extraction from the MOF structure and subsequent conversion to MeTFA on solvolysis rather than methane functionalization. This provides a rationalization for why similar yields are observed under reaction conditions with Fe-BTC and various additives.

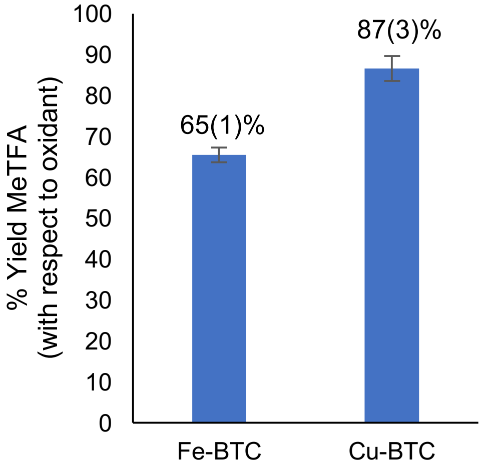

Figure 4.20. Comparison of Fe-BTC and Cu-BTC for the partial oxidation of methane to MeTFA. Conditions: CH_4 (300 psi), Cu-BTC or Fe-BTC (0.1 mmol), HTFA (8 mL), 180 °C, 1 h. All reactions were set up under ambient atmosphere. Yields are calculated by (mmol MeTFA)/(mmol oxidant)*100 not on a per-iron or per-copper basis.

4.8 Conclusions and Future Directions

Mechanistic studies of the OxE process with iodate/chloride indicate that light alkane functionalization likely occurs through a pathway that involves the formation of free radicals that abstract H-atoms from alkane C–H bonds. The selectivity of the process for mono-functionalized products is proposed to be a manifestation of the polar effect, wherein the TFA moiety of the functionalized product (*e.g.*, MeTFA) is protected from over-oxidation reduces the polarity of the transition state for H-atom abstraction relative to that of the substrate. As a result, there is a higher barrier to oxidation of the product even though its C–H bond is weaker than that of the starting alkane. Thus, the OxE process with iodate/chloride demonstrates the efficacy of a radical-based process for light alkane functionalization and uses catalytic amounts of chloride to generate chlorine radicals capable of H-atom abstraction *in situ*. Therefore, we have sought to apply this chemistry to more readily air-recyclable oxidants while maintaining the motif of product protection that is crucial to the OxE process.

We have begun to examine the scope of potentially viable oxidants for the next-generation OxE processes. Metal oxides based on cerium and bismuth, which have been studied as catalysts or additives for oxyhalogenation chemistry, were largely unsuccessful, although minimal yields of functionalized products were observed. As oxyhalogenation chemistry requires significantly higher temperatures than are within our current capabilities, the lackluster performance of these oxidants may be improved when tested at elevated temperatures. Alternatively, these oxidants could be too strongly oxidizing and overcome the protecting effect to over-oxidize functionalized products. In contrast, higher yields of functionalized products have been obtained with nitrates as well as manganese-, iron- and copper-based oxidants.

The efficacy of nitrates in the presence of chloride salts demonstrates the ability to transfer the OxE chemistry to other oxidants, while maintaining the high selectivity for mono-functionalized products obtained in the original OxE process. The addition of iodine, which has been proposed to be a crucial intermediate in the original OxE process,[8] resulted in significantly higher yields of functionalized products with NH_4NO_3. Furthermore, similar to the OxE process, the addition of greater amounts of iodine results in lower yields of functionalized product. Chloride, another proposed intermediate in the OxE process using iodate and chloride,[8] has been shown to improve yields of functionalized products significantly, although ~10% yield relative to oxidant was obtained in the absence of chloride. Mechanistic studies are required to determine if recycling of the oxidant is possible with dioxygen and to elucidate the nature of the reaction mechanism, as the production of nitroalkanes was unexpected. As there is precedent for the recycling of NO to NO_2, which could form from the reduction of nitrate, with dioxygen,[4] future studies with nitrates will focus on the re-oxidation of the salts *in situ* using co-oxidants or dioxygen.

A variety of manganese-based oxidants have been shown to mediate methane functionalization under OxE conditions. MnO_2, Mn_3O_4 and Mn_2O_3 are the most effective, each with > 60% yield of MeTFA relative to oxidant. As a readily available and relatively inexpensive oxidant, MnO_2 has been used for optimization studies. It has been demonstrated that iodine was necessary to obtain these high yields and clear ^{1}H NMR spectra for analysis. Surprisingly, the addition of chloride is unnecessary for methane functionalization using MnO_2 and the other manganese oxides which were tested, in contrast to what was observed in the iodate/chloride and periodate/chloride studies.[9-10]

A noteworthy facet of the original OxE process with iodate/chloride is its capacity to functionalize light alkanes with minimal over-oxidation of the starting alkane. MeTFA is also relatively stable under reaction conditions with MnO_2/I_2, with > 80% of the starting amount of MeTFA remaining after 16 h at 140 °C, which is comparable to the ~85% that remained when iodate/chloride was used. Thus, over-oxidation of MeTFA is slow for the MnO_2-based oxidation as well. Solvent studies demonstrated that, similar to the iodate/chloride process, functionalization with MnO_2 is not as efficient in less acidic media. Mechanistic studies will seek to elucidate active intermediate species in efforts to extend this chemistry to less acidic and more affordable solvents.

We propose that the Mn-based oxidants could be disproportionate to give higher oxidation state manganese species {e.g., Mn(V)} active for methane functionalization. As chloride is not required, the high valent Mn oxidant likely performs H-atom abstraction to give alkyl radicals. As in the case of the OxE reaction with iodate/chloride, iodine could trap these alkyl radicals to generate alkyl iodides which are converted to alkyl trifluoroacetate esters in HTFA solvent.

Iron- and copper-based oxidants Fe-BTC and Cu-BTC result in methane functionalization in HTFA in the absence of any additives. As other Fe(III) and Cu(II) oxidants have resulted in minimal functionalization, additional studies are required to determine the role of the metal organic framework and its stability or instability under the reaction conditions. We propose that additives are not needed as the oxidant is able to trap radicals efficiently itself, but further mechanistic studies are necessary.

4.9 Experimental Section

General Considerations. *Caution: Many of the reagents and conditions described herein are potentially hazardous. Safety procedures should be consulted prior to the use of concentrated acids, mixtures of hydrocarbons and oxygen and strong oxidants.*

Unless noted otherwise, all reactions were performed under ambient atmosphere. All chemicals were purchased from commercial sources and used as received. Gases were purchased from GTS-Welco and were used as received. NMR analysis was performed using a Varian Inova 500 or NMRS 600 spectrometer. NMR spectra of reaction mixtures were obtained using neat HTFA or HOAc with a C_6D_6 capillary as an internal lock reference. Nitromethane or acetic acid were added as internal standards and used to reference ^1H NMR spectra (δ 4.18 and 2.04, respectively). High pressure reactions were performed custom-built stainless-steel reactors.[9-10]

General Procedures

Methane functionalization with KCl/NH_4IO_3 for comparison to other oxidants. A custom-built stainless-steel reactor with a Teflon liner[9-10] was charged with a stir bar, KCl (0.1 mmol), NH_4IO_3 (1.1 mmol) and HTFA (8 mL). The reactor was sealed and pressurized with 300 psi of methane. After the mixture was stirred at 800 rpm at 180 °C for 1 h, the reactor was allowed to cool to room temperature. The reactor was then vented carefully, and HOAc was added as an internal standard. After stirring, an aliquot was removed for centrifugation. The supernatant was analyzed by ^1H NMR. A representative ^1H NMR spectrum is shown below. This procedure was performed in triplicate.

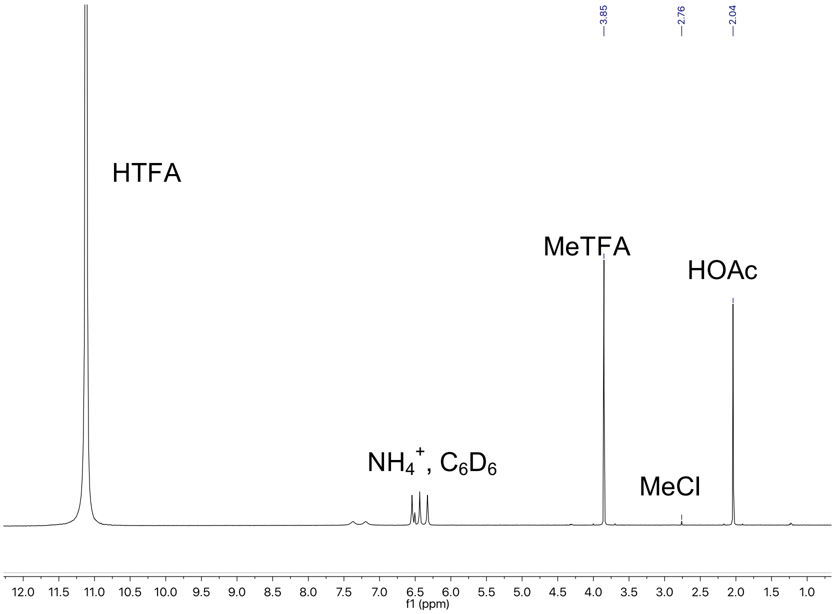

Figure 4.21. Representative ^1H NMR spectrum of methane functionalization with KCl/NH_4IO_3 in HTFA. Conditions: CH_4 (300 psi), KCl (0.1 mmol), NH_4IO_3 (1.1 mmol), HTFA (8 mL), 180 °C, 1 h. HOAc (0.35 mmol) was added as an internal standard.

Methane functionalization with nitrate oxidants. A custom-built stainless-steel reactor with a Teflon liner[9-10] was charged with a stir bar, KCl (0-0.5 mmol), nitrate oxidant (ceric ammonium nitrate, NH_4NO_3 or KNO_3, 1.1 mmol), I_2 (0-0.2 mmol) and HTFA (8 mL). The reactor was sealed and pressurized with 300 psi of methane. After the mixture was stirred at 800 rpm at 180 °C for 1-4 h, the reactor was allowed to cool to room temperature. The reactor was then vented carefully, and HOAc was added as an internal standard. After stirring, an aliquot was removed for centrifugation. The supernatant was analyzed by ^{1}H NMR. A representative ^{1}H NMR spectrum is shown below. Each condition was performed in triplicate.

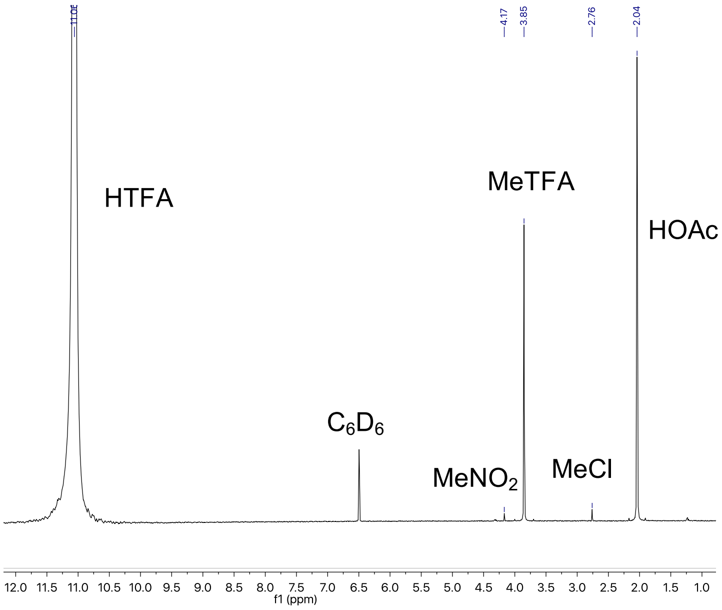

Figure 4.22. Representative ^{1}H NMR spectrum of methane functionalization with $KCl/NH_4NO_3/I_2$ in HTFA. Conditions: CH_4 (300 psi), KCl (0.1 mmol), NH_4NO_3 (1.1 mmol), I_2 (0.1 mmol), HTFA (8 mL), 180 °C, 2 h. HOAc (0.35 mmol) was added as an internal standard.

Ethane functionalization with KCl/NH_4NO_3. A custom-built stainless-steel reactor with a Teflon liner[9-10] was charged with a stir bar, KCl (0.1 mmol), NH_4NO_3 (1.1 mmol) and HTFA (8 mL). The reactor was sealed and pressurized with 300 psi of methane. After the mixture was stirred at 800 rpm at 180 °C for 2 h, the reactor was allowed to cool to room temperature. The reactor was then vented carefully, and HOAc was added as an internal standard. After stirring, an aliquot was removed for centrifugation. The supernatant was analyzed by ^{1}H NMR. A representative ^{1}H NMR spectrum is shown below. Nitroethane formation was confirmed by spiking a sample with a known standard. This procedure was performed in triplicate.

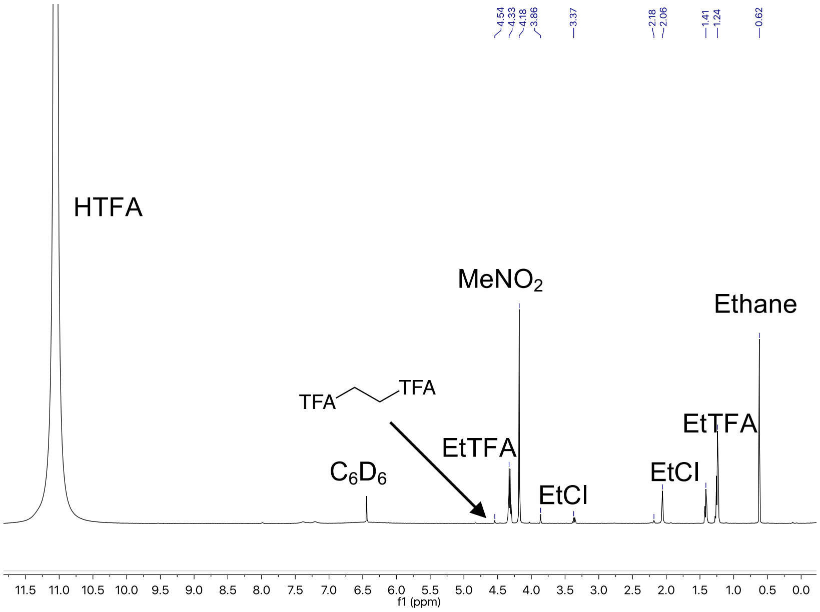

Figure 4.23. Representative ^{1}H NMR spectrum of ethane functionalization with KCl/NH_4NO_3 in HTFA. Conditions: CH_3CH_3 (300 psi), KCl (0.1 mmol), NH_4NO_3 (1.1 mmol), HTFA (8 mL), 180 °C, 2 h. Nitromethane (0.37 mmol) added as an internal standard.

Methane functionalization with $NaBiO_3$. A custom-built stainless-steel reactor with a Teflon liner[9-10] was charged with a stir bar, KCl (0.1 mmol), $NaBiO_3$ (1.1 mmol), I_2 (0-0.0.5 mmol) and HTFA (8 mL). The reactor was sealed and pressurized with 300 psi of methane. After the mixture was stirred at 800 rpm at 180 °C for 1 h, the reactor was allowed to cool to room temperature. The reactor was then vented carefully, and HOAc was added as an internal standard. After stirring, an aliquot was removed for centrifugation. The supernatant was analyzed by ^{1}H NMR. A representative ^{1}H NMR spectrum is shown below. Each condition was performed in triplicate.

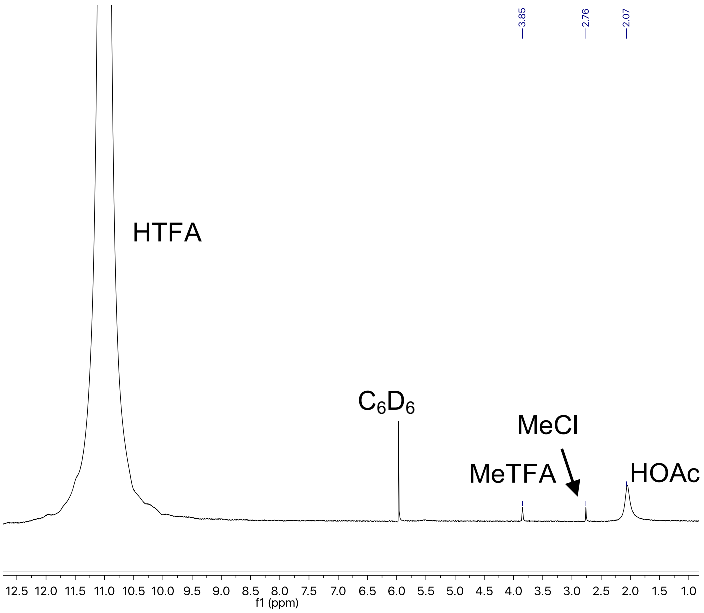

Figure 4.24. Representative ^{1}H NMR spectrum of methane functionalization with KCl/NaBiO$_3$ in HTFA. Conditions: CH$_4$ (300 psi), KCl (0.1 mmol), NH$_4$NO$_3$ (1.1 mmol), HTFA (8 mL), 180 °C, 1 h. HOAc (0.35 mmol) was added as an internal standard.

MeTFA decay in the presence of NaBiO$_3$. A custom-built stainless-steel reactor with a Teflon liner[9-10] was charged with a stir bar, MeTFA (0.65 mmol) KCl (0-0.1 mmol), NaBiO$_3$ (1.1 mmol), I$_2$ (0-0.0.5 mmol) and HTFA (8 mL). The reactor was sealed and pressurized with 300 psi of argon. After the mixture was stirred at 800 rpm at 80 °C for 2 h, the reactor was allowed to cool to room temperature. The reactor was then vented carefully, and HOAc was added as an internal standard. After stirring, an aliquot was removed for centrifugation. The supernatant was analyzed by ^{1}H NMR. A representative ^{1}H NMR spectrum is shown below. This procedure was performed in triplicate.

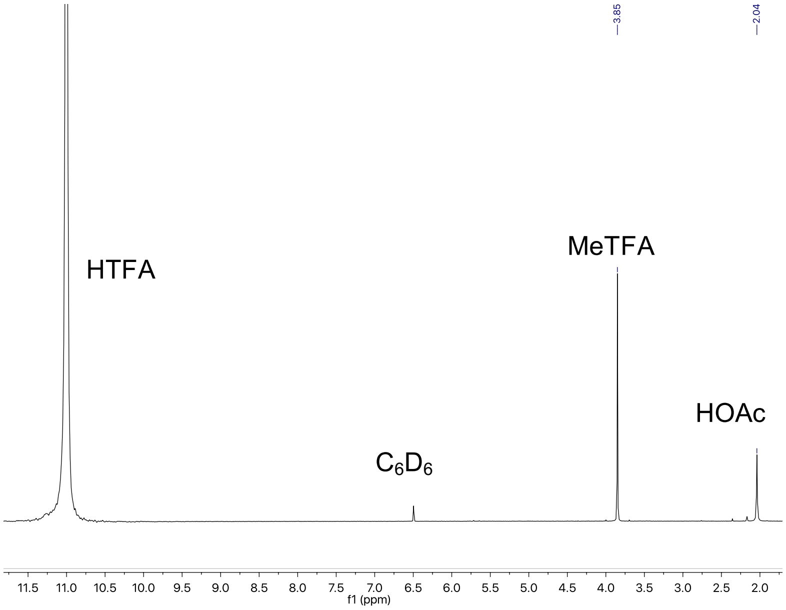

Figure 4.25. Representative ^{1}H NMR spectrum of MeTFA decay in the presence of $NaBiO_3$. Conditions: Argon (300 psi), MeTFA (0.65 mmol), KCl (0.1 mmol), NH_4NO_3 (1.1 mmol), HTFA (8 mL), 80 °C, 2 h. HOAc (0.35 mmol) was added as an internal standard.

Ethane functionalization with $NaBiO_3$. A custom-built stainless-steel reactor with a Teflon liner[9-10] was charged with a stir bar, KCl (0 or 0.1 mmol), $NaBiO_3$ (1.1 mmol) and HTFA (8 mL). The reactor was sealed and pressurized with 300 psi of ethane. After the mixture was stirred at 800 rpm at 80 °C for 2 h, the reactor was allowed to cool to room temperature. The reactor was then vented carefully, and nitromethane was added as an internal standard. After stirring, an aliquot was removed for centrifugation. The supernatant was analyzed by ^{1}H NMR. A representative ^{1}H NMR spectrum is shown below. Each condition was performed in triplicate.

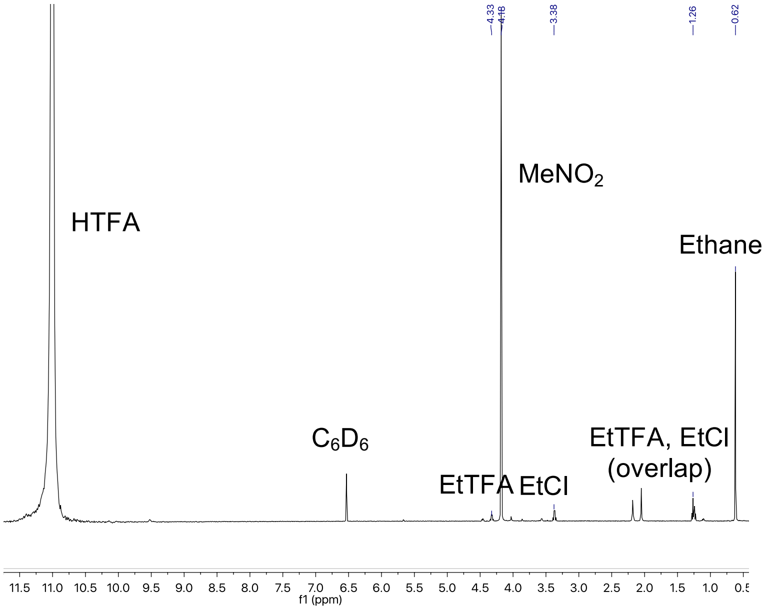

Figure 4.26. Representative ^{1}H NMR spectrum of ethane functionalization with KCl/$NaBiO_3$ in HTFA. Conditions: CH_4 (300 psi), KCl (0.1 mmol), $NaBiO_3$ (1.1 mmol), HTFA (8 mL), 80 °C, 2 h. Nitromethane (0.37 mmol) was added as an internal standard.

Propane functionalization with $NaBiO_3$. A custom-built stainless-steel reactor with a Teflon liner[9-10] was charged with a stir bar, KCl (0 or 0.1 mmol), $NaBiO_3$ (1.1 mmol) and HTFA (8 mL). The reactor was sealed and pressurized with 100 psi of propane. After the mixture was stirred at 800 rpm at 80 °C for 2 h, the reactor was allowed to cool to room temperature. The reactor was then vented carefully, and HOAc was added as an internal standard. After stirring, an aliquot was removed for centrifugation. The supernatant was analyzed by ^{1}H NMR. A representative ^{1}H NMR spectrum is shown below. Each condition was performed in triplicate.

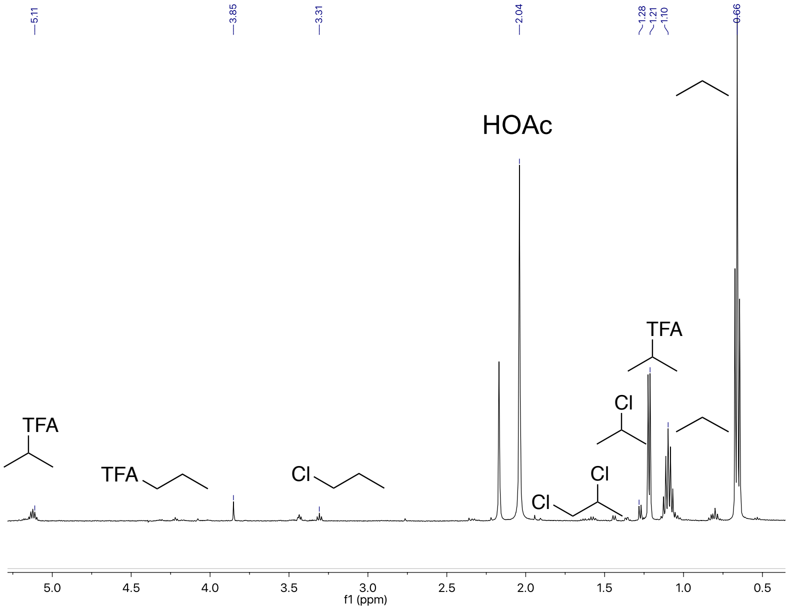

Figure 4.27. Representative ^{1}H NMR spectrum of propane functionalization with KCl/NaBiO$_3$ in HTFA. Conditions: CH$_4$ (300 psi), KCl (0.1 mmol), NaBiO$_3$ (1.1 mmol), HTFA (8 mL), 80 °C, 2 h. HOAc (0.35 mmol) was added as an internal standard.

Methane functionalization with CeO$_2$. A custom-built stainless-steel reactor with a Teflon liner[9-10] was charged with a stir bar, KCl (0.1 or 0.3 mmol), CeO$_2$ (1.1 mmol), I$_2$ (0 or 0.1 mmol) and HTFA (8 mL). The reactor was sealed and pressurized with 300 psi of methane. After the mixture was stirred at 800 rpm at 180 °C for 1 h, the reactor was allowed to cool to room temperature. The reactor was then vented carefully, and nitromethane was added as an internal standard. After stirring, an aliquot was removed for centrifugation. The supernatant was analyzed by ^{1}H NMR. A representative ^{1}H NMR spectrum is shown below. Each condition was performed in triplicate.

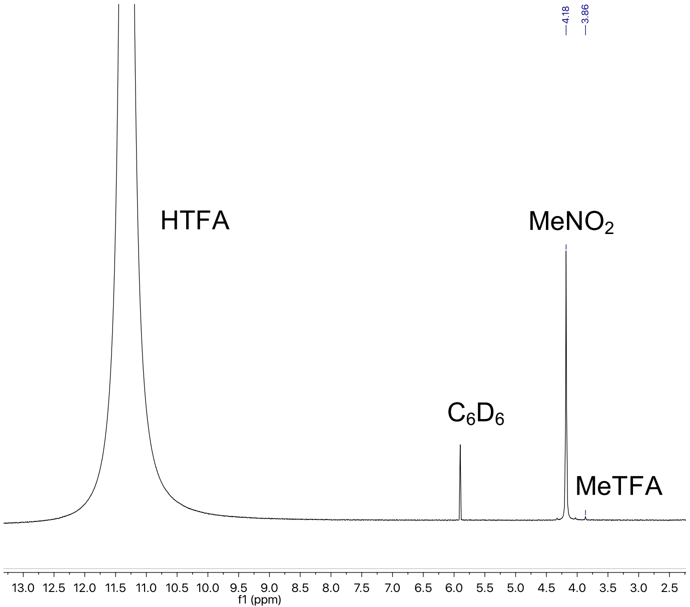

Figure 4.28. Representative ^{1}H NMR spectrum of methane functionalization with KCl/CeO_2. Conditions: CH_4 (300 psi), KCl (0.1 mmol), CeO_2 (1.1 mmol), HTFA (8 mL), 180 °C, 1 h. Nitromethane (0.37 mmol) was added as an internal standard.

Methane functionalization with MnO_2. A custom-built stainless-steel reactor with a Teflon liner[9-10] was charged with a stir bar, KCl (if added, 0.1 mmol), MnO_2 (1.1-3.3 mmol), I_2 (0.05-0.5 mmol) and HTFA (8 mL). The reactor was sealed and pressurized with 100 or 300 psi of methane. After the mixture was stirred at 800 rpm at 180 °C for 1 h, the reactor was allowed to cool to room temperature. The reactor was then vented carefully, and nitromethane was added as an internal standard. After stirring, a 1 mL aliquot was added to a centrifuge tube with $NaBiO_3$. The centrifuge tube was shaken and then centrifuged. The supernatant was analyzed by ^{1}H NMR. Representative ^{1}H NMR spectra are shown below. Each condition was performed in triplicate.

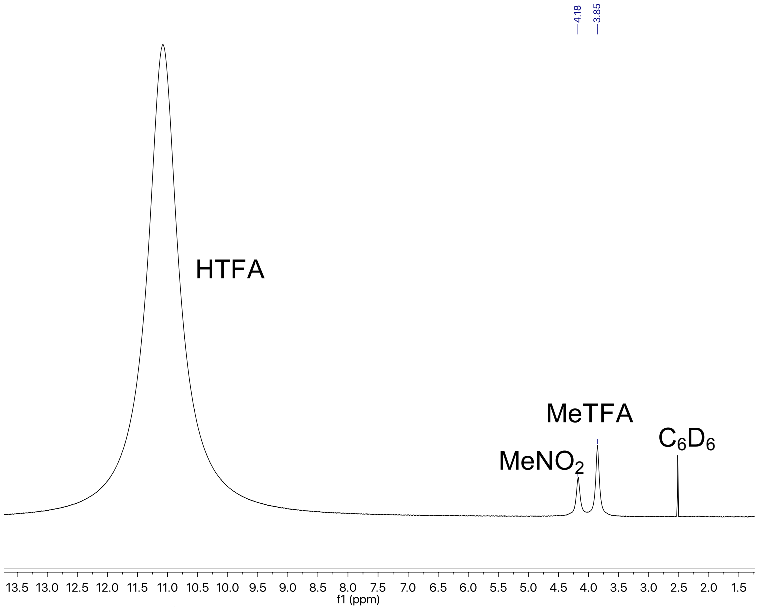

Figure 4.29. Representative ^{1}H NMR spectrum of methane functionalization with MnO_2/I_2 in the absence of KCl. Conditions: CH_4 (300 psi), MnO_2 (1.1 mmol), I_2 (0.1 mmol), HTFA (8 mL), 180 °C, 1 h. Nitromethane (0.37 mmol) was added as an internal standard.

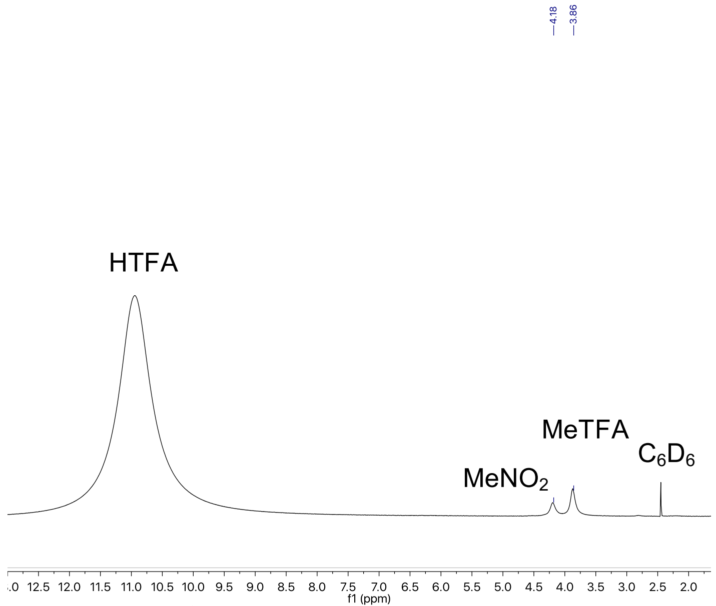

Figure 4.30. Representative ^{1}H NMR spectrum of methane functionalization with $KCl/MnO_2/I_2$. Conditions: CH_4 (300 psi), KCl (0.1 mmol), MnO_2 (1.1 mmol), I_2 (0.1 mmol), HTFA (8 mL), 180 °C, 1 h. Nitromethane (0.37 mmol) was added as an internal standard.

Screening Mn oxidants for methane functionalization. A custom-built stainless-steel reactor with a Teflon liner[9-10] was charged with a stir bar, Mn oxidant (1.1 mmol;

MnO_2, Mn_2O_3, Mn_3O_4, $KMnO_4$, K_2MnO_4 or $Mn(OAc)_3{\cdot}2H_2O$), I_2 (0.15 mmol) and HTFA (8 mL). The reactor was sealed and pressurized with 300 psi of methane. After the mixture was stirred at 800 rpm at 180 °C for 1 h, the reactor was allowed to cool to room temperature. The reactor was then vented carefully, and nitromethane was added as an internal standard. After stirring, a 1 mL aliquot was added to a centrifuge tube with $NaBiO_3$. The centrifuge tube was shaken and then centrifuged. The supernatant was analyzed by ^1H NMR. Representative ^1H NMR spectra are shown below. Each condition was performed in triplicate.

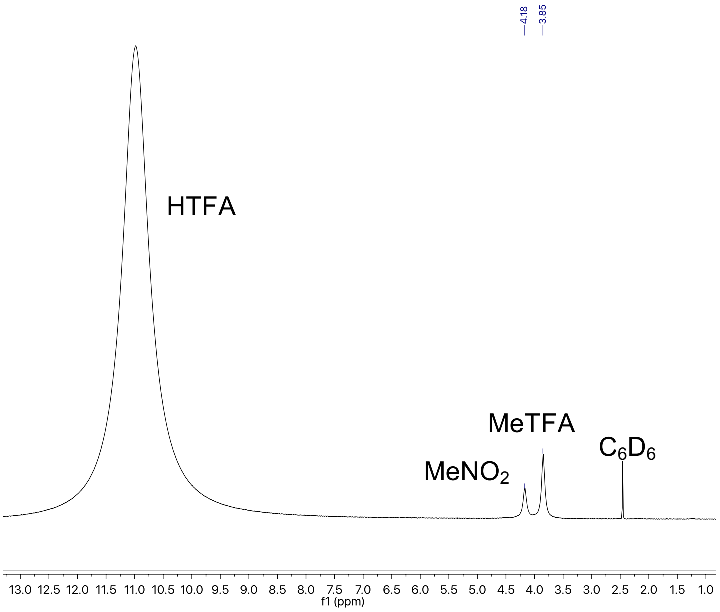

Figure 4.31. Representative ^1H NMR spectrum of methane functionalization with MnO_2/I_2. Conditions: CH_4 (300 psi), MnO_2 (1.1 mmol), I_2 (0.15 mmol), HTFA (8 mL), 180 °C, 1 h. Nitromethane (0.37 mmol) was added as an internal standard.

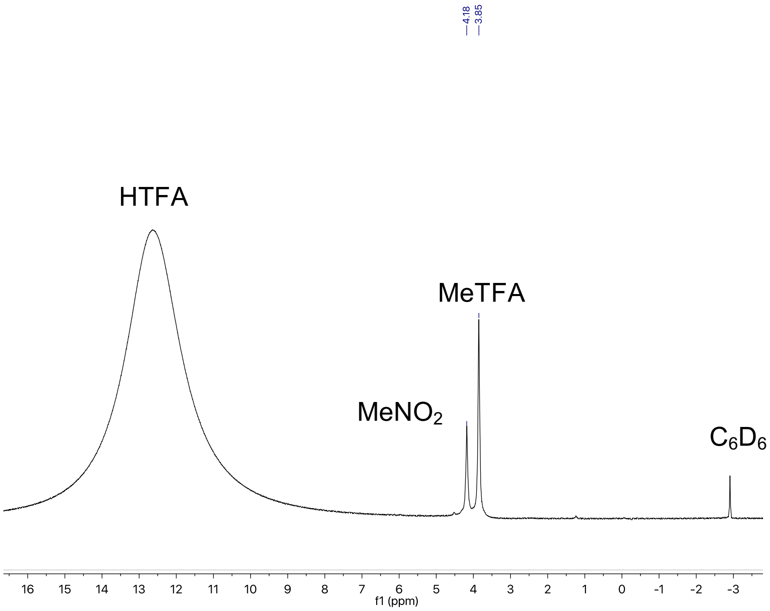

Figure 4.32. Representative ^{1}H NMR spectrum of methane functionalization with Mn_2O_3/I_2. Conditions: CH_4 (300 psi), Mn_2O_3 (1.1 mmol), I_2 (0.15 mmol), HTFA (8 mL), 180 °C, 1 h. Nitromethane (0.37 mmol) was added as an internal standard.

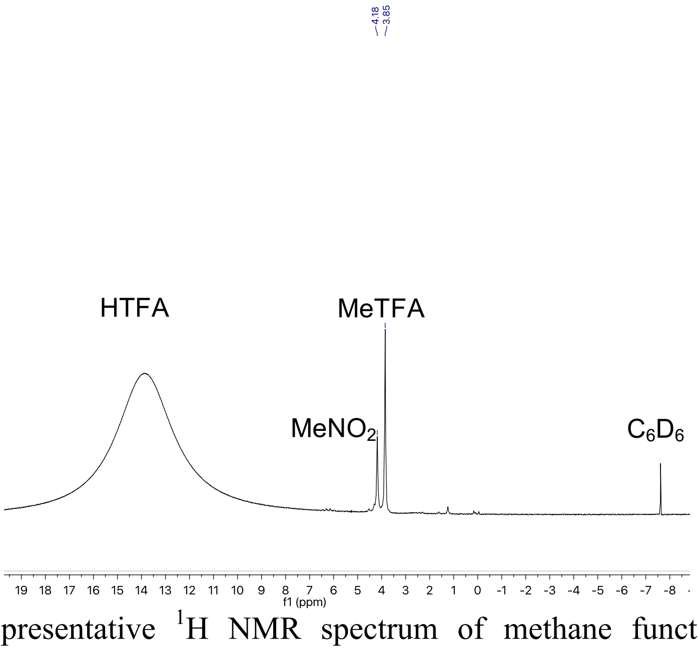

Figure 4.33. Representative ^{1}H NMR spectrum of methane functionalization with Mn_3O_4/I_2. Conditions: CH_4 (300 psi), Mn_3O_4 (1.1 mmol), I_2 (0.15 mmol), HTFA (8 mL), 180 °C, 1 h. Nitromethane (0.37 mmol) was added as an internal standard.

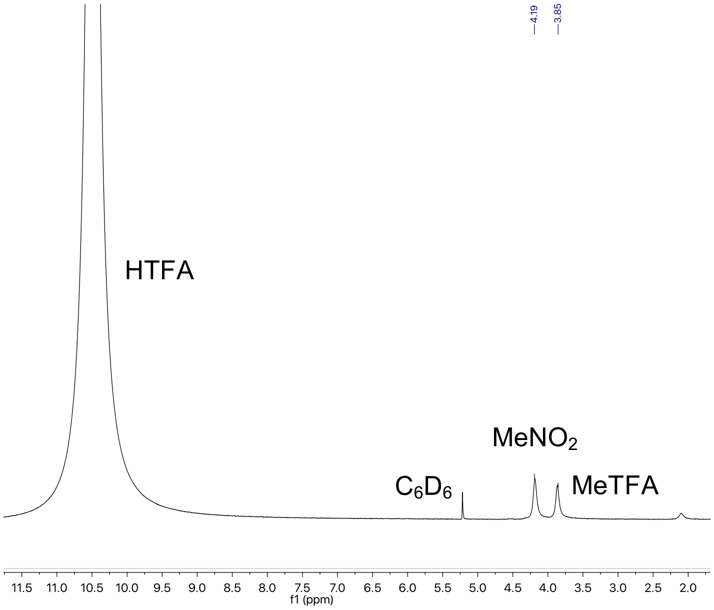

Figure 4.34. Representative ^1H NMR spectrum of methane functionalization with $KMnO_4/I_2$. Conditions: CH_4 (300 psi), $KMnO_4$ (1.1 mmol), I_2 (0.15 mmol), HTFA (8 mL), 180 °C, 1 h. Nitromethane (0.37 mmol) was added as an internal standard.

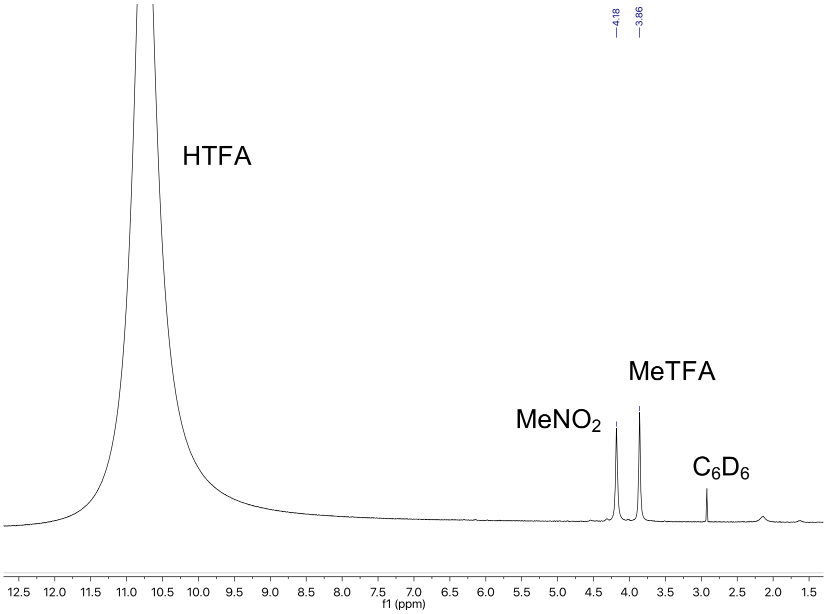

Figure 4.35. Representative ^1H NMR spectrum of methane functionalization with K_2MnO_4/I_2. Conditions: CH_4 (300 psi), K_2MnO_4 (1.1 mmol), I_2 (0.15 mmol), HTFA (8 mL), 180 °C, 1 h. Nitromethane (0.37 mmol) was added as an internal standard.

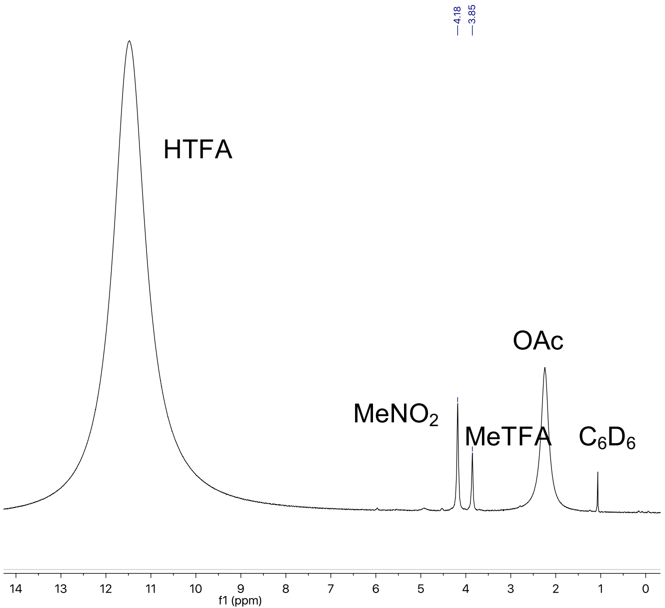

Figure 4.36. Representative ^{1}H NMR spectrum of methane functionalization with $Mn(OAc)_3 \cdot 2H_2O/I_2$. Conditions: CH_4 (300 psi), $Mn(OAc)_3 \cdot 2H_2O$ (1.1 mmol), I_2 (0.15 mmol), HTFA (8 mL), 180 °C, 1 h. Nitromethane (0.37 mmol) was added as an internal standard.

Increasing $Mn(OAc)_3 \cdot 2H_2O$ loading for methane functionalization. A custom-built stainless-steel reactor with a Teflon liner[9-10] was charged with a stir bar, $Mn(OAc)_3 \cdot 2H_2O$ (3.3 mmol), I_2 (0.15 mmol) and HTFA (8 mL). The reactor was sealed and pressurized with 300 psi of methane. After the mixture was stirred at 800 rpm at 180 °C for 2 h, the reactor was allowed to cool to room temperature. The reactor was then vented carefully, and nitromethane was added as an internal standard. After stirring, a 1 mL aliquot was added to a centrifuge tube with $NaBiO_3$. The centrifuge tube was shaken and then centrifuged. The supernatant was analyzed by ^{1}H NMR. A representative ^{1}H NMR spectrum is shown below. This procedure was performed in triplicate.

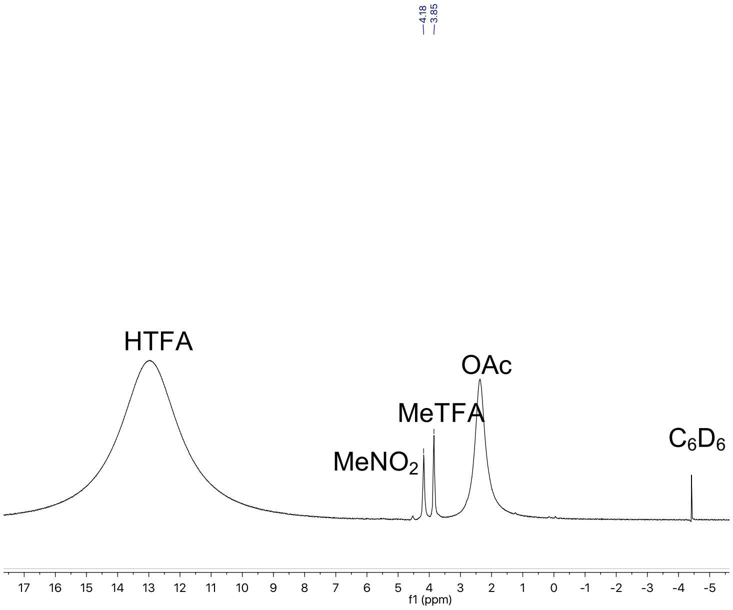

Figure 4.37. Representative ^{1}H NMR spectrum of methane functionalization with Mn(OAc)$_3$·2H$_2$O (2.2 mmol)/I$_2$. Conditions: CH$_4$ (300 psi), Mn(OAc)$_3$·2H$_2$O (2.2 mmol), I$_2$ (0.15 mmol), HTFA (8 mL), 180 °C, 2 h. Nitromethane (0.37 mmol) was added as an internal standard.

Study of MeTFA functionalization and decay with MnO$_2$/I$_2$. Functionalization reactions were set up following the general procedure for methane functionalization listed above using MnO$_2$ (1.1 mmol), I$_2$ (0.15 mmol) and HTFA (8 mL). The reactor was pressurized with 300 psi of methane and heated at 140 °C for 1-5 h. For decay experiments, a custom-built stainless-steel reactor with a Teflon liner[9-10] was charged with a stir bar, MeTFA (0.63 mmol), MnO$_2$ (1.1 mmol), I$_2$ (0.15) and HTFA (8 mL). To obtain the 0 h time point, the reactor was not pressurized or heated before following the standard work-up procedure. Otherwise, the reactor was sealed before being pressurized with 300 psi of argon and heated at 180 °C for 1-16 h. The reactor was then vented carefully, and nitromethane was added as an internal standard. After stirring, a 1 mL aliquot was added to a centrifuge tube with NaBiO$_3$. The centrifuge tube was shaken and then centrifuged. The supernatant was analyzed by ^{1}H NMR. A representative ^{1}H NMR spectrum from a

MeTFA decay reaction is shown below. All data are given as averages of at least three experiments with standard deviations shown.

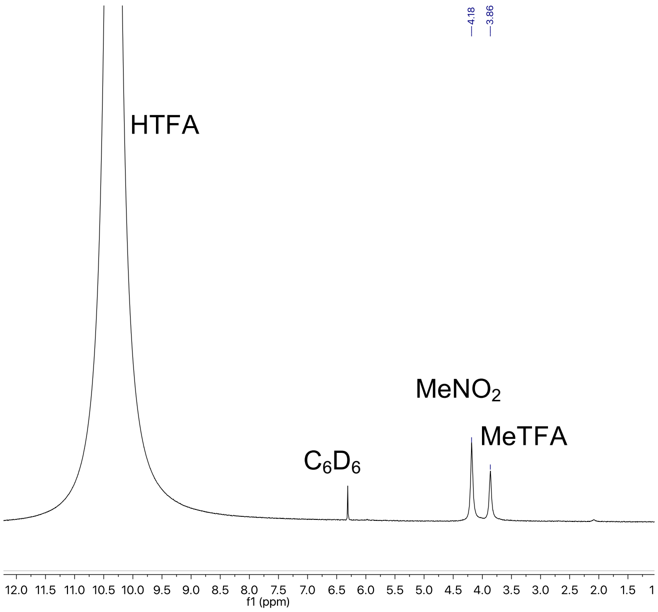

Figure 4.38. Representative ^{1}H NMR spectrum of MeTFA decay in the presence of MnO_2/I_2. Conditions: MeTFA (0.63 mmol), Ar (300 psi), MnO_2 (1.1 mmol), I_2 (0.15 mmol), HTFA (8 mL), 140 °C, 2 h. Nitromethane (0.37 mmol) was added as an internal standard.

Solvent screening for methane functionalization with MnO_2/I_2. A custom-built stainless-steel reactor with a Teflon liner[9-10] was charged with a stir bar, MnO_2 (1.1 mmol), I_2 (0.15 mmol) and solvent {8 mL; HOAc or HTFA/H_2O (7:1 vol/vol)}. The reactor was sealed and pressurized with 300 psi of methane. After the mixture was stirred at 800 rpm at 180 °C for 1 h, the reactor was allowed to cool to room temperature. The reactor was then vented carefully, and nitromethane was added as an internal standard. After stirring, a 1 mL aliquot was added to a centrifuge tube with $NaBiO_3$. The centrifuge tube was shaken and then centrifuged. The supernatant was analyzed by ^{1}H NMR. Representative ^{1}H NMR spectra are shown below. Each condition was performed in triplicate.

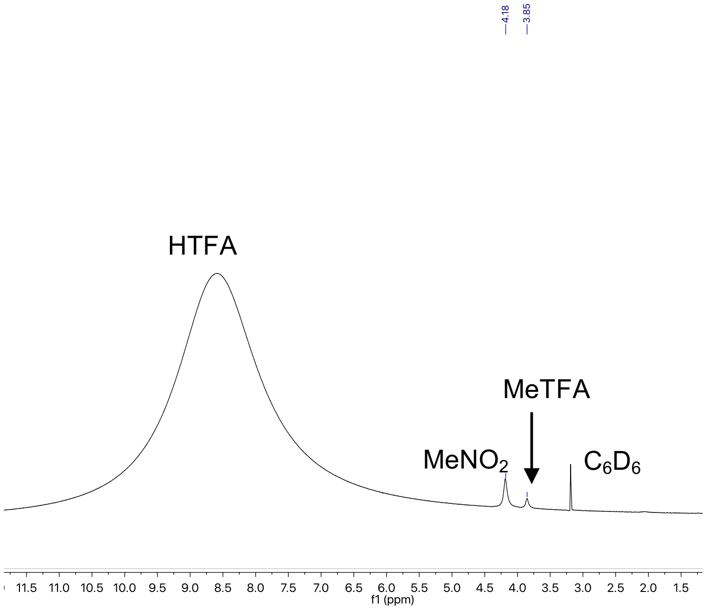

Figure 4.39. Representative ^{1}H NMR spectrum of methane functionalization with MnO_2/I_2 in dilute HTFA. Conditions: CH_4 (300 psi), MnO_2 (1.1 mmol), I_2 (0.15 mmol), HTFA/H_2O (7:1 vol/vol), 180 °C, 1 h. Nitromethane (0.37 mmol) was added as an internal standard.

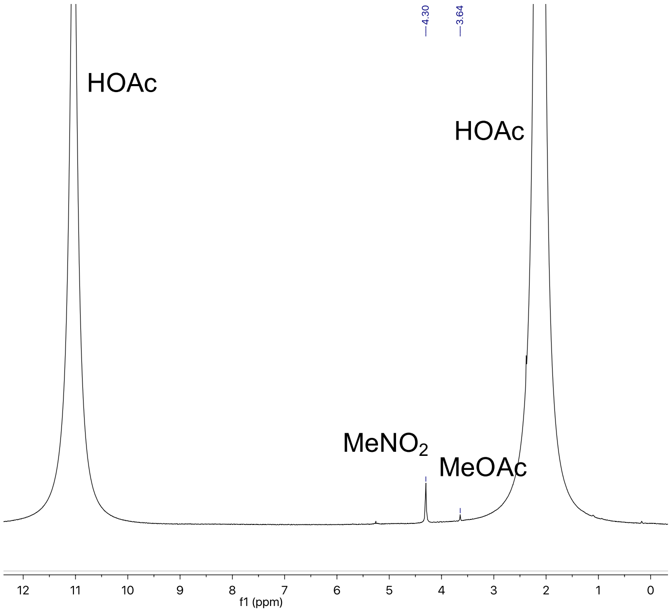

Figure 4.40. Representative ^{1}H NMR spectrum of methane functionalization with MnO_2/I_2 in HOAc. Conditions: CH_4 (300 psi), MnO_2 (1.1 mmol), I_2 (0.15 mmol), HOAc (8 mL), 180 °C, 1 h. Nitromethane (0.37 mmol) was added as an internal standard.

General procedure for the use of Fe-based oxidants for methane functionalization.

A custom-built stainless-steel reactor with a Teflon liner[9-10] was charged with a stir bar, KCl (if added, 0.1-0.3 mmol), Fe oxidant (1.1 mmol; Fe_2O_3 or Fe-BTC), I_2 (if added, 0.1 mmol) and HTFA (8 mL). The reactor was sealed and pressurized with 300 psi of methane. After the mixture was stirred at 800 rpm at 180 °C for 1 h, the reactor was allowed to cool to room temperature. The reactor was then vented carefully, and nitromethane was added as an internal standard. After stirring, an aliquot was removed and centrifuged. The supernatant was analyzed by ^{1}H NMR. Representative ^{1}H NMR spectra are shown below. Each condition was performed in triplicate.

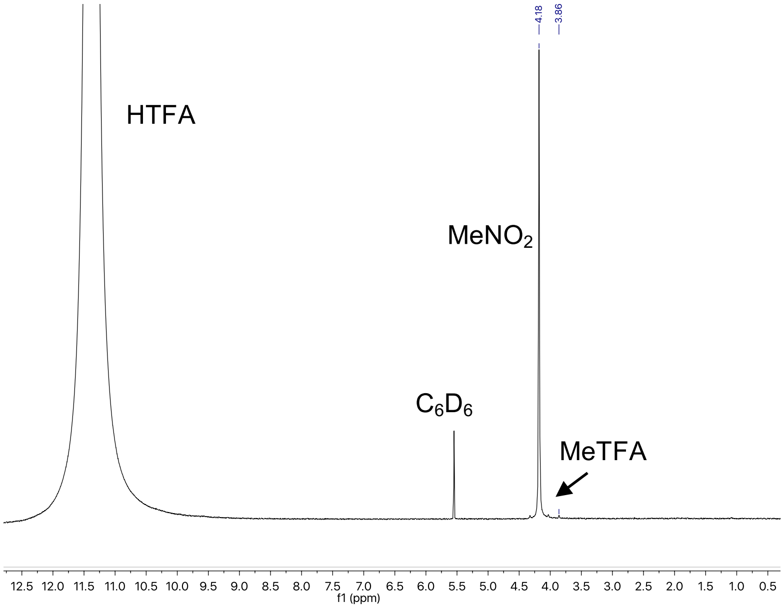

Figure 4.41. Representative ^{1}H NMR spectrum of methane functionalization with KCl/Fe_2O_3 in HTFA. Conditions: CH_4 (300 psi), KCl (0.1 mmol), Fe_2O_3 (1.1 mmol), HTFA (8 mL), 180 °C, 1 h. Nitromethane (0.37 mmol) was added as an internal standard.

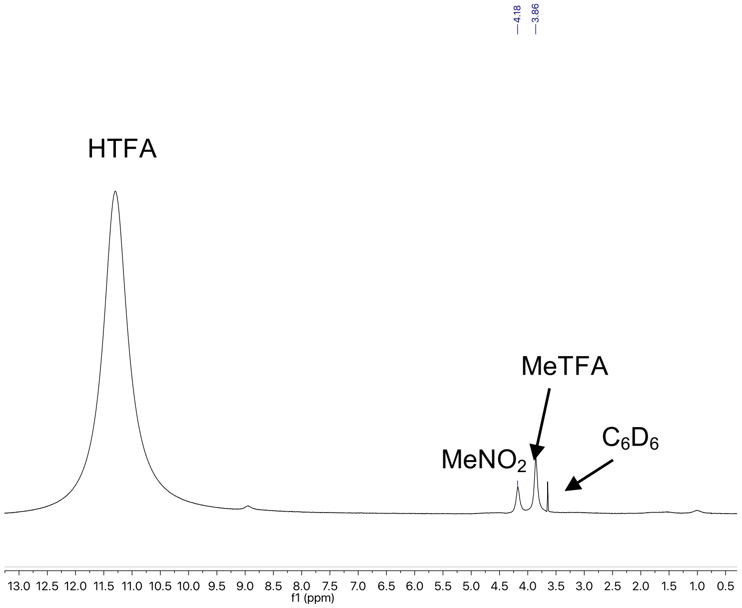

Figure 4.42. Representative ^{1}H NMR spectrum of methane functionalization with KCl/Fe-BTC in HTFA. Conditions: CH_4 (300 psi), KCl (0.1 mmol), Fe-BTC (1.1 mmol), HTFA (8 mL), 180 °C, 1 h. Nitromethane (0.37 mmol) was added as an internal standard.

General procedure for the use of Cu-BTC for methane functionalization. A custom-built stainless-steel reactor with a Teflon liner[9-10] was charged with a stir bar, Cu-BTC oxidant (0.1 mmol) and HTFA (8 mL). The reactor was sealed and pressurized with 300 psi of methane. After the mixture was stirred at 800 rpm at 180 °C for 1 h, the reactor was allowed to cool to room temperature. The reactor was then vented carefully, and nitromethane was added as an internal standard. After stirring, an aliquot was removed and centrifuged. The supernatant was analyzed by ^{1}H NMR. Representative ^{1}H NMR spectra are shown below. The reaction was performed in triplicate.

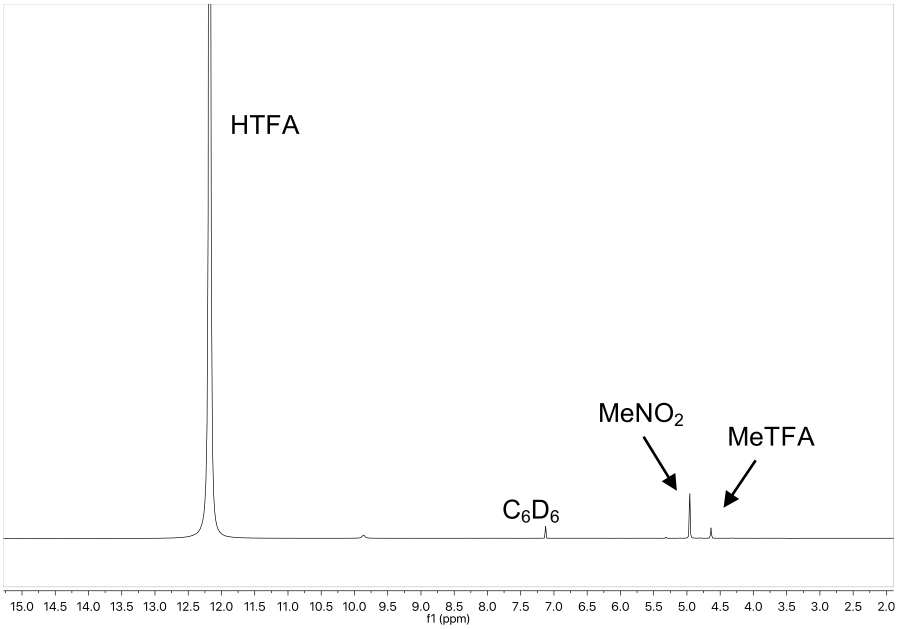

Figure 4.43. Representative ^{1}H NMR spectrum of methane functionalization with Cu-BTC in HTFA. Conditions: CH_4 (300 psi), Cu-BTC (0.1 mmol), HTFA (8 mL), 180 °C, 1 h. Nitromethane (0.37 mmol) was added as an internal standard.

4.10 References

1. *CRC Handbook of Chemistry and Physics*. 65th ed.; CRC Press: Boca Raton, FL, 1984.

2. Tang, Y.; Li, Y.; Yu, Z.; Bai, Y.; Chen, Y.; Sun, Y.; Wan, P. *Green Chem.* **2012**, *14*, 334-337.

3. Gerken, J. B.; Stahl, S. S. *ACS Cent. Sci.* **2015**, *1*, 234-243.

4. Sheng, X.; Ma, H.; Chen, C.; Gao, J.; Yun, G.; Xu, J. *Catal. Commun.* **2010**, *11*, 1189-1192.

5. Scharfe, M.; Capdevila-Cortada, M.; Kondratenko, V. A.; Kontratenko, E. V.; Colussi, S.; Trovarelli, A.; López, N.; Pérez-Ramírez, J. *ACS Catal.* **2018**, *8* (4), 2651-2663.

6. Scharfe, M.; Lira-Parada, P. A.; Paunović, V.; Moser, M.; Amrute, A. P.; Pérez-Ramírez, J. *Angew. Chem. Int. Ed.* **2016**, *55* (9), 3068-3072.

7. Leyva-Pérez, A.; Cómbita-Merchán, D.; Cabrero-Antonino, J. R.; Al-Resayes, S. A.; Corma, A. *ACS Catal.* **2013**, *3* (2), 250-258.

8. Schwartz, N. A.; Boaz, N. C.; Kalman, S. E.; Zhuang, T.; Goldberg, J. M.; Fu, R.; Nielsen, R. J.; Goddard III, W. A.; Groves, J. T.; Gunnoe, T. B. *ACS Catal.* **2018**, *8*, 3138-3149.

9. Fortman, G. C.; Boaz, N. C.; Munz, D.; Konnick, M. M.; Periana, R. A.; Groves, J. T.; Gunnoe, T. B. *J. Am. Chem. Soc.* **2014**, *136*, 8393-8401.

10. Kalman, S. E.; Munz, D.; Fortman, G. C.; Boaz, N. C.; Groves, J. T.; Gunnoe, T. B. *Dalton Trans.* **2015**, *44*, 5294-5298.

11. Chen, W.; Kocal, J. A.; Brandvold, T. A.; Bricker, M. L.; Bare, S. R.; Broach, R. W.; Greenlay, N.; Popp, K.; Walenga, J. T.; Yang, S. S.; Low, J. J. *Catal. Today* **2009**, *140*, 157-161.

12. Strassner, T.; Ahrens, S.; Muehlhofer, M.; Munz, D.; Zeller, A. *Eur. J. Inorg. Chem.* **2013**, *2013* (21), 3659-3663.

13. Wang, X.; Liu, Y.; Zhang, Y.; Zhang, T.; Chang, H.; Zhang, Y.; Jiang, L. *Appl. Catal. B* **2018**, *229*, 52-62.

14. Fu, R.; Nielsen, R. J.; Schwartz, N. A.; Goddard III, W. A.; Gunnoe, T. B.; Groves, J. T., DFT Mechanistic Study of Methane Monooxygenation by Hypervalent Iodine Alkane Oxidation (HIAO) Process. *Manuscript submitted* **2018**.

15. Magistro, A. J.; Nicholas, P. P.; Carroll, R. T. *J. Org. Chem.* **1969,** *34* (2), 271-273.

16. Carroll, R. T.; De Witt, E. J.; Trapasso, L. E. Oxychlorination of lower alkanes. 3,173,962, 1965.

17. Krause, E.; Roka, K. Process for the chlorination of hydrocarbons. 1,591,984, 1926.

18. Mikami, Y.; Dhakshinamoorthy, A.; Alvaro, M.; Garcia, H. *ChemCatChem* **2013**, *5*, 1964-1970.

19. Dhakshinamoorthy, A.; Alvaro, M.; Garcia, H. *Chem. Eur. J.* **2011**, *17*, 6256-6262.

20. Peng, L.; Wu, S.; Yang, X.; Hu, J.; Fu, X.; Li, M.; Bai, L.; Huo, Q.; Guan, J. *New J. Chem.* **2017**, *41*, 2891-2894.

21. Nagarjun, N.; Dhakshinamoorthy, A. *Mol. Catal.* **2019**, *463*, 54-60.

22. Dhakshinamoorthy, A.; Alvaro, M.; Garcia, H. *J. Catal.* **2009**, *267*, 1-4.

23. Dhakshinamoorthy, A.; Alvaro, M.; Garcia, H. *ACS Catal.* **2011**, *1*, 48-53.

24. Rosen, A. S.; Notestein, J. M.; Snurr, R. Q. *ACS Catal.* **2019**, *9*, 3576-3587.

5 Photochemical Functionalization of Light Alkanes

5.1 Introduction

Selective partial oxidation of light alkanes is a longstanding goal of the catalysis community, as has been discussed in the previous Chapters. The majority of reported approaches toward this goal have utilized the energy from heat to overcome reaction barriers. This Chapter, however, is focused on the use of light rather than heat for the functionalization of light alkanes.

There is precedent for the photochemical partial oxidation of light alkanes using photo-mediated processes, albeit a limited precedent when compared to the literature regarding thermal functionalization. Vogler and Kunkely reported the photocatalytic oxidation of methane to methanol with perrhenate in aqueous media using H_2O_2 to regenerate perrhenate *in situ* (Scheme 5.1).[1] UV-vis studies indicated that ReO_4^- was regenerated during the reaction, but yields of methanol were not reported. Flow chemistry has also been explored for photochemical light alkane functionalization by Hu, Guo and coworkers, who reported the use of cerium salts as photocatalysts for the alkylation, arylation and amination of methane and ethane using visible light.[2] Aerobic stoichiometric photochemical partial oxidation using chlorine dioxide as an oxidant was reported by Ohkubo and coworkers (Scheme 5.2).[3] The process was selective for methanol and formic acid formation with 99% methane conversion. The use of a biphasic reaction mixture (H_2O/perfluorohexane) minimized the over-oxidation of products as photochemical functionalization occurred in the fluorous phase while product accumulation occurred in the aqueous phase. Heterogeneous photocatalysis has been reported by Xie and coworkers using a TiO_2-

supported iron species for the conversion of methane to methanol, achieving 15% conversion of methane and 90% selectivity for methanol.[4]

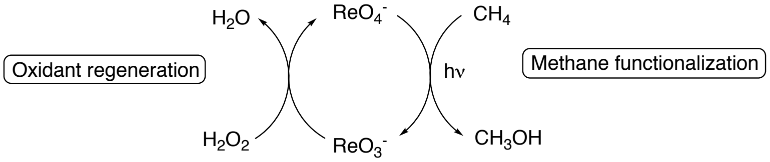

Scheme 5.1. Proposed catalytic cycle for photocatalytic methane functionalization with perrhenate in aqueous media.[1]

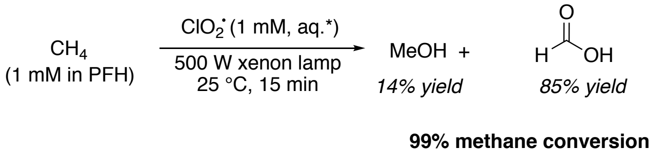

(PFH = perfluorohexane)
*aqueous solution contains equimolar $NaClO_2$ and HCl

Scheme 5.2. Chlorine dioxide radical as an oxidant for the oxidation of methane to methanol and formic acid in an aqueous/fluorous biphasic mixture.[3]

5.2 Photo-OxE for the Functionalization of Light Alkanes

5.2.1 Introduction

The results discussed in this section have been submitted to *ACS Catalysis.* This work has been a collaboration between the Gunnoe group and the Groves group (Princeton University). Preliminary photochemical light alkane functionalization experiments using iodate and chloride were performed by Dr. Steven Kalman of the Gunnoe group, and Dr. Nicholas Boaz of the Groves group began the study of photochemical functionalization of the model substrates adamantane and norbornane using iodate and chloride. Subsequent reactions examining the photochemical functionalization of cyclohexane were performed by Dr. Jonathan Goldberg of the Groves group.

5.2.2 Photo-OxE of Methane

The iodate/chloride OxE process converts light alkanes methane, ethane and propane to mono-functionalized esters in high yields relative to the starting alkane under thermal conditions.[5-6] However, one of the major limitations of the process is the undesired oxidation of solvent under the oxidizing conditions at elevated temperatures (~200 °C). This provided impetus to study the potential activity of the OxE process at lower temperatures, however, alkane functionalization was shown to be minimal at temperatures < 100 °C.[5] Thus, given the findings discussed in Chapter 2, we proposed that the reactive intermediates demonstrated to be effective for light alkane functionalization by the OxE process could potentially be generated and reactive under milder reaction conditions using photolysis to achieve photochemical oxy-esterification, or photo-OxE.

The optimal conditions for OxE were used for a preliminary screening using photolysis. Without optimization, the functionalization of methane by KCl and NH_4IO_3 in HTFA after 24 h of photolysis from a mercury arc lamp gave 16(5)% yield of MeTFA relative to methane with a 35:1 ratio of MeTFA:MeCl (Scheme 5.3). This finding compares favorably to the thermal reaction, especially given that the highest MeTFA yield obtained with the thermal OxE process using iodate/chloride was 24%.[5] Furthermore, the generation of 4(1) mmol of MeTFA demonstrated that the photo-OxE process is catalytic in chloride, as only 0.67 mmol of KCl was used. The success of these un-optimized reactions resulted in further investigation of the photo-OxE process. To confirm that the high intensity light from the mercury arc lamp was required for methane functionalization, an ambient light control reaction was performed (Scheme 5.4). Under ambient light in the laboratory, < 0.2% total yield of MeX (X = TFA and Cl) was obtained after 24 h, highlighting the necessity of the mercury arc lamp.

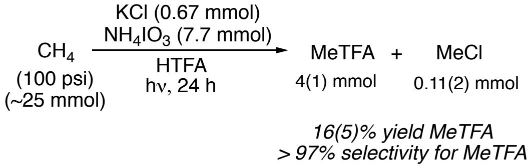

Scheme 5.3. Photochemical partial oxidation of methane using the mercury arc lamp. Conditions: CH_4 (100 psi), KCl (0.67 mmol), NH_4IO_3 (7.7 mmol), HTFA (8 mL), 24 h photolysis using the mercury arc lamp. The percent yield of MeTFA is based on the amount of added methane. The standard deviation is based on a minimum of three experiments.

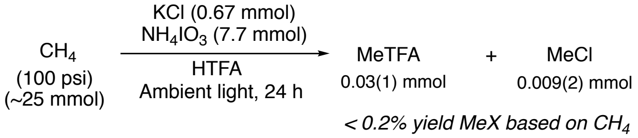

Scheme 5.4. Oxidation of methane using the OxE system under ambient light. Conditions: CH_4 (100 psi), KCl (0.67 mmol), NH_4IO_3 (7.7 mmol), HTFA (8 mL), 24 h exposure to ambient laboratory light in a fume hood.

The initial report of the thermal OxE process using iodate/chloride found that yields of mono-functionalized products increased with increasing chloride loading.[5] Thus, one of the first steps in optimization of the photo-OxE process was to determine the optimal loading of KCl. As shown in Figure 5.1, the yield of MeTFA increases from 16(5)% to ~25% when increasing the amount of KCl from 0.67 to 2.01 mmol. In the absence of chloride, trace MeTFA is produced. Selectivities for MeTFA remain high (> 90%) when using the higher chloride loadings of 2.01 mmol and 3.35 mmol. However, with larger amounts of chloride (*e.g.*, 6.7 mmol), the MeTFA yield and selectivity decrease as MeCl production increases and dichloromethane (DCM), an undesired product of over-oxidation forms. With 6.7 mmol of KCl, the selectivity for MeTFA decreases to 70%. Based on the chloride screening, 2.01 mmol of KCl was used in additional experiments as it enabled the highest yields with lower deviations than were observed when using 3.35 mmol of KCl.

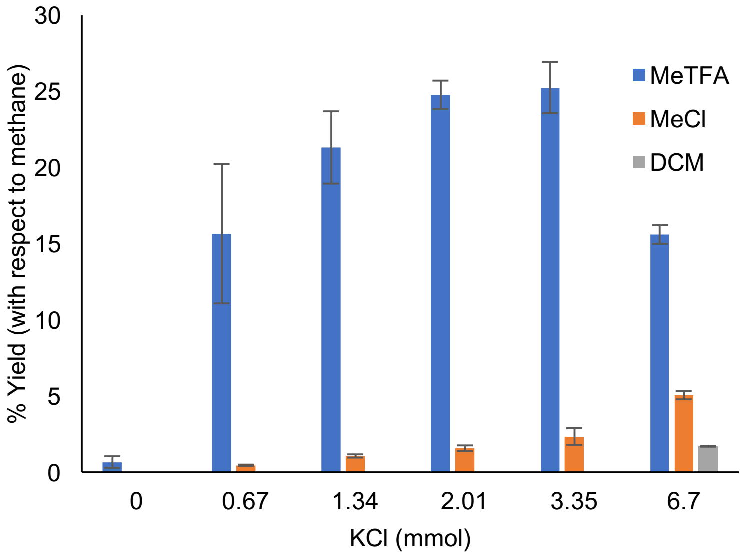

Figure 5.1. Effect of starting KCl amount on MeX yield. Conditions: CH_4 (100 psi), KCl (0.67-26.7 mmol), NH_4IO_3 (7.7 mmol), HTFA (8 mL), 24 h photolysis. Error bars denote standard deviations based on a minimum of three experiments.

To optimize the photo-OxE process further, reaction times were extended to 48 h and methane pressures were varied. When using 100 psi of methane (~25 mmol), 39(4)% yield of MeTFA, based on methane, was obtained after 48 h (Figure 5.2), a significant increase relative to the 25(1)% yield observed after 24 h. This yield of ~40% mono-functionalized alkyl ester product is greater than the highest yield obtained using thermal OxE with iodate (24% yield MeX), and the concentration of product is approximately four-fold higher, with ~1.2 M using photo-OxE compared to ~0.23 M for thermal OxE.[5] When decreasing the methane pressure to 50 psi, MeTFA was obtained in 48(4)% yield with 95% selectivity, slightly exceeding the highest yield obtained under thermal OxE using periodate as the oxidant, 41%.[6] With 25 psi of methane, lower average yields of MeTFA are observed and there is greater variability between experiments.

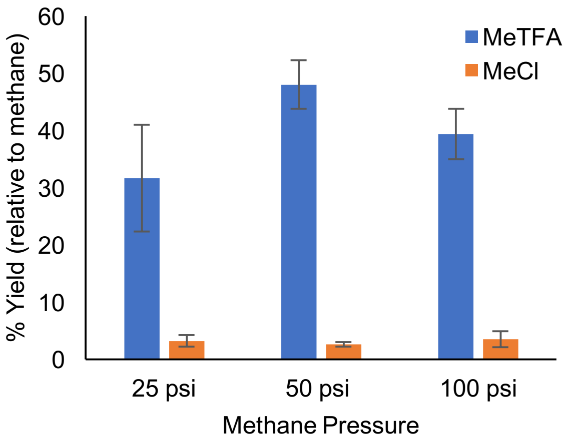

Figure 5.2. Effect of methane pressure on photochemical OxE of methane. Conditions: CH_4 (25, 50, or 100 psi), KCl (2.01 mmol), NH_4IO_3 (7.7 mmol), HTFA (8 mL), 48 h photolysis using the mercury arc lamp. Error bars denote standard deviations based on at least three experiments.

Subsequently, we sought to determine the solvent scope of the photo-OxE process. Although the highest yields of MeTFA are obtained when using HTFA as the solvent, similar to the thermal process, functionalization also occurs in more weakly acidic solvents (Figure 5.3). In dilute HTFA (3:1 HTFA/H_2O) and dichloroacetic acid (pKa 1.35 versus 0.52 for HTFA),[7] MeX yields of 16(2)% and 17(1)% are observed. These findings are particularly significant given that previous examples of light alkane functionalization processes, which operate efficiently in superacidic media, exhibit low tolerance to water or less acidic solvents.[8] As addressed in Chapter 2, acetic acid was studied as a reaction solvent for the thermal OxE process. Although MeOAc formation was observed in the reaction of methane with KCl and NH_4IO_3 in HOAc, it was determined that it was the result of solvent oxidation rather than methane functionalization.[9] Additionally, the generation of intermediates that are likely responsible for methane oxidation was not observed by UV-vis spectroscopy when HOAc was used as the solvent, in agreement with DFT calculations.[9-10] Thus, HOAc serves as a useful point of comparison between the thermal and photochemical OxE processes. Unlike the thermal process, only trace MeOAc, ~0.1% relative to methane, is formed under photochemical conditions (Scheme 5.5). This result is in agreement with previous results indicating that the species responsible for alkane functionalization is not generated in the weakly acidic HOAc, and demonstrates the potential utility of photolysis as a means of reducing the extent of solvent oxidation.

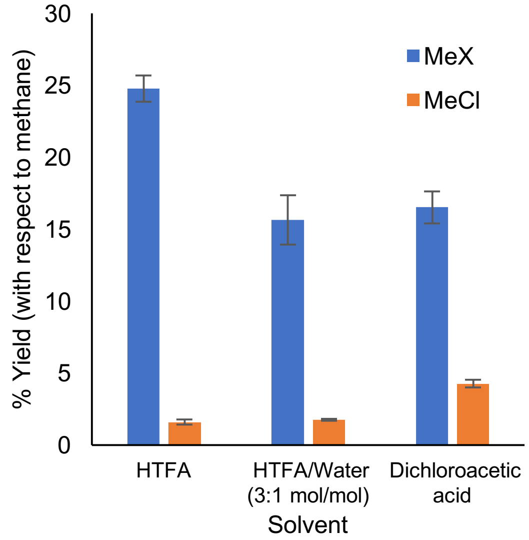

Figure 5.3. Photochemical partial oxidation of methane by KCl/NH_4IO_3 in different solvent combinations. MeX is the corresponding acetate ester for each acid. Conditions: CH_4 (100 psi), KCl (2.01 mmol), NH_4IO_3 (7.7 mmol), solvent (8 mL), 24 h photolysis. Error bars denote standard deviations based on at least three experiments.

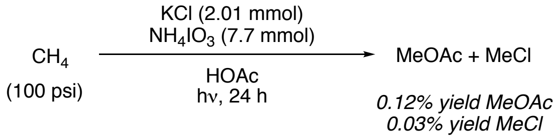

Scheme 5.5. Photochemical partial oxidation of methane using KCl/NH_4IO_3 in HOAc.

The potential utility of compact fluorescent light (CFL) as an irradiation source was subsequently tested. Although the yields of MeX are lower with the 105 W CFL than the mercury arc lamp, methane functionalization is observed in yields similar to the best yields obtained using the thermal OxE system with iodate (Figure 5.4). The yields of MeTFA after 24 h using CFL and the mercury arc lamp are ~10% and ~25%, respectively.

Extending the reaction using the mercury arc lamp does not lead to increased yields, whereas with the CFL, ~25% yield of MeTFA is obtained following 72 h of irradiation. Additional irradiation time with the CFL beyond 72 h does not result in further improved yields.

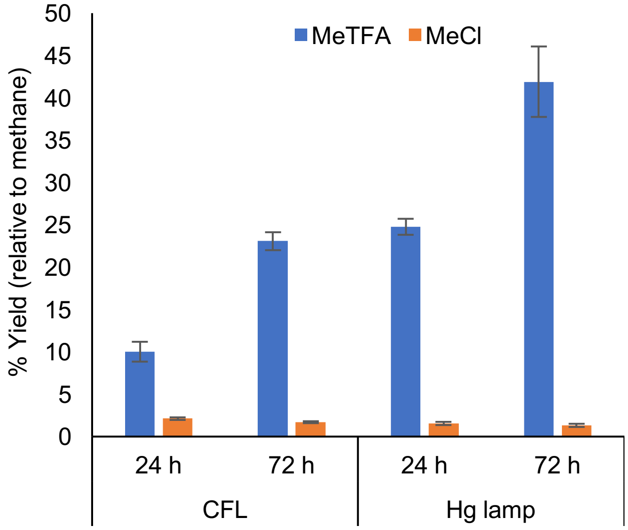

Figure 5.4. Comparison of irradiation by the mercury arc lamp and a 105 W compact fluorescent light (CFL) for photochemical partial oxidation of methane by KCl/NH_4IO_3. Conditions: CH_4 (100 psi), KCl (2.01 mmol), NH_4IO_3 (7.7 mmol), solvent (8 mL), 24 h photolysis. Error bars denote standard deviations based on at least three experiments.

Given the success of the thermal OxE system using periodate as the oxidant, periodate was also tested for the photo-OxE process (Figure 5.5). Although the combination of periodate and chloride results in methane conversion to MeTFA and MeCl, the yields with periodate are comparable to those with iodate after 24 h, and are lower after 48 h. The standard deviations with periodate were also significant after 48 h.

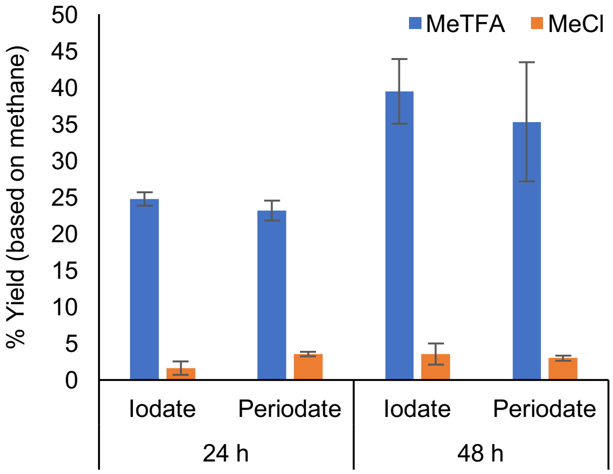

Figure 5.5. Comparison of photochemical functionalization of methane with iodate versus periodate. Conditions: CH_4 (100 psi), KCl (2.01 mmol), NH_4IO_3 or KIO_4 (7.7 mmol), HTFA, (8 mL), 24 or 48 h photolysis using the mercury arc lamp. Error bars denote standard deviations based on three trials for each condition except for the 48 h trial with periodate, which is based on six trials.

5.2.3 Photo-OxE of Ethane

Given the success of the photo-OxE process for methane functionalization, there was motivation to determine the scope of the photochemical reaction using other light alkanes. The photochemical functionalization of ethane was studied using the mercury arc lamp under the conditions that were optimized for methane (2.01 mmol KCl, 7.7 mmol NH_4IO_3). The yields of functionalized product obtained using low pressures of ethane are very high. With 25 psi of methane, 82(5)% yield of EtX (X = TFA or Cl) was observed (Figure 5.6). With higher ethane pressure, the EtX yields are lower, however, they remain higher than or comparable to the ethane functionalization results demonstrated in the initial report of the thermal process with iodate/chloride.[5] The selectivity for mono-functionalized products, EtTFA and EtCl, is high relative to di-functionalized products, 1-iodo-2-trifluoroacetoxyethane, 1-chloro-2-trifluoroacetoxyethane, 1,2-bis(trifluoroacetoxy)ethane and 1,2-dichloroethane (Figure 5.6). There is also ^1H NMR evidence for the formation of a 1,1-difunctionalized product when using low ethane pressures. A COSY spectrum indicates that there is coupling between a doublet (δ 1.72, *J* = 5.8 Hz) and a quartet (δ 6.39, *J* =5.8 Hz), in good agreement with literature reports of 1,1-bis(trifluoroacetoxy)ethane (Figure 5.20).[11-12] This product forms in trace amounts with 50 or 100 psi of ethane, whereas with 25 psi of ethane, assuming the doublet corresponds to a methyl group, a 1.6(8)% yield is observed relative to ethane. Similarly, at higher ethane pressures, fewer di-functionalized products are observed when compared with lower ethane pressures (Figures 5.18 and 5.19). This finding suggests that at high conversions of alkane (> 80%), over-oxidation occurs, but is minimal.

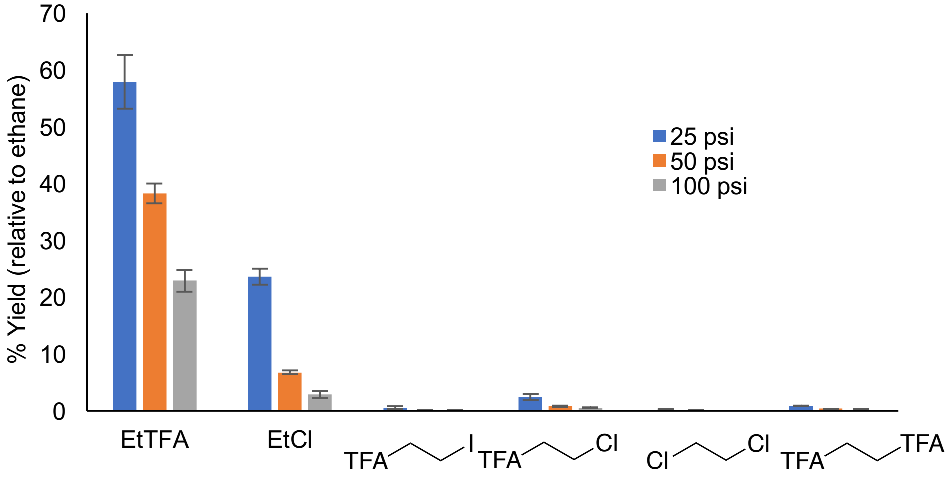

Figure 5.6. Photochemical functionalization of ethane with KCl/NH_4IO_3. Conditions: CH_3CH_3 (25, 50 or 100 psi), KCl (2.01 mmol), NH_4IO_3 (7.7 mmol), HTFA (8 mL), 24 h photolysis. Error bars denote standard deviations based on three experiments.

5.2.4 Photo-OxE of Propane

Propane is also functionalized by the photo-OxE process (Figure 5.7). Yields of functionalized product are lower with propane when compared with methane or ethane, but optimized yields are comparable with those obtained under thermal conditions.[5] Using 25 psi of propane, 38% total yield of functionalized products is observed, while under thermal conditions, 40% yield was observed.[5] However, the concentration of functionalized products under photochemical conditions is approximately four times higher than under thermal conditions, 0.32 M and 0.07 M, respectively. Similar to the findings with ethane, di-functionalized products are also formed under photo-OxE conditions, but the mono-functionalized products are the major products.

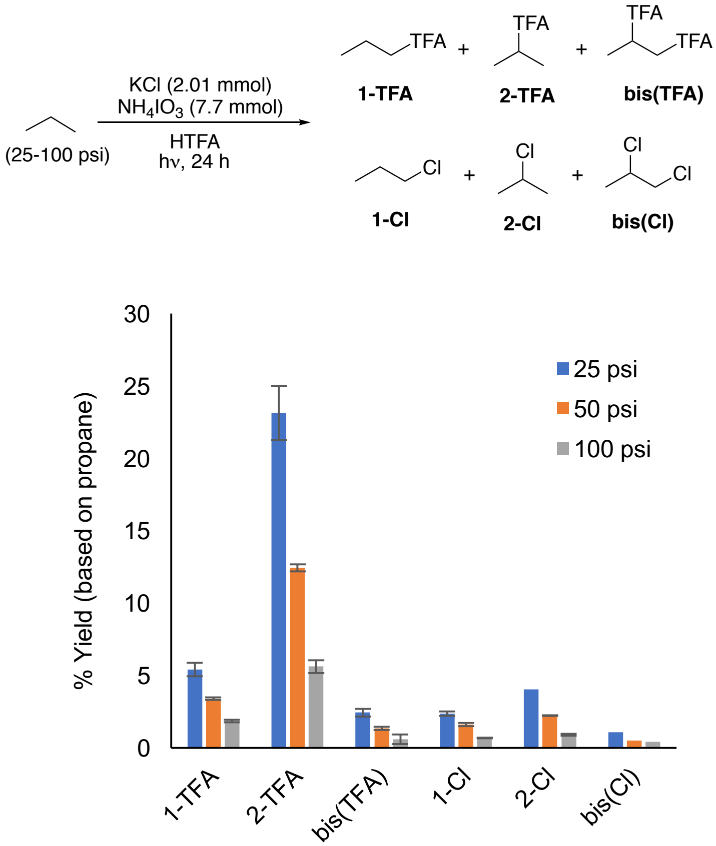

Figure 5.7. Photochemical functionalization of propane (25-100 psi) with KCl (2.01 mmol) and NH_4IO_3 (7.7 mmol) in HTFA with 24 h of photolysis using the mercury arc lamp. Error bars denote standard deviations based on at least three experiments.

5.3 Mechanistic Studies of the Photo-OxE Process

5.3.1 Stability of MeTFA under Photo-OxE Conditions

In an effort to further compare thermal OxE and photo-OxE processes, the stability of MeTFA under photochemical conditions was studied by monitoring the rate of functionalization of methane and the consumption of MeTFA over time (Figure 5.8). Similar to the findings in the thermal study, MeTFA was stable under the oxidizing photo-OxE reaction conditions with KCl and NH_4IO_3. This indicates that the product protection by the TFA moiety is not limited to the thermal reaction and that it can be applied to other functionalization processes. Because the concentration of methane in solution is unknown, these data cannot be used to determine absolute rates of functionalization, however, as in the thermal study, these processes can be compared to one another approximately using the slopes of the linear fits from plots of MeX production versus time. The plot of methane functionalization versus time is approximately linear for the first 24 h, and that of MeTFA decay versus time is linear for the entire data set, thus fits of those data were used to obtain slopes of functionalization and decay, respectively (Figure 5.25). Consequently, the ratio of methane functionalization to MeTFA consumption is 13.4, very similar to the ratio of 13.5 observed in the thermal process (see Chapter 2). EtTFA was also found to be rather stable under photo-OxE conditions, with 71(2)% of EtTFA remaining after 24 h (Scheme 5.6). Overall, 85% of the initial EtTFA could be accounted for, taking into consideration the amount of 1,2-bis(trifluoroacetoxy)ethane that formed during the reaction.

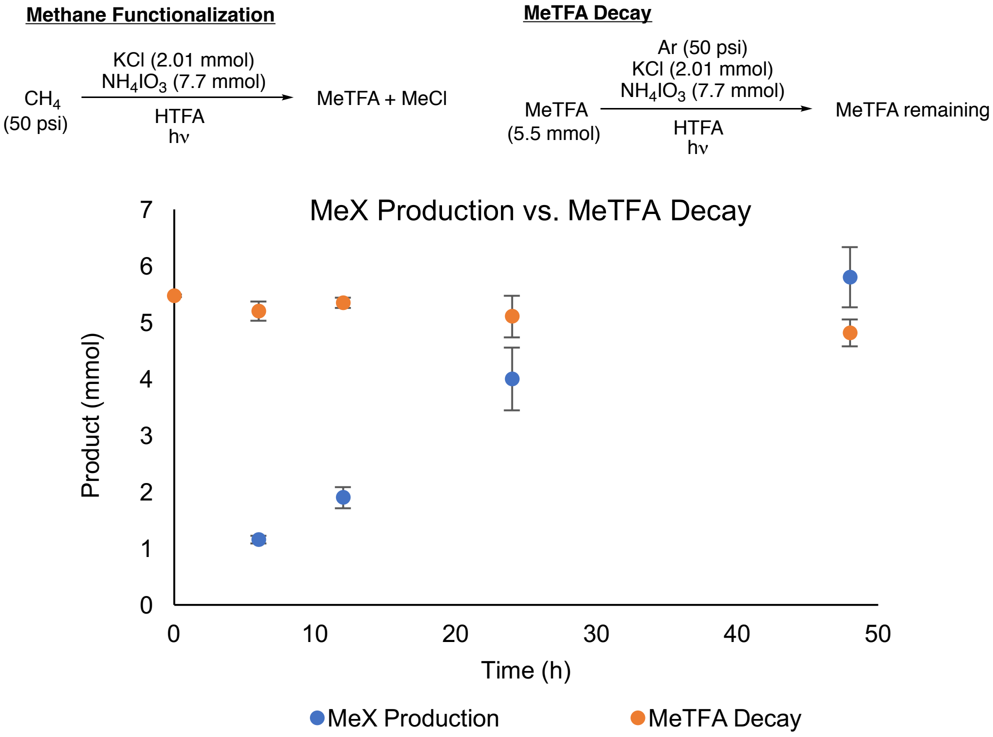

Figure 5.8. Methane functionalization vs MeTFA decay in the presence of KCl, NH_4IO_3 and HTFA under photochemical reaction conditions as a function of time. Standard deviations are based on at least three experiments.

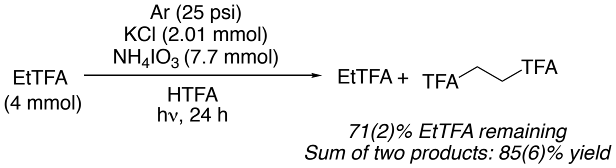

Scheme 5.6. EtTFA decay in the presence of KCl, NH_4IO_3 and HTFA after 24 h photolysis. Standard deviations are based on three experiments.

5.3.2 Comparison to Radical Chlorination & Effect of Added Iodine

To compare the photo-OxE process to radical chlorination, methane functionalization was tested using *N*-chlorosuccinimide (NCS) and benzoyl peroxide as the radical initiator. With NCS and benzoyl peroxide in HTFA, methane is converted to MeCl and CH_2Cl_2 under photochemical reaction conditions. However, as was observed with the thermal OxE process, MeTFA is produced when iodine is added to the reaction (Scheme 5.7). The addition of iodine also serves to minimize over-oxidation to CH_2Cl_2. With and without added iodine, CH_2Cl_2 accounts for < 9% and 25%, respectively, of functionalized products. As in the thermal process, these data demonstrate the efficacy of I_2 as a radical trap under chlorination conditions. The yields of functionalized products by the photo-OxE process are not improved by the addition of iodine at the start of the reaction (Figure 5.9), demonstrating yet another similarity to the thermal process. Thus, iodine likely serves to trap methyl radical to form MeI, which is then converted to MeTFA in HTFA (Scheme 5.8). Iodine increases the selectivity for MeTFA over MeCl, but it does not likely play a direct role in methane C–H bond breaking.

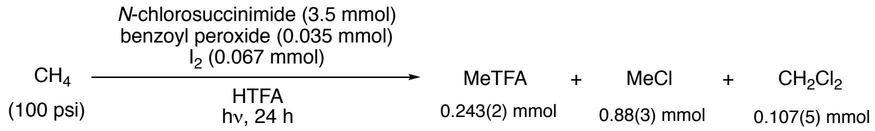

Scheme 5.7. Addition of iodine to chlorination by *N*-chlorosuccinimide and benzoyl peroxide results in formation of MeTFA. Standard deviations are based on at least three experiments.

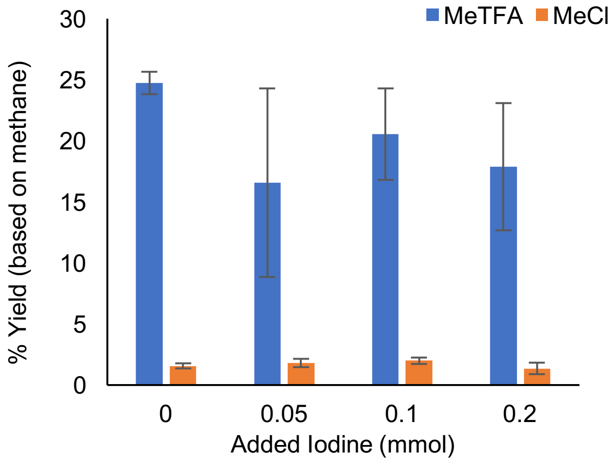

Figure 5.9. Photochemical functionalization of methane with KCl/NH_4IO_3 as a function of added iodine. Conditions: CH_4 (100 psi), KCl (2.01 mmol), NH_4IO_3 (7.7 mmol), I_2 (0-0.2 mmol), HTFA, (8 mL), 24 h photolysis. Error bars denote standard deviations based on at least three experiments.

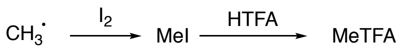

Scheme 5.8. Proposed pathway where iodine acts a trapping agent for methyl radical to generate MeI which is converted to MeTFA in HTFA solvent.

5.3.3 Studies with Cyclohexane

Given the superb performance of the photo-OxE process, we sought to understand the potential mechanistic differences between the thermal and photochemical reactions. While the previous studies examining the 3°:2° reactivity and kinetic isotope effect studies for the thermal process utilized adamantane as a model substrate (see Chapter 2), adamantane could not be used for mechanistic studies of the photochemical process due to its poor solubility in HTFA at the room temperature. Also, using adamantane would give ambiguous KIE results.[13-15] Thus, cyclohexane was used instead for the photochemical studies and was also examined under thermal conditions for comparative purposes (Table 5.1). While these results provide a comparison between the thermal and photochemical reactions with cyclohexane, the mechanistic conclusions might not extend to the reactions with light alkanes.

Preliminary studies with cyclohexane used an equimolar amount of substrate and NH_4IO_3 oxidant with 0.25 eq. of chloride relative to cyclohexane (Table 5.1). Only trace amounts of functionalized products were observed on reaction in the dark at room temperature after 24 h. On heating the reaction mixture at 100 °C for 1 h, five functionalization products were observed by GC-MS, including the mono-functionalized products CyTFA and CyCl which are predicted to be generated through an H-atom abstraction pathway. The formation of the di-functionalized products is proposed to occur through an initial dehydrogenation of cyclohexane to cyclohexene,[16] followed by the addition of Cl_2, ICl or ICl_3 (generated *in situ*) across the double bond to give a dihalocyclohexane intermediate (Scheme 5.9). As evidence of this potential pathway, *trans*-1,2-dichlorocyclohexane was detected as a product of the reaction.[17] The dihalosubstituted intermediate is then proposed to undergo solvolysis in HTFA, which would result in the formation of 1,2-bis(trifluoroacetoxy)cyclohexane and 2-chloro-1-trifluoroacetoxy-cyclohexane,[18] which were observed by GC-MS and ^{1}H NMR spectroscopy. Significantly higher yields of functionalized products are observed using a variety of light sources, and the highest are obtained using the UV reactor.

Table 1. Cyclohexane functionalization under OxE conditions (thermal and photochemical).[a]

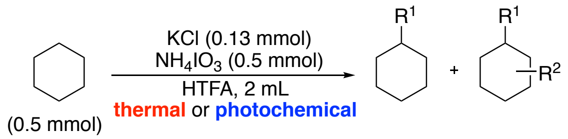

Product Yields (%)

	Dark, RT 24 h	100 °C 1 h	26W CFL 24 h	105W CFL 24 h	Blue LED 24 h	UV-reactor 18 h	UV-reactor 24 h, cooling#
R^1 = TFA	trace	2.7(8)	13.3(3)	11.7(6)	14(2)	30(2)	20.2(3)
R^1 = Cl	trace	1.6(1)	4.5(1)	4.7(3)	1.9(4)	ND	trace
R^1 = R^2 = TFA	ND	trace	1.1(1)	1.3(1)	2.4(2)	4.7(2)	4.2(1)
R^1 = R^2 = Cl	ND	trace	1.6(1)	2.2(3)	3.0(1)	ND	2.2(1)
R^1 = Cl; R^2 = TFA	ND	trace	*6.4(3)	*5.6(3)	*5.9(3)	*10.1(5)	*9.3(1)
Total product yield		4.3(8)	26.9(5)	25.5(8)	27(2)	45(2)	35.9(3)

[a]Products were quantified using GC-MS vs. an internal standard (tetradecane). #Reaction run with cyclohexane (1 mmol), NH_4IO_3 (1 mmol), KCl (0.25 mmol), HTFA (1 mL) and cooled with a curtain of N_2 flowing over the top of the vials. *Denotes detection and quantification by ^{1}H NMR spectroscopy. ND = not detected.

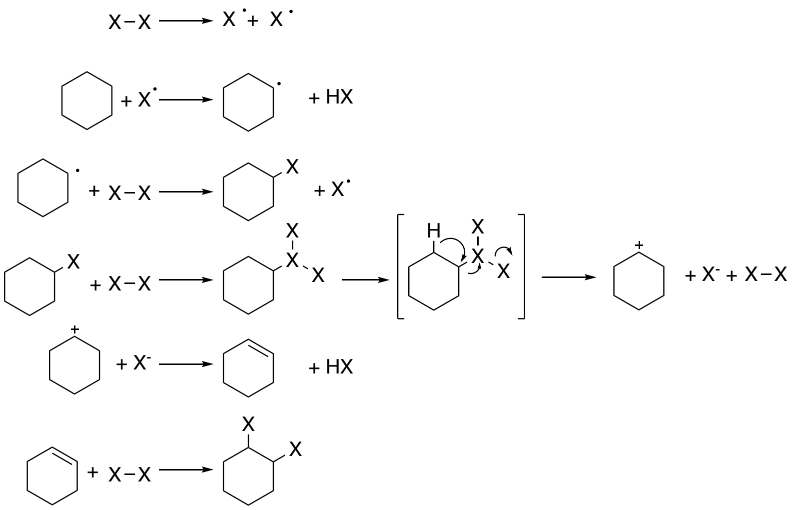

Scheme 5.9. Proposed mechanism for the di-functionalization of cyclohexane via initial dehydrogenation to generate a cyclohexene intermediate and subsequent addition of Cl_2, ICl or ICl_3. X = I, Cl. Adapted from reference.[16]

Whether using photochemical or thermal means to generate the active species for the OxE reaction, di-functionalized products were obtained in significant yields indicating that multiple reaction pathways could be occurring simultaneously. However, that should not inhibit estimation of the the isotope effect as it can be examined as a function of the initial H-atom abstraction from cyclohexane. Using a 1:1 mixture of perprotio- and perdeuterocyclohexane, the ratio of combined protio and combined deutero products was obtained under both thermal and photochemical reaction conditions (k_H/k_D, Table 5.1). This ratio differed significantly between the photochemical and thermal OxE processes, giving k_H/k_D values of 2.1(2) and 1.06(3), respectively. This difference indicates that different mechanisms are likely operative for thermally and photochemically driven cyclohexane functionalization. The k_H/k_D value for the photochemical process is in good agreement with the k_H/k_D of 1.14(1) observed in the study of the reaction of atomic chlorine with cyclohexane-h_{12}/d_{12} by Li and Pirasteh.[19-20]

As UV-vis spectroscopy has been used to demonstrate that the addition of KCl and NH_4IO_3 or KIO_4 to HTFA generates Cl_2, ICl and/or ICl_3 (Figure 5.31),[5, 9] the potential for chlorine atom reactivity under photochemical reaction conditions was examined using KIE studies. The reactions were also performed under thermal conditions for comparison. The reactions of ICl_3 and ICl with a 1:1 mixture of cyclohexane-h_{12} and cyclohexane-d_{12}, under thermal conditions gave k_H/k_D = 2.3(2) and 4.3(1), respectively, which are indicative of significant kinetic isotope effects (Table 5.2). However, while the k_H/k_D observed when using KCl/NH_4IO_3 or KCl/KIO_4 is similar to that of ICl_3, previous studies (*i.e.*, the selectivity study with propane comparing reactivity of KCl/NH_4IO_3 with NCS/benzoyl peroxide, see Chapter 2) indicate that the thermal OxE process might not operate via a purely chlorine-radical-based mechanism.[9] Calculations suggest that the formation of $IO_2\cdot$ is possibly generated *in situ*,[9-10] thus, there may be additional pathways (*i.e.*, in addition to chlorine radical-based H-atom abstraction) for H-atom abstraction in the thermal process.

The KIE values for the thermal and photochemical OxE processes with iodate/chloride differ significantly {2.1(2) versus 1.06(3)}, as do those with periodate/chloride {1.94(3) versus 1.08(3)}, indicating that the active species of the thermal and photochemical processes are likely different. Furthermore, under those reaction conditions, ICl_3 and ICl give k_H/k_D = 1.15(1) and 1.21(4), respectively (Table 5.2). The values for all photochemical conditions are similar to that of the reported process with Cl_2 (k_H/k_D = 1.1-1.2).[19-20] Therefore, it is possible that the mechanism of the photo-OxE process involves H-atom abstraction solely by chlorine radicals, whereas other intermediates play a role in the thermal reaction. As there is evidence for the formation of Cl_2, ICl and ICl_3 *in situ*, each could act as a source of chlorine.[21-24]

Table 5.2. OxE kinetic isotope effect experiments with cyclohexane under thermal and photochemical conditions.[a]

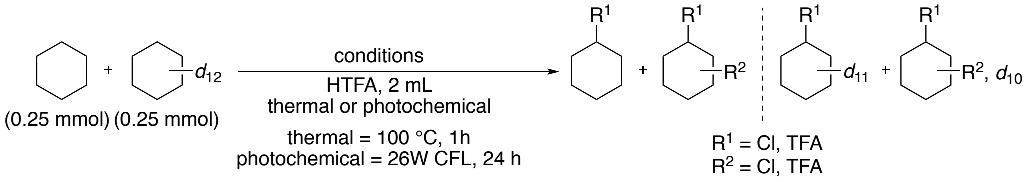

Entry	Thermal/Photochemical	Condition	k_H/k_D[b]
1	**thermal**	KCl/NH_4IO_3	2.1(2)
2		KCl/KIO_4	1.94(3)
3		ICl_3	2.3(2)
4		ICl	4.3(1)
5	**photochemical**	KCl/NH_4IO_3	1.06(3)
6		KCl/KIO_4	1.08(3)
7		ICl_3	1.15(1)
8		ICl	1.21(4)

[a] Conditions: KCl (0.14 mmol), NH_4IO_3 (0.25 mmol) or KIO_4 (0.25 mmol); ICl_3 (0.25 mmol); ICl (0.28 mmol). [b] k_H/k_D ratios reflect total protiated vs. total deuterated products. Product ratios were determined by GC-MS. Standard deviations are based on at least three experiments.

5.4 Photochemical Functionalization of Light Alkanes with Ammonium Nitrate

As nitrates were demonstrated to be effective oxidants for the functionalization of light alkanes under thermal conditions (Chapter 4), NH_4NO_3 was examined as an oxidant for the photochemical functionalization of methane (Scheme 5.10). As an initial screening, the total yield of MeX (X = TFA, NO_2, Cl) based on NH_4NO_3 is high, > 60%. Thus, ammonium nitrate is an efficient oxidant under photochemical conditions, and additional studies are needed to optimize this process and to elucidate its reaction mechanism.

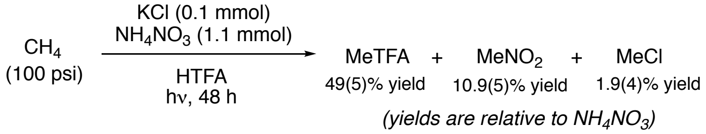

Scheme 5.10. Photochemical functionalization of methane with KCl/NH_4NO_3 in HTFA. Conditions: CH_4 (100 psi), KCl (0.1 mmol), NH_4IO_3 (1.1 mmol), HTFA (8 mL), 48 h photolysis with mercury arc lamp. Yields are reported relative to NH_4NO_3. Standard deviations are based on at least three experiments.

5.5 Photochemical Functionalization of Light Alkanes with MnO_2

Manganese(IV) dioxide was also demonstrated to be an effective oxidant for the thermal functionalization of methane (Chapter 4). As an initial screening of reaction conditions for photo-OxE, the effect of different additives was examined (Figure 5.10). In contrast to the thermal studies where KCl did not have an effect on the methane functionalization reaction using MnO_2 (see Chapter 4), the addition of KCl is critical for the photochemical reaction using MnO_2. With only added iodine, the MeTFA yield is < 11% relative to oxidant. However, when KCl and I_2 are both added, 96(12)% yield relative to MnO_2 is obtained.

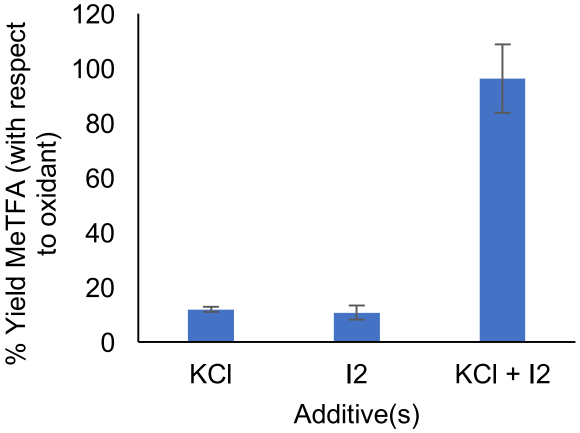

Figure 5.10. Photochemical functionalization of methane with MnO_2 in HTFA. Conditions: CH_4 (100 psi), KCl (if added, 0.1 mmol), MnO_2 (1.1 mmol), I_2 (if added, 0.1 mmol) and HTFA (8 mL), 24 h photolysis with the mercury arc lamp. Standard deviations are based on at least three experiments.

To optimize yields based on methane, the KCl/MnO_2/I_2 process was studied under different pressures of methane. With 100 and 50 psi of methane, the MeTFA yield based on oxidant is > 90%. At a lower methane pressure, this corresponds to a higher yield of MeTFA based on methane at 50 psi, 8.0(2)% versus 4.2(6)% when using 100 psi of methane. The yield based on methane using 25 psi of methane is ~9%, however the yield based on oxidant decreases sharply. Thus, 50 psi of methane was used in further attempts to optimize the yield of MeTFA based on methane. The scale of the reaction was subsequently examined (Figure 5.11). By doubling the starting amounts of KCl, MnO_2 and I_2, the MeTFA yield relative to methane increases, but not by a factor of two. Instead, the increase in MeTFA yield is from 8.0(2)% to 10.7(6)% as the yield based on oxidant decreases with increased oxidant loading (Figure 5.12).

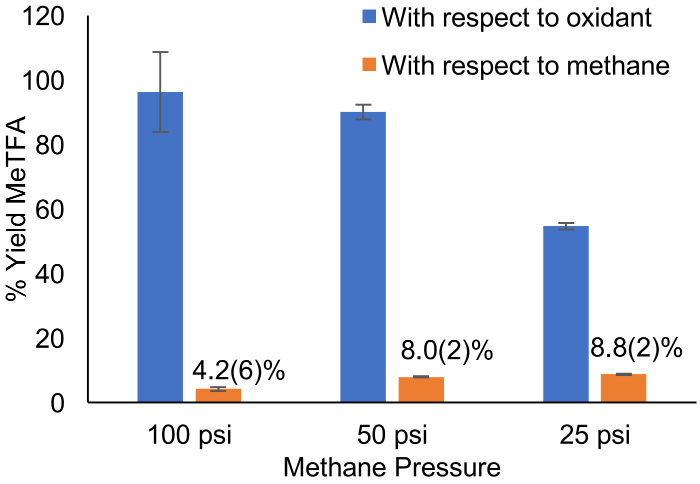

Figure 5.11. Photochemical functionalization of methane with $KCl/MnO_2/I_2$ in HTFA as a function of methane pressure. Conditions: CH_4, KCl (0.1 mmol), MnO_2 (1.1 mmol), I_2 (0.1 mmol) and HTFA (8 mL), 24 h photolysis with mercury arc lamp. Standard deviations are based on at least three experiments.

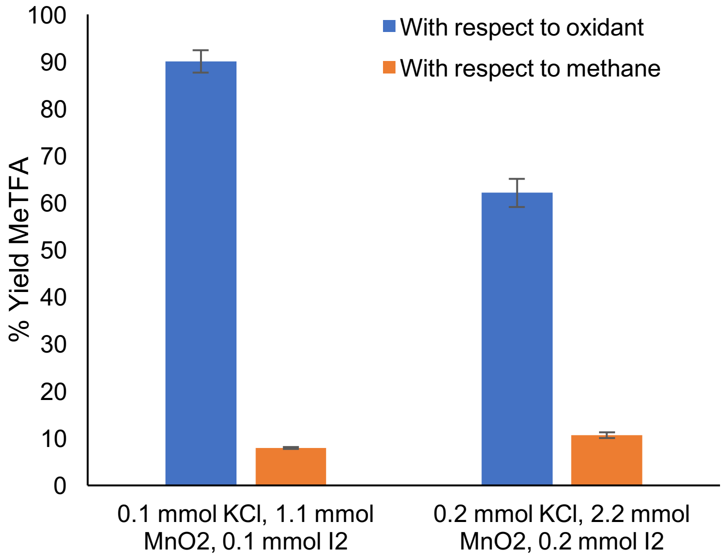

Figure 5.12. Photochemical functionalization of methane with KCl/MnO_2/I_2 in HTFA. Conditions: CH_4 (50 psi), KCl (0.1 or 0.2 mmol), MnO_2 (1.1 or 2.2 mmol), I_2 (0.1 or 0.2 mmol) and HTFA (8 mL), 24 h photolysis with the mercury arc lamp. Standard deviations are based on at least three experiments.

On evaluating the effect of water on the photochemical reaction with MnO_2, it was found that the process exhibits a high tolerance for water, contrary to what was observed thermally (Figure 5.13). With 1 mL of added H_2O, the yield of MeTFA relative to methane only decreases by 2.5%, to 8.1(4)%. Although the yields of MeTFA at present are lower than those obtained using the OxE process, the use of manganese oxides as oxidants is appealing due to its potential for more facile recyclability from air than is possible with iodate or periodate. The addition of O_2 to the methane functionalization reaction with Mn_2O_3 by Chen and coworkers enabled catalytic turnover of the Mn oxidant.[25] In contrast, the addition of O_2 to the original OxE process with iodate did not result in improved yields, and as periodate is a stronger oxidant than iodate, it is unlikely that it would be recycled more easily.

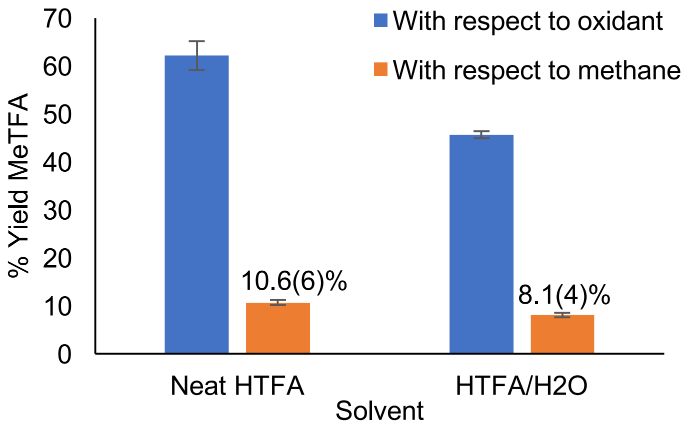

Figure 5.13. Photochemical functionalization of methane with KCl/MnO_2/I_2 in HTFA or HTFA/H_2O. Conditions: CH_4 (50 psi), KCl (0.2 mmol), MnO_2 (2.2 mmol), I_2 (0.2 mmol) and HTFA (8 mL) or HTFA/H_2O (8 mL/1 mL), 24 h photolysis with the mercury arc lamp. Standard deviations are based on at least three experiments.

5.6 Tetrabutylammonium Decatungstate as a Photocatalyst for the Partial Oxidation of Light Alkanes

5.6.1 Introduction

The aforementioned processes in this Chapter demonstrate that a range of traditional oxidants are capable of selective partial oxidation of methane under photochemical conditions. However, all of these reactions are stoichiometric. These findings motivated the extension of this chemistry to study the use of photocatalysts as oxidants with the ultimate goal of using dioxygen as the oxidant. Photocatalysts differ from the previously studied oxidants in that they absorb radiation to generate excited species that can promote electron- and energy-transfer processes.[26] Thus, instead of requiring a strong oxidant which can convert chloride to molecular chlorine *in situ* to give chlorine radicals on irradiation, it was proposed that a photocatalyst could be used to oxidize chloride to chlorine and then regenerate the original photocatalyst in solution (Scheme 5.11)

Proposed OxE Catalytic Cycle

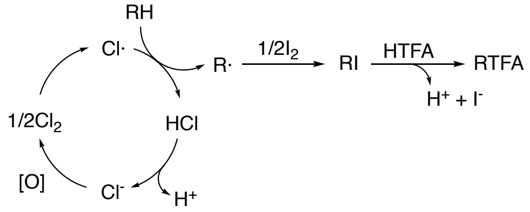

Envisioned Combination of Photocatalysis and OxE Using Oxygen

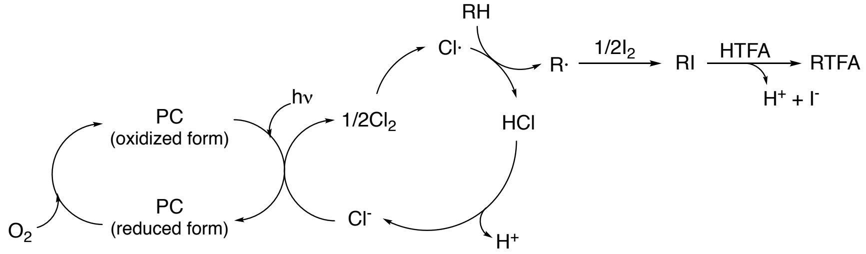

Scheme 5.11. Comparison of the proposed catalytic cycle for OxE and a simplified form of the envisioned catalytic cycle using a photocatalyst (PC) for chloride oxidation in a process similar to OxE where the terminal oxidant is O_2.

Tetrabutylammonium decatungstate (TBADT, Scheme 5.12) is an established polyoxometalate photocatalyst for the oxidation of alkanes, alkenes, alcohols, amides and amines.[27-30] Recently, TBADT has also been demonstrated to functionalize unactivated sp^3 C–H bonds under aerobic conditions in flow.[31] While there are many examples of C–H functionalization of alkanes using TBADT,[30-35] its use for the functionalization of light alkanes has not been reported.

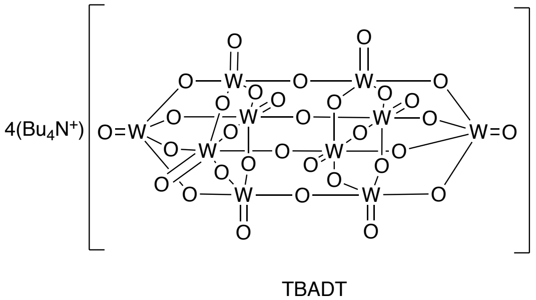

TBADT

Scheme 5.12. Structure of tetrabutylammonium decatungstate (TBADT).

The mechanistic pathways through which TBADT photocatalysis operates have been the subjects of extensive study.[36] Functionalization is generally thought to occur via single electron transfer (SET) or hydrogen atom transfer (HAT) (Scheme 5.13). Which pathway is operable depends upon the substrate's redox properties. As **wO** (*i.e.*, TBADT's reactive excited state) has a redox potential of approximately +2.44 V vs. SCE (saturated calomel electrode),[37] if a substrate has a redox potential < +2.44 V vs. SCE then SET can take place, to form the alkyl radical cation.[38] However, if the redox potential of the substrate does not match that value, then HAT is possible, resulting in the generation of alkyl radical (Scheme 5.13). In either case, this results in the production of mono-reduced TBADT, $(W_{10}O_{32})^{5-}$. $[W_{10}O_{32}]^{5-}$ undergoes rapid disproportionation to give the $[W_{10}O_{32}]^{4-}$, the oxidized form which can resume photocatalysis, and $[W_{10}O_{32}]^{6-}$.[38-39] The reduced form can be oxidized by O_2 to the original active photocatalyst.[27, 40] As a result, aerobic photocatalysis with TBADT is a burgeoning field,[31-34] and the photocatalyst is a highly attractive candidate for new photochemical oxidation processes.

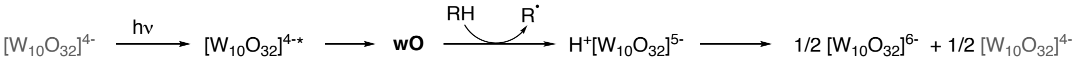

Scheme 5.13. SET pathway for alkane functionalization with TBADT. **wO** = TBADT's reactive excited state. Adapted from reference.[38]

5.6.2 Photocatalytic Functionalization of Methane using Tetrabutylammonium Decatungstate

TBADT was studied as a photocatalyst for methane functionalization. Under the initial screening conditions, the combination of KCl and TBADT in HTFA solvent gave ~10 TO MeX product (X = TFA, Cl) relative to TBADT (Scheme 5.14). Air is used as the reactions are set up under ambient atmosphere. The reaction favors the production of MeTFA with a > 20:1 ratio of MeTFA:MeCl. In the absence of KCl, no functionalization is observed.

Thus, TBADT acts as a photocatalyst for the functionalization of methane under similar conditions to the photo-OxE process.

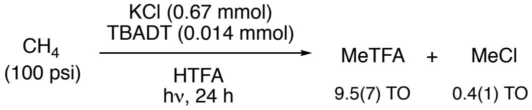

Scheme 5.14. Photochemical functionalization of methane with KCl/TBADT. Conditions: CH_4 (100 psi), KCl (0.67 mmol), TBADT (0.014 mmol), HTFA (8 mL), 24 h photolysis with the mercury arc lamp. Turnovers (TOs) are based on TBADT. Yields and standard deviations are based on three experiments.

Subsequent studies examined the effect of added iodine, as the radical trap has been proposed to enable the high yields of mono-functionalization obtained with the OxE processes.[9] The addition of 0.05 mmol of iodine results in improved yields from 10(1) TO of MeTFA in the absence of iodine to 17(3) TO of MeTFA (Figure 5.14). At higher loadings of iodine, average yields of MeTFA decrease slightly, but, since the standard deviations increase, the yields remain statistically identical.

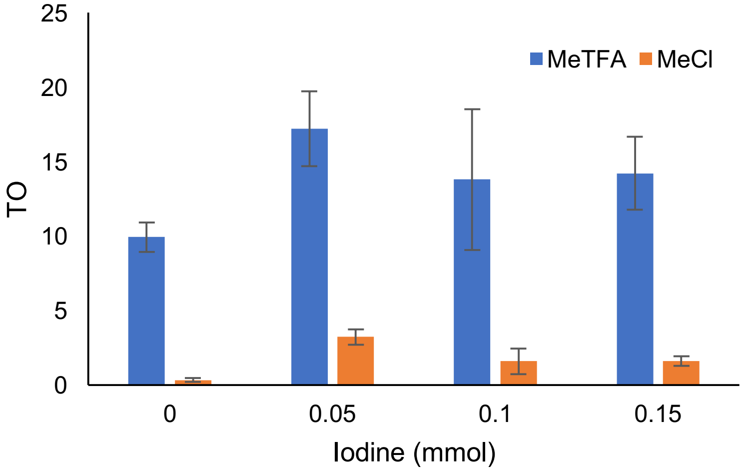

Figure 5.14. Photochemical functionalization of methane with KCl/TBADT as a function of added iodine. Conditions: CH_4 (100 psi), KCl (0.67 mmol), TBADT (0.014 mmol), I_2 (0-0.15 mmol), HTFA (8 mL), 24 h photolysis with the mercury arc lamp. Error bars denote standard deviations based on at least three experiments.

The effect of the reaction atmosphere was studied (Figure 5.15). Although the reaction of KCl/TBADT is complete after 24 h, if the reactions are purged with dioxygen, slightly higher yields are possible and catalysis is extended past 24 h. After 48 h with O_2, 16(3) TO of MeTFA are obtained (Figure 5.15). Using the strong oxidant $K_2S_2O_8$ to recycle TBADT *in situ* results in 0.29(2) mmol of MeTFA 0.064(4) mmol of MeCl, corresponding to 21(2) TO and 4.6(3) TO, respectively (Scheme 5.15). However, with KCl and $K_2S_2O_8$ in the absence of TBADT, statistically identical yields of MeTFA and MeCl are obtained, indicating that $K_2S_2O_8$ is not merely recycling reduced TBADT *in situ* (Scheme 5.15).

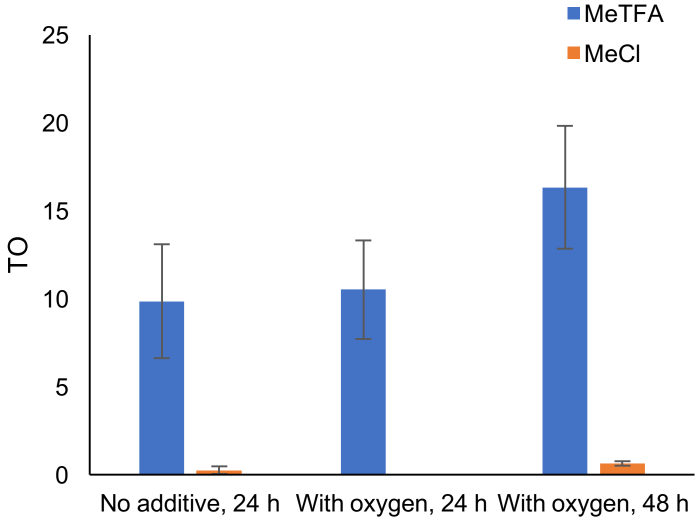

Figure 5.15. Photochemical functionalization of methane with KCl/TBADT with and without O_2 purging. Conditions: CH_4 (150 psi), KCl (0.67 mmol), TBADT (0.014 mmol), HTFA (8 mL), photolysis with the mercury arc lamp. Air denotes experiments set up in air, and O_2 denotes experiments where reactors were purged with O_2 for 10 min prior to pressurizing with methane. Error bars denote standard deviations based on at least three experiments.

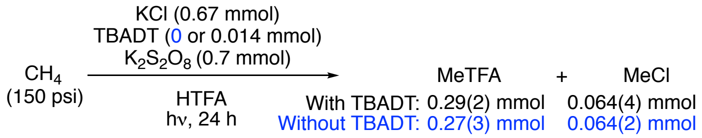

Scheme 5.15. Photochemical functionalization of methane with KCl/TBADT using $K_2S_2O_8$ as an *in situ* oxidant. Conditions: CH_4 (150 psi), KCl (0.67 mmol), TBADT (0 or 0.014 mmol), $K_2S_2O_8$ (0.7 mmol), HTFA (8 mL), 24 h photolysis with the mercury arc lamp.

In the OxE processes, the strong acid HTFA has been proposed to be necessary to generate the active species in solution. However, for photocatalysis with TBADT, such a strong acid may not be necessary. HOAc was used to determine if the reaction could occur in less acidic reaction media. In HOAc, no evidence of methane functionalization was observed after 24 h of photolysis under the standard conditions (100 psi CH_4, 0.67 mmol KCl, 0.014 TBADT, 8 mL solvent). Developing greater understanding of the requirements for solvents for photocatalysis with TBADT is the subject of further study.

5.7 Summary & Future Directions

Extending the thermal OxE process to photochemical reaction conditions has been extremely successful. The primary advancement of the photo-OxE process is its demonstration of the general nature of the ester's protecting effect for partial oxidation, at least in carboxylic acid solvent. The mono-functionalized product with weaker (homolytic) C–H bonds than the starting alkane is stable under highly oxidizing conditions and in the presence of chlorine radical, a capable H-atom abstraction source. This stability enables high yields and selectivity for the mono-functionalized product, and the protecting effect of the ester could be applied to other functionalization systems, both thermal and photochemical.

The photo-OxE process using iodate and chloride for the partial oxidation of light alkanes is highly efficient and selective for partial oxidation products. Yields of RX (R = Me, Et; X = TFA, Cl) are particularly high with methane and ethane (~50% and 80%, respectively). These results are significant as this demonstrates the use of a radical-based process for selective partial oxidation under photochemical conditions with high conversions. Mechanistic studies indicate that the photo-OxE process likely occurs by a chlorine radical-based H-atom abstraction pathway, whereas multiple H-atom abstraction agents are predicted to be generated under thermal conditions. Additionally, the photo-OxE process exhibits greater tolerance to water and less acidic solvents than the thermal OxE process.

In addition to being effective oxidants for thermal methane functionalization (Chapter 4), nitrates and manganese(IV) dioxide are also capable oxidants for photochemical methane functionalization. The use of ammonium nitrate in combination with KCl in HTFA resulted in > 60% yield of MeX (X = TFA, NO_2, Cl) relative to oxidant under un-optimized conditions with the mercury arc lamp. With MnO_2, comparisons between the thermal and photochemical processes indicate that the two processes likely occur by different mechanisms as chloride was required under photochemical conditions but not under thermal conditions. The photochemical oxidation process with KCl, MnO_2 and I_2 is selective for the formation of MeTFA, and nearly quantitative yields of MeTFA based on oxidant are observed, although MeTFA yields based on methane are limited to ~11% at present. The photochemical process with MnO_2 also operates in dilute HTFA, an advantage over previous light alkane functionalization processes which require superacidic solvent media.[8]

Further optimization of the photochemical functionalization of light alkanes using nitrates and transition metal-based oxidants is required. It is likely that the addition of iodine would serve to improve yields of functionalized product further, as was observed under thermal conditions. Optimization of the chloride loading could also have a significant impact on the reaction. Another major facet of future studies will be the *in situ* regeneration of the oxidant. To develop a process that can be used at scale for light alkane functionalization, O_2 must be the terminal oxidant. Future studies, similar to those outlined in Chapter 4, will involve the study of co-oxidants that can themselves be regenerated by O_2 and which can oxidize reduced oxidant species such that functionalization can proceed.

The use of a known photocatalyst, TBADT, further demonstrates the potential range of the OxE process. The photochemical reactions are catalytic in TBADT, with a maximum of 17(3) TO observed under optimized conditions. The addition of iodine results in slightly improved yields, potentially due to the role of iodine as a radical trap as was proposed for the thermal OxE process with iodate. Although further optimization studies are required, the studies with TBADT demonstrate proof-of-concept that the protection strategy can be applied to photocatalytic systems for selective partial oxidation of light alkanes. Primary future goals for photocatalysis with TBADT are to develop a greater understanding of the potential solvent media that can be used and to optimize conditions for re-oxidation of the photocatalyst. Although the use of added O_2 has resulted in longer-lived catalysis, further studies are required to develop more effective methods for the *in situ* regeneration of the photocatalyst in order to improve its longevity.

In addition to re-oxidation, the photocatalytic process could be improved through immobilization strategies. Preparation of heterogenized forms of decatungstate has been the subject of extensive study,[41-46] and applying those techniques could aid the recyclability of the photocatalyst. Two additional photocatalyst candidates will be examined, $Ru(bpz)_3(PF_6)_2$ and $(Ir[dF(CF_3)ppy]_2(dtbpy))PF_6$ {bpz = 2,2-bipyrazine; $[dF(CF_3)ppy]$ = 2-(2,4-difluorophenyl)-5-(trifluoromethyl)pyridine; dtbpy = 4,4'-di-*tert*-butyl-2,2'-bipyridine} (Scheme 5.16). These photocatalysts were chosen for their strong oxidizing capabilities. $Ru(bpz)_3(PF_6)_2$ and $(Ir[dF(CF_3)ppy]_2(dtbpy))PF_6$ have excited state potentials of +1.45 V vs SCE and 1.21 V vs SCE, respectively.[47-48] Thus, both should be able to generate reactive species for H-atom abstraction *in situ* in an extension of the OxE chemistry which uses light to recycle the photocatalyst.

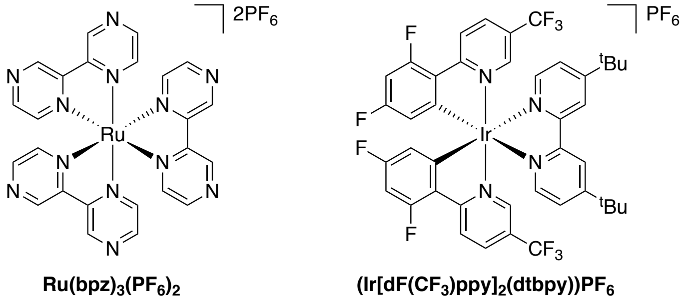

Scheme 5.16. Photocatalyst candidates for future studies, $Ru(bpz)_3(PF_6)_2$ and $(Ir[dF(CF_3)ppy]_2(dtbpy))PF_6$.

Mechanistic studies will seek to elucidate the operative reaction mechansims of these processes and, in turn, to enable further optimization of these photochemical functionalization processes. The photochemical reactions appear to exhibit similarities to the photo-OxE process which likely operates by a chlorine-radical-based mechanism. Obtaining the k_H/k_D for the photochemical reaction with cyclohexane-h_{12}/d_{12} would enable comparisons between the reactions with these oxidants and Cl_2, ICl, and ICl_3. UV-vis studies could also help to determine the active species present *in situ.*

5.8 Experimental Section

General Considerations. *Caution: Many of the reagents and conditions described herein are potentially hazardous. Safety procedures should be consulted prior to the use of concentrated acids, mixtures of hydrocarbons and oxygen and strong oxidants.*

Unless noted otherwise, all reactions were performed under ambient atmosphere. All chemicals were purchased from commercial sources, and other than *N*-chlorosuccinimide, all were used as received. *N*-Chlorosuccinimide was recrystallized from acetic acid prior to use. Tetrabutylammonium decatungstate was prepared according to a literature procedure.[49] Gases were purchases from GTS-Welco and used as received. All lamps were purchased from commercial sources and used as received. The mercury arc lamp (Hanovia, medium pressure, UV lamp, 450 W) was purchased from Ace Glass, the 105 W compact fluorescent lightbulb (CFL, 420 W equivalent, 5000 K full spectrum) was purchased from Amazon and the 26W CFL (2700 K) was purchased from Grainger. The UV reactor is a Rayonet Photochemical Reactor (RPR-100), and the blue LED is a Kessil H150-blue 30 W High Luminous *DEX 2100 LED*. NMR analysis was performed using a Bruker, Avance 500, Avance III 600 or Avance DRX-600 or a Varian Inova 500 spectrometer. NMR spectra of reaction mixtures from the functionalization of methane, ethane and propane were obtained using neat HTFA or HOAc with a C_6D_6 capillary as an internal lock reference. Nitromethane or acetic acid were added as internal standards and used to reference ^1H NMR spectra (δ 4.18 and 2.04, respectively). GC-MS analysis was performed using an Agilent Technologies 7890A gas chromatograph equipped with a fused silica column and electron impact mass analyzer. High pressure reactions were performed in glass reactors from Andrews Glass with custom-built Swagelok reactor tops.

General Procedures

Photochemical functionalization of light alkanes by OxE. A Fisher-Porter reactor was charged with a stir bar, KCl (0.67-6.7 mmol), NH_4IO_3 or KIO_4 (7.7 mmol), HTFA (8 mL), and I_2 (if added, 0.05-0.2 mmol) prior to being sealed and pressurized with the light alkane. The reactor was stirred on a stir plate inside a photolysis chamber with either a mercury arc lamp or lamp with a CFL bulb. The lamp was turned on for the reaction time, with an additional 15 min added to the reaction time when the mercury arc lamp was used to account for the warm-up time of the bulb. After the reaction, the lamp was turned off and the reactor was vented. Internal standard (nitromethane or HOAc) was added and the reaction mixture was stirred. An aliquot was then removed for centrifugation and the supernatant was used for ^{1}H NMR analysis. Representative ^{1}H NMR spectra are shown below. Data are reported as averages of at least three experiments with standard deviations.

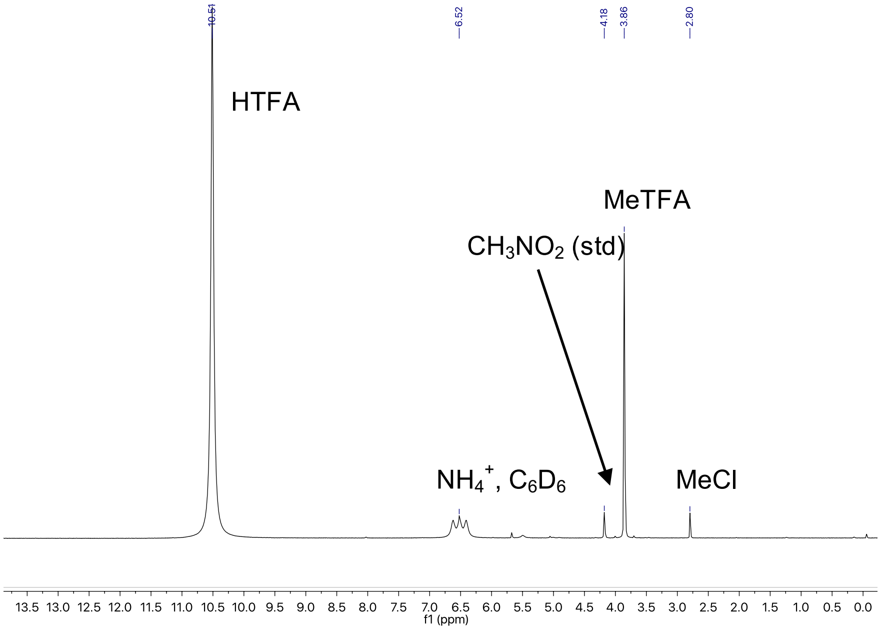

Figure 5.16. Representative ^{1}H NMR spectrum for photochemical methane functionalization with KCl/NH_4IO_3. Conditions: CH_4 (100 psi), KCl (2.01 mmol), NH_4IO_3 (7.7 mmol), HTFA (8 mL), 24 h photolysis using Hg lamp. Nitromethane (0.56 mmol) was added as an internal standard.

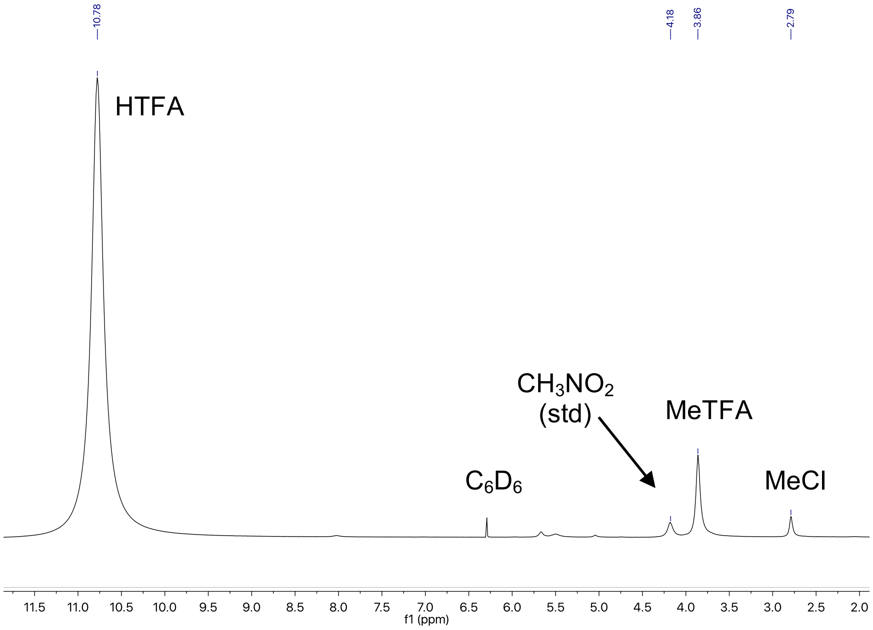

Figure 5.17. Representative ^1H NMR spectrum for photochemical methane functionalization with KCl/KIO_4. Conditions: CH_4 (100 psi), KCl (2.01 mmol), NH_4IO_3 or KIO_4 (7.7 mmol), HTFA (8 mL), 24 h photolysis with Hg lamp. Nitromethane (0.56 mmol) was added as an internal standard.

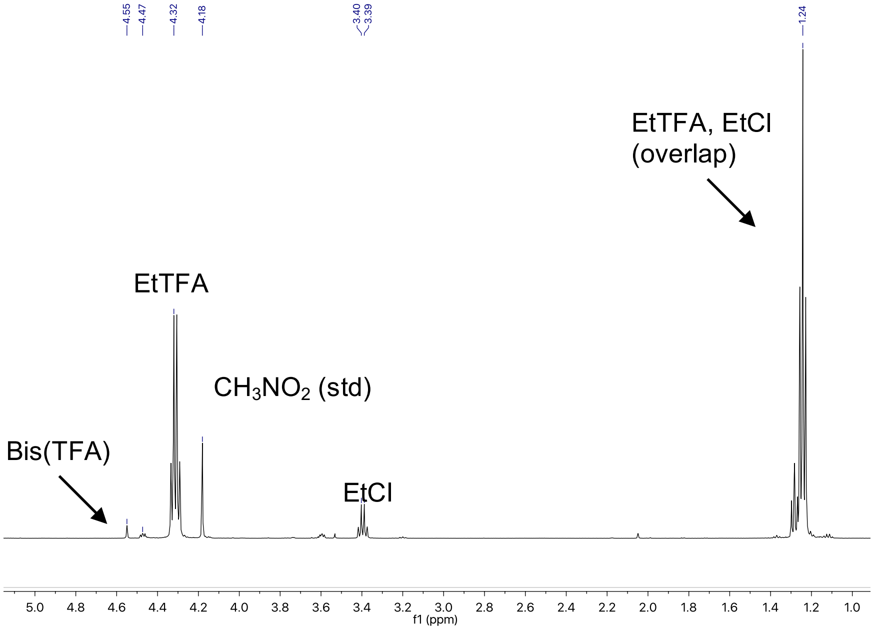

Figure 5.18. Representative ^1H NMR spectrum for photochemical ethane functionalization. Conditions: CH_3CH_3 (100 psi), KCl (2.01 mmol), NH_4IO_3 (7.7 mmol), HTFA (8 mL), 24 h photolysis with Hg lamp. Nitromethane (0.56 mmol) was added as an internal standard.

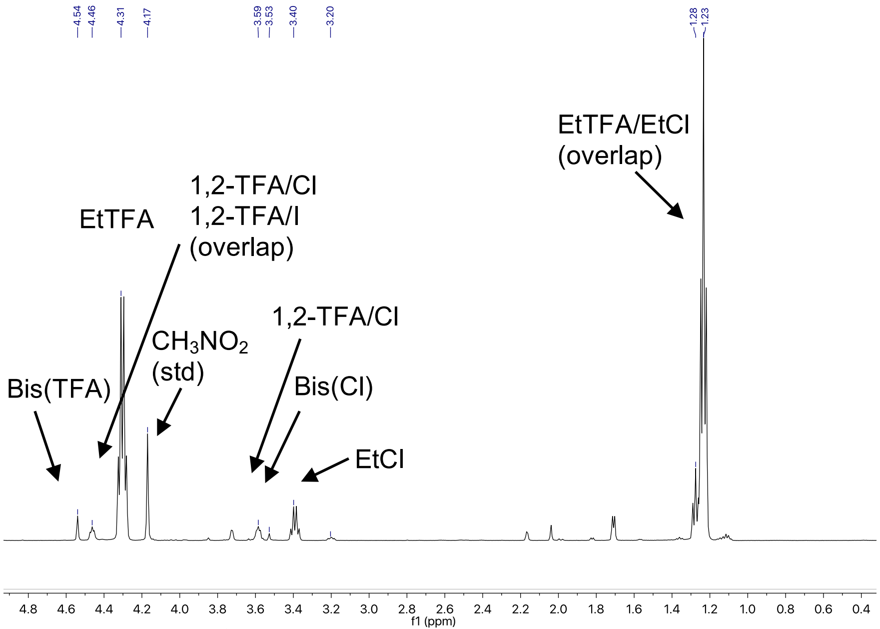

Figure 5.19. Representative ^{1}H NMR spectrum for photochemical ethane functionalization at low ethane pressure. Conditions: CH_3CH_3 (25 psi), KCl (2.01 mmol), NH_4IO_3 (7.7 mmol), HTFA (8 mL), 24 h photolysis with Hg lamp. Nitromethane (0.37 mmol) was added as an internal standard. 1,2-X,Y refers to 1,2-disubstituted ethane products.

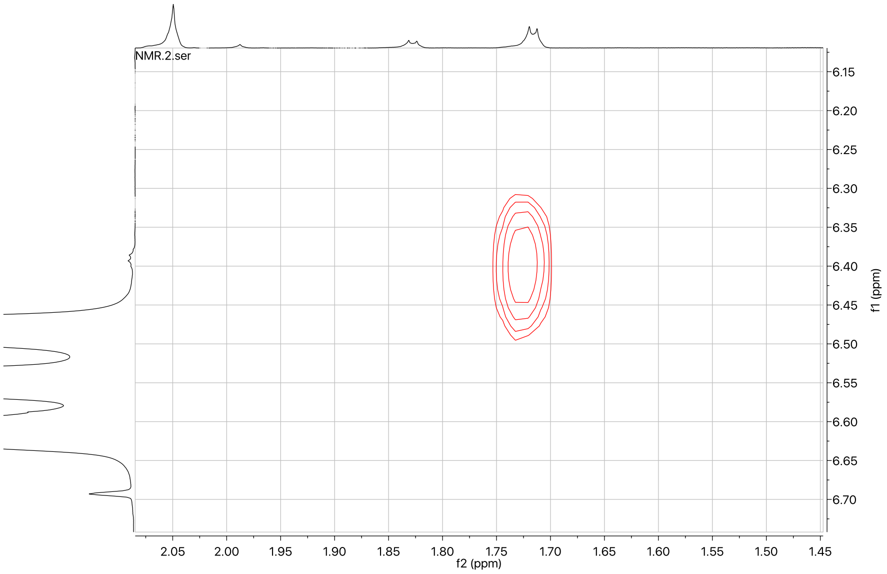

Figure 5.20. COSY spectrum for photochemical ethane functionalization, zoomed in to illustrate cross peak. Conditions: CH_3CH_3 (25 psi), KCl (2.01 mmol), NH_4IO_3 (7.7 mmol), HTFA (8 mL), 24 h photolysis with Hg lamp. Nitromethane (0.37 mmol) was added as an internal standard.

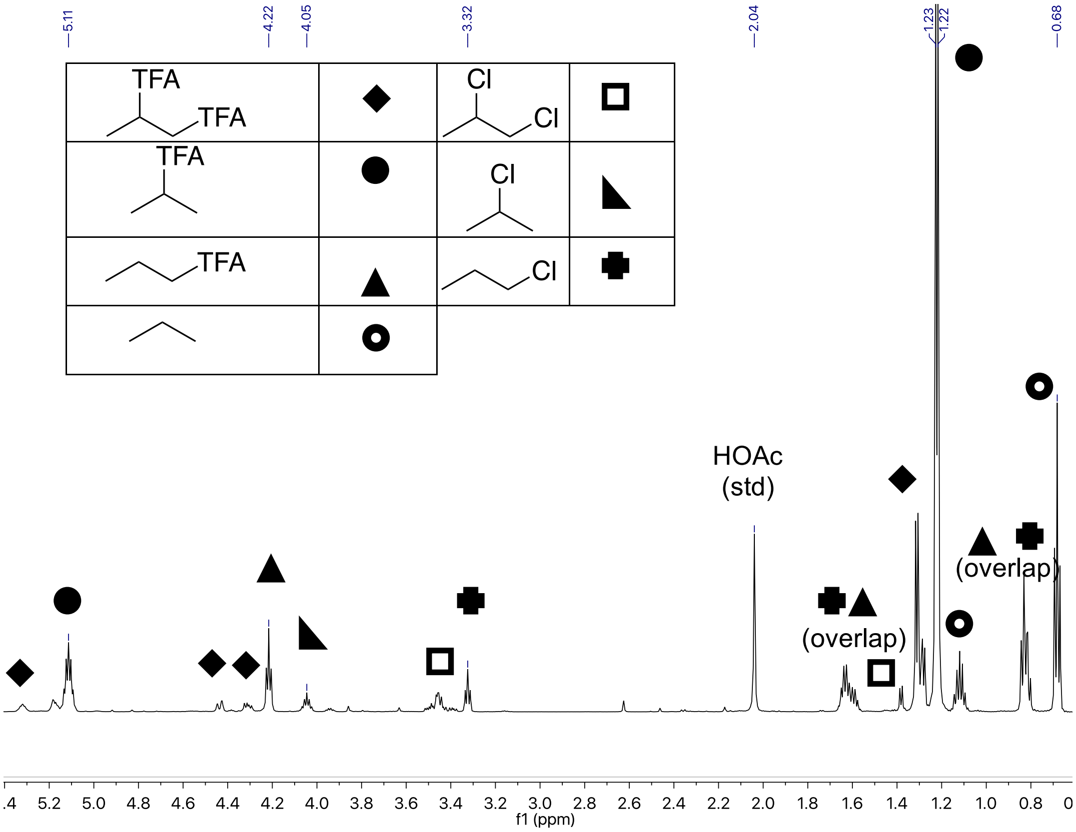

Figure 5.21. Representative ^{1}H NMR spectrum for photochemical propane functionalization. Conditions: Propane (100 psi), KCl (2.01 mmol), NH_4IO_3 (7.7 mmol), HTFA (8 mL), 24 h photolysis with Hg lamp. Acetic acid (0.53 mmol) was added as an internal standard.

Solvent screening for the photo-OxE process. A Fisher-Porter reactor was charged with a stir bar, KCl (2.01 mmol), NH_4IO_3 (7.7 mmol) and dichloroacetic acid (8 mL), HTFA/H_2O (3:1 mol/mol, 8 mL) or glacial HOAc (8 mL) prior to being sealed and pressurized with the 100 psi of methane. The reactor was stirred on a stir plate inside a photolysis chamber with a mercury arc lamp. The lamp was turned on for 24 h, with an additional 15 min added to the reaction time to account for the warm-up time of the bulb. After the reaction, the lamp was turned off and the reactor was vented. Internal standard was added and the reaction mixture was stirred. An aliquot was then removed for centrifugation and the supernatant was used for ^{1}H NMR analysis. Representative ^{1}H NMR spectra for dichloroacetic acid and HOAc are shown below. ^{1}H NMR spectra in dilute HTFA are similar to those in neat HTFA. Data are reported as averages of at least three experiments with standard deviations.

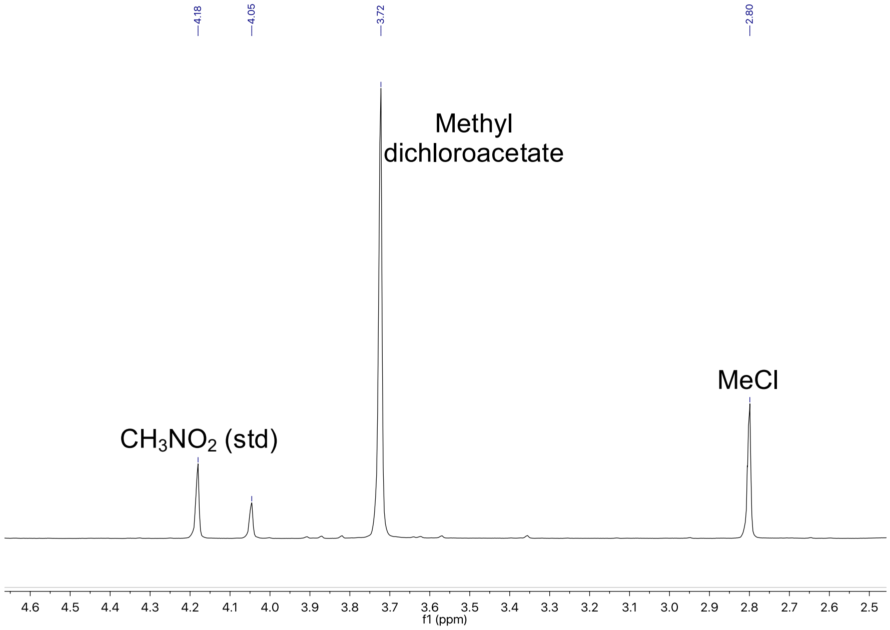

Figure 5.22. Representative ^{1}H NMR spectrum for photochemical methane functionalization in dichloroacetic acid. Conditions: CH_4 (100 psi), KCl (2.01 mmol), NH_4IO_3 (7.7 mmol), dichloroacetic acid (8 mL), 24 h photolysis with Hg lamp. Nitromethane (0.56 mmol) was added as an internal standard.

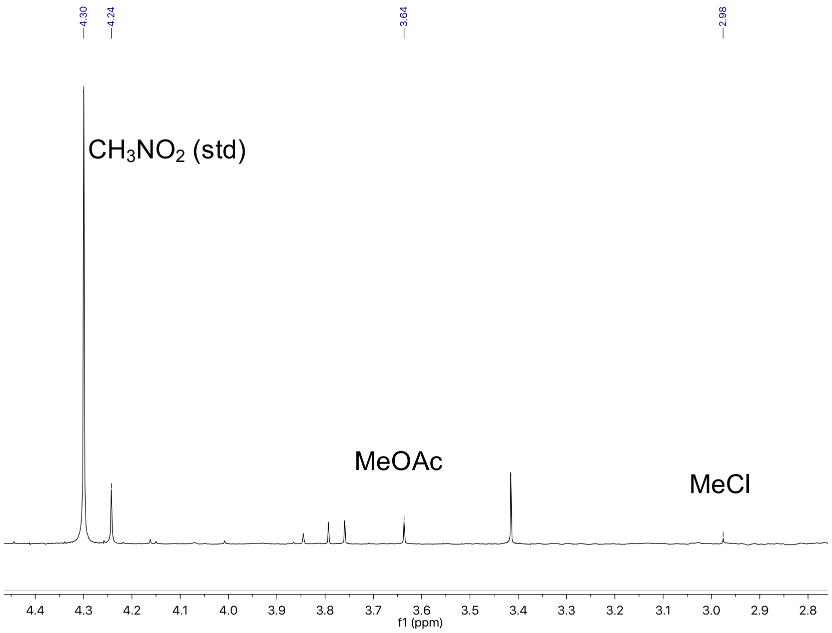

Figure 5.23. Representative ^{1}H NMR spectrum for photochemical methane functionalization in HOAc. Conditions: CH_4 (100 psi), KCl (2.01 mmol), NH_4IO_3 (7.7 mmol), HOAc (8 mL), 24 h photolysis with Hg lamp. Nitromethane (0.56 mmol) was added as an internal standard.

Study of MeTFA functionalization and decay. Functionalization reactions were set up following the general procedure listed above using KCl (2.01 mmol), NH_4IO_3 (7.7 mmol), HTFA (8 mL). The reactor was pressurized with 50 psi of methane and photolyzed using the mercury arc lamp for reaction times of 6, 18 or 24 h. For decay experiments, a Fisher-Porter reactor was charged with a stir bar, MeTFA (5.5 mmol), KCl (2.01 mmol), NH_4IO_3 (7.7 mmol), HTFA (8 mL) before being pressurized with 50 psi of argon. The reaction mixture was photolyzed using the mercury arc lamp for 6, 12, 24 or 48 h. A representative ^{1}H NMR spectrum from a MeTFA decay reaction is shown below. All data are given as averages of at least three experiments with standard deviations shown.

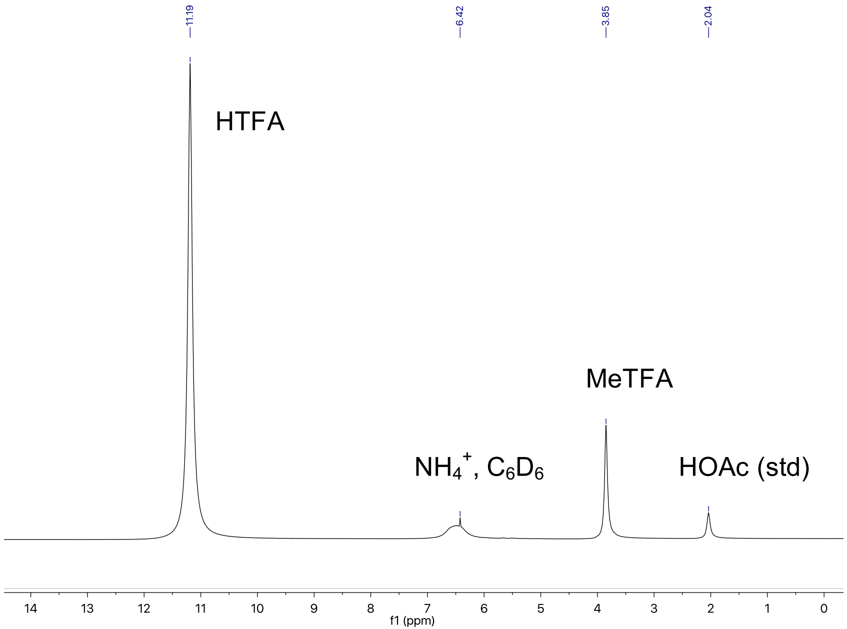

Figure 5.24. Representative ^{1}H NMR spectrum from the reaction of methyl trifluoroacetate with KCl/NH_4IO_3 in HTFA. Conditions: Argon (50 psi), MeTFA (5.5 mmol) KCl (2.01 mmol), NH_4IO_3 (7.7 mmol), HTFA (8 mL), Hg lamp photolysis, 12 h. Acetic acid (1.4 mmol) was added as an internal standard.

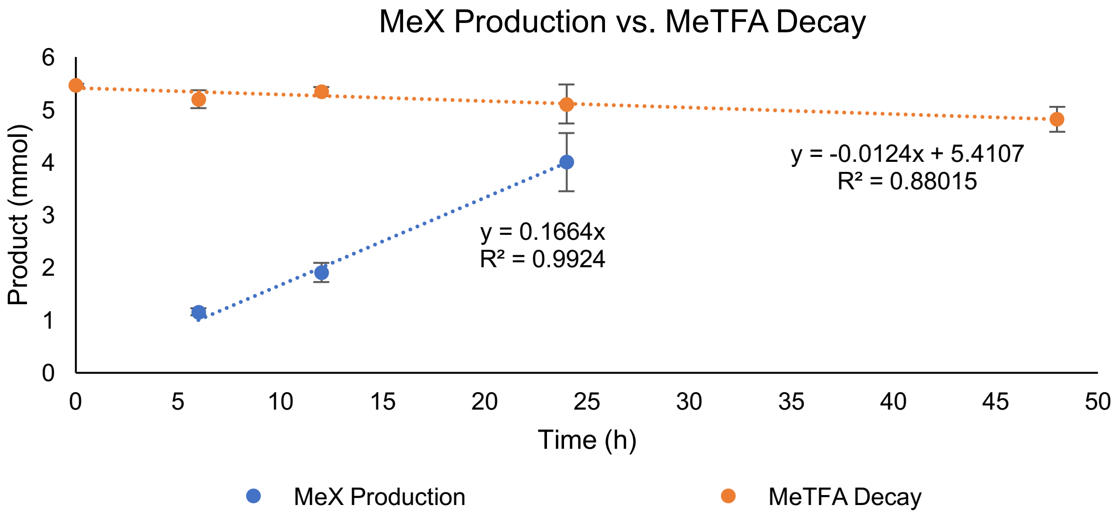

Figure 5.25. Linear fits for MeTFA (blue) production for the reaction of KCl (2.01 mmol), NH_4IO_3 (7.7 mmol) and HTFA (8 mL) with methane (50 psi) under photolysis with the Hg lamp. The decay of MeTFA (orange) was monitored using MeTFA (5.5 mmol), 50 psi Ar, KCl (2.01 mmol), NH_4IO_3 (7.7 mmol) and HTFA (8 mL). The initial amount of MeTFA for the decay series was determined by setting up controls and taking ^{1}H NMR spectra immediately to account for loss due to volatility.

Chlorination with *N*-chlorosuccinimide and benzoyl peroxide with or without added iodine. A Fisher Porter reactor was charged with a stir bar, *N*-chlorosuccinimide (3.5 mmol), benzoyl peroxide (0.035 mmol), I_2 (0 or 0.067 mmol) and HTFA (8 mL). The reactor was then sealed and pressurized with 100 psi of methane. The reactor was stirred in the photolysis chamber with the mercury arc lamp and photolyzed for 24 h. After the reaction, the lamp was turned off and the reactor was vented. Internal standard was added and the reaction mixture was stirred. An aliquot was then removed for centrifugation and the supernatant was used for ^{1}H NMR analysis. Representative ^{1}H NMR spectra are shown below. Data given in Scheme 5.5 are the average of at least three experiments with standard deviations shown.

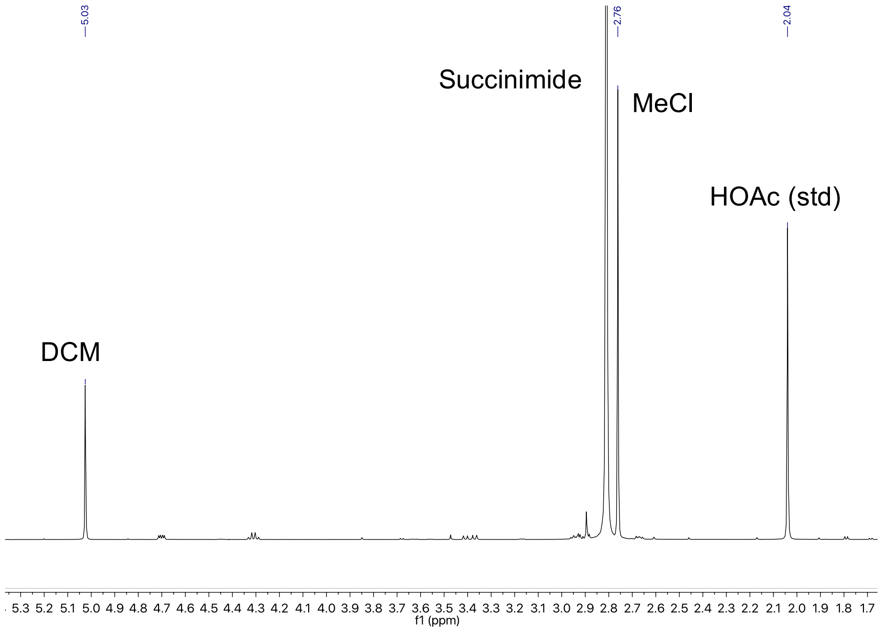

Figure 5.26. Representative ^{1}H NMR spectrum for photochemical methane functionalization with *N*-chlorosuccinimide without added iodine. Conditions: CH_4 (100 psi), *N*-chlorosuccinimide (3.5 mmol), benzoyl peroxide (0.035 mmol), HTFA (8 mL), 24 h of photolysis with Hg lamp. Acetic acid (0.53 mmol) was added as an internal standard.

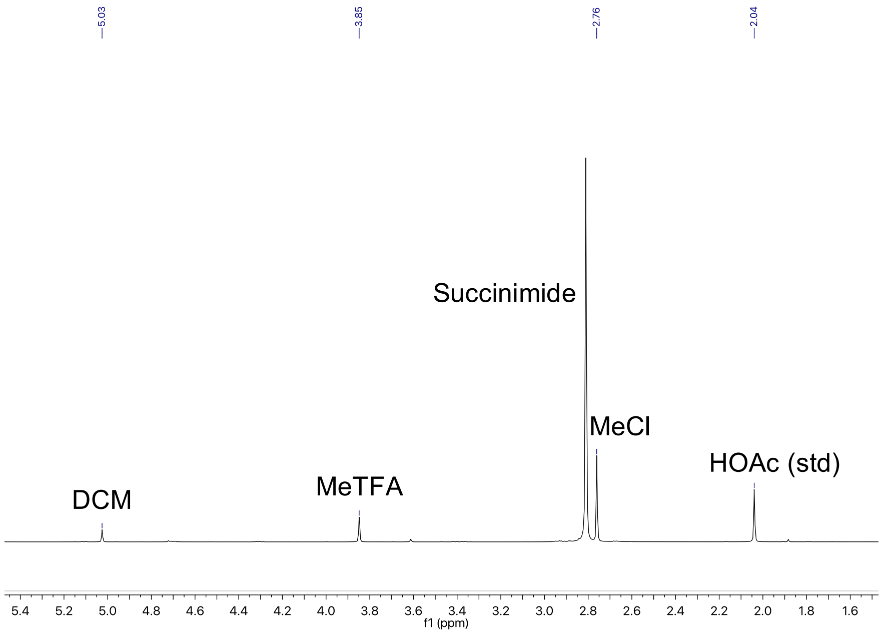

Figure 5.27. Representative ^{1}H NMR spectrum for photochemical methane functionalization with *N*-chlorosuccinimide with added iodine. Conditions: CH_4 (100 psi), *N*-chlorosuccinimide (3.5 mmol), benzoyl peroxide (0.035 mmol), I_2 (0.067 mmol), HTFA (8 mL), 24 h of photolysis with the mercury arc lamp. Acetic acid (0.53 mmol) was added as an internal standard.

Cyclohexane functionalization. A microwave vial (8 mL) was charged with a stir bar, KCl (0.13 mmol), NH_4IO_3 (0.51 mmol), HTFA (2 mL) and cyclohexane (0.5 mmol). The vial was sealed with a crimp cap with a septum. **Thermal:** The vial was placed in an oil bath at 100 °C and heated and stirred for 1 h. **Photochemical:** The vial was placed in front of the light source and stirred at room temperature for 24 h, unless specified otherwise. **Work-up:** Following the reaction, the vial was cooled to room temperature and was then filtered through a PTFE filter into a new vial with internal standard (0.24 mmol tetradecane). The reaction vial was rinsed with 5 mL dichloromethane and the rinsing was filtered into the work-up vial with tetradecane as the internal standard. The combined filtrate and internal standard mixture was washed with H_2O (2 × 10 mL). The layers were separated and the organic layer was dried over $MgSO_4$. An aliquot was analyzed by GC-

MS and product amounts were determined by comparison to the internal standard. For ^{1}H NMR analysis, the product mixture was dried under vacuum and the residue was dissolved in $CDCl_3$ for the identification and quantification of 2-chloro-1-trifluoroacetoxy-cyclohexane. Reported data are the average of three experiments with the standard deviations shown. Representative data are shown below.

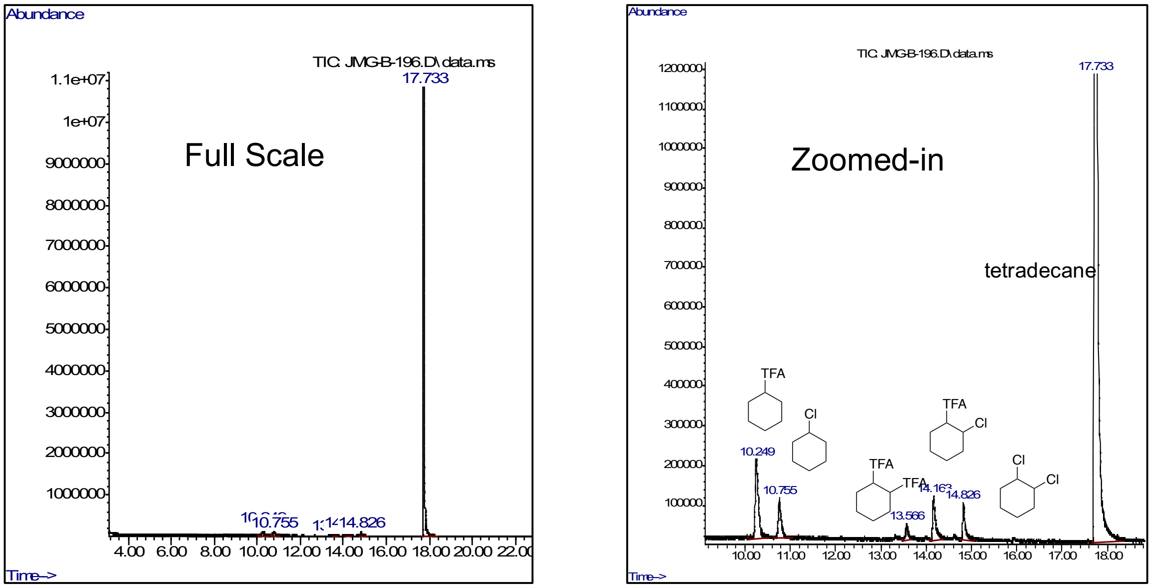

Figure 5.28. Representative GC-MS trace for the functionalization of cyclohexane. Conditions: Cyclohexane (0.5 mmol), KCl (0.13 mmol), NH_4IO_3 (0.5 mmol), HTFA (2 mL), 100 °C, 1 h. Tetradecane (0.24 mmol) was added as an internal standard.

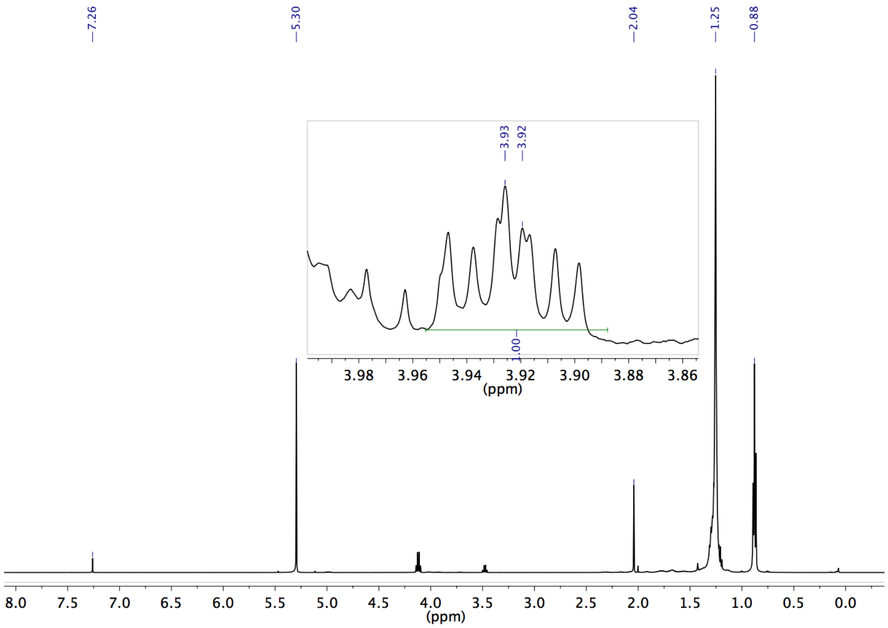

Figure 5.29. Representative ^{1}H NMR spectrum ($CDCl_3$) for the functionalization of cyclohexane. Inset shows characteristic peak for 2-chloro-1-trifluoroacetoxy-cyclohexane. Conditions: Cyclohexane (0.5 mmol), KCl (0.13 mmol), NH_4IO_3 (0.5 mmol), HTFA (2 mL), 100 °C, 1 h. Tetradecane (0.24 mmol) was added as an internal standard.

Kinetic isotope effect studies. A microwave vial (8 mL) was charged with either KCl (0.14 mmol) and NH_4IO_3 (0.25 mmol), KCl (0.14 mmol) and KIO_4 (0.25 mmol) or ICl (0.28 mmol) or ICl_3 (0.25 mmol). HTFA (2 mL), cyclohexane-h_{12} (0.25 mmol) and cyclohexane-d_{12} (0.25 mmol) were also added to the vial. The vial was sealed with a crimp cap with a septum. The mixture was then reacted under the photochemical or thermal conditions described above. Following the reaction, the vial's contents were filtered through a PTFE filter. The reaction vial was rinsed with 5 mL dichloromethane and the rinsing was filtered into the work-up vial. The combined filtrate and internal standard mixture was washed with H_2O (2 × 10 mL). The layers were separated and the organic layer was dried over $MgSO_4$. An aliquot was analyzed by GC-MS. Reported data are the average of three experiments with the standard deviations shown. A representative GC-MS trace is shown below.

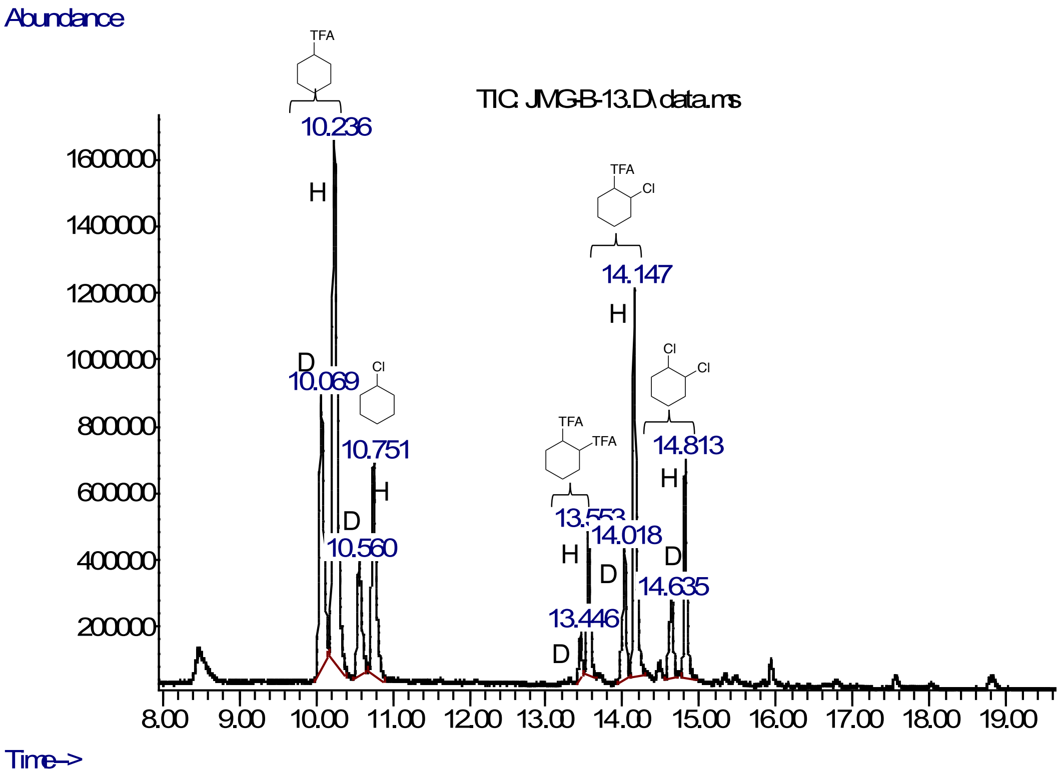

Figure 5.30. Representative GC-MS trace for the kinetic isotope effect experiments with cyclohexane. Conditions: cyclohexane (0.25 mmol), cyclohexane-d_{12} (0.25 mmol), KCl (0.14 mmol), NH_4IO_3 (0.27 mmol), HTFA (2 mL), 100 °C, 1 h. In each set of peaks for a given product, the fully protio product is indicated by an "H" and the fully deutero product is indicated by a "D."

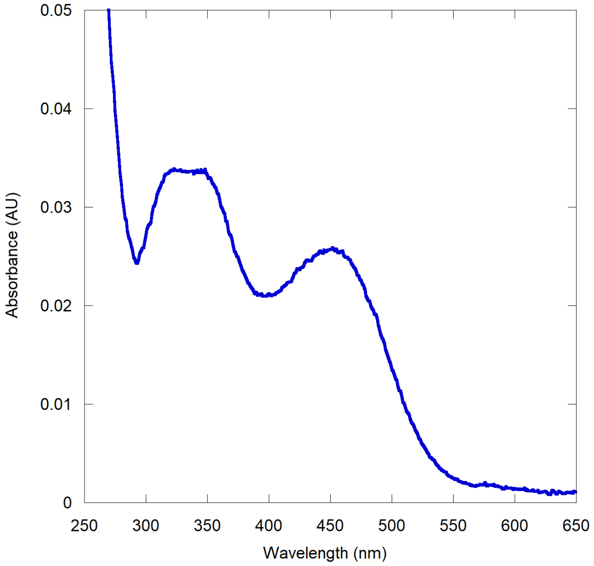

Figure 5.31. UV-vis spectrum obtained on the combination of KCl (0.15 mmol) and KIO_4 (0.5 mmol) to HTFA (2 mL) after filtering off the solids and diluting to 4 mL.

Photochemical Functionalization of Methane with KCl/NH_4NO_3. A Fisher-Porter reactor was charged with a stir bar, KCl (0.1 mmol), NH_4IO_3 (1.1 mmol) and HTFA (8 mL) prior to being sealed and pressurized with the 100 psi of methane. The reactor was stirred on a stir plate inside a photolysis chamber with a mercury arc lamp. The lamp was turned on for 48 h, with an additional 15 min added to the reaction time to account for the warm-up time of the bulb. After the reaction, the lamp was turned off and the reactor was vented. Internal standard (HOAc) was added and the reaction mixture was stirred. An aliquot was then removed for centrifugation and the supernatant was used for ^{1}H NMR analysis. Nitromethane formation was verified by spiking a reaction mixture with a known standard. A representative ^{1}H NMR spectrum is shown below. Data are reported as averages of at least three experiments with standard deviations.

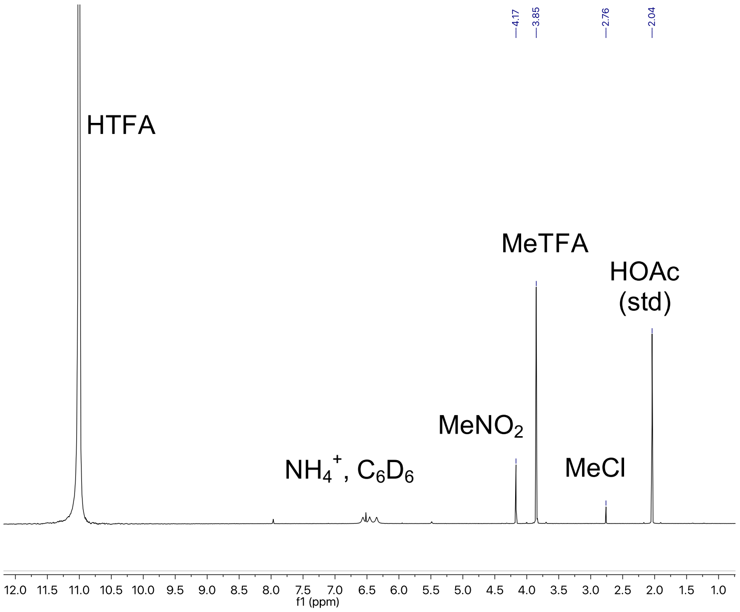

Figure 5.32. Representative ^{1}H NMR spectrum for photochemical methane functionalization with KCl/NH$_4$NO$_3$. Conditions: CH$_4$ (100 psi), KCl (0.1 mmol), NH$_4$NO$_3$ (1.1 mmol), HTFA (8 mL), 24 h of photolysis with the mercury arc lamp. Acetic acid (0.35 mmol) was added as an internal standard.

Photochemical Functionalization of Methane with MnO$_2$. A Fisher-Porter reactor was charged with a stir bar, KCl (if added, 0.1 mmol), MnO$_2$ (1.1 mmol), I$_2$ (if added, 0.1 mmol) and HTFA (8 mL) prior to being sealed and pressurized with the 100 psi of methane. The reactor was stirred on a stir plate inside a photolysis chamber with a mercury arc lamp. The lamp was turned on for 48 h, with an additional 15 min added to the reaction time to account for the warm-up time of the bulb. After the reaction, the lamp was turned off and the reactor was vented. Nitromethane was added as the internal standard and the reaction mixture was stirred. A 1 mL aliquot was then removed and added to a centrifugation tube with NaBiO$_3$ and shaken prior to centrifugation. The supernatant was used for ^{1}H NMR analysis. A representative ^{1}H NMR spectrum is shown below. Data are reported as averages of at least three experiments with standard deviations.

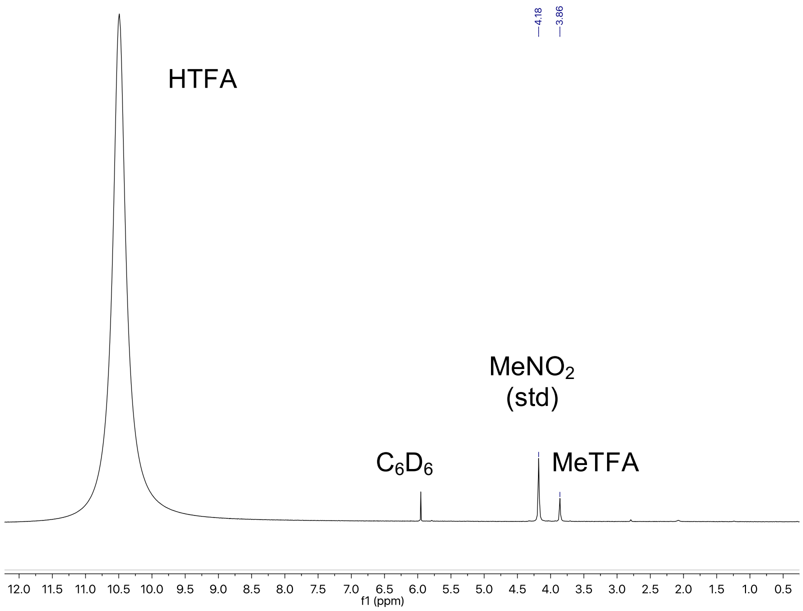

Figure 5.33. Representative ^{1}H NMR spectrum for photochemical methane functionalization with KCl/MnO$_2$. Conditions: CH$_4$ (100 psi), KCl (0.1 mmol), MnO$_2$ (1.1 mmol), HTFA (8 mL), 24 h of photolysis with the mercury arc lamp. Nitromethane (0.37 mmol) was added as an internal standard. 300 mg of NaBiO$_3$ was used for work-up.

Photochemical Functionalization of Methane with TBADT. A Fisher-Porter reactor was charged with a stir bar, KCl (if added, 0.67 mmol), TBADT (0.014 mmol), I$_2$ (if added, 0.1-0.3 mmol), K$_2$S$_2$O$_8$ (if added, 0.7 mmol) and acid (8 mL) prior to being sealed and pressurized with methane. If oxygen was used, the reaction mixture was purged with O$_2$ for 10 min prior to pressurizing with methane. The reactor was stirred on a stir plate inside a photolysis chamber with a mercury arc lamp. The lamp was turned on for the allotted reaction time, with an additional 15 min added to the reaction time to account for the warm-up time of the bulb. After the reaction, the lamp was turned off and the reactor was vented. When HTFA was used as the solvent, acetic acid was added as the internal standard and the reaction mixture was stirred. If acetic acid was used, nitromethane was added as the internal standard. A 1 mL aliquot was then removed for centrifugation. The supernatant was used for ^{1}H NMR analysis. A representative ^{1}H NMR spectrum is shown below. Data are reported as averages of at least three experiments with standard deviations.

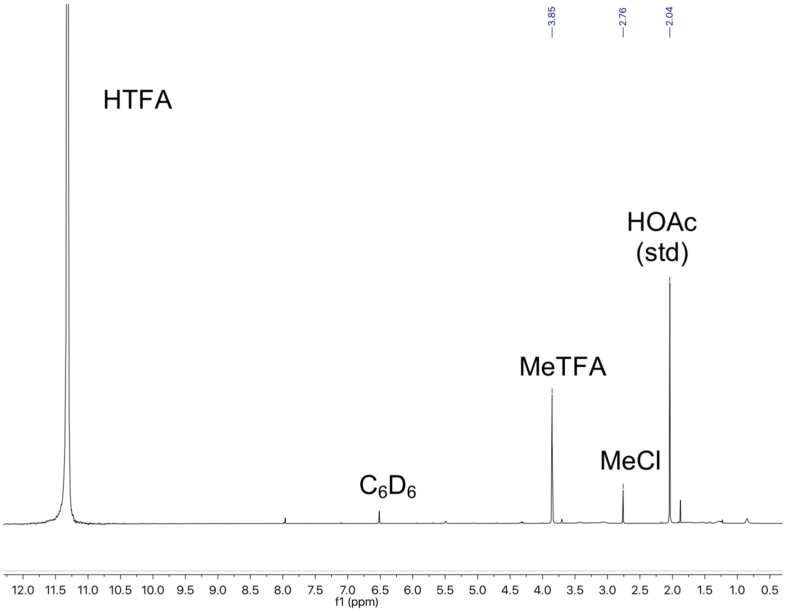

Figure 5.34. Representative ^{1}H NMR spectrum for photochemical methane functionalization with KCl/TBADT. Conditions: CH_4 (100 psi), KCl (0.67 mmol), TBADT (0.014 mmol), I_2 (0.05 mmol), HTFA (8 mL), 24 h of photolysis with the mercury arc lamp. Acetic acid (0.35 mmol) was added as an internal standard.

5.9 References

1. Kunkely, H.; Vogler, A. *Z. Naturforsch.* **2013,** *68b*, 891-894.

2. Hu, A.; Guo, J.-J.; Pan, H.; Zuo, Z. *Science* **2018,** *361* (6403), 668-672.

3. Ohkubo, K.; Hirose, K. *Angew. Chem. Int. Ed.* **2017,** *56*, 1-5.

4. Xie, J.; Jin, R.; Li, A.; Bi, Y.; Ruan, Q.; Deng, Y.; Zhang, Y.; Yao, S.; Sankar, G.; Ma, D.; Tang, J. *Nature Catalysis* **2018,** *1*, 889-896.

5. Fortman, G. C.; Boaz, N. C.; Munz, D.; Konnick, M. M.; Periana, R. A.; Groves, J. T.; Gunnoe, T. B. *J. Am. Chem. Soc.* **2014,** *136*, 8393-8401.

6. Kalman, S. E.; Munz, D.; Fortman, G. C.; Boaz, N. C.; Groves, J. T.; Gunnoe, T. B. *Dalton Trans.* **2015,** *44*, 5294-5298.

7. Dissociation Constants of Organic Acids and Bases. In *CRC Handbook of Chemistry and Physics*, 97th ed.; Haynes, W. M., Ed. Taylor & Francis Group: Boca Raton, FL, 2017; pp 88-97.

8. Conley, B. L.; Tenn, W. J.; Young, K. J. H.; Ganesh, S. K.; Meier, S. K.; Ziatdinov, V. R.; Mironov, O.; Oxgaard, J.; Gonzales, J.; Goddard, W. A.; Periana, R. A. *J. Mol Catal. A: Chem.* **2006,** *251* (1-2), 8-23.

9. Schwartz, N. A.; Boaz, N. C.; Kalman, S. E.; Zhuang, T.; Goldberg, J. M.; Fu, R.; Nielsen, R. J.; Goddard III, W. A.; Groves, J. T.; Gunnoe, T. B. *ACS Catal.* **2018,** *8*, 3138-3149.

10. Fu, R.; Nielsen, R. J.; Schwartz, N. A.; Goddard III, W. A.; Gunnoe, T. B.; Groves, J. T., DFT Mechanistic Study of Methane Monooxygenation by Hypervalent Iodine Alkane Oxidation (HIAO) Process. *Manuscript submitted* **2018**.

11. Ternay, A. L., Jr.; Deavenport, D.; Bledsoe, G. *J. Org. Chem.* **1974,** *39* (22), 3268-3271.

12. Hogan, T.; Sen, A. *J. Am. Chem. Soc.* **1997,** *119*, 2642-2646.

13. Kramer, G. M. *Tetrahedron* **1986,** *42* (4), 1071-1077.

14. Rudakov, E. S.; Volkova, L. K. *Russ. Chem. Bull.* **2008,** *57* (8), 1611-1626.

15. Adams, D. R.; Bailey, P. D.; Collier, I. D.; Leah, S. A. H.; Ridyard, C. *Chem. Commun.* **1996,** (3), 333-334.

16. Tanner, D. D.; Rowe, J. E. *J. Org. Chem.* **1986,** *51* (4), 457-460.

17. Böhme, H.; Schmitz, R. *Chem. Ber.* **1955,** *88* (3), 357-361.

18. Cech, F.; Linskeseder, M.; Zbiral, E. *Monatsh. Chem.* **1976,** *107* (6), 1429-1436.

19. Li, Z.; Pirasteh, A. *Int. J. Chem. Kinet.* **2006,** *38* (6), 386-398.

20. Aschmann, S. M.; Atkinson, R. *J. Chem. Kinet.* **1995,** *27* (6), 613-622.

21. Christie, M. I.; Roy, R. S.; Thrush, B. A. *Trans. Faraday Soc.* **1959,** *55* (7), 1149-1152.

22. Hess, W. W.; Huyser, E. S.; Kleinber, J. *J. Org. Chem.* **1964,** *29* (5), 1106-1109.

23. Kelly, C. C.; Yu, W. H. S.; Wijnen, M. H. J. *Can. J. Chem.* **1970,** *48* (4), 603-606.

24. Kelly, C. C.; Wijnen, M. H. J. *J. Phys. Chem.* **1969,** *73* (7), 2447-2448.

25. Chen, W.; Kocal, J. A.; Brandvold, T. A.; Bricker, M. L.; Bare, S. R.; Broach, R. W.; Greenlay, N.; Popp, K.; Walenga, J. T.; Yang, S. S.; Low, J. J. *Catal. Today* **2009,** *140*, 157-161.

26. Maldotti, A.; Molinari, A.; Amadelli, R. *Chem. Rev.* **2002,** *102*, 3811-3836.

27. Tzirakis, M. D.; Lykakis, I. N.; Orfanopoulos, M. *Chem. Soc. Rev.* **2009,** *38* (2609-2621).

28. Angioni, S.; Ravelli, D.; Emma, D.; Dondi, D.; Fagnoni, M.; Albini, A. *Adv. Synth. Catal.* **2008,** *350*, 2209-2214.

29. Yamase, T.; Takabayashi, N.; Kaji, M. *J. Chem. Soc., Dalton Trans.* **1984,** *0*, 793-799.

30. Hill, C. L. *Synlett* **1995**, 127-132.

31. Laudadio, G.; Govaerts, S.; Wang, Y.; Ravelli, D.; Koolman, H. F.; Fagnoni, M.; Djuric, S. W.; Noël, T. *Angew. Chem. Int. Ed.* **2018,** *57*, 4078-4082.

32. Giannotti, C.; Richter, C. *Int. J. Photoenergy* **1999,** *1* (2), 69-73.

33. Wu, W.; Fu, Z.; Tang, S.; Zou, S.; Wen, X.; Meng, Y.; Sun, S.; Deng, J.; Liu, Y.; Yin, D. *Appl. Catal. B* **2015,** *164*, 113-119.

34. Ermolenko, L. P.; Giannotti, C. *J. Chem. Soc., Perkin Trans. 2* **1996,** *0*, 1205-1210.

35. Zheng, Z.; Hill, C. L. *Chem. Commun.* **1998,** *0*, 2467-2468.

36. Tanielian, C. *Coord. Chem. Rev.* **1998,** *178-180*, 1165-1181.

37. De Waele, V.; Poizat, O.; Fagnoni, M.; Bagno, A.; Ravelli, D. *ACS Catal.* **2016,** *6*, 7174-7182.

38. Ravelli, D.; Fagnoni, M.; Fukuyama, T.; Nishikawa, T.; Ryu, I. *ACS Catal.* **2018,** *8*, 701-713.

39. Ravelli, D.; Protti, S.; Fagnoni, M. *Acc. Chem. Res.* **2016,** *49*, 2232-2242.

40. Nomiya, K.; Sugie, Y.; Miyazaki, T.; Miwa, M. *Polyhedron* **1986,** *5* (7), 1267-1271.

41. Fornal, E.; Giannotti, C. *Photochem. Photobiol., A* **2007,** *188*, 279-286.

42. Shi, D.; He, C.; Sun, W.; Ming, Z.; Meng, C.; Duan, C. *Chem. Commun.* **2016,** *52*, 4714-4717.

43. Carraro, M.; Gardan, M.; Scorrano, G.; Drioli, E.; Fontananova, E.; Bonchio, M. *Chem. Commun.* **2006**, 4533-4535.

44. Bonchio, M.; Carraro, M.; Scorrano, G.; Fontananova, E.; Drioli, E. *Adv. Synth. Catal.* **2003,** *345*, 1119-1126.

45. Tzirakis, M. D.; Lykakis, I. N.; Panagiotou, G. D.; Bourikas, K.; Lycourghiotis, A.; Kordulis, C.; Orfanopoulos, M. *J. Catal.* **2007,** *252*, 178-189.

46. Zou, Y.; Ding, H.; Feng, S. *Chem. Mater.* **2001,** *13*, 4058-4064.

47. Haga, M.; Dodsworth, E. S.; Eryavec, G.; Seymour, P.; Lever, A. B. P. *Inorg. Chem.* **1985,** *24* (12), 1901-1906.

48. Lowry, M. S.; Goldsmith, J. I.; Slinker, J. D.; Rohl, R.; Pascal, R. A.; Malliaras, G. G.; Bernhard, S. *Chem. Mater.* **2005,** *17* (23), 5712-5719.

49. Protti, S.; Ravelli, D.; Fagnoni, M.; Albini, A. *Chem. Commun.* **2009,** (47), 751-753.

6 Oxidative Alkenylation of Toluene with 1-Pentene

6.1 Introduction to Olefin Hydroarylation and Arene Alkenylation

6.1.1 Current Industrial Methods for Alkyl and Alkenyl Arene Production

Alkyl and alkenyl arenes are widely used in the production of plastics, elastomers and detergents.[1-4] For example, 25 million metric tons of styrene, the monomeric building block of the common plastic polystyrene, were produced globally in 2010.[5] In industry, alkyl arenes have historically been produced using Friedel-Crafts alkylation catalysis with Lewis and Brønsted acids, and conversion of alkyl arenes to alkenyl arenes (such as ethylbenzene to styrene) requires dehydrogenation at high temperatures (≥ 550 °C) using metal oxide catalysts (Scheme 6.1).[1] High reaction temperatures are often required (~400 °C) for the alkylation reaction, and recycling the catalyst is often not possible as it is neutralized following the reaction, which results in the production of stoichiometric amounts of halogenated waste.[1, 6] Friedel-Crafts catalysis also suffers from low selectivity for mono-functionalized products as alkylated arenes are activated toward further reaction, which results in the generation of poly-functionalized products.[1] As a result, a transalkylation step is required to optimize the yield of the mono-functionalized product (Scheme 6.1). Zeolite catalysts (*i.e.*, porous crystalline aluminosilicates) can also be used to produce alkyl arenes.[2] Although zeolites offer substantial advantages compared to traditional Friedel-Crafts catalysts, arene alkylation by zeolites also operates by an acid-based mechanism. Thus, many of the features of Friedel-Crafts catalysis are present when using zeolite catalysts.

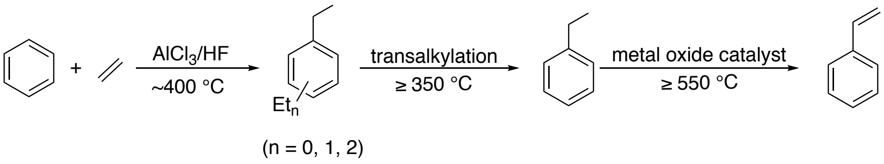

Scheme 6.1. Friedel-Crafts alkylation of benzene to yield ethylbenzene, and subsequent dehydrogenation to produce styrene.[7]

The acid-based mechanism for arene alkylation has significant drawbacks. Electron-deficient arenes are unreactive or react slowly under acid-based arene alkylation conditions.[8] Additionally, because the acid-based mechanism involves a carbocation intermediate, 1-aryl alkanes cannot be produced from simple α-olefins such as propylene, and 1-pentene (*e.g.*, cumene is produced exclusively from benzene and propylene, Scheme 6.2).[9] Thus, Friedel-Crafts or zeolite-based arene alkylation using hydrocarbons is always selective for Markovnikov products. For benzene alkylation using long-chain α-olefins, not only are 2-aryl alkanes produced but also other internal alkanes, n-aryl alkanes (where n > 2), are produced. Table 6.1 shows additional examples where acid-based catalysis with $AlCl_3$ results in the selective formation of the branched alkyl arene product(s). Additionally, Friedel-Crafts catalysis often results in polyalkylation as the alkyl arene is activated toward further alkylation. As a result, for the large-scale synthesis of alkyl arenes transalkylation processes are often required to maximize the yield of mono-functionalized product (Scheme 6.1). Another disadvantage of acid-based catalysis is its regioselectivity. As it is an electrophilic aromatic substitution reaction, regioselectivity is dictated by activating or deactivating substituents on the aromatic ring. In effect, this limits the scope of products that can be generated using this method, as for example, the generation of *para*-alkylated nitroarenes would not be feasible using acid-based catalysis.

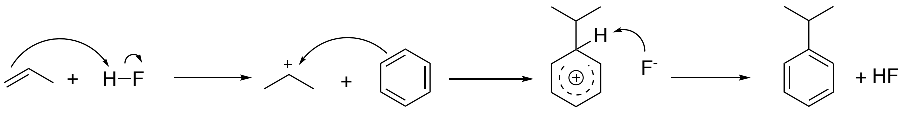

Scheme 6.2. Acid-based mechanism of Friedel-Crafts alkylation for benzene with propylene results in the production of cumene (branched Markovnikov product). *n*-Propylbenzene (linear anti-Markovnikov product) is not generated due to the instability of the intermediate primary carbocation.

Table 6.1. Selected examples of acid-based alkylation with AlCl$_3$.[a] Adapted from reference.[10]

Arene	α-Olefin	*o:m:p*	L:B	Product(s)
Benzene[a]	Propylene	n/a	100% branched	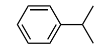
Benzene[b]	Isobutylene	n/a	100% branched	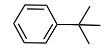
Benzene[c]	1-Hexene	n/a	100% branched	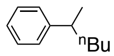
Toluene[d]	Propylene	3:1:2.6	> 98% branched	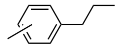
				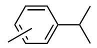

[a,c]Data and conditions are from reference.[9] [b]Data and conditions are from reference.[11] [d]Data and conditions are from reference.[12]

6.1.2 Transition Metal-Catalyzed Olefin Hydroarylation and Oxidative Alkenylation

Transition metal-catalyzed olefin hydroarylation and oxidative arene alkenylation offer potential advantages over traditional acid-mediated alkylation catalysis for the production of alkyl arenes and alkenyl arenes, respectively.[13-14] The transition metal catalyzed processes often operate by a different and non-acid based pathway. A general and commonly proposed catalytic cycle for olefin hydroarylation as well as a related cycle for oxidative olefin hydroarylation are shown in Scheme 6.3. For olefin hydroarylation (Scheme 6.3, blue), ethylene can coordinate to a metal-aryl complex (a phenyl ligand is depicted in Scheme 6.3) and then insert into the metal-phenyl bond to generate a phenethyl intermediate. Upon benzene coordination and C–H activation, the alkyl arene product is released to regenerate the starting metal-aryl complex. In oxidative arene alkenylation

(Scheme 6.3, red), the metal-phenethyl intermediate undergoes *β*-hydride elimination to generate a hydride complex with coordinated styrene (Scheme 6.3). Dissociation of the aryl olefin (styrene in Scheme 6.3) and reaction of the M–H with an oxidation can regenerate the catalyst.

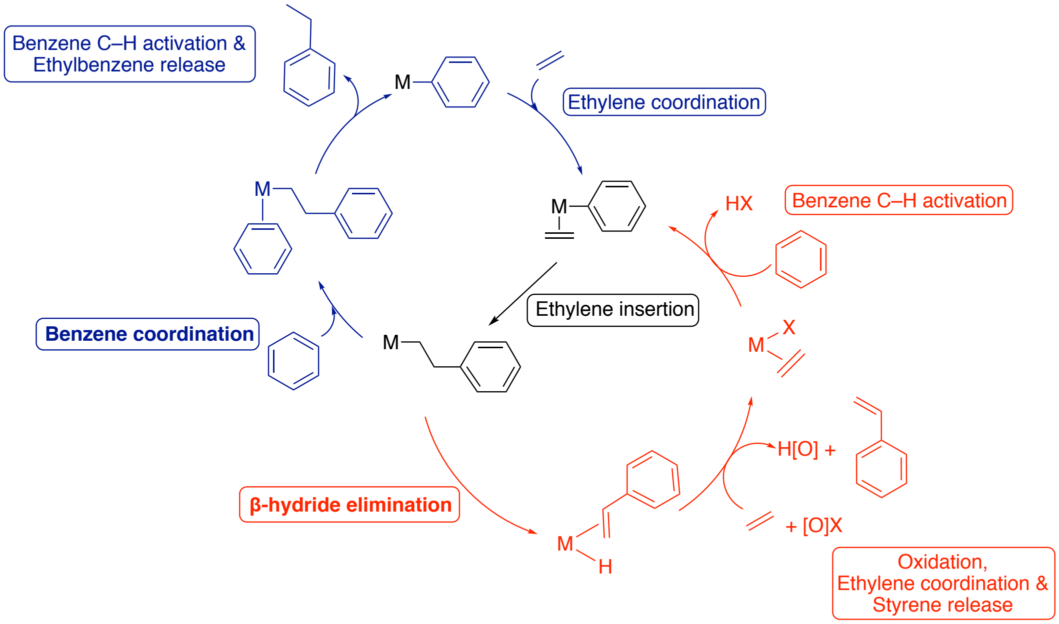

Scheme 6.3. Frequently invoked catalytic cycles for transition metal catalyzed hydrophenylation of ethylene (blue) and oxidative arene alkenylation (red). Steps involved in both catalytic cycles are in black. [O] = oxidant; M = metal complex; X = conjugate base of HX.

Because these processes operate via olefin insertion into metal-aryl bonds, the production of linear products (*i.e.*, 1-aryl alkanes or 1-aryl alkenes) from *α*-olefins is possible. However, prior to the Gunnoe group's recent rhodium-based catalysts,[7, 10, 15] highly selective generation of linear products using hydrocarbon substrates had not been reported. Olefin hydroarylation and oxidative arene alkenylation have been extensively studied by our group using ruthenium-,[14, 16-24] platinum-[25-30] and rhodium-based catalysts.[7, 10, 15, 31] Examples that are most directly related to the results described in this Chapter are discussed below.

6.1.3 Use of Rh-Based Catalysts for Arene Alkenylation

The Gunnoe group reported the use of Pt(II) catalysts for the production of styrene, but turnovers were limited as the catalysts decomposed to inactive Pt(0) after formation of ~1 TO of styrene.[26-29] It was speculated, based on kinetic studies, that the generation of Pt(II)-hydride intermediates provide a kinetically accessible pathway for bimolecular (*i.e.*, reaction of two Pt complexes) reduction to form elemental Pt. In an effort to improve the longevity of catalysis, Rh(I) catalyst precursors were studied. Some data suggest that reduction to Rh(0) is less thermodynamically favorable than reduction of Pt(II) to Pt(0).[7] In our initial efforts, (^{Fl}DAB)Rh(TFA)(η^2-C_2H_4) (^{Fl}DAB = *N*,*N'*-bis(pentafluorophenyl)-2,3-dimethyl-1,4-diaza-1,3-butadiene) was used as a catalyst precursor for arene alkenylation with CuX_2 {X = acetate (OAc), trifluoroacetate (TFA), pivalate (OPiv) and 2-ethyl hexanoate (OHex)} as *in situ* oxidant.[7] Yields discussed in previous reports and herein are often based on the CuX_2 oxidant, which is typically the limiting reagent (with the exception of reactions where *in situ* regeneration of Cu(II) with air or O_2 is possible). The generation of one equivalent of styrene requires the reduction of two equivalents of CuX_2,

(^{Fl}DAB)Rh(TFA)(η^2-C_2H_4) converts benzene, ethylene and CuX_2 oxidants to styrene, CuX and HX with optimized yields of ≥ 95% (based on the limiting reagent CuX_2) with nearly 100% selectivity for styrene.[7] Catalyst longevity up to 96 h was observed with > 800 turnovers (TO) of styrene observed under optimized conditions (Scheme 6.4).[7]

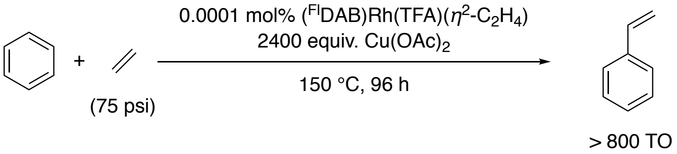

Scheme 6.4. Oxidative ethylene hydrophenylation with (^{Fl}DAB)Rh(TFA)(η^2-C_2H_4) (^{Fl}DAB = *N*,*N*'-bis(pentafluorophenyl)-2,3-dimethyl-1,4-diaza-1,3-butadiene; TFA = trifluoroacetate) as a catalyst precursor. Conditions: Benzene (10 mL), ethylene (75 psi), 0.0001 mol% (^{Fl}DAB)Rh(TFA)(η^2-C_2H_4) relative to benzene, 2400 equiv. $Cu(OAc)_2$ (relative to Rh), 150 °C, 96 h. The reaction was run in duplicate which yielded 817 and 852 TO of styrene.[7] The theoretical yield was 1200 TO.

The Gunnoe group extended this Rh-based catalysis to α-olefins in efforts to study the linear:branched selectivity.[32] The nomenclature of alkyl/alkenyl arenes in industry can be misleading, where linear alkyl or alkenyl arenes are mixtures comprised primarily of 2-aryl alkanes or alkenes with linear (i.e., unbranched) alkane or alkene chains. As discussed above, acid-catalyzed processes do not generate 1-aryl alkanes or alkenes.[33] Thus, we differentiate between linear alkyl arenes with n-aryl alkanes (n > 1) and 1-aryl alkanes or alkenes by denoting the latter as "super" linear alkyl or alkenyl arenes (or SLABs).

Whereas acid-catalyzed arene alkylation always favors the production of branched products (*i.e.*, n-aryl alkanes where n > 1; *e.g.*, always > 98% branched),[9, 11-12] with [Rh(η^2-C_2H_4)$_2$(μ-OAc)]$_2$, linear products are favored regardless of the arene or α-olefin (Table 6.2). In this study, the lowest observed linear:branched (L:B) ratio when using [Rh(μ-OAc)(η^2-C_2H_4)$_2$]$_2$ with $Cu(OAc)_2$ as the oxidant was ~8:1. Further, the products of rhodium catalysis favored *meta*- and *para*-substituted alkenyl arenes, likely as a result of steric effects, whereas $AlCl_3$-catalyzed reactions favored the production of *ortho*- and *para*-substituted alkenyl arenes as predicted by the activation of those positions toward electrophilic aromatic substitution.

Table 6.2. Selected examples of arene alkenylation using $[Rh(\eta^2\text{-}C_2H_4)_2(\mu\text{-}OAc)]_2$ and $Cu(OAc)_2$ versus traditional alkylation with $AlCl_3$. Adapted from reference.[10]

Catalyst	Arene	α-Olefin	*o:m:p*	L:B	TON	Products
$AlCl_3$[b]	Benzene	Propylene	n/a	100% branched	95	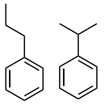
$[Rh(\mu\text{-}OAc)(\eta^2\text{-}C_2H_4)_2]_2$	Benzene	Propylene	n/a	8:1	80(4)	
$AlCl_3$[c]	Benzene	Isobutylene	n/a	100% branched	NR	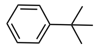
$[Rh(\mu\text{-}OAc)(\eta^2\text{-}C_2H_4)_2]_2$	Benzene	Isobutylene[e]	n/a	100% linear	100(2)	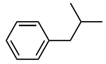
$AlCl_3$[d]	Toluene	Propylene	3:1:2.6	> 98% branched	NR	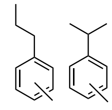
$[Rh(\mu\text{-}OAc)(\eta^2\text{-}C_2H_4)_2]_2$	Toluene	Propylene	1:8.9:9.3	9.4:1	86(17)	

[a]L:B ratios with $[Rh(\eta^2\text{-}C_2H_4)_2(\mu\text{-}OAc)]_2$ were determined after hydrogenation of the unsaturated products. NR = not reported. Conditions using $[Rh(\eta^2\text{-}C_2H_4)_2(\mu\text{-}OAc)]_2$: 0.01 mol% $[Rh(\eta^2\text{-}C_2H_4)_2(\mu\text{-}OAc)]_2$ relative to arene, 25 psi gaseous olefin or 2000 equiv. of olefin, 150 °C, 48 h, 240 equiv. $Cu(OAc)_2$ relative to $[Rh(\eta^2\text{-}C_2H_4)_2(\mu\text{-}OAc)]_2$. Hydrogenation was performed using 5% Pt/C under hydrogen atmosphere. [b]Data and conditions from reference.[9] [c]Data and conditions from reference.[11] [d]Data and conditions from reference.[12] [e]72 h.

6.2 Introduction to Polyethylene Naphthalate (PEN)

Polyethylene naphthalate (PEN), a polyester similar to polyethylene terephthalate (PET), has naphthyl rings rather than the phenyl rings of PET (Scheme 6.5).[34] Although PET has many commercial applications, as discussed in Chapter 3, PEN offers potential advantages over PET. PEN has a more rigid structure, resulting in greater dimensional stability.[35] Further, PEN exhibits better resistance to heat and has a higher barrier to gas permeability.[34, 36] As a result, the PEN polymer is likely better for storing substances prone to oxidation, especially in the food sector.

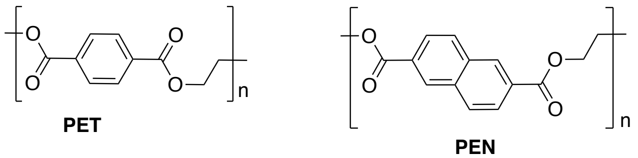

Scheme 6.5. Structures of polyethylene terephthalate (PET) and polyethylene naphthalate (PEN).

PEN is produced through the polymerization of ethylene glycol with naphthalate monomer, typically either 2,6-naphthalenedicarboxylic acid or the methyl ester derivative.[34] 2,6-Naphthalenedicarboxylic acid is produced from the oxidation of 2,6-dimethylnaphthalene (2,6-DMN). The primary method for 2,6-DMN synthesis requires harsh reaction conditions (*i.e.*, use of potassium metal and anhydrous HF) and requires multiple steps (Scheme 6.6).[35, 37] Hence, the expense of 2,6-DMN is a major inhibition for economic synthesis of PEN. Consequently, the production of PEN has been limited in spite of its advantages over the current polyester market leader PET.[34]

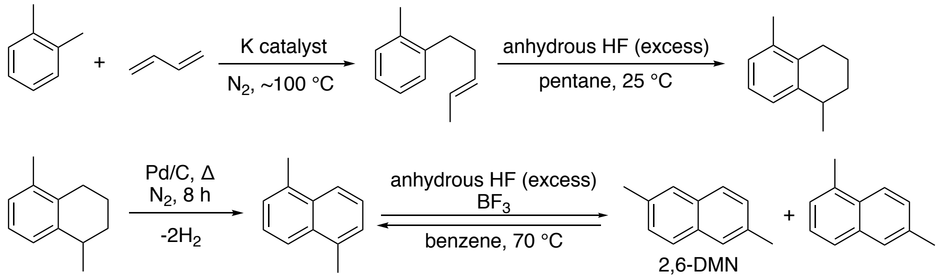

Scheme 6.6. Overview of the industrial route for the synthesis of 2,6-dimethylnaphthalene from *o*-xylene and butadiene. K catalyst = calcined CaO stirred with potassium metal at 150 °C. Adapted from references.[35,37-38]

Because of the aforementioned synthetic challenges, the development of a more economical route for the synthesis of 2,6-DMN is desirable. As there are existing technologies capable of converting *n*- and 2-pentenyltoluenes to 2,6-DMN,[39-41] efficient production of these pentenyltoluenes could provide an alternative to current processes for 2,6-DMN production. [42-43] The selectivity of such a process for *n*-pentenyltoluenes and 2-pentyltoluenes is critical as 3-pentenyltoluenes cannot be ring-closed to give 2,6-DMN. Further, the ring-closure to form 2,6-DMN is more efficient with *n*-pentyltoluenes than 2-pentyltoluenes.

The Gunnoe group's Rh-based catalysis has demonstrated the capability to convert arenes and α-olefins to alkenyl arenes with high L:B ratios.[10, 15] Thus, we speculated that our oxidative arene alkenylation chemistry is well-suited to enable production of *n*- and 2-pentenyltoluenes, favoring the *n*-pentyltoluenes, which can be most readily ring-closed, from 1-pentene and toluene (Scheme 6.7). Importantly, toluene is an inexpensive arene and 1-pentene is a byproduct of Fischer-Tropsch reduction of CO. Thus, we proposed that our Rh-based catalysis would offer advantages in selectivity over acid-based catalysis, which favors the formation of the 2- and 3-pentyltoluenes and does not produce the most highly desired *n*-pentyltoluenes (Scheme 6.8). This Chapter details studies of the oxidative alkenylation of toluene with 1-pentene as the α-olefin to produce pentenyltoluenes (Scheme 6.7).

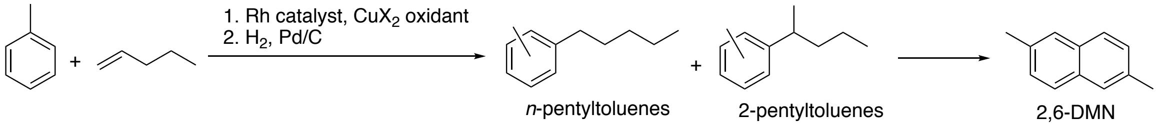

Scheme 6.7. Envisioned process for a possible route to 2,6-DMN from toluene and 1-pentene using a Rh catalyst with a CuX$_2$ oxidant. A hydrogenation step is included for clarity (*vide infra*).

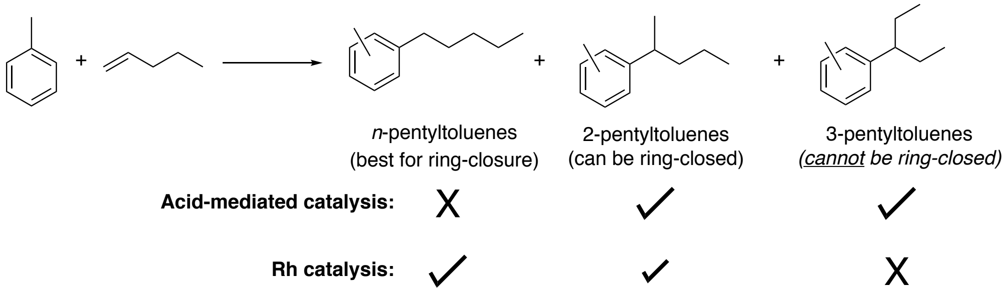

Scheme 6.8. Comparison of pentyltoluene products from acid- and Rh-based functionalization and implications for 2,6-DMN production. Products from Rh catalysis are shown following a hydrogenation step for clarity. *n*-Pentyltoluenes cannot be produced by acid-based catalysis. *M*-, *p*- and *o*-isomers are not shown as 2,6-DMN can be produced from isomerization of other DMNs. The checkmark for 2-pentyltoluene for Rh catalysis is smaller to indicate the greater selectivity for the linear product.

6.3 Oxidative Alkenylation of Toluene with 1-Pentene

6.3.1 Introduction

The report using $[Rh(\eta^2\text{-}C_2H_4)_2(\mu\text{-}OAc)]_2$ as a catalyst for arene alkenylation examined the conversion of toluene and propylene and the conversion of benzene and 1-pentene.[10] However, toluene and 1-pentene were not combined in this study due to the complexity of the resulting product mixture. The conversion of toluene and propylene to propenyltoluenes was studied, and the selectivity for L:B products was 9.4:1 (Table 6.1).[10] The conversion of benzene with 1-pentene to pentenylbenzenes was also examined, giving an 8:1 ratio of *n*-pentylbenzene:2-pentylbenzene after hydrogenation (Table 6.1).[10] These results demonstrated that toluene and 1-pentene could serve as substrates for oxidative olefin hydroarylation and indicated that high L:B ratios were likely possible using the rhodium salt $[Rh(\eta^2\text{-}C_2H_4)_2(\mu\text{-}OAc)]_2$ as a catalyst precursor and $Cu(OPiv)_2$ as an oxidant. Michael Webster-Gardiner performed preliminary experiments examining the use of rhodium catalysts for the alkenylation of toluene with 1-pentene to generate pentenyltoluenes. Bill Schinksi (retired, Chevron) served as an additional advisor for this work.

6.3.1 Results and Discussion

The oxidative arene alkenylation of toluene with 1-pentene using $Cu(OPiv)_2$ as the oxidant could result in the production of multiple possible byproducts in addition to the desired *n*- and 2-pentenyltoluenes and undesired 3-pentenyltoluenes. Such possible byproducts include C_{10} species resulting from olefin coupling, biaryl products resulting from toluene coupling, pentenyl pivalates and products resulting from the hydroarylation of any of the aforementioned products and byproducts. As *E*- and *Z*-isomers of each of the alkenyl products could be produced, the resultant product mixture is complicated. Further, *m*-, *p*- and *o*- products could be generated for each product incorporating a substituted toluene (*i.e.*, pentenyltoluenes). Separation and quantification of these products is challenging. But, hydrogenation of the product mixture allows for a simplified analysis as it avoids the complications resulting from geometric isomers (*i.e.*, both *E*- and *Z*-products funnel to the same alkyl derivative).

In agreement with the previous study that used $[Rh(\eta^2\text{-}C_2H_4)_2(\mu\text{-}OAc)]_2$ as an arene alkenylation pre-catalyst, toluene and 1-pentene are converted to pentenyltoluenes using 0.01 mol% Rh with varying concentrations of 1-pentene and Cu(II) oxidant in neat toluene at 150 °C. To simplify analysis, the reaction mixtures were hydrogenated using H_2 and Pd/C. High L:B (*i.e.*, *n*-pentyltoluene:2-pentyltoluene) ratios were observed, and production of 3-pentyltoluenes is not observed under any of the studied reaction conditions indicating that isomerization of 1-pentene is slow under the reaction conditions. Typically, L:B ratios of > 5:1 are observed, with higher ratios of ~12:1 observed under certain conditions (Table 6.2). In order to optimize catalysis, a variety of reaction conditions have been examined. For each experiment in this Chapter, the mol% Rh is relative to toluene and the equivalents of 1-pentene and Cu(II) oxidant are relative to Rh.

The effect of varying the 1-pentene concentration has been examined using 0.01 mol% of $[Rh(\eta^2\text{-}C_2H_4)_2(\mu\text{-}OAc)]_2$ and 240 eq. of $Cu(OPiv)_2$ at 150 °C (Table 6.2). The L:B ratios increase with increasing 1-pentene concentration. The highest L:B ratio of 12(1):1 was obtained using 2000 eq. of 1-pentene (relative to Rh), a marked increase from the 5.59(9):1 obtained using 250 eq. of 1-pentene. Higher concentrations of olefin might facilitate more rapid dissociation of pentenyltoluenes and reduce the extent of isomerization to generate the branched products. However, the total yield of pentyltoluenes remained similar under all studied conditions, ~65% based on $Cu(OPiv)_2$ as the limiting reagent (Table 6.2). Under all conditions, the production of *meta*- and *para*-pentyltoluenes in agreement with the previous study using $[Rh(\eta^2\text{-}C_2H_4)_2(\mu\text{-}OAc)]_2$ providing evidence against an acid-catalyzed mechanism.[10] Under each set of conditions, *meta*, *para* and *ortho* products account for ~62-70%, ~30-35% and < 2% of the total, respectively.

Table 6.3. Effect of 1-pentene loading on pentyltoluene and decane production.[a]

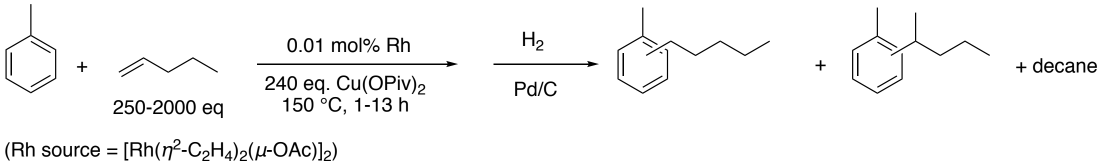

Eq. 1-Pentene	L:B	% Yield Pentyltoluenes	Eq. Decane Produced
250	5.5(9):1	60(4)%	ND
500	7.5(8):1	73(5)%	2.6(7)
1000	9.3(9):1	64(4)%	7.81(5)
2000	12(1):1	47(4)%	18(1)*

[a]% Yield represents the total % yield of pentyltoluenes based on the amount of the copper oxidant. Averages and standard deviations are based on three experiments. *Decane was not fully hydrogenated in one of the three trials, thus data for decane formation are from two experiments.

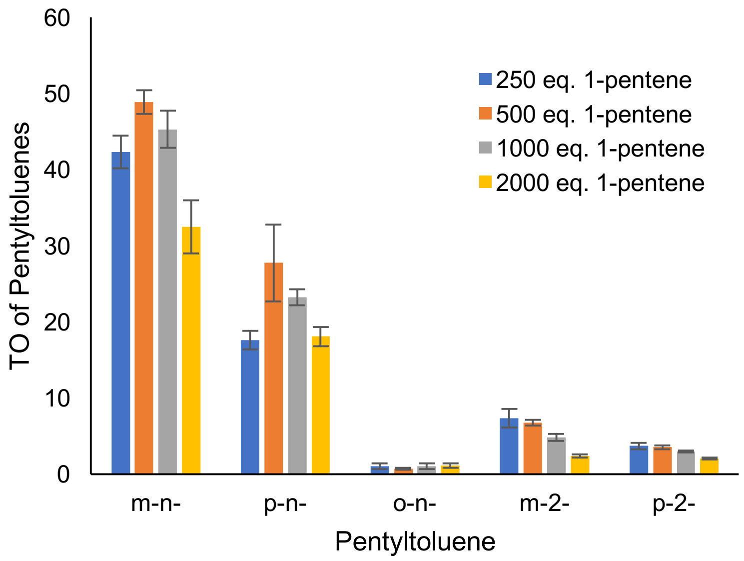

Figure 6.1. Pentyltoluene product distribution as a function of 1-pentene loading. Error bars denote standard deviations based on three experiments.

The yield of pentyltoluenes is potentially limited by the decomposition of the Rh catalyst under reaction conditions and the generation of undesired byproducts. For example, pentyl pivalate and C_{10} products have been detected by GC-MS. At high 1-pentene concentrations (> 500 eq. relative to Rh), C_{10} species are generated (Tables 6.2 and 6.3). Upon hydrogenation, the various C_{10} products are converted to *n*-decane, and at higher olefin concentrations, 4-methylnonane has also been detected by GC-MS. As 1-pentene is a relatively costly reactant and the formation of byproducts is undesirable, we sought to minimize olefin coupling. Thus, there is a balance between achieving the highest L:B ratio possible while minimizing the formation of undesired C_{10} products. As such, the 1-pentene loadings in studies discussed herein use either 500 eq. or 1000 eq. of the olefin.

Subsequent experiments examined the effect of varying the copper(II) amount. The L:B ratios are high, ~10:1, and statistically identical using between 120 and 360 eq. of $Cu(OPiv)_2$ (Table 6.3). The overall yield of pentyltoluene products is also statistically identical for each of the three conditions (Table 6.3), indicating that product formation increases proportionally with increased amount of Cu(OPiv)$_2$. There is a slight increase in the formation of C$_{10}$ products with the highest Cu(OPiv)$_2$ amount. The formation of decane (on hydrogenation) is likely Rh-catalyzed. Decane was not observed in control reactions performed in the absence of [Rh(η^2-C$_2$H$_4$)$_2$(μ-OAc)]$_2$. As in the olefin optimization study, the formation of *meta*- and *para*-pentyltoluenes is favored (Figure 6.2).

Table 6.4. Effect of copper(II) oxidant concentration on pentyltoluene and decane production.[a]

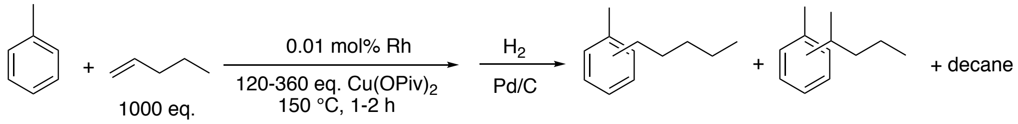

(Rh source = [Rh(η^2-C$_2$H$_4$)$_2$(μ-OAc)]$_2$)

Eq. Cu(OPiv)$_2$	L:B	% Yield Pentyltoluenes	Eq. Decane Produced
120	11(2):1	64(5)%	6.6(6)
240	9.3(9):1	64(4)%	7.81(5)
360	11(1):1	65(3)%	13(2)

[a] % Yield represents the total % yield of pentyltoluenes based on the amount of the copper oxidant. Averages and standard deviations are based on three experiments.

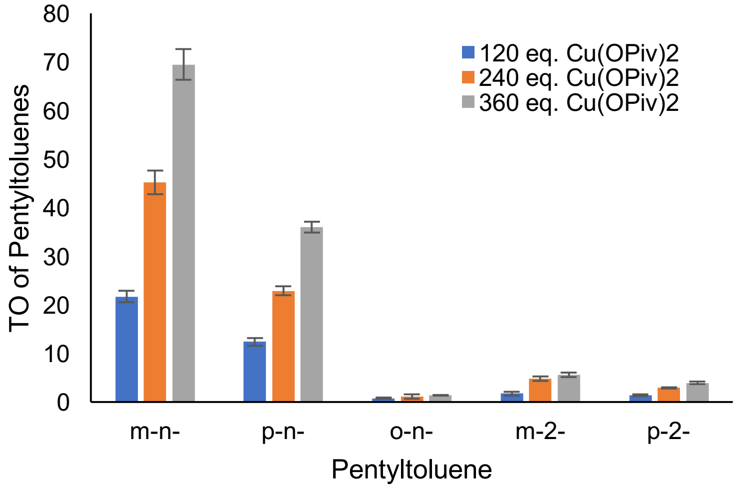

Figure 6.2. Pentyltoluene product distribution as a function of Cu(OPiv)$_2$ loading. Error bars denote standard deviations based on three experiments.

To determine if using another soluble copper(II) oxidant would result in an improved L:B ratio or pentyltoluene yield, $Cu(OHex)_2$ and $Cu(Ole)_2$ (OHex = 2-ethylhexanoate, Ole = oleate) were tested under identical reaction conditions. Although the pentyltoluene yields are statistically identical and the amounts of decane produced are similar for $Cu(OPiv)_2$ and $Cu(OHex)_2$, the yield of pentyltoluenes is significantly lower with $Cu(Ole)_2$. The L:B ratio varies based on the oxidant, from 11(1) with $Cu(Ole)_2$ to 9.3(9):1 with $Cu(OPiv)_2$ to 5.8(4):1 with $Cu(OHex)_2$ (Table 6.4). The reason for these changes is unknown, but $Cu(OPiv)_2$ was used as the oxidant for additional studies given its ability to obtain a high L:B ratio and yield of pentyltoluenes. The formation of *meta*- and *para*-pentyltoluenes is favored regardless of the copper(II) oxidant (Figure 6.3).

Table 6.5. Effect of oxidant identity on pentyltoluene and decane production.[a]

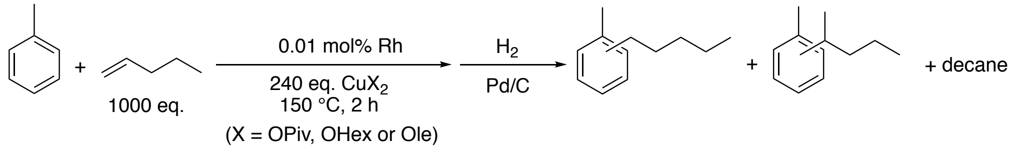

(Rh source = $[Rh(\eta^2\text{-}C_2H_4)_2(\mu\text{-}OAc)]_2$)

Cu(II) Oxidant	L:B	% Yield Pentyltoluenes	Eq. Decane Produced
$Cu(OPiv)_2$	9.3(9):1	64(4)%	7.81(5)
$Cu(OHex)_2$	5.8(4):1	70(4)%	11(1)
$Cu(Ole)_2$	11(1):1	17(1)%	3.3(2)

[a]% Yield represents the total % yield of pentyltoluenes based on the amount of the copper oxidant. Averages and standard deviations are based on three experiments.

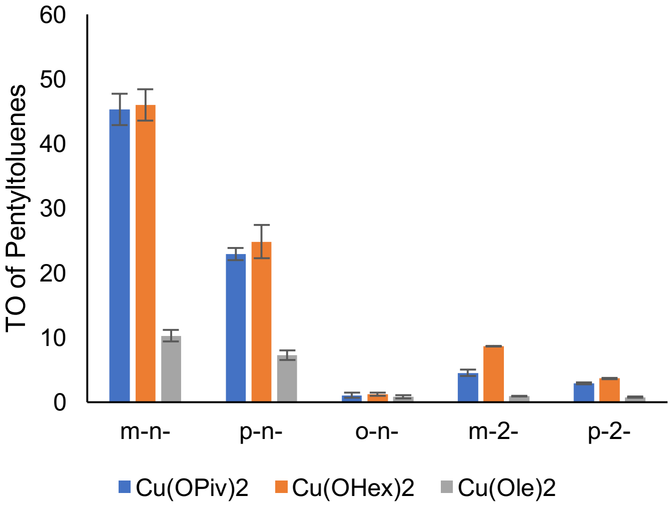

Figure 6.3. Pentyltoluene product distribution as a function of CuX_2 (X = OPiv, OHex, Ole) oxidant identity. Error bars denote standard deviations based on three experiments.

The effect of varying the reaction temperature was also examined. For each temperature from 120-180 °C, the L:B ratio is high (Table 6.5). The large deviations are possibly due to poor signal-to-noise for the branched products. However, as the trial with the larger amount of 2-pentyltoluenes also had a higher overall yield, the L:B for that trial was ~7:1, indicating that it was still highly selective for the production of *n*-pentyltoluene. Yields of pentyltoluenes are similar across this temperatures, with the highest yield 64(5)% obtained at 150 °C. Decane formation is statistically identical for all three reaction temperatures (Table 6.4). As demonstrated previously, the formation of *meta*- and *para*-pentyltoluenes is favored at each temperature (Figure 6.4).

Table 6.6. Effect of reaction temperature on pentyltoluene and decane production.[a]

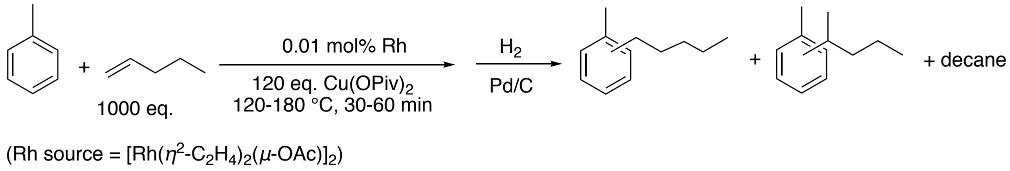

Temperature (°C)	L:B	% Yield Pentyltoluenes	Eq. Decane Produced
120	13(9):1	52(8)%	6(1)
150	11(2):1	64(5)%	6.6(6)
180	17(5):1	47.7(7)%	5.9(9)

[a] % Yield represents the total % yield of pentyltoluenes based on the amount of the copper oxidant. Averages and standard deviations are based on three experiments.

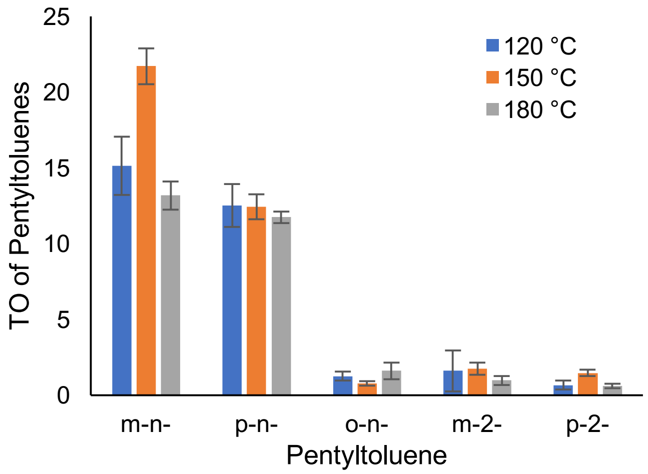

Figure 6.4. Pentyltoluene product distribution as a function of reaction temperature. Error bars denote standard deviations based on three experiments.

The concentration of the rhodium catalyst in the aforementioned experiments and in the initial report discussing the use of [Rh(η^2-C$_2$H$_4$)$_2$(μ-OAc)]$_2$ is 0.01 mol% relative to arene.[10] As rhodium is expensive, it would be preferable to use a lower concentration. Using the lower concentration of 0.001 mol% Rh, the L:B ratio improves from 7.5(8):1 when 0.01 mol% is used to 10(1):1 (Table 6.6). The formation of C$_{10}$ products is effectively reduced when using the lower Rh concentration, but their formation is minimal, < 3 equivalents, under these reaction conditions with 0.01 mol% Rh. The percent yield of pentyltoluenes is much lower when using the lower Rh concentration, decreasing from 73(5)% to 44(2)% (Table 6.6). While the L:B ratio improves with the lower Rh concentration, the significant decrease in yield is problematic as the goal of this chemistry is to develop a process for facile generation and isolation of pentenyltoluene products. With either Rh concentration, the formation of *meta*- and *para*-pentyltoluenes is favored (Figure 6.5).

Table 6.7. Effect of Rh concentration on pentyltoluene and decane production.[a]

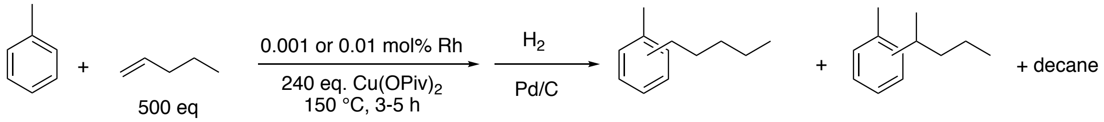

(Rh source = $[Rh(\eta^2\text{-}C_2H_4)_2(\mu\text{-}OAc)]_2$)

Mol% Rh	L:B	% Yield Pentyltoluenes	Eq. Decane Produced
0.001	10(5):1	44(2)%	Trace
0.01	7.5(8):1	73(5)%	2.6(7)

[a] % Yield represents the total percent yield of pentyltoluenes based on the amount of the copper oxidant. Averages and standard deviations are based on three experiments.

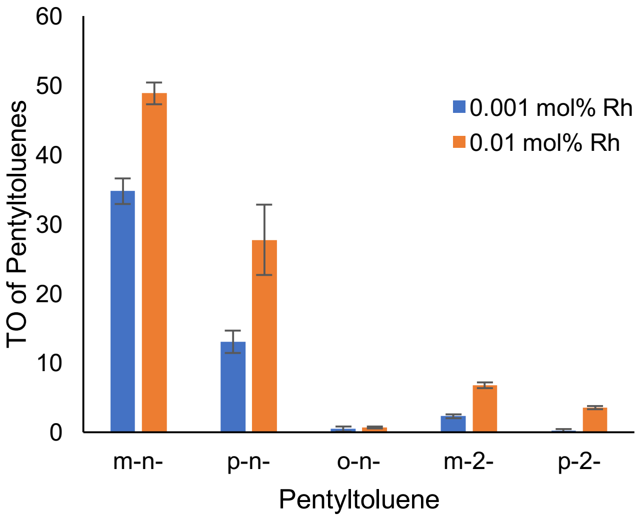

Figure 6.5. Pentyltoluene product distribution as a function of rhodium concentration. Error bars denote standard deviations based on three experiments.

As the goal of this research is to develop a process to efficiently produce pentenyltoluenes as precursors for 2,6-DMN, the pentenyltoluenes from a test reaction were isolated using conditions from Table 6.3 with 360 equivalents of $Cu(OPiv)_2$. Following work-up (see Experimental section), 88 mg of pentenyltoluenes were isolated, 32% yield based on $Cu(OPiv)_2$. This demonstrates that Rh-catalyzed alkenylation of toluene can be used to produce a desirable precursor to next-generation plastics.

6.4 Conclusions & Future Directions

Following hydrogenation, the Rh-catalyzed oxidative alkenylation of toluene with 1-pentene selectively produces *n*- and 2-pentyltoluenes. The linear (*n*-) pentyltoluene is the major product under the studied reaction conditions, and the undesired 3-pentyltoluene, which cannot be used in the ring closure reaction to generate 2,6-DMN is not observed. High L:B ratios on the order of ~10:1 are observed under a variety of reaction conditions. The reaction operates over a range of temperatures (120-180 °C) and high L:B ratios are obtained with a variety olefin, oxidant or rhodium catalyst concentrations.

Future studies will focus on the use of 1-hexene as the olefinic substrate, as hexenyltoluenes can also be converted 2,6-dimethylnaphthalene. 1-Hexene would provide a possible economical advantage over 1-pentene, as it is available from a variety of commercial sources, while 1-pentene is primarily produced by a single manufacturer.[44] Thus, the commercialization of this alkenylation reaction would be aided if it could operate effectively using another olefin source. Additional studies will center on the use of air-stable rhodium catalysts in order to prolong catalyst longevity and increase product yield, as additional efforts will require scale-up of this process and on the isolation of pentenyltoluene and hexenyltoluene products.

6.5 Experimental Section

General Considerations. All alkenylation reactions were performed under inert atmosphere in a glovebox. The purity of the glovebox atmosphere was maintained by nitrogen purges and was monitored using an oxygen analyzer (O_2 < 15 ppm for all reactions). Reactions were performed in glass Fischer-Porter reactors. Toluene was distilled over calcium hydride prior to use and was stored over molecular sieves. $Cu(OPiv)_2$ and $[Rh(\eta\text{-}C_2H_4)_2(\mu\text{-}OAc)]_2$ were synthesized according to literature procedures.[45-46] *n*-Pentyltoluenes were independently synthesized according to adapted literature procedures and were used as authentic standards for quantification.[47] All other chemicals were purchased from commercial sources and used as received. Hydrogen was purchased from GTS-Welco and used as received.

GC-MS was performed using a Shimadzu GCMS-QP2010 Plus instrument with a 30 m × 0.25 mm SHRXI-5MS column with a 0.25 μm thickness. Electron impact (EI) ionization was used. Products were quantified using a linear regression analysis of gas chromatograms relative to standard samples. Plots of peak areas versus molar ratios were gave regression lines using cyclooctane as the internal standard for pentyltoluene and decane formation. For the normal (*n*-) *m*-, *p*- and *o*-pentyltoluene products, the slope and correlation coefficient of the regression lines were 1.34 and 0.998 (*n*-*m*-pentyltoluene), 1.85 and 0.997 (*n*-*p*-pentyltoluene) and 1.84 and 0.998 (*n*-*o*-pentyltoluene), respectively. For decane, the slope and correlation coefficient were 2.08 and 0.998, respectively. Production of 2-pentyltoluene products was quantified using the slope and correlation coefficient for a curve of cumene:*n*-propylbenzene which enabled an approximation of the ratio of *n*- to 2-pentyltoluene products. The slope and correlation coefficient of the regression line were 0.998 and 0.98 for cumene:*n*-propylbenzene, respectively.

General Procedures

Catalytic Oxidation Alkenylation of Toluene with 1-Pentene. For a representative catalytic reaction, a stock solution was prepared with 0.01 mol% of Rh {Rh source = [Rh(η^2-C_2H_4)$_2$(μ-OAc)]$_2$}, cyclooctane (63 µL, 10 eq. relative to Rh), and toluene (50 mL). Glass Fischer-Porter reactors were charged with a stir bar, 10 mL of stock solution, 1-pentene and Cu(II) oxidant. The reactors were sealed and pressurized with 50 psi of nitrogen. Reactors were heated in an oil bath and stirred. The reaction was stopped when all of the copper(II) was consumed, indicated by a color change of the reaction mixture.[7] Reactions were allowed to cool prior analysis by GC-MS and subsequent hydrogenation.

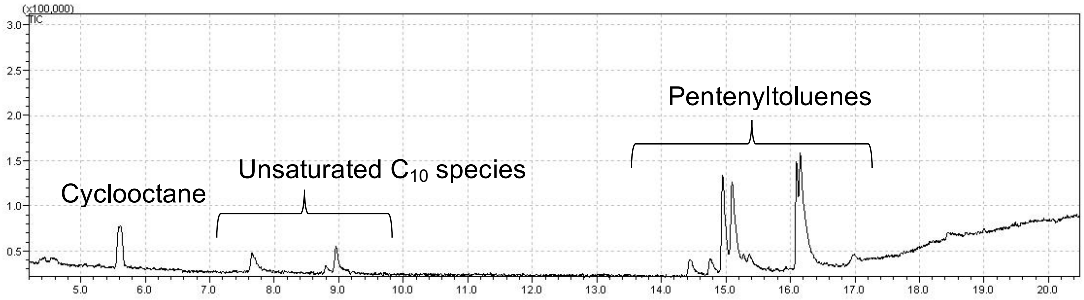

Figure 6.6. Representative GC-MS trace of a reaction mixture from the catalytic oxidative alkenylation of toluene with 1-pentene. Conditions: 0.01 mol % Rh {Rh source = [Rh(η^2-C_2H_4)$_2$(μ-OAc)]$_2$} relative to toluene, 10 eq. cyclooctane relative to Rh), toluene, 240 eq. Cu(OHex)$_2$ relative to Rh, 1000 eq. 1-pentene relative to Rh, 150 °C, 2 h.

Hydrogenation Procedure. Glass Fischer-Porter reactors were charged with a stir bar, an aliquot of the reaction mixture (0.1 mL), 10% Pd/C (8 mg) and 200 proof ethanol (4 mL). The reactors were sealed and the headspace was evacuated before being pressurized with 100 psi of H_2. The reactions stirred overnight at room temperature. The reactors were carefully vented and the mixture was analyzed by GC-MS.

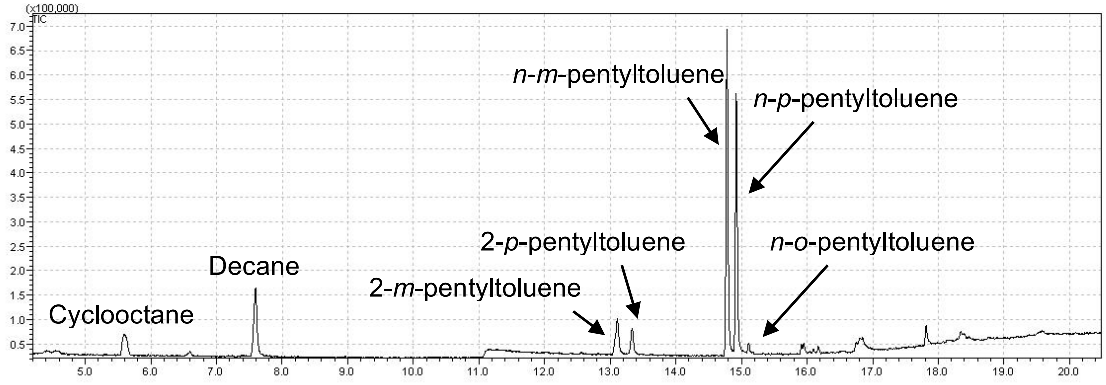

Figure 6.7. Representative GC-MS trace of a reaction mixture from the catalytic oxidative alkenylation of toluene with 1-pentene (reaction conditions shown in Figure 6.6) following hydrogenation according to the above procedure.

Pentenyltoluene Isolation Procedure. Following catalysis, the reactor was cooled to room temperature. The reaction mixture was diluted with ~40 mL of EtOAc, 10 mL of 10% aqueous NaOH solution and 50 mL DI H_2O. The layers were separated and the aqueous layer was extracted with 3 × 40 mL of EtOAc. The organic layers were combined. The organic layer was washed with DI H_2O (3 × 40 mL), dried over $MgSO_4$ and filtered. The filtrate was concentrated *in vacuo* and then purified by column chromatography using silica as the solid phase and cyclohexane/EtOAc as the eluent. After concentrating *in* vacuo, the yellow product was then filtered through a plug of alumina, eluting with cyclohexane. The filtrate was concentrated *in vacuo* and then purified by column chromatography using a silica column and eluting with pentane. The product was concentrated *in vacuo* and characterized by GC-MS.

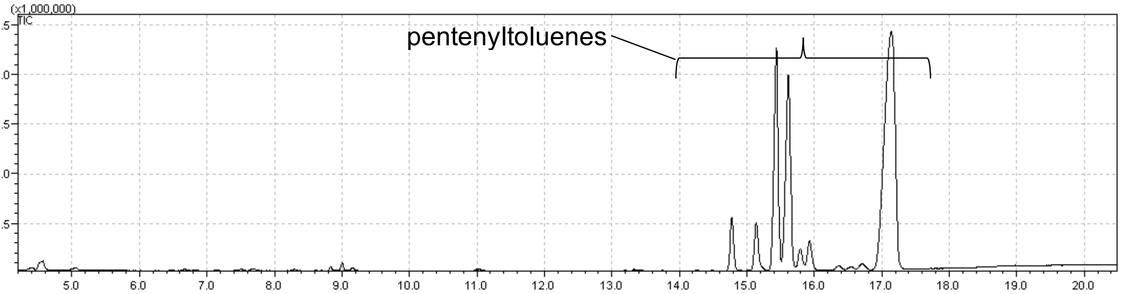

Figure 6.8. GC-MS trace of isolated pentenyltoluenes (reaction conditions described above).

6.6 References

1. Wittcoff, H. A.; Reuben, B. G.; Plotkin, J. S., *Industrial Organic Chemicals*. 3rd ed.; John Wiley & Sons: Hoboken, NJ, 2013.

2. Perego, C.; Pollesel, P., Advances in Nanoporous Materials. Ernst, S., Ed. Elsevier Science: Oxford, 2009; Vol. 1, pp 97-149.

3. Kocal, J. A.; Vora, B. V.; Imai, T. *Appl. Catal. A* **2001,** *221*, 295-301.

4. Hibbs, J., Anionic Surfactants. In *Chemistry and Technology of Surfactants*, Farn, R. J., Ed. Blackwell Publishing: Oxford, 2006; pp 91-123.

5. New Process for Producing Styrene Cuts Costs, Saves Energy, and Reduces Greenhouse Gas Emissions. https://www1.eere.energy.gov/office_eere/pdfs/exelus_case_study.pdf.

6. Rueping, M.; Nachtsheim, B. J. *Beilstein J. Org. Chem.* **2010,** *6* (6).

7. Vaughan, B. A.; Webster-Gardiner, M. S.; Cundari, T. R.; Gunnoe, T. B. *Science* **2015,** *348* (6233), 421-424.

8. Bandini, M.; Tragni, M.; Umani-Ronchi, A. *Adv. Synth. Catal.* **2009,** *351*, 2521-2524.

9. Matsumoto, T.; Taube, D. J.; Periana, R. A.; Taube, H.; Yoshida, H. *J. Am. Chem. Soc.* **2000,** *122*, 7414-7415.

10. Webster-Gardiner, M. S.; Chen, J.; Vaughan, B. A.; McKeown, B. A.; Schinski, W.; Gunnoe, T. B. *J. Am. Chem. Soc.* **2017,** *139* (15), 5474-5480.

11. Olah, G. A.; Flood, S. H.; Moffatt, M. E. *J. Am. Chem. Soc.* **1964,** *86*, 1060-1064.

12. Olah, G. A.; Flood, S. H.; Kuhn, S. J.; Moffatt, M. E.; Overchuck, N. A. *J. Am. Chem. Soc.* **1964,** *86*, 1046-1054.

13. Dong, Z.; Ren, Z.; Thompson, S. J.; Xu, Y.; Dong, G. *Chem. Rev.* **2017,** *117*, 9333-9403.

14. Foley, N. A.; Lee, J. P.; Ke, Z.; Gunnoe, T. B.; Cundari, T. R. *Acc. Chem. Res.* **2009,** *42* (5), 585-597.

15. Chen, J.; Nielsen, R. J.; Goddard, W. A., III; McKeown, B. A.; Dickie, D. A.; Gunnoe, T. B. *J. Am. Chem. Soc.* **2018,** *140*, 17007-17018.

16. Lail, M.; Arrowood, B. N.; Gunnoe, T. B. *J. Am. Chem. Soc.* **2003,** *125*, 7506-7507.

17. Lail, M.; Bell, C. M.; Conner, D.; Cundari, T. R.; Gunnoe, T. B.; Petersen, J. L. *Organometallics* **2004,** *23* (5007-5020).

18. DeYonker, N. J.; Foley, N. A.; Cundari, T. R.; Gunnoe, T. B.; Petersen, J. L. *Organometallics* **2007,** *26*, 6604-6611.

19. Foley, N. A.; Lail, M.; Gunnoe, T. B.; Cundari, T. R.; Boyle, P. D.; Petersen, J. L. *Organometallics* **2007,** *26*, 5507-5516.

20. Foley, N. A.; Lail, M.; Lee, J. P.; B., G. T.; Cundari, T. R.; Petersen, J. L. *J. Am. Chem. Soc.* **2007,** *129*, 6765-6781.

21. Foley, N. A.; Ke, Z.; Gunnoe, T. B.; Cundari, T. R.; Petersen, J. L. *Organometallics* **2008,** *27*, 3007-3017.

22. Morello, G. R.; Cundari, T. R.; Gunnoe, T. B. *J. Organomet. Chem.* **2012,** *697*, 15-22.

23. Burgess, S. A.; Joslin, E. E.; Gunnoe, T. B.; Cundari, T. R.; Sabat, M.; Myers, W. H. *Chem. Sci.* **2014,** *5*, 4355-4366.

24. Joslin, E. E.; Quillian, B.; Gunnoe, T. B.; Cundari, T. R.; Sabat, M.; Myers, W. H. *Inorg. Chem.* **2014,** *53*, 6270-6279.

25. McKeown, B. A.; Foley, N. A.; Lee, J. P.; Gunnoe, T. B. *Organometallics* **2008,** *27*, 4031-4033.

26. McKeown, B. A.; Gonzalez, H. E.; Friedfeld, M. R.; Gunnoe, T. B.; Cundari, T. R.; Sabat, M. *J. Am. Chem. Soc.* **2011,** *133*, 19131-19152.

27. McKeown, B. A.; Gonzalez, H. E.; Friedfeld, M. R.; Brosnahan, A. M.; Gunnoe, T. B.; Cundari, T. R.; Sabat, M. *Organometallics* **2013,** *32*, 2857-2865.

28. McKeown, B. A.; Gonzalez, H. E.; Gunnoe, T. B.; Cundari, T. R.; Sabat, M. *ACS Catal.* **2013,** *3*, 1165-1171.

29. McKeown, B. A.; Gonzalez, H. E.; Michaelos, T.; Gunnoe, T. B.; Cundari, T. R.; Crabtree, R. H.; Sabat, M. *Organometallics* **2013,** *32* (3903-3913).

30. McKeown, B. A.; Prince, B. M.; Ramiro, Z.; Gunnoe, T. B.; Cundari, T. R. *ACS Catal.* **2014,** *4*, 1607-1615.

31. Vaughan, B. A.; Khani, S. K.; Gary, J. B.; Kammert, J. D.; Webster-Gardiner, M. S.; McKeown, B. A.; Davis, R. J.; Cundari, T. R.; Gunnoe, T. B. *J. Am. Chem. Soc.* **2017,** *139* (4), 1485-1498.

32. Cao, Y.; Kessas, R.; Naccache, C.; Ben Taarit, Y. *Appl. Catal., A* **1999,** *184*, 231-238.

33. Kosswig, K., Surfactants. In *Ullmann's Encyclopedia of Industrial Chemistry*, Wiley-VCH: 2012; Vol. 13, pp 24791-24830.

34. Chen, P.; Kotek, R. *Polym. Rev.* **2008,** *48*, 392-421.

35. Lillwitz, L. D. *Appl. Catal. A* **2001,** *221*, 337-358.

36. Pang, K.; Kotek, R.; Tonelli, A. *Prog. Polym. Sci.* **2006,** *31*, 1009-1037.

37. Eberhardt, G. G.; Peterson, H. J. *J. Org. Chem.* **1965,** *30*, 82-84.

38. Suld, G.; Stuart, A. P. *J. Org. Chem.* **1964,** *29* (10), 2939-2946.

39. Chen, C.-Y.; Schinski, W. L.; O'Rear, D. J.; Harris, T. V. Method of making dimethylnaphthalenes. 5,955,641, 1999.

40. Santilli, D. S.; Chen, C.-Y. Method of making 2,6-dimethylnaphthalene from other dimethylnaphthalene isomers andn from dimethyltetralins/dimethyldecalins with a methyl group on each ring. 6,015,930, 2000.

41. Del Rossi, K. J.; Green, L. A.; Huss, A., Jr.; Kirker, G. W.; Landis, M. E. Process for Preparing Dimethylnaphthalene. 5,043,501, 1991.

42. de Klerk, A.; Furimsky, E., *Catalysis in the Refining of Fischer-Tropsch Syncrude*. Royal Society of Chemistry: 2010.

43. Fabri, J.; Graeser, U.; Simo, T. A., Toluene. In *Ullmann's Encyclopedia of Industrial Chemistry*, Wiley: Weinheim, Germany, 2012; pp 26081-26092.

44. RSA Olefins. https://www.cchange.ac.za/rsa-olefins/.

45. Xie, L.-H.; Suh, M. P. *Chem. Eur. J.* **2011,** *17*, 13653.

46. Werner, H.; Poelsma, S.; Schneider, M. E.; Windmüller, B.; Barth, D. *Chem. Ber.* **1996,** *129* (6), 647-652.

47. Batsomboon, P.; Phakhodee, W.; Ruchirawat, S.; Ploypradith, P. *J. Org. Chem.* **2009,** *74*, 4009-4012.

7 Appendix

DFT mechanistic study of methane mono-esterification by hypervalent iodine alkane oxidation process

Ross Fu[†], Robert J. Nielsen[†], Nichole S. Liebov[‡], William A. Goddard III[†*], T. Brent Gunnoe[‡], John T. Groves[§]

[†]Materials and Process Simulation Center (139-74), California Institute of Technology, Pasadena, CA 91125, USA

[‡]Department of Chemistry, University of Virginia, Charlottesville, VA 22904, USA

[§]Department of Chemistry, Princeton University, Princeton, NJ 08544, USA

KEYWORDS. DFT, methane, monooxidation, monooxygenation, iodine

ABSTRACT: Recent experiments report high yield (up to 40%) and selectivity (generally > 85%) for the direct partial oxidation of methane to methyl trifluoroacetate in trifluoroacetic acid solvent using hypervalent iodine as the oxidant and in the presence of substoichiometric amounts of chloride anion. We develop here the reaction mechanism for these results based on DFT calculations at the M06-2X/6-311G**++/aug-pVTZ-PP level of plausible intermediates and transition states. We find a mechanistic process that explains both reactivity as well as selectivity of the system. In this oxy-esterification (OxE) system **$IO_2Cl_2^-$ and/or $IOCl_4^-$ act as key transient intermediates**, leading to the generation of the high-energy radicals $IO_2\cdot$ and $Cl\cdot$ that mediate methane C–H bond cleavage. These studies suggest new experiments to validate the OxE mechanism.

INTRODUCTION

Natural gas is a naturally-occurring hydrocarbon mixture composed chiefly of methane that is generally found in the same places as petroleum.[1] However, methane is a gas with a very low boiling point of −161.5°C, making it difficult to liquefy, and consequently expensive to store and transport.[2] Because natural gas sells for a much lower price than petroleum on the world market, it is often uneconomical to harvest.[3] And because it is also a potent greenhouse gas with 72 times the climate change potential of CO_2, release into the atmosphere can have significantly deleterious environmental effects.[4] It has been estimated that 140 billion cubic meters of natural gas are flared annually.[5]

Much effort has been expended towards partially oxidizing methane to methanol onsite.[6] As a liquid under standard conditions and a common chemical feedstock, methanol is both easier to store and transport, and also more valuable than methane.[7] A frequently used industrial process is called steam-methane reformation (SMR). A mixture of methane and steam is passed through a nickel catalyst at high temperatures and pressures to form synthesis gas (CO and H_2), which is then recombined in a second catalytic process to form methanol. Unfortunately, this process is both highly energy and capital intensive, and it is generally not feasible to be located near remote extraction sites.[8] Another strategy for methane functionalization is methane oxychlorination, which involves the catalyzed reaction of methane with HCl and O_2 to form methyl chloride and water. The products can further react to produce methanol and regenerate HCl.[9] Unfortunately, this process produces a large amount of over-oxidized byproducts such as methylene chloride, chloroform, and carbon tetrachloride. In fact, a common limitation of radical based mechanisms such as oxychlorination is the fact that the C–H bond of methane, 104 kcal/mol, is stronger than that of methanol (96 kcal/mol) or methyl chloride (100 kcal/mol), leading to abundant over-oxidized side products.[10]

In the 1960s, Shilov and coworkers discovered that platinum salts in aqueous HCl solution could activate methane under mild conditions, producing methyl chloride (and consequently methanol by hydrolysis) through an electrophilic two-electron C–H activation mechanism.[11] In the ensuing decades, much work has been done to improve catalyst stability, find less expensive alternatives to platinum, and replace Pt(IV) with dioxygen as the stoichiometric terminal oxidant.[12] One of the most promising developments is the Catalytica process developed by Periana and coworkers, in which methane in oleum solution (H_2SO_4/SO_3) is oxidized to methyl bisulfate via diverse late-transition metals such as Pt, Pd, Hg, and Au.[13] In all of these cases, the reaction is selective for methyl bisulfate production, often with negligible over-oxidation. This has been attributed to the presence of the electron withdrawing group $–OSO_3H$

which serves as a protecting group, removing electron density from the methyl C–H bond and slowing over-oxidation by electrophilic catalysts.[14] Currently, the chief drawback of the Catalytica family of methane oxidation systems is the use of superacidic media such as oleum, which must be constantly replenished due to H_2O being produced by the reaction, rendering cost-effective product extraction very difficult.

Our work on the partial oxidation of methane has focused on the search for processes efficient under less acidic environments, in particular trifluoroacetic acid (TFAH).[15] For instance, we have characterized a number of rhodium complexes with C–H activation ability in TFAH.[16] Recently, we have reported the ability of hypervalent iodine complexes to oxidize light alkanes (methane, ethane and propane) under mild conditions. Hypervalent iodine complexes were reported to activate C–H bonds in an electrophilic 2-electron oxidation.[17] Since then, we have also seen that simple iodate and other iodine oxide salts oxidize methane and other light alkanes in the presence of catalytic amounts of chloride anion.[18] In addition to 2-election pathways, our work on the hypervalent iodine oxide reactions indicate that 1-electron radical pathways should be explored.

In this contribution, we use density functional theory (DFT) to determine the mechanism for the oxidation of methane to methyl trifluoroacetate in TFAH solution using hypervalent iodine oxide as the oxidant. Our results explain current observations for a range of iodine based oxidants. In particular, we provide a comprehensive characterization of the mechanism of iodate oxidation, and suggest how it may be extended to other iodine sources. In addition, our calculations are valid for TFAH and predict non-reactivity in acetic acid. We also present our experimental work conducted in parallel to our calculations that accounts for reactivity in acetic acid and supports our calculated results.

MATERIALS AND METHODS

General calculations

All quantum mechanical calculations were carried out using the Jaguar software version 8.4 developed by Schrödinger Inc.[19] Geometry optimizations were carried out on initial guess structures, and vibrational frequencies were calculated to confirm the optimized geometries as intermediates (no negative curvatures) or transition states (one negative curvature) and to calculate the zero-point energy, entropy, and temperature corrections to obtain the free energy profile. Calculations were performed using the M06-2X density functional[20] with the Grimme post-SCF D3 correction for van der Waals interactions.[21] The double-ζ 6-31G** basis set[22] was used for all elements except bromine and iodine (which used the Peterson pseudopotential along with a diffuse-augmented correlation-consistent triple-ζ basis set without *f* functions, i.e. aug-cc-PVTZ-PP(-f)[23]) for geometry optimization and frequency calculations. All calculations were performed using a temperature set to 498.15 K. A comparison of relevant calculated and experimental reaction enthalpies is given in Table S4.

Construction of the solvation energy

Solvation energies ΔE_{solv} were calculated using the PBF Poisson-Boltzmann implicit continuum solvation model[24] using the triple-ζ 6-311G**++ basis set[25] for all elements except bromine and iodine, which used the aug-cc-PVTZ-PP basis set with Peterson pseudopotential and *f* functions.[23] This model treats any arbitrary solvent with two parameters: its dielectric constant ε and its probe radius *r*. The probe radius is calculated according to the formula $\boldsymbol{r} = \sqrt[3]{\mathbf{3\Delta MW/4\pi N_A\rho}}$, where *r* is the probe radius in Å, MW is the molecular weight, N_A is Avogadro's number, ρ is the density, and Δ is the liquid packing density and estimated at 0.5 (for comparison, Δ = 0.74 for FCC and HCP crystals).[26] Solvent energies were calculated using a dielectric constant of 8.55 for TFAH.[27] Using the above formula, the probe radius was thereby set to 2.451 Å.

Construction of the free energy

The state energies for each species in the gas phase were calculated using the formulae $U_{\mathrm{gas}} = E_{\mathrm{gas}} + \mathrm{ZPE} + U_{\mathrm{lib}}$, $H_{\mathrm{gas}} = U_{\mathrm{gas}} + pV$, and $G_{\mathrm{gas}} = H_{\mathrm{gas}} - TS$, where U_{lib} is the total contribution of temperature-dependent librational (translational, rotational, and vibrational) effects to the internal energy. For each species in the solution phase, the free energy was calculated as $G_{\mathrm{sol}} = G_{\mathrm{gas}} + \Delta E_{\mathrm{solv}} + \Delta G_{\mathrm{gas}\rightarrow\mathrm{solv}}$, where ΔE_{solv} is the solvation energy as described above and $\Delta G_{\mathrm{gas}\rightarrow\mathrm{solv}} = kT\ln(24.5)$ represents the free energy change of compressing 1 mol of an ideal gas (volume 24.5 L at 25°C) to 1 L (for 1 M standard concentration). In the specific case of individual atoms or ions such as $Br^{\cdot}$ or Cl^-, ZPE = 0 and $H_{\mathrm{tot}} = 5/2kT$, and *S* is taken from Chase.[28]

Experimental methods

All reactions were prepared in air. Glacial acetic acid (HOAc), acetic acid-d_4, methyl acetate (MeOAc), ammonium iodate (NH_4IO_3), and potassium chloride (KCl) were purchased from commercial sources and used as received. Methane and argon were purchased from GTS-Welco and used as received. ^1H NMR spectra were recorded on a Varian Inova 500 MHz NMR spectrometer, using neat samples each with C_6D_6 in a sealed capillary as an internal lock reference. Chemical shifts are reported relative to standards of nitromethane (CH_3NO_2) (^1H NMR δ 4.30). GC-MS data were obtained on a Shimadzu GC-2010 instrument equipped with a Restek RT-Qbond 30 m × 8 mm fused silica PLOT column. Reactions were carried out in in-house-built high-pressure stainless steel VCO reactors using Swagelok parts. Each reactor had a Teflon liner and stir bar and was heated in an aluminum block.

RESULTS

The ability of simple iodate salts to oxidize methane was reported by Fortman et al.[18a] A wide variety of iodine containing species were investigated in that contribution, and the chemistry was subsequently extended to simple periodate salts in a follow-up contribution.[18b] Table 1 is a summary of the reactions methane undergoes in TFAH, when various iodine oxidants and other additives are added.

Table 1. Summary of experimentally determined methane oxidation reactions in TFAH with various iodine oxidants and other additives.[a]

Entry	Species	Additive	Yield MeTFA; MeX
1	I_2	–	–
2	I_2	KCl	–
3	I_2	NH_4IO_3	2%
4	ICl	–	–
5	ICl_3	–	5%; 43% MeCl
6	$I(TFA)_3$	–	7%
7	$I(TFA)_3$	KCl	43%
8	NH_4IO_3	KCl	21%; <1% MeCl
9	$(IO_2)_2S_2O_7$	–	<1%
10	$(IO_2)_2S_2O_7$	KCl	48%
11	I_2O_4	–	2%; 15% MeI
12	I_2O_4	KCl	30%; 17% MeI
13	$(IO)_2SO_4$	–	5.3%
14	$(IO)_2SO_4$	KCl	31%
15	KIO_4	KCl	41%; 1% MeCl

[a] Yields for all entries except for **8** and **15** are reported relative to the amount of iodine source, which was 0.4 mmol. Yields for entries **8** (NH_4IO_3) and **15** (KIO_4) are relative to methane (8.4 mmol for NH_4IO_3 and 2.9 mmol for KIO_4). The experiment with KIO_4 (entry 15) was performed at 200 °C, whereas all other experiments were performed at 180 °C.

In the following sections, we will address the individual observations in each entry of Table 1.

Entries 1-2. The lack of reaction with elemental iodine is of little surprise, as iodine radicals are generally thought of as being too weak to break the C–H bonds of methane. This is confirmed by our calculations (equations 1-3). From equation 2, we see that abstracting a hydrogen atom from methane by an iodine radical is endergonic by 25.8 kcal/mol. More importantly, by combining equations 2 and 3 we see that conversion of methane and iodine to methyl iodide and hydrogen iodide is both endothermic and endergonic.

$$\mathrm{I_2} \rightarrow 2\mathrm{I}\cdot \qquad \Delta H^{a} = 36.5;\ \Delta G = 32.2 \tag{1}$$

$$\mathrm{I}\cdot + \mathrm{CH_4} \rightarrow \mathrm{HI} + \mathrm{CH_3}\cdot \qquad \Delta H^{a} = 31.7;\ \Delta G = 25.8 \tag{2}$$

$$\mathrm{CH_3}\cdot + \mathrm{I_2} \rightarrow \mathrm{CH_3I} + \mathrm{I}\cdot \qquad \Delta H^{a} = -19.0;\ \Delta G = -16.9 \tag{3}$$

[a] Values based on experimental BDEs.[29] All numbers in kcal/mol.

Entry 3. Although I_2 and KIO_3 have been reported to oxidize methane in oleum,[30] the same reaction was not observed in the more weakly acidic TFAH. The oleum reaction is proposed to involve I^+ as a reactive intermediate, but we find that this species is too unstable to be accessible in TFAH (equation 4). TFAI may be seen as a lower-energy analogue (equation 5); however, the O–I bond dissociation energy is still too high (equation 6).

$$\mathrm{I_2} + \mathrm{TFAH} \rightarrow \mathrm{I^+} + \mathrm{HI} + \mathrm{TFA^-} \qquad \Delta H = 97.4;\ \Delta G = 86.2 \tag{4}$$

$$\mathrm{I_2} + \mathrm{TFAH} \rightarrow \mathrm{HI} + \mathrm{TFAI} \qquad \Delta H = 38.8;\ \Delta G = 38.7 \tag{5}$$

$$\mathrm{TFAI} \rightarrow \mathrm{TFA}\cdot + \mathrm{I}\cdot \qquad \Delta H = 52.1;\ \Delta G = 39.5 \tag{6}$$

Entry 4. ICl has a BDE of 51 kcal/mol, and breaking the bond is too endergonic to occur to any significant extent under reaction conditions (equation 7).

However, if we assume that it could break into chlorine and iodine radicals, we see from equation 8 that the chlorine radicals are able to break the C–H bonds of methane. The resulting methyl radicals would react with additional ICl to form iodine radicals (equation 9), which may be able to regenerate additional chlorine radicals (equations 10). Hence our DFT shows that ICl cannot initiate methane oxidation, although it may be able to sustain a reaction that has already been initiated by a different radical source.

$$\mathrm{ICl} \rightarrow \mathrm{I}\cdot + \mathrm{Cl}\cdot \qquad \Delta H^{a} = 51; \; \Delta G = 45.1 \qquad (7)$$

$$\mathrm{Cl}\cdot + \mathrm{CH_4} \rightarrow \mathrm{HCl} + \mathrm{CH_3}\cdot \qquad \Delta H^{a} = -0.2; \; \Delta G = -5.6 \qquad (8)$$

$$\mathrm{CH_3}\cdot + \mathrm{ICl} \rightarrow \mathrm{CH_3Cl} + \mathrm{I}\cdot \qquad \Delta H^{a} = -30.0; \; \Delta G = -29.5 \qquad (9)$$

$$\mathrm{I}\cdot + \mathrm{ICl} \rightarrow \mathrm{I_2} + \mathrm{Cl}\cdot \qquad \Delta H^{a} = 14.5; \; \Delta G = 12.9 \qquad (10)$$

[a]Values based on experimental BDEs.[29] All numbers in kcal/mol.

Entry 5. ICl_3 actually exists in the solid form as the dimer I_2Cl_6,[31] although under reaction conditions it is monomeric (equation 11). It is known to be a powerful oxidizer and chlorine source. In our mechanism, ICl_3 generates chlorine atoms (equation 12), which abstract the hydrogen from methane to generate methyl radicals. The methyl radical abstracts chlorine from another equivalent of ICl_3 to generate the product, methyl chloride (equation 13). Finally, radical propagation is achieved through the decomposition of $ICl_2\cdot$, which generates additional chlorine radicals (equation 14).

$$\mathrm{I_2Cl_6} \Leftrightarrow 2\mathrm{ICl_3} \qquad \Delta H = 6.1; \; \Delta G = -0.6 \qquad (11)$$

$$\mathrm{ICl_3} \rightarrow \mathrm{ICl_2}\cdot + \mathrm{Cl}\cdot \qquad \Delta H = 41.0; \; \Delta G = 28.3 \qquad (12)$$

$$\mathrm{Cl}\cdot + \mathrm{CH_4} \rightarrow \mathrm{HCl} + \mathrm{CH_3}\cdot \qquad \Delta H^{a} = -0.2; \; \Delta G = -5.6 \qquad (8)$$

$$\mathrm{CH_3}\cdot + \mathrm{ICl_3} \rightarrow \mathrm{CH_3Cl} + \mathrm{ICl_2}\cdot \qquad \Delta H = -46.9; \; \Delta G = -46.3 \qquad (13)$$

$$\mathrm{ICl_2}\cdot \rightarrow \mathrm{ICl} + \mathrm{Cl}\cdot \qquad \Delta H = 25.7; \; \Delta G = 17.9 \qquad (14)$$

[a]Values based on experimental BDEs.[29] All numbers in kcal/mol.

This is our first entry in which methane is oxidized to a significant extent, although the main product is methyl chloride. Equations 11 and 12 show that dissociation to the monomer ICl_3 is favorable and I–Cl bond homolysis is accessible. According to experimental observations,[18a] methyl chloride does not convert to methyl trifluoroacetate under reaction conditions. However, methyl iodide is rapidly converted via S_N2 attack to methyl trifluoroacetate, even at room temperature, but only under basic conditions such as for the NH_4IO_3/KCl case (entry **8**) or the KIO_4/KCl case (entry **17**).

Entries 6-7. In 2014, Konnick et al. reported the ability of the hypervalent I(III) compound $(C_6F_5)I(TFA)_2$ to oxidize methane to MeTFA in TFAH solution.[32] Their mechanism, supported by DFT calculations, involved the electrophilic 2-electron activation of methane to form an organoiodine(III) intermediate, which is then attacked via S_N2 to form MeTFA. However, our calculations which examine $I(TFA)_3$ instead find that the analogous closed-shell transition state is too high in energy (Scheme 1). Hence, we believe an alternative mechanism is needed to explain the reactivity in entries 6 and 7.

Scheme 1. Closed shell mechanism of methane oxidation by I(TFA)$_3$.

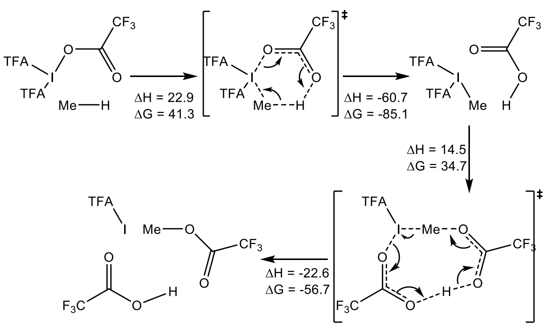

Instead, we propose a radical mechanism initiated by the homolysis of an I–TFA bond (Scheme 2). Both radical fragments TFA· and $I(TFA)_2\cdot$ can then either activate methane (red) or decompose (blue). Finally, the methyl radical can react with another equivalent of $I(TFA)_3$ to form the product MeTFA and propagate the reaction (equation 15).

Scheme 2. Open shell mechanism of methane activation by I(TFA)$_3$^{a}.

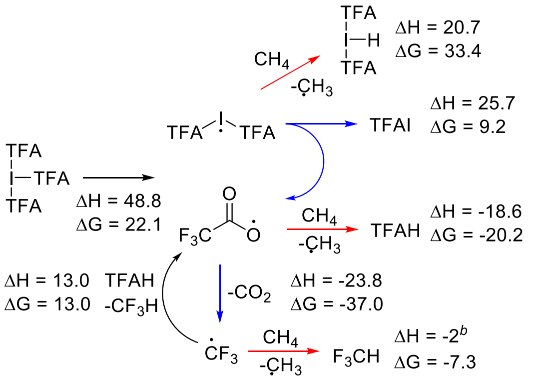

[a]Methane activation in red; decomposition in blue. [b]Values based on experimental BDEs.[29] All numbers in kcal/mol.

$$\mathrm{CH_3}\cdot + \mathrm{I(TFA)_3} \rightarrow \mathrm{CH_3TFA} + \mathrm{ITFA_2}\cdot \qquad \Delta H = -52.9; \; \Delta G = -54.8 \qquad (15)$$

From a close examination of Scheme 2, we see that a number of decomposition pathways may affect the yield of $CH_3\cdot$ radical generation, hence explaining the low yield observed for entry 6. Our case is bolstered by the experimental observation of fluoroform formation as a side product as reported by Konnick et al.,[32] indicating that their hypervalent iodine reaction may have a radical component as well. Also, evidence of radical CF_3 formation is found for the conversion of methane and iodate/chloride in TFAH.[18]

In comparing entries 6 to 7, we see that the addition of chloride greatly improves yield from 7% to 43%. We first consider the possibility of $I(TFA)_3$ and Cl^- forming adducts (equations 16-18), and we see that substitution of TFA by Cl is favorable for all three reactions. However, we consider that only the formation of $I(TFA)_2Cl$ is feasible since only substoichiometric amounts of KCl are added.

$$\mathrm{I(TFA)_3 + Cl^- \rightarrow I(TFA)_2Cl + TFA^-} \qquad \Delta H = -6.5;\ \Delta G = -14.5 \qquad (16)$$

$$\mathrm{I(TFA)_2Cl + Cl^- \rightarrow I(TFA)Cl_2 + TFA^-} \qquad \Delta H = -2.9;\ \Delta G = -11.2 \qquad (17)$$

$$\mathrm{I(TFA)Cl_2 + Cl^- \rightarrow ICl_3 + TFA^-} \qquad \Delta H = -6.8;\ \Delta G = -12.2 \qquad (18)$$

From $I(TFA)_2Cl$, we may expect thermal homolysis to break either the I–TFA (equation 19) or I–Cl (equation 20) bond. Either way, radicals are formed that can activate methane as in Scheme 2.

$$\mathrm{I(TFA)_2Cl \rightarrow I(TFA)Cl\cdot + TFA\cdot} \qquad \Delta H = 48.8;\ \Delta G = 27.7 \qquad (19)$$

$$\mathrm{I(TFA)_2Cl \rightarrow I(TFA)_2\cdot + Cl\cdot} \qquad \Delta H = 47.8;\ \Delta G = 34.8 \qquad (20)$$

The resulting methyl radicals can react with additional $I(TFA)_2Cl$ to form MeTFA (equation 21) in preference to MeCl (equation 22), which provides an explanation for why only MeTFA is observed as an oxidized product.

$$\mathrm{CH_3\cdot + I(TFA)_2Cl \rightarrow CH_3TFA + I(TFA)Cl\cdot} \qquad \Delta H = -52.8;\ \Delta G = -55.1 \qquad (21)$$

$$\mathrm{CH_3\cdot + I(TFA)_2Cl \rightarrow CH_3Cl + I(TFA)_2\cdot} \qquad \Delta H = -40.0;\ \Delta G = -39.8 \qquad (22)$$

Non-radical paths for CH_4 activation using potential I(III) intermediates were sought, but no thermally accessible transition states were found (see Supporting Information, Scheme S1).

Entry 8. The reaction of methane and iodate salts in the presence of catalytic amounts of chloride is the chief focus of the report by Fortman et al.[18a] and may be considered the "canonical" hypervalent iodine oxidation reaction. Hence, we devote the bulk of our analysis to this reaction and its variations.

We begin by noting that while iodate is quite basic in TFAH solution under reaction conditions (equation 23) and thus protonated to HIO_3, chloride, iodide, and water are all weak bases (equations 24-26, respectively) and remain unprotonated.

$$\mathrm{IO_3^- + TFAH \rightarrow HIO_3 + TFA^-} \qquad \Delta H = 0.3;\ \Delta G = -2.4 \qquad (23)$$

$$\mathrm{Cl^- + TFAH \rightarrow HCl + TFA^-} \qquad \Delta H = 10.6;\ \Delta G = 6.9 \qquad (24)$$

$$\mathrm{I^- + TFAH \rightarrow HI + TFA^-} \qquad \Delta H = 19.3;\ \Delta G = 15.1 \qquad (25)$$

$$\mathrm{H_2O + TFAH \rightarrow H_3O^+ + TFA^-} \qquad \Delta H = 26.4;\ \Delta G = 25.2 \qquad (26)$$

Furthermore, we note that if elemental iodine is in the system (as it is the eventual fate of iodate in the reaction[18]), it can complex to chloride and iodide (equations 27-28, respectively). This would further decrease the thermodynamic activity of these halides and thus make their protonation even less likely.

$$\mathrm{Cl^- + I_2 \rightarrow I_2Cl^-} \qquad \Delta H = -10.9;\ \Delta G = -3.4 \qquad (27)$$

$$\mathrm{I^- + I_2 \rightarrow I_3^-} \qquad \Delta H = -9.4;\ \Delta G = -2.9 \qquad (28)$$

Having established that iodate is initially protonated to HIO_3, we wish to ascertain if the TFAH environment may result in TFA/aqua/chloro adducts being formed. In order to approach this rigorously, we begin by noting that HIO_3 is an I(V) complex with only oxo and hydroxo ligands. In water, an oxo ligand can interconvert with two hydroxo ligands. In TFAH, an oxo can interconvert with two TFA ligands. And in the presence of a chloride salt, hydroxo and TFA ligands may interconvert with chloro ligands. Thus, we would expect HIO_3 in wet TFAH with chloride to exist as a multitude of iodine complexes with a combination of oxo, hydroxo, chloro, and TFA substituents such that the overall oxidation state of the iodine is +5.

A complete accounting of I(V) species in $TFAH/H_2O$ with optional chloro ligands, along with their relative energies, is given in Table S1. From this table, we can extract the lowest energy I(V) species containing at least one I–Cl bond (Scheme S2). By calculating the difference in energy between each species and the corresponding species with the I–Cl bond broken, we can find the BDEs and free energies for homolytically cleaving each I–Cl bond (see Supporting Information, Scheme S2, in red). These values are in excellent agreement with the previous coupled-cluster work by Dixon and coworkers.[33] However, we did not find a species with a readily homolyzible bond. The lowest energy species are $IO_2Cl_2^-$ and $IOCl_4^-$, but breaking the I–Cl bond of these species is endergonic by 44.1 and 37.7 kcal/mol, respectively, which is too unfavorable to be considered as contributing processes. By contrast, the species $IOCl_3$ and ICl_5 can have their I−Cl bonds broken at a free energy cost of 23.8 and 17.1 kcal/mol, respectively, but they are significantly less stable than $IO_2Cl_2^-$ (G_{rel} of 10.3 and 20.1 compared to −6.5 for $IO_2Cl_2^-$) and hence not likely to be present in solution.

In considering how the reaction might proceed, we decided to investigate more closely the role of elemental iodine. We have observed experimentally that elemental iodine is formed as a final product in our reaction.[18a] Elemental iodine is well known to be a radical inhibitor, due to the relative inertness (as far as radicals go) of I·.[34] Hence, we decided to add the assumption that the system at steady state would include a significant concentration of I·, either produced from 1), the reaction of other radicals with I_2, or 2), the autolysis of I_2 itself, which according to equation 1 is endergonic by a relatively accessible 32.2 kcal/mol. A steady state approximation for the reaction kinetics should also affect our calculation for the overall reaction barrier, given later in this section.

We thus look at the reaction of several I(V) species with I· (Figure S1), and we are gratified to find that the abstraction of Cl is generally facile. In particular, we see that our low energy anionic species $IO_2Cl_2^-$ and $IOCl_4^-$ also have the lowest barriers for reacting with I·, generating ICl and IO_2Cl^- (which spontaneously decomposes to IO_2· and Cl^-) or $IOCl_3^-$, respectively (equations 29-30).

$$\mathrm{I}\cdot + \mathrm{IO_2Cl_2^-} \rightarrow \mathrm{ICl} + \mathrm{IO_2Cl^-}\cdot \qquad \Delta G^{\ddagger} = 4.5;\ \Delta G = 0.6 \qquad (29)$$

$$\mathrm{IO_2Cl^-}\cdot \rightarrow \mathrm{IO_2}\cdot + \mathrm{Cl^-}$$

$$\mathrm{I}\cdot + \mathrm{IOCl_4^-} \rightarrow \mathrm{ICl} + \mathrm{IOCl_3^-}\cdot \qquad \Delta G^{\ddagger} = 8.3;\ \Delta G = -7.4 \qquad (30)$$

Both ICl and $IOCl_3^-$ can generate Cl radicals: ICl through reaction with I·, and $IOCl_3^-$ through auto-dissociation (equations 31-32).

$$\mathrm{I}\cdot + \mathrm{ICl} \rightarrow \mathrm{I_2} + \mathrm{Cl}\cdot \qquad \Delta H^{a} = 14.5;\ \Delta G = 12.9 \qquad (10)$$

$$\mathrm{IOCl_3^-}\cdot \rightarrow \mathrm{IOCl_2^-} + \mathrm{Cl}\cdot \qquad \Delta H = 26.6;\ \Delta G = 17.7 \qquad (31)$$

^{a}Values based on experimental BDEs.[29] All numbers in kcal/mol.

Both IO_2· and Cl· radicals are able to initiate hydrogen abstraction from methane (equations 32 and 8, respectively). The HCl produced by equation 8 is then deprotonated and absorbed by I_2 (equations 24 and 27), while the HIO_2 produced by equation 32 disproportionates to HIO_3 and HOI (equation 33), which can then convert to additional ICl (equation 34). A more detailed treatment of HIO_2 and other I(III) species can be found below in the section for entries 11-14.

$$\mathrm{IO_2}\cdot + \mathrm{CH_4} \rightarrow \mathrm{HIO_2} + \mathrm{CH_3}\cdot \qquad \Delta H = 14.3;\ \Delta G = 10.3 \qquad (32)$$

$$\mathrm{Cl}\cdot + \mathrm{CH_4} \rightarrow \mathrm{HCl} + \mathrm{CH_3}\cdot \qquad \Delta H^{a} = -0.2;\ \Delta G = -5.6 \qquad (8)$$

$$2\mathrm{HIO_2} \rightarrow \mathrm{HIO} + \mathrm{HIO_3} \qquad \Delta H = -21.6;\ \Delta G = -21.3 \qquad (33)$$

$$\mathrm{HIO} + \mathrm{I_2Cl^-} + \mathrm{TFAH} \rightarrow \mathrm{ICl} + \mathrm{I_2} + \mathrm{H_2O} + \mathrm{TFA^-} \qquad \Delta H = 0.4;\ \Delta G = -10.2 \qquad (34)$$

^{a}Values based on experimental BDEs.[29] All numbers in kcal/mol.

Due to the presence of elemental iodine in the reaction, the methyl radicals produced will most likely react with I_2 to produce CH_3I (equation 35), which is converted to the product CH_3TFA under reaction conditions (equation 36). Finally, the iodine radicals can recombine to form additional I_2 (equation 37), and the iodide produced in equation 36 can comproportionate with HIO to produce additional elemental iodine (equation 38).

$$\mathrm{CH_3}\cdot + \mathrm{I_2} \rightarrow \mathrm{CH_3I} + \mathrm{I}\cdot \qquad \Delta H^{a} = -19.0;\ \Delta G = 16.9 \qquad (35)$$

$$\mathrm{CH_3I} + \mathrm{TFA^-} \rightarrow \mathrm{CH_3TFA} + \mathrm{I^-} \qquad \Delta H = -9.4;\ \Delta G = -2.9 \qquad (36)$$

$$2\mathrm{I}\cdot \rightarrow \mathrm{I_2} \qquad \Delta H^{a} = -36.5;\ \Delta G = -32.2 \qquad (37)$$

$$\mathrm{I^-} + \mathrm{HIO} + \mathrm{TFAH} \rightarrow \mathrm{I_2} + \mathrm{H_2O} + \mathrm{TFA^-} \qquad \Delta H = -21.0;\ \Delta G = -23.7 \qquad (38)$$

^{a}Values based on experimental BDEs.[29] All numbers in kcal/mol.

Scheme 3 shows the synthesis of the above equations into a full mechanism for the conversion of methane to methyl trifluoroacetate for the iodate-based OxE process. The mechanism proceeds through typical phases of initiation, propagation, and termination. During initiation, the lowest energy I(V)−Cl species are formed, and I· radical is generated. Propagation begins with the I· radical reacting with the I(V) species to create the more reactive radicals IO_2· and Cl· (reactive radical activation). The radicals IO_2· and Cl· then abstract hydrogen atoms from methane, which rebounds on elemental iodine to form methyl iodide and regenerate I· (methane activation and iodine radical regeneration). Finally, methyl iodide can undergo S_N2 attack by TFA^- to produce the methyl TFA product, and the iodide and HIO_2 can disproportionate and comproportionate to form additional iodate and elemental iodine (iodate regeneration).

In order to estimate the overall kinetic barrier for Scheme 3, we consider a steady-state approximation for [I·], using the method in Carey and Sundberg's *Advanced Organic Chemistry* page 683.[35] We approximate that the rate of formation and destruction of I· to be equal, i.e. $k_1[\mathrm{I_2}] = k_{-1}[\mathrm{I}\cdot]^2$, where $k_1[\mathrm{I_2}]$ is the rate of initiation (equation 1) and $k_{-1}[\mathrm{I}\cdot]^2$ the rate of termination. Then, $[\mathrm{I}\cdot] = \sqrt{k_1/k_{-1}}[\mathrm{I_2}]^{1/2}$. We can also say that the rate of the reaction is the rate of a propagation step, for example equation 29: rate = $k_{29}[\mathrm{I}\cdot][\mathrm{IO_2Cl_2^-}] = k_{29}\sqrt{k_1/k_{-1}}[\mathrm{I_2}]^{1/2}[\mathrm{IO_2Cl_2^-}]$. Hence, the rate constant is $k = k_{29}\sqrt{k_1/k_{-1}}$. Using the Eyring-Polanyi equation $k = \frac{k_BT}{h}\exp\left(-\frac{\Delta G^\ddagger}{RT}\right)$,[36] we see that overall activation barrier is then $\Delta G^\ddagger = -RT\ln\left(\frac{h}{k_BT}k_{29}\sqrt{k_1/k_{-1}}\right) = \Delta G_{29}^\ddagger - \frac{1}{2}RT\ln(k_1/k_{-1}) = \Delta G_{29}^\ddagger + \frac{1}{2}\Delta G_1^\ddagger - \frac{1}{2}\Delta G_{-1}^\ddagger$. If we assume that the dissociation and reformation of $\mathrm{I_2}$ has minimal barrier, we can approximate $\Delta G_1^\ddagger \approx \Delta G_1$ and $\Delta G_{-1}^\ddagger \approx 0$. Since we have calculated $\Delta G_{29}^\ddagger$ as 4.5 kcal/mol (Scheme 3) and ΔG_1 as 32.2 kcal/mol (equation 1), we estimate the effective barrier to be about 20.6 kcal/mol.

Scheme 3. Overall summary of the mechanism for the iodate-based OxE process for methane oxidation. All numbers in kcal/mol. *Values based on experimental BDEs.[29]

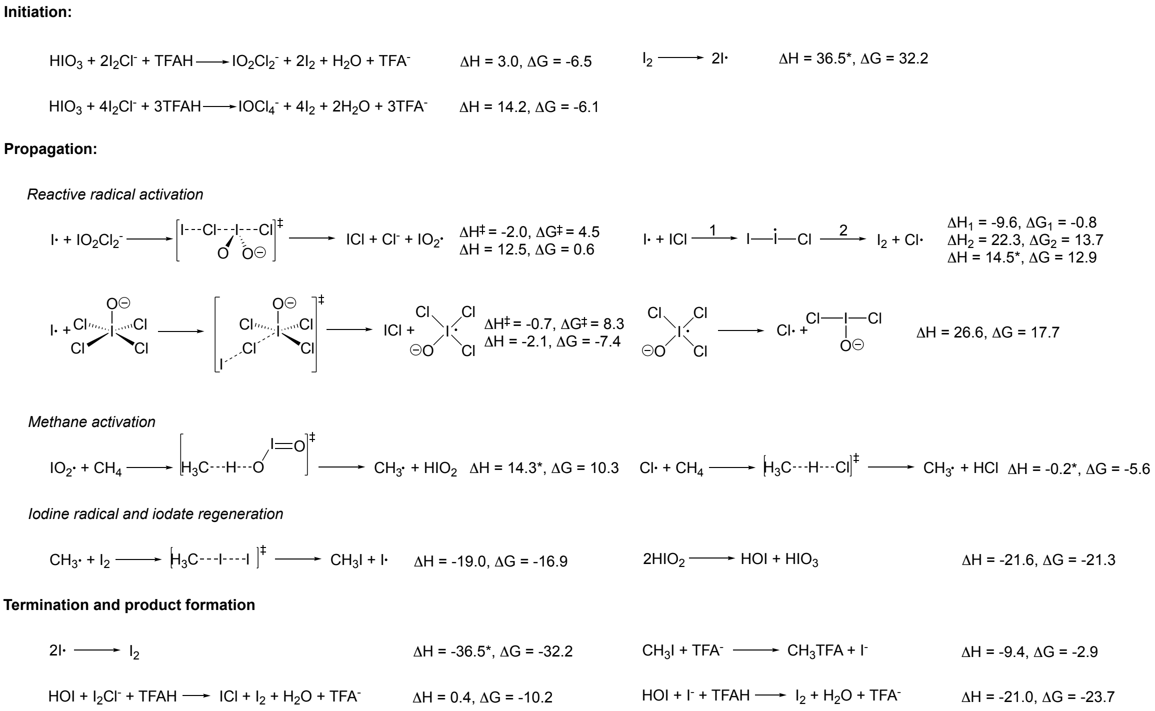

Equation 39 shows the overall reaction of the iodate/chloride oxidation.

$$\begin{aligned} &2\mathrm{HIO_3} + 5\mathrm{CH_4} + 5\mathrm{TFAH} \rightarrow \mathrm{I_2} + 6\mathrm{H_2O} + 5\mathrm{CH_3TFA} \qquad \Delta H = -234.1;\ \Delta G = -228.3 \end{aligned} \tag{39}$$

Entry 8, acetic acid variation. Previously, we showed that the reaction of methane and iodate/chloride in acetic acid produces methyl acetate (MeOAc).[18a] However, on further evaluation, it was found that MeOAc formed under these conditions is the result of the reaction with acetic acid only and that the majority of the MeOAc is not derived from methane oxidation. Control reactions in the absence of methane gave statistically identical MeOAc yields as reactions that include methane, approximately 30% yield with respect to oxidant using 0.67 mmol KCl and 7.7 mmol of $\mathrm{NH_4IO_3}$ in acetic acid. Furthermore, GC-MS analysis of the reaction of perprotio-methane in acetic acid-d_4 indicated that the fully deuterated derivative $\mathrm{CD_3CO_2CD_3}$ accounts for > 90% of methyl acetate production, while the product that would arise from methane functionalization, $\mathrm{CD_3CO_2CH_3}$, accounts for < 2% of the methyl acetate product.

Using DFT, it is readily apparent that the same mechanism proposed for the iodate-based OxE process in TFAH when translated to acetic acid solvent will not work. The biggest difference between acetic acid and TFAH is the much milder acidity of acetic acid. In equation 23, we see that iodate is quite basic in TFAH and is expected to be fully protonated. However, by comparison we can see from equation 40 that iodate is a weak base in HOAc and is expected to remain in the anionic form. Chloride is expected to remain anionic in both cases (equations 24 and 41); however, in HOAc it is not expected to be absorbed by elemental iodine (compare equation 42 to 27).

$$\mathrm{IO_3^- + HOAc \rightarrow HIO_3 + OAc^-} \qquad \Delta H = 17.0;\ \Delta G = 13.7 \qquad (40)^a$$

$$\mathrm{Cl^- + HOAc \rightarrow HCl + OAc^-} \qquad \Delta H = 32.3;\ \Delta G = 27.9 \qquad (41)^a$$

$$\mathrm{Cl^- + I_2 \rightarrow I_2Cl^-} \qquad \Delta H = -6.2;\ \Delta G = 1.3 \qquad (42)^a$$

[a]Values calculated for HOAc solution All numbers in kcal/mol.

The calculated energies of various I(V)−Cl species compared to this new IO_3^-/Cl^- baseline reveal that they are much higher in energy (Figure S2). We are simply unable to form the same quantities of the I(V)−Cl intermediates necessary to generate high energy radicals. We also note that the H−O bond in acetic acid is much weaker (BDE 112 kcal/mol) than that in TFAH (124.5 kcal/mol); hence, radicals that are generated are much more likely to react with the acetic acid solvent, abstracting H atoms to form species such as $\cdot CH_2CO_2H$ and $CH_3CO_2\cdot$, which may decompose to liberate CO_2 and form other radicals such as $CH_3\cdot$ that ultimately become MeOAc.

Entries 9-10. The mechanism for IO_3^- and Cl^- as described for entry 8 can easily hold if the iodate source is replaced by $(IO_2)_2S_2O_7$. We would expect any water in the system to hydrolyze $(IO_2)_2S_2O_7$ to HIO_3 and H_2SO_4 (equations 43-44). Hence, it is expected the same mechanism with improved yield due perhaps to the improved acidity of the system.

$$\mathrm{(IO_2)_2S_2O_7 + 2H_2O \rightarrow 2HIO_3 + H_2S_2O_7} \qquad \Delta H = -59.1;\ \Delta G = -65.6 \qquad (43)$$

$$\mathrm{H_2S_2O_7 + H_2O \rightarrow 2H_2SO_4} \qquad \Delta H = -26.8;\ \Delta G = -32.2 \qquad (44)$$

Note that $HS_2O_7^-$ and HSO_4^-, like Cl^- and I^-, are weak bases in TFAH, but $S_2O_7^{2-}$ and SO_4^{2-} are favorable in reacting with TFAH and are thus protonated (equations 45-48).

$$\mathrm{HS_2O_7^- + TFAH \rightarrow H_2S_2O_7 + TFA^-} \qquad \Delta H = 16.0;\ \Delta G = 16.9 \qquad (45)$$

$$\mathrm{S_2O_7^{2-} + TFAH \rightarrow HS_2O_7^- + TFA^-} \qquad \Delta H = -4.6;\ \Delta G = -3.9 \qquad (46)$$

$$\mathrm{HSO_4^- + TFAH \rightarrow H_2SO_4 + TFA^-} \qquad \Delta H = 3.3;\ \Delta G = 3.3 \qquad (47)$$

$$\mathrm{SO_4^{2-} + TFAH \rightarrow HSO_4^- + TFA^-} \qquad \Delta H = -24.0;\ \Delta G = -26.8 \qquad (48)$$

Also note that H_3O^+ is a weak acid in TFAH (equation 49), and since the reaction generates H_2O as a byproduct, we would expect H_3O^+ and not $TFAH_2^+$ to be the active Brønsted acid in acidic wet TFAH solution. Although $H_2S_2O_7$, H_2SO_4, HCl, and HI are all considered strong acids in aqueous solution, due to the much lower dielectric constant of TFAH, none of them are likely to protonate H_2O in TFAH solution (equations 50-53).

$$\mathrm{H_3O^+ + TFAH \rightarrow H_2O + TFAH_2^+} \qquad \Delta H = 20.3;\ \Delta G = 21.5 \qquad (49)$$

$$\mathrm{H_2S_2O_7 + H_2O \rightarrow HS_2O_7^- + H_3O^+} \qquad \Delta H = 10.3;\ \Delta G = 8.3 \qquad (50)$$

$$\mathrm{H_2SO_4 + H_2O \rightarrow HSO_4^- + H_3O^+} \qquad \Delta H = 23.1;\ \Delta G = 21.9 \qquad (51)$$

$$\mathrm{HCl + H_2O \rightarrow Cl^- + H_3O^+} \qquad \Delta H = 15.7;\ \Delta G = 18.2 \qquad (52)$$

$$\mathrm{HI + H_2O \rightarrow I^- + H_3O^+} \qquad \Delta H = 7.1;\ \Delta G = 10.0 \qquad (53)$$

We also note that with the conversion of $(IO_2)_2S_2O_7$ to HIO_3 and H_2SO_4, the system is still not acidic enough to remove chloride from its sequestration by elemental iodine (equations 54-55).

$$\mathrm{H_2S_2O_7 + I_2Cl^- \rightarrow HS_2O_7^- + I_2 + HCl} \qquad \Delta H = 5.5;\ \Delta G = -6.6 \qquad (54)$$

$$\mathrm{H_2SO_4 + I_2Cl^- \rightarrow HSO_4^- + I_2 + HCl} \qquad \Delta H = 18.3;\ \Delta G = 7.0 \qquad (55)$$

Although in basic solution the energies of I(V) species can be referenced to the species HIO_3, I_2Cl^-, I_2, H_2O, TFAH, and TFA^-, in acidic solution they should be referenced to the species HIO_3, I_2Cl^-, I_2, H_2O, TFAH, H_2SO_4, and HSO_4^-. The columns in Table S1 that are marked "acid" show the energies of the I(V) species recalculated to this new reference. As in the basic case of the IO_3^-/Cl^- system, the lowest energy species formed are still $IO_2Cl_2^-$ and $IOCl_4^-$, with the only difference being that $IOCl_4^-$ is now favored over $IO_2Cl_2^-$. Scheme S3 shows the new initiation steps for the methane oxidation in acidic condition (i.e., $(IO_2)_2S_2O_7$), whereas the propagation and termination steps remain the same as for Scheme 3.

Entries 11-14. I_2O_4 and $(IO)_2SO_4$ can be analyzed as ionic species, consisting of a linear polymeric cationic $(IO)_n^{n+}$ chain with either IO_3^- or SO_4^{2-} as the counterion.[37] The iodine atoms in $(IO)_n^{n+}$ have a formal positive charge, and the counterions may be coordinated to them (strongly so in the solid and in low dielectric solvents; more weakly in high dielectric solvents such as ethanol and dimethylformamide).[37b] We see that the $(IO)_n^{n+}$ chain itself must be active in effecting methane oxidation, since entry 14 shows that the reaction works with an inert sulfate counterion. In general, it is known that I(V) salts are more stable than I(III), and indeed, both I_2O_4 and $(IO)_2SO_4$ are known to disproportionate to HIO_3 and I_2 in hot water and sulfuric acid, respectively.[37a] We would thus expect HIO_3 to be likely formed in hot TFAH as well.

Our computational studies initially indicated that $(IO)_n^{n+}$ chains in TFAH are unstable with respect to dissociation into $I{=}O^+$ monomers (equation 56).[38] However, iodate or sulfate is the counterion, and both are very basic (equations 23 and 48), leading to the formation of TFA^-, which can very favorably react with IO^+ to form TFA−I=O (equation 57). The TFA−I=O produced can further add a water or TFAH molecule across the I=O double bond (equations 58-59), or polymerize (equations 60-61). Table S2 shows a comprehensive listing of all monomeric I(III) species that may be formed in TFAH solution. The lowest energy monomeric species is ICl_3 in both basic and acidic systems. Since the polymerization of $I(OH)TFA_2$ is approximately thermoneutral (equation 61), and since ICl_3 is significantly lower in energy than $I(OH)TFA_2$ (equation 62), we can restrict our mechanistic considerations to monomeric I(III) species only.

$(\mathrm{IO})_n^{n+} \rightarrow \mathrm{IO}^+ + (\mathrm{IO})_{n-1}^{(n-1)+}$ $\Delta H \sim -17$ to -20; $\Delta G \sim -30$ to -33 (56)[38b]

$\mathrm{IO}^+ + \mathrm{TFA}^- \rightarrow \mathrm{I(O)TFA}$ $\Delta H = -39.1$; $\Delta G = -25.3$ (57)

$\mathrm{I(O)TFA} + \mathrm{H_2O} \rightarrow \mathrm{I(OH)_2TFA}$ $\Delta H = -24.4$; $\Delta G = -9.2$ (58)

$\mathrm{I(O)TFA} + \mathrm{TFAH} \rightarrow \mathrm{I(OH)TFA_2}$ $\Delta H = -24.8$; $\Delta G = -6.1$ (59)

$\mathrm{H[I(O)TFA]_nTFA} + \mathrm{I(O)TFA} \rightarrow \mathrm{H[I(O)TFA]_{n+1}TFA}$ $\Delta H \sim -29$ to -24; $\Delta G \sim -8$ to -4 (60)[39]

$\mathrm{H[I(O)TFA]_nTFA} + \mathrm{I(OH)TFA_2} \rightarrow \mathrm{H[I(O)TFA]_{n+1}TFA} + \mathrm{TFAH}$ $\Delta H \sim -4$ to 1; $\Delta G \sim -2$ to 2 (61)[40]

$\mathrm{I(OH)TFA_2} + 3\mathrm{I_2Cl^-} + \mathrm{TFAH} \rightarrow \mathrm{ICl_3} + 3\mathrm{I_2} + \mathrm{H_2} + 3\mathrm{TFA^-}$ $\Delta H = 26.6$; $\Delta G = -15.5$ (62)

We now see that the species involved here form the same collection of species in the reactions of entry 5 (ICl_3) and entry 7 ($ITFA_3/Cl^-$). As in the case of entry 7, MeTFA and not MeCl is formed due to the catalytic amounts of Cl^- preventing the build-up of ICl_3 itself. We can also consider a disproportionation route to form I(V) that can enter that mechanistic route. In one such example, monomeric I(O)TFA favorably disproportionates to IO_2TFA (equation 63), which can then convert to HIO_3 (equation 64). The I(V) mechanism as for the iodate reaction (entry 8) then applies. The TFAI byproduct can convert to ICl (equation 65) and enter the I(V) mechanism from there.

$2\mathrm{I(O)TFA} \rightarrow \mathrm{IO_2TFA} + \mathrm{ITFA}$ $\Delta H = -22.9$; $\Delta G = -20.7$ (63)

$\mathrm{IO_2TFA} + \mathrm{H_2O} \rightarrow \mathrm{HIO_3} + \mathrm{TFAH}$ $\Delta H = -10.0$; $\Delta G = -12.8$ (64)

$\mathrm{TFAI} + \mathrm{I_2Cl^-} \rightarrow \mathrm{ICl} + \mathrm{I_2} + \mathrm{TFA^-}$ $\Delta H = 1.9$; $\Delta G = -10.0$ (65)

Entry 15. Periodate can actually refer to two different ions: metaperiodate (IO_4^-) and the water adduct orthoperiodate ($H_4IO_6^-$).[37a] Whereas orthoperiodate is generally known to be the preferred species in aqueous solution, we wanted to ascertain if metaperiodate persists under our reaction conditions (potentially wet TFAH). Scheme S4 shows that both addition of water and protonation to IO_4^- is unfavorable; hence, we can begin our analysis with the IO_4^- species itself.

In the presence of elemental iodine, comproportionation to iodate is favorable (equation 66). In the absence of I_2, chloride may serve as a reducing agent instead (equations 67-68).

$5\mathrm{IO_4^-} + \mathrm{I_2} + \mathrm{H_2O} \rightarrow 5\mathrm{IO_3^-} + 2\mathrm{HIO_3}$ $\Delta H = -27.6$; $\Delta G = -40.4$ (66)

$\mathrm{IO_4^-} + \mathrm{Cl^-} \rightarrow \mathrm{IO_3^-} + \mathrm{ClO^-}$ $\Delta H = 24.0$; $\Delta G = 18.5$ (67)

$\mathrm{ClO^-} + \mathrm{TFAH} \rightarrow \mathrm{HOCl} + \mathrm{TFA^-}$ $\Delta H = -18.9$; $\Delta G = -20.6$ (68)

As shown in Scheme 3, in the presence of chloride the iodate can oxidize methane to CH_3TFA and generate HIO_2 (equation 32), which then disproportionates to regenerate HIO_3 through several other iodine oxyacids (equations 33-34). The hypochlorous acid produced in equations 67-68 can react with these iodine oxyacids, aiding in the regeneration of HIO_3 (equations 69-70).

$\mathrm{HOCl} + \mathrm{HIO_2} + \mathrm{I_2} + \mathrm{TFA^-} \rightarrow \mathrm{I_2Cl^-} + \mathrm{HIO_3} + \mathrm{TFAH}$ $\Delta H = -35.6$; $\Delta G = -22.8$ (69)

$\mathrm{HOCl} + \mathrm{ICl} + \mathrm{H_2O} + 2\mathrm{I_2} + 2\mathrm{TFA^-} \rightarrow 2\mathrm{I_2Cl^-} + \mathrm{HIO_2} + 2\mathrm{TFAH}$ $\Delta H = -14.5$; $\Delta G = 8.7$ (70)

Because IO_3^- is generated from IO_4^- (equation 66), our mechanism for IO_3^- (entry 8) should also be valid for IO_4^-. However, since IO_4^- can be expected to make a much richer set of chloro, TFA, oxo, and hydroxo complexes than IO_3^-, we have only demonstrated the feasibility of one possible reaction pathway (IO_4^- to methane oxidation via IO_3^-) without discounting the possibility of other pathways. Equation 71 shows the overall reaction of the periodate/chloride oxidation, which is even more downhill than iodate/chloride oxidation (compare to equation 39).

$2\mathrm{HIO_4} + 7\mathrm{CH_4} + 7\mathrm{TFAH} \rightarrow \mathrm{I_2} + 8\mathrm{H_2O} + 7\mathrm{CH_3TFA}$ $\Delta H = -374.4$; $\Delta G = -372.5$ (71)

DISCUSSION

As mentioned above, a common limitation of radical mechanisms is the difficulty of preventing over-oxidation. For example, free radical chlorination of methane at reasonable conversions often yields a mixture of methyl chloride, methylene chloride, chloroform, and/or carbon tetrachloride.[41] Methane oxidation by electrophilic C–H activation can be selective for CH_3X (X = TFA, SO_3H, etc.) due to the electron-withdrawing nature of X acting as a protecting group.[14] In the iodate/chloride OxE process, methane and ethane were oxidized to CH_3TFA and EtTFA respectively, with conversions greater than 20% and with formation of minimal over-oxidized products.[18a] Is it possible that TFA could serve as a protecting group against radical oxidation?

Consider the immediate result of a radical H-atom abstraction on CH_3TFA: the formation of the radical $\cdot CH_2TFA$. A case could be made that a lone pair on the O atom of TFA directly bound to the CH_2 can stabilize the radical via the formation of a two-centered, three-electron bond.[35] This would make radical attack on CH_3TFA and thus over-oxidation more likely, similar to observations for methane oxychlorination. A case could also be made that in the transition state $[TFACH_2\text{---}H\text{---}Cl]\cdot^{\ddagger}$, the C has partial cationic character due to the electronegative nature of the Cl atom. The presence of the electron-withdrawing TFA group thus destabilizes the transition state in what is termed a radical polar effect, and hence inhibits over-oxidation.[42]

In order to investigate the competing trends of lone pair stabilization and polar effect destabilization, we examine several radical abstraction reactions and compare them to equation 8 (equations 72-76). Our insights from the comparisons are summarized in Table 2.

$$\mathrm{Cl}\cdot + \mathrm{CH_4} \rightarrow \mathrm{HCl} + \mathrm{CH_3}\cdot \qquad \Delta G^{\ddagger} = 3.2; \ \Delta G = -5.6 \tag{8}$$

$$\mathrm{Br}\cdot + \mathrm{CH_4} \rightarrow \mathrm{HBr} + \mathrm{CH_3}\cdot \qquad \Delta G^{\ddagger} = 15.5; \ \Delta G = 8.6 \tag{72}$$

$$\mathrm{Cl}\cdot + \mathrm{CH_3TFA} \rightarrow \mathrm{HCl} + \mathrm{TFACH_2}\cdot \qquad \Delta G^{\ddagger} = 6.1; \ \Delta G = -6.3 \tag{73}$$

$$\mathrm{Br}\cdot + \mathrm{CH_3TFA} \rightarrow \mathrm{HBr} + \mathrm{TFACH_2}\cdot \qquad \Delta G^{\ddagger} = 19.6; \ \Delta G = 7.9 \tag{74}$$

$$\mathrm{Cl}\cdot + \mathrm{CH_3Cl} \rightarrow \mathrm{CH_2Cl}\cdot + \mathrm{HCl} \qquad \Delta G^{\ddagger} = 3.6; \ \Delta G = -7.6 \tag{75}$$

$$\mathrm{Cl}\cdot + \mathrm{CH_2Cl_2} \rightarrow \mathrm{CHCl_2}\cdot + \mathrm{HCl} \qquad \Delta G^{\ddagger} = 4.3; \ \Delta G = -8.9 \tag{76}$$

Table 2. Comparison of radical H-abstractions to isolate polar and lone pair effects.

Comparison	$\Delta\Delta G^{\ddagger}$	$\Delta\Delta G$
CH_4 v. CH_3TFA + Cl· (eqs. 8 v. 73)	2.9	−0.7
CH_4 v. CH_3TFA + Br· (eqs. 72 v. 74)	4.1	−0.7
CH_4 v. CH_3Cl + Cl· (eqs. 8 v. 75)	0.4	−2.0
CH_3Cl v. CH_2Cl_2 + Cl· (eqs. 75 v. 76)	0.7	−1.3

As shown in the final column of Table 2, the calculated $\Delta\Delta G$s confirm the lone pair stabilization effect: In all cases, ΔG for the reaction $\mathrm{Y}\cdot + \mathrm{CX}_n\mathrm{H}_{4-n} \rightarrow \mathrm{HY} + \mathrm{CX}_n\mathrm{H}_{3-n}\cdot$ is lower if X is a substituent such as Cl or TFA as opposed to H.

From examining the $\Delta\Delta G^{\ddagger}$ column instead, we see that the transition state for H atom abstraction for CH_3TFA + Y· (Y = Cl or Br) is about 3-4 kcal/mol higher than the corresponding transition state for CH_4 + Y·. This is the polar effect, and it can be confirmed by Mulliken charges (Table S3). The charge on carbon in CH_4 is −0.60 due to the relative electronegativity of carbon versus hydrogen. For CH_3TFA and CH_3Cl, this increases to −0.33 and −0.40, respectively; due to the electron withdrawing TFA or Cl groups, which have Mulliken charges −0.27 and −0.12, respectively. In the transition states $[CH_3\text{---}H\text{---}Cl]\cdot^{\ddagger}$ and $[CH_3\text{---}H\text{---}Br]\cdot^{\ddagger}$, the charge on C is increased to −0.52 and −0.51, respectively; an illustration of the polar effect due to the electronegative Cl and Br atoms. In the comparison of CH_3TFA to the transition states $[TFACH_2\text{---}H\text{---}Cl]\cdot^{\ddagger}$ and $[TFACH_2\text{---}H\text{---}Br]\cdot^{\ddagger}$, the charge on TFA is increased from −0.27 to −0.16 and −0.07, which is quite destabilizing due to the electron-withdrawing nature of the TFA substituent. The charge on Cl for CH_3Cl and $[ClCH_2\text{---}H\text{---}Cl]\cdot^{\ddagger}$ similarly increases from −0.12 to 0.10, but this is less destabilizing due to the greater polarizability of Cl. As for CH_2Cl_2 and $[Cl_2CH\text{---}H\text{---}Cl]\cdot^{\ddagger}$, the average charge on the Cl's increases from −0.01 to 0.16. Thus, we see the relative lack of over-oxidation protection for CH_3Cl and CH_2Cl_2.

This analysis explains the reason for the increased $\Delta G^{\ddagger}$ of CH_3TFA activation, and thus the origin of protection against over-oxidation.

CONCLUSION

We have examined existing experimental data regarding the oxidation of methane to methyl trifluoroacetate using a wide variety of hypervalent iodine complexes, and used DFT to model viable mechanistic pathways for each reaction. Although there is a wide variety of iodine reagents capable of effecting the reaction, the tendency of iodine complexes to disproportionate into I_2 and I(V) serves as a "funnel" that unites the sundry iodine precursors into the same mechanism based on iodic acid. In our common iodate/OxE mechanism, iodic acid is converted to $IO_2Cl_2^-$ or $IOCl_4^-$ as the key intermediate, which reacts with iodine radicals present in the system to form $IO_2\cdot$ and $Cl\cdot$ radicals. These radicals are able to mediate the C−H bond cleavage of methane, leading to CH_3I and ultimately the final product, CH_3TFA, which is protected from further oxidation by the polar effect.

We thus report a simple and unifying solution to the mechanism of the iodate/OxE process, a problem that initially appears to involve an intractable soup of chemical species. These insights may serve as a starting point for further investigations into this class of oxidation reactions.

ASSOCIATED CONTENT

Supporting Information. Additional schemes and tables and a spreadsheet containing raw data for all chemical species studied. This material is available free of charge via the Internet at http://pubs.acs.org.

AUTHOR INFORMATION

Corresponding Author

*Author to whom correspondence should be addressed. Email: wag@wag.caltech.edu

Author Contributions

All calculations were carried out by RF, with strategies suggested by RF, RJN, and WAG. Experimental work was carried out by NSL under mentorship by TBG. Critical guidance was provided by JTG and TBG. The manuscript was written through contributions of all authors. All authors have given approval to the final version of the manuscript.

Funding Sources

This research was sponsored by the U.S. Department of Energy, Office of Energy Efficiency and Renewable Energy, Advanced Manufacturing Office, under contract DE-AC05-00OR22725 with UT-Battelle, LLC. The funding for this computational project came from various gifts to the Materials and Process Simulation Center (MSC) at Caltech. The computers used were funded from DURIP grants to the MSC.

ABBREVIATIONS

BDE, bond dissociation energy; DFT, density functional theory; OxE, oxy-esterification; OAc, acetate; PBF, Poisson-Boltzmann Finite element method; SCF, self-consistent field; SMR, steam-methane reformation; TFA, trifluoroacetate.

REFERENCES

1. *General Chemistry: An Atoms First Approach*; Halpern, J., Ed.; Howard University: Washington, 2014.
2. Chapter 15.7: Fossil Fuels. In *General Chemistry for Engineering*; Halpern, J.; Sinex, S.; Johnson, S.; Eds.; Prince George's Community College: Largo, MD, 2016.
3. U.S. Energy Information Administration. Independent Statistics & Analysis: Natural Gas. https://www.eia.gov/dnav/ng/hist/rngwhhdm.htm (accessed January 29, 2017).
4. Pachauri, R. K.; Reisinger, A. *The Fourth Assessment Report of the Intergovernmental Panel on Climate Change*; Working Group 1: Geneva, Switzerland, 2007, Chapter 2.
5. The World Bank. Global Gas Flaring Reduction Partnership (GGFR). http://www.worldbank.org/en/programs/gasflaringreduction (accessed January 29, 2017).
6. Cheng, W.-H.; Kung, H. H. *Methanol Production and Use*; Marcel Dekker: New York, NY, 1994; pp 283−317.
7. ICIS. Methanol Prices, Markets, & Analysis. http://www.icis.com/chemicals/methanol/ (accessed January 29, 2017).
8. National Renewable Energy Laboratory. Subcontract Report NREL/SR-510-39943: Equipment Design and Cost Estimation for Small Modular Biomass Systems, Synthesis Gas Cleanup, and Oxygen Separation Equipment. http://www.nrel.gov/docs/fy06osti/39943.pdf (accessed January 29, 2017)
9. a. Bal'zhinimaev, B. S.; Paukshtis, E. A.; Kovalev, E. V.; Suknev, A. P.; Shalygin, A. S. (Uchrezhdenie RAN Institut Kataliza im. G. K. Boreskova SO RAN). Method of Selective Catalytic Oxychlorination of Methane to Methyl Chloride. RU Patent 2446881C2, April 10, 2012; b. Aglulin, A. G. *Kinet. Catal.* **2009**, *50*, 427−434; c. Stauffer, J. E. Process for the Chlorination of Methane. World Patent 9008117A1, July 26, 1990; d. Rozanov, V. N.; Gvozd, E. V.; Kernerman, V. A.; Svetlanov, E. B.; Trushechkina, M. A.; Treger, Y. A. *Kinet. Catal.* **1989**, *30*, 148−154; e. Riegel, H.; Schindler, H. D.; Sze, M. C. (CE Lummus). Oxychlorination of Methane. U.S. Patent 4,207,268A, June 10, 1980.
10. Labinger, J. A. *J. Mol. Catal.* **2004**, *220*, 27−35.
11. a. Goldshlegger, N. F.; Tyabin, M. B.; Shilov, A. E.; Shteinman, A. A. *Zh. Fiz. Khim.* **1969**, *43*, 2174−2175; b. Goldshlegger, N. F.; Eskova, V. V.; Shilov, A. E.; Shteinman, A. A. *Zh. Fiz. Khim.* **1972**, *46*, 1353−1354; c. Shilov, A. E.; Shul'pin, G. B. *Activation and Catalytic Reactions of Saturated Hydrocarbons in the Presence of Metal Complexes*; Kluwer Academic Publishers: Dordrecht, 2000; pp 259−317.
12. a. Fekl, U.; Goldberg, K. I. *Adv. Inorg. Chem.* **2003**, *54*, 259−320; b. Lersch, M.; Tilset, M. *Chem. Rev.* **2005**, *105*, 2471−2526.
13. a. Chepaikin, E. G. *Russ. Chem. Rev.* **2011**, *80*, 363−396; b. Jones, C. J.; Taube, D.; Ziatdinov, V. R.; Periana, R. A.; Nielsen, R. J.; Oxgaard, J.; Goddard, W. A., III. *Angew. Chem., Int. Ed.* **2004**, *43*, 4626−4629; c. Periana, R. A.; Taube, D. J.; Gamble, S.; Taube, H.; Satoh, T.; Fujii, H. *Science* **1998**, *280*, 560−564; d. Periana, R. A.; Taube, D. J.; Taube, H.; Evitt, E. R. (Catalytica, Inc.). *Catalytic Process for Converting Lower Alkanes to Esters, Alcohols, and to Hydrocarbons*. U.S. Patent 5,306,855A, April 26, 1994; e. Kao, L. C.; Hutson, A. C.; Sen, A. *J. Am. Chem. Soc.* **1991**, *113*, 700−701.

14. a. Ahlquist, M.; Nielsen, R. J.; Periana, R. A.; Goddard III, W. A. *J. Am. Chem. Soc.* **2009**, *131*, 17110-17115; b. Fu, R.; Nielsen, R. J.; Goddard, W. A. III; Fortman, G. C.; Gunnoe, T. B. *ACS Catal.* **2014**, *4*, 4455−4465.
15. Hashiguchi, B. G.; Konnick, M. M.; Bischof, S. M.; Gustafson, S. J.; Devarajan, D.; Gunsalus, N.; Ess, D. H.; Periana, R. A. *Science* **2014**, *343*, 1232−1237.
16. a. O'Reilly, M. E.; Fu, R.; Nielsen, R. J.; Sabat, M.; Goddard, W. A. III; Gunnoe, T. B. *J. Am. Chem. Soc.* **2014**, *136*, 14690–14693; b. Munz, D.; Webster-Gardiner, M. S.; Fu, R.; Strassner, T.; Goddard, W. A. III; Gunnoe, T. B. *ACS Catal.* **2015**, *5*, 769–775; c. Webster-Gardiner, M. S.; Fu, R.; Fortman, G. C.; Nielsen, R. J.; Gunnoe, T. B.; Goddard, W. A. III. *Catal. Sci. Technol.* **2015**, *5*, 96–100; d. Fu, R.; O'Reilly, M. E.; Nielsen, R. J.; Goddard, W. A. III; Gunnoe, T. B. *Chem. Eur. J.* **2015**, *21*, 1286–1293; c. Webster-Gardiner, M. S.; Piszel, P. E.; Fu, R.; Chen, J.; McKeown, B. A.; Nielsen, R. J.; Goddard, W. A. III; Gunnoe, T. B. *J. Mol. Catal. A: Chem*. **2017**, *426B*, 381–388.
17. a. Olah, G. A.; Gupta, B.; Felberg, J. D.; Ip, W. M.; Husain, A.; Karpeles, R.; Lammertsma, K.; Melhotra, A. K.; Trivedi, N. J. *J. Am. Chem. Soc.* **1985**, *107*, 7097−7105; b. Ding, K.; Metiu, H.; Stucky, G. D. *ACS Catal.* **2013**, *3*, 474−477; c. Dohi, T.; Kita, Y. *ChemCatChem* **2014**, *6*, 76−78; d. Moteki, S. A.; Usui, A.; Zhang, T.; Solorio Alvarado, C. R.; Maruoka, K. *Angew. Chem., Int. Ed.* **2013**, *52*, 8657−8660; e. Ding, K.; Zhang, A.; Stucky, G. D. *ACS Catal.* **2012**, *2*, 1049−1056; f. Buddrus, J.; Plettenberg, H. *Angew. Chem., Int. Ed. Engl.* **1976**, *15*, 436.
18. a. Fortman, G. C.; Boaz, N. C.; Munz, D.; Konnick, M. M.; Periana, R. A.; Groves, J. T.; Gunnoe, T. B. *J. Am. Chem. Soc.* **2014**, *136*, 8393−8401; b. Kalman. S. E.; Munz, D.; Fortman, G. C.; Boaz, N. C.; Groves, J. T.; Gunnoe, T. B. *Dalton Trans.*, **2015**, *44*, 5294−5298.
19. Bochevarov, A. D.; Harder, E.; Hughes, T. F.; Greenwood, J. R.; Braden, D. A.; Philipp, D. M.; Rinaldo, D.; Halls, M. D.; Zhang, J.; Friesner, R. A. *Intl. J. Quant. Chem.* **2013**, *113*, 2110–2142.
20. Zhao, Y.; Truhlar, D. G. *Theor. Chem. Account* **2008**, *120*, 215–241.
21. Grimme, S.; Antony, J.; Erlich, S.; Krieg, H. *J. Chem. Phys.* **2010**, *132*, 154104.
22. a. Hehre, W. J.; Ditchfield, R.; Pople, J. A. *J. Chem. Phys.* **1972**, *56*, 2257–2261; b. Francl, M. M.; Pietro, W. J.; Hehre, W. J.; Binkley, J. S.; Gordon, M. S.; Defrees, D. J.; Pople, J. A. *J. Chem. Phys.* **1982**, *77*, 3654–3665.
23. a. Peterson, K. A. *J. Chem. Phys.* **2003**, *119*, 11099–11112; b. Peterson, K. A.; Figgen, D.; Goll, E; Stoll, H.; Dolg, M. *J. Chem. Phys.* **2003**, *119*, 11113–11123; c. Metz, B.; Stoll, H.; Dolg, M. *J. Chem. Phys*. **2000**, *113*, 2563–2569.
24. a. Tannor, D. J.; Marten, B.; Murphy, R.; Friesner, R. A.; Sitkoff, D.; Nicholls, A.; Ringnalda, M. N.; Goddard, W. A. III; Honig, B. *J. Am. Chem. Soc.* 1994, *116*, 11875–11882; b. Marten, B.; Kim, K.; Cortis, C.; Friesner, R. A.; Murphy, R. B.; Ringnalda, M. N.; Sitkoff, D.; Honig, B. *J. Phys. Chem*. 1996, *100*, 11775–11788.
25. a. Clark, T.; Chandrasekhar, J.; Spitznagel, G. W.; Schleyer, P. V. *J. Comput. Chem.* **1983**, *4*, 294–301; b. Krishnan, R.; Binkley, J. S.; Seeger, R.; Pople, J. A. *J. Chem. Phys.* **1980**, *72*, 650–654.
26. Jaguar 8.4 User Manual, page 357, see note 86.
27. Harris, F. E.; O'Konski, C. T. *J. Am. Chem. Soc.* **1954**, *76*, 4317–4318.
28. Chase, M. W. Jr. *NIST-JANAF Themochemical Tables, Fourth Edition*, *J. Phys. Chem. Ref. Data, Monograph 9,* 1998, 1–1951.
29. Speight, J. *Lange's Handbook of Chemistry*, 17th ed.; McGraw-Hill: Boston, 2016; pp. 176–187.
30. a. Michalkiewicz, B.; Jarosińska, M.; Łukasiewicz, I. *Chem. Eng. J.* **2009**, *154*, 156−161; b. Gang, X.; Zhu, Y.; Birch, H.; Hjuler, H. A.; Bjerrum, N. *J. Appl. Catal., A* **2004**, *261*, 91−98; c. Periana, R. A.; Mirinov, O.; Taube, D. J.; Gamble, S. *Chem. Commun*. **2002**, 2376−2377; d. Bjerrum, N. J.; Xiao, G.; Hjuler, H. A. (Statoil Research Centre). Process and Catalyst System for the Oxidation of Gaseous Hydrocarbons into Alcohols. World Patent 9924383A1, May 20, 1999.
31. Boswijk, K. H. ; Wiebenga, E. H. *Acta Crystallogr.* **1954**, *7*, 417–423.
32. Konnick, M. M.; Hashiguchi, B. G.; Devarajan, D.; Boaz, N. C.; Gunnoe, T. B.; Groves, J. T.; Gunsalus, N.; Ess, D. H.; Periana, R. A. *Angew. Chem., Int. Ed.* **2014**, *53*, 10490−10494.
33. Grant, D. J.; Garner, E. B. III; Matus, M. H.; Nguyen, M. T.; Peterson, K. A.; Francisco, J. S.; Dixon, D. A. *J. Phys. Chem. A*, **2010**, *114*, 4254–4265.
34. Sememov, N. N. *Some Problems in Chemical Kinetics and Reactivity*; Princeton University Press: Princeton, NJ, 2017; p. 191.
35. Carey, F. A.; Sundberg, R. J. *Advanced Organic Chemistry, Part A: Structure and Mechanisms*, 5th ed.; Springer: Berlin, 2008.
36. a. Eyring, H. *J. Chem. Phys.* **1935**, *3*, 107–115; b. Hammett, L. P. *Physical Organic Chemistry*, 1st ed.; McGraw-Hill: New York and London, 1940.
37. a. Wiberg, N.; Holleman, A. F. *Holleman-Wiberg's Inorganic Chemistry*; Academic Press: Cambridge, 2001; b. Dasent, W. E.; Waddington, T. E. *J. Chem. Soc.* **1960**, 3350−3356.
38. a. For $(IO)_n^{n+}$ specifically, we optimized the geometry in solution phase, since a gas phase optimization would inevitably fail due to the large amount of positive charge; b. $n = 2$: $\Delta H = 19.9$, $\Delta G = 30.0$; $n = 3$: $\Delta H = 16.9$, $\Delta G = 29.9$; $n = 4$: $\Delta H = 18.1$, $\Delta G = 32.8$.
39. $n = 0$: $\Delta H = -24.8$, $\Delta G = -6.1$; $n = 1$: $\Delta H = -23.9$, $\Delta G = -4.2$; $n = 2$: $\Delta H = -28.8$, $\Delta G = -7.5$; $n = 3$: $\Delta H = -27.9$, $\Delta G = -5.8$; $n = 5$: $\Delta H = -28.7$, $\Delta G = -8.3$.
40. $n = 0$: $\Delta H = 0$, $\Delta G = 0$; $n = 1$: $\Delta H = 0.9$, $\Delta G = 1.9$; $n = 2$: $\Delta H = -4.1$, $\Delta G = -1.4$; $n = 3$: $\Delta H = -3.2$, $\Delta G = 0.3$; $n = 5$: $\Delta H = -3.9$, $\Delta G = -2.2$.
41. Carey, F.A. *Organic Chemistry*, 6th Ed.; McGraw Hill: New York, 2006.
42. Viehe, H. G.; Janousek, Z; Merényi, R. *Substituent Effects in Radical Chemistry*; D. Reidel: Dordrecht, Holland, 1986.